University of Strathclyde

Department of Biomedical Engineering

THE DEVELOPMENT OF A REMOTELY EXPANDABLE ANASTOMOSIS DEVICE FOR USE IN PAEDIATRIC CARDIOTHORACIC SURGERY

Craig Simpson

This thesis is submitted in fulfilment of the requirements of the degree of Doctor of Philosophy PhD

2017

‘This thesis is the result of the author’s original research. It has been composed by the author and has not been previously submitted for examination which has led to the award of a degree.’

Signed:

Date:

Abstract

Congenital Heart Disease (CHD) is one of the main causes of infant mortality in the UK and United States. In 2011, 47% of infants born with CHD in the UK did not survive to their first birthday. Often forms of CHD require the implantation of conduits (tubes) to redirect the blood flow around the reconstructed anatomy in the early days of life. In all cases, these children will require review surgery, often several times to replace the implanted conduit as the child grows. Critically every review procedure carries with it an increased mortality risk. This project represents the first stage in the development of a conduit/ anastomosis technology, which will grow in response to the growing child, matching haemodynamic demand and eliminating the need for revision surgery.

Two prototypes were designed and developed. Each using an active drive mechanism to expand a stainless steel expansion strip with the slow and controlled movement required for such an application. Each of the designs were silicone coated using custom designed injection moulding techniques ensuring biocompatibility.

Power and control systems were designed for each iteration taking into account their expansion methods to achieve the desired expansion rate of 12mm to 20mm in diameter of the implantation period.

Three consecutive implantation studies were carried out throughout the device's development. In the first study, the device was implanted into the right ventricle of a cadaveric pig to determine any potential impediments that would need to be addressed for implantation into live animal models. The second implantation was carried out on 6 piglets, successfully establishing CPB procedures. The third implantation was successfully carried out on 3 piglets, 2 of which survived the duration of the testing, confirming a successful encapsulation method to ensure biocompatibility, however it appeared the device failed to expand due to power line breakdown.

Acknowledgements

Foremost, I would like to thank my primary supervisor, Professor Terry Gourlay, for all the help and guidance he provided throughout the course of this project, showing great patience along the way, he, along with my colleagues, Dr Craig Robertson, Dr Monica Rozeik played major roles in the development of this project and the formation of this thesis. Coining the phrases *'what if....'* And *'it'll be fine!'* which will stick with me forever.

Also I would like to thank the technicians Stephen Murray, for his help in the workshop offering technical and practical input while passing on his fabrication skills, and John Mclean, who provided his electronics expertise.

I would also like to thank the rest of the staff in the Biomedical Engineering Dept. for keeping spirits high, and to EPSRC for funding my PhD.

Thank you to my parents, for their patience and support throughout my years at university, my sister, Karen, who actually bound this thesis, and a big thank you to my girlfriend, Sarah, for her encouragement and continual support. I got there in the end!

Contents

List of Figures

List of Tables

Chapter 1.

A Review on Congenital Heart Disease

1. A Review on Congenital Heart Disease

The Oxford Dictionary of Sports Science and Medicine defines Congenital Heart Disease as 'a structural defect of the heart present at birth'. These malformations of the heart may manifest as a number of pathologies that result in poor heart function due to inappropriate blood flow distribution, flow restriction and structural malformation. These conditions almost always require intervention and are often life threatening if not repaired. (Hoffman et al. 2002)

In 2010, 20% of all infant deaths recorded in the United States of America (USA) were caused by congenital malformations, deformations and chromosomal anomalies. 1,148 of which were due to the infant having major malformations of the heart. (Murphy et al. 2013) In the same year 1,487 infants were born in the United Kingdom (UK) with congenital heart anomalies, and in 2011 47% of infants born with CHD in the UK did not survive to their first birthday. (Townsend N et al. 2013)

Although the number of infant deaths associated with CHD has dropped dramatically from just under 4000, from 1979 to 1983 to around 600 during 2004 – 2008, shown in figure 3 provided by British Heart Foundation. Despite this improvement in outcome, CHD is still the biggest cause of infant mortality. (Townsend N et al. 2013)

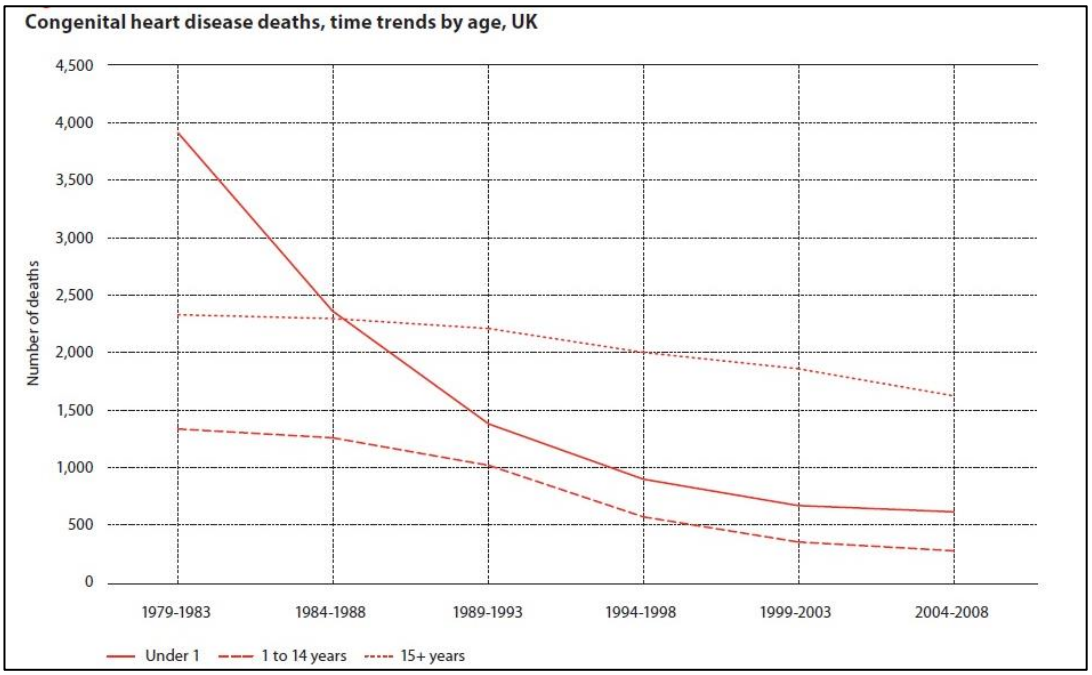

Figure 1 - Table from the British Heart Disease, Children and Young People Statistics 2013

There are a number of different types of CHD, conditions involving developmental anomalies that alter the normal architecture of the heart, vessels and valves.

1.1. Prenatal Heart Development

The heart begins to form 5 weeks into embryological development. The chambers begin to form the atrial and ventricular septa, splitting the heart into its 4 chambers. The respiratory needs of the growing foetus are supplied by the mother through the sinus venous, during this time the blood does not flow to the lungs for oxygenation. The formation of the foramen ovale allows the blood to pass between the right to left atria. A flap of tissue prevents backflow and allows the heart to circulate blood sufficiently.

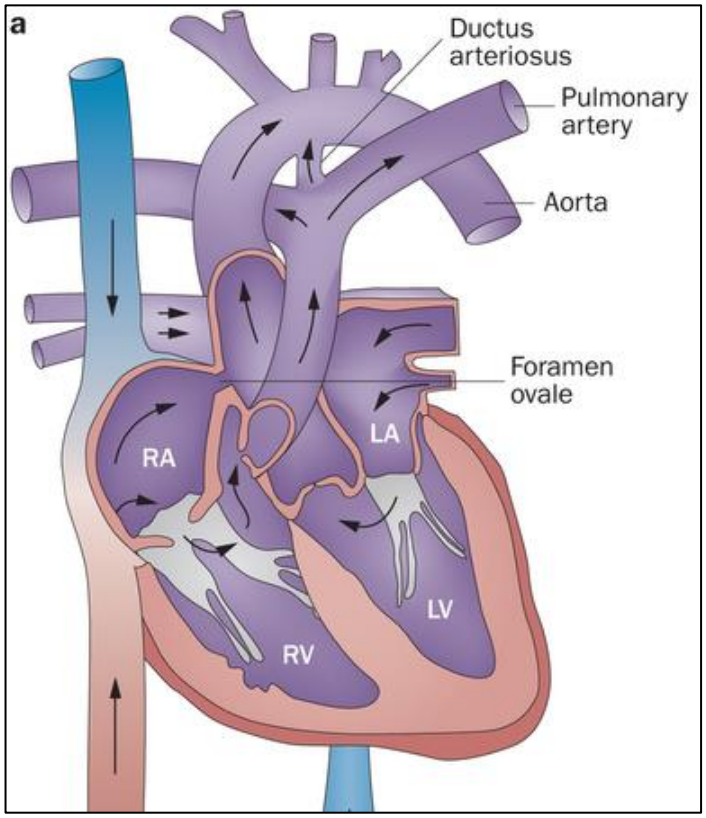

Figure 2 - The Prenatal Heart depicting the Parent Ductus Arteriosus and Foramen Ovale (Hunter et al. 2014)

The ductus arteriosus is a natural shunt connecting the pulmonary artery to the proximal descending aorta. This allows the blood in the right ventricle to bypass the non-functional lungs in the prenatal infant.

1.2. Septal Defects

A septal defect is a congenital condition that involves malformation of the walls separating the different chambers of the heart, which causes the mixing of oxygenated and deoxygenated blood within these chambers. The consequences of septal defects on the functionality of the cardiovascular system and the effect on the infant depend on the severity of the defect. Some defects can be small and remain unnoticed, closing within a week of birth. However patients with sizable defects can show signs of cyanosis, tiredness and shortness of breath, along with audible heart murmurs. (Penny et al. 2011) Septal defects can be atrial or ventricular in nature.

1.2.1. Atrial Septal Defect (ASD)

Atrial septal defects are holes located in the wall separating the atria of the heart which allow the blood to mix throughout the two atrial chambers. This is often accompanied by other forms of congenital malformations. ASDs causes' oxygen-rich blood from the left atrium to mix with oxygen-poor blood in the right atrium (or vice versa) (*Figure 3*) and ultimately reduces the oxygen level of the blood reaching the systemic circulation, such as the brain, organs and tissues.

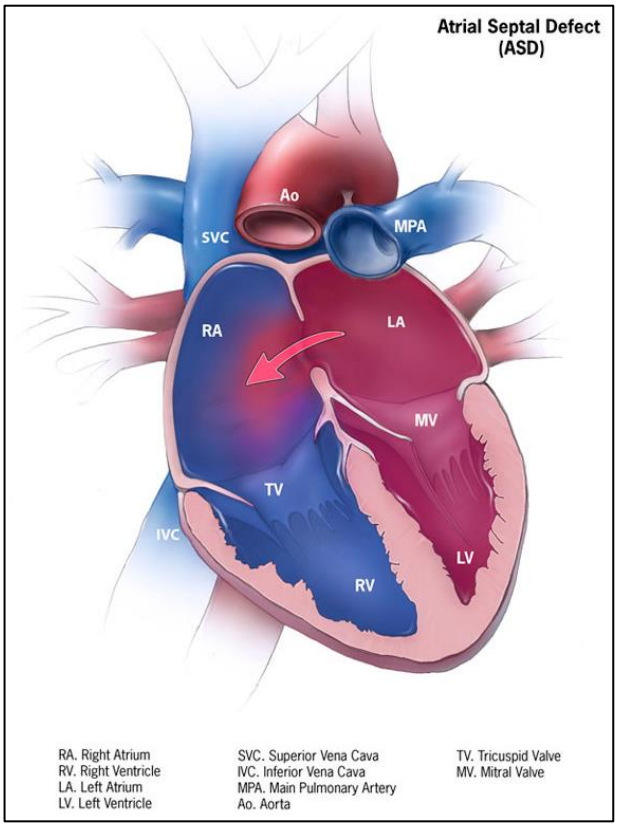

Figure 3 - Atrial Septal Defect (ASD) (Source CC0 1.0 Public Domain Dedication)

1.2.2. Ventricular Septal Defect (VSD)

Similar to ASDs, ventricular ruptures are formed during the foetal development of the heart. Some of these can cause a left ventricular free wall rupture – resulting in catastrophic acute myocardial infarction and often immediate death. However, 15 – 20% are formed in the septal

wall of the ventricles causing the oxygenated and deoxygenated blood to mix inside the heart. (*Figure 4*) This condition is called Ventricular Septal Defect (VSD). (Bull 1986)

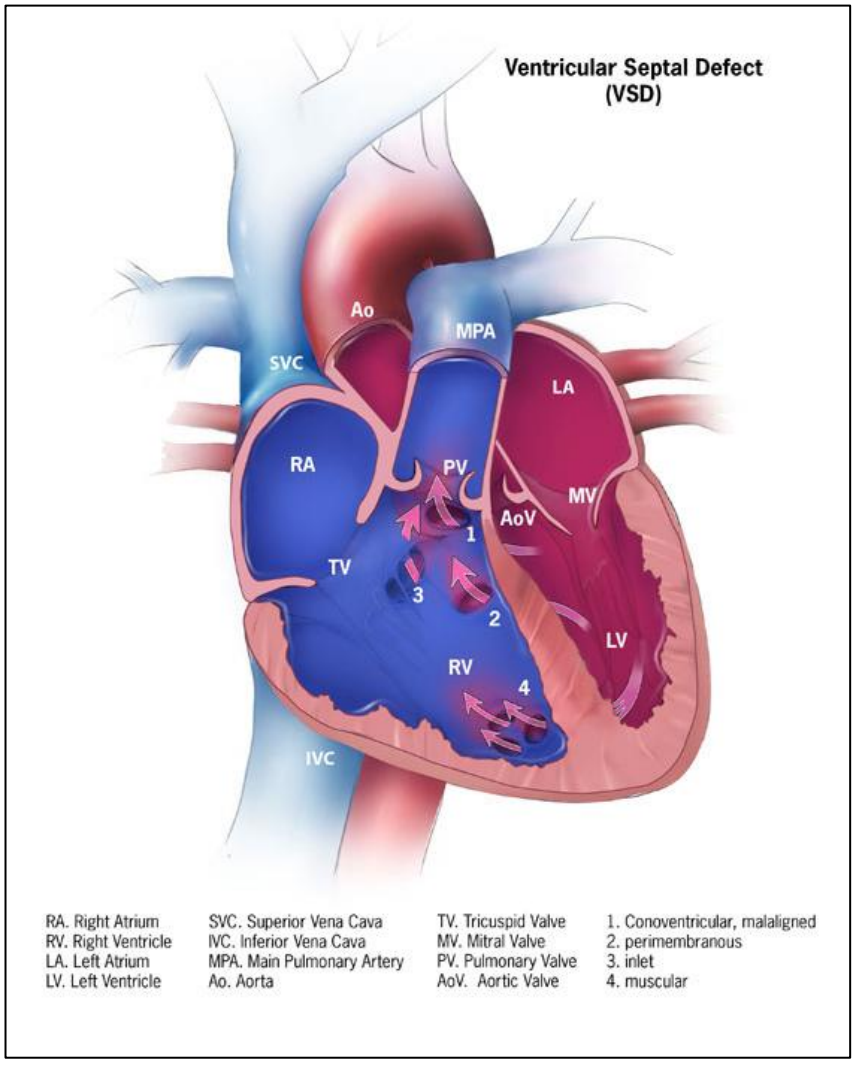

Figure 4 - Ventricular Septal Defect (VSD) (Source CC0 1.0 Public Domain Dedication)

The British Heart Foundation reported in 2008 that – of the 3,377 children born with congenital anomalies of the cardiovascular system, in England and Wales, 423 involved a VSD. It can be found accompanying many other congenital heart anomalies such as tetralogy of fallot (see Chapter 1.6) and truncus arteriosus. (see Chapter 1.8) (Giboney 1983, Townsend N et al. 2013)

1.2.3. Atrioventricular Septal Defect (AVSD)

When maldevelopment of the wall separating the atria and ventricles occurs it is called a complete atrioventricular septal defect (AVSD). Instead of classical separate mitral and tricuspid valves, the valves effectively form a single junction with a common 5 leaflet atrioventricular valve. Due to this valve spanning both sides of the heart, both atrial and ventricular septal defects are present to allow oxygenated and deoxygenated blood to mix freely within all chambers of the heart. (*Figure 5*) A partial atrioventricular septal defect occurs when the defects on the septal walls are further away from the junction, meaning the mitral and tricuspid valves remain separate. (Brawn 2005)

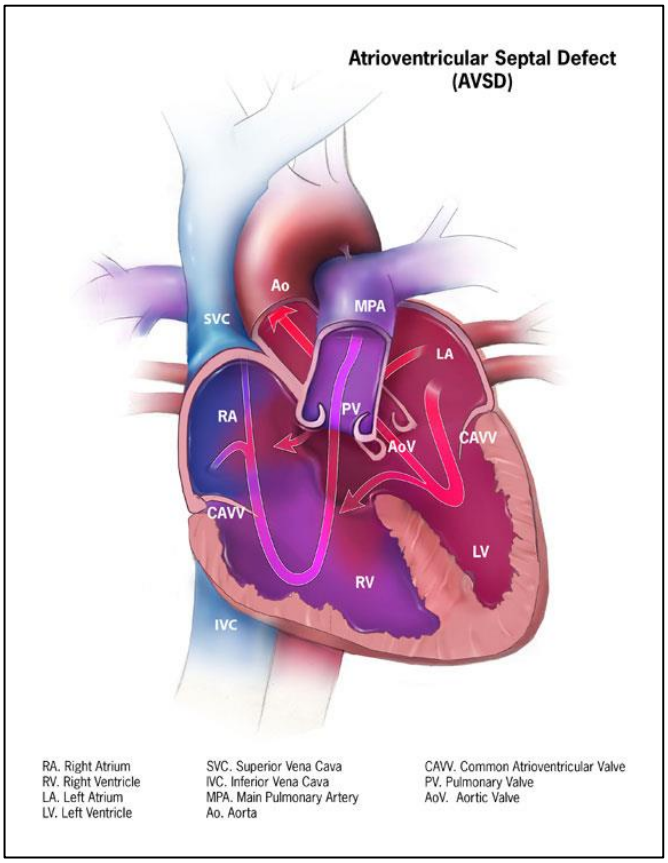

Figure 5 - Atrioventricular Septal Defect (AVSD) (Source CC0 1.0 Public Domain Dedication)

According to a study carried out by the British Isles Network of Congenital Anomaly Registers in 2010, the number of cases involving this malformation has dropped in recent years from 4.8% of 10,000 births in England and wales in 2007 to 3.8% in 2010. (Springett A et al. 2012)

1.3. Coarctation of the Aorta

Coarctation of the aorta describes an unusually narrow section of the aorta. During the normal foetal development of the child, the ductus arteriosus (Chapter1.1.) redirects the blood flow from the pulmonary artery to the proximal descending aorta, and allows the blood to bypass the lungs. (*Figure 2*). Following child birth, this vessel should close within 24 hours allowing normal functionality of the lungs. However in a child with coarctation of the aorta, this produces increased pressure at this narrowing, and therefore less blood is pumped to the body from the heart, which causes increased pressure in the left ventricle and ultimately induces enlargement of the heart.

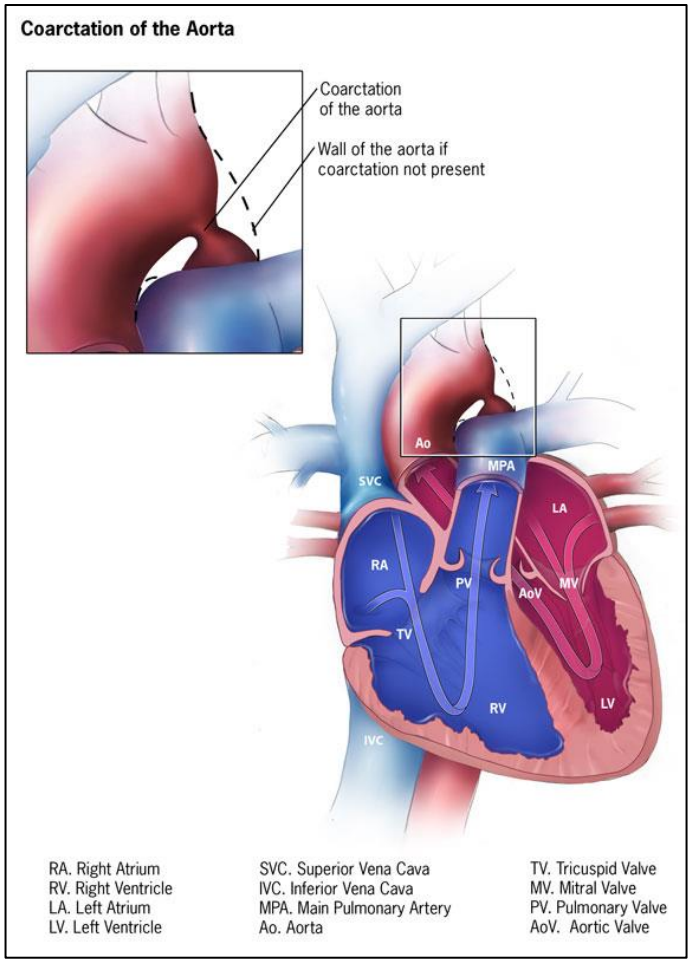

Figure 6 - Coarctation of the Aorta (Source CC0 1.0 Public Domain Dedication)

1.4. Transposition of the Great Arteries (TGA)

When the great arteries of the heart (pulmonary and the aorta) switch position during the early development stages, this is called Transposition of the Great Arteries (TGA). (Schniker 1952) Normally the lungs receive deoxygenated blood from the right side of the heart (via the pulmonary artery) where it is oxygenated and returns to the left side of the heart. This configuration is reversed with TGA, and the aorta arises from the right ventricle and the pulmonary artery arises from the left ventricle. Due to this switch, pulmonary and systemic circuits run in parallel rather than in series. The systemic blood is delivered to the systemic arterial circulation without ever passing through the lungs for oxygenation, and the pulmonary venous blood is delivered back into the pulmonary arterial circuit, never reaching the rest of the body. *(Figure 7)*

Survival of the child depends on whether other forms of congenital heart disease are present. For example, if ventricular or atrial septal defects are present, this would allow some blood to mix within the heart, resulting in small amounts of oxygenated blood being delivered to the rest of the body and deoxygenated blood to reach the lungs. Similarly, if a patient with ductus arteriosus, in which the ductus arteriosus does not completely close after child birth, it would join the pulmonary artery to the aorta and allow for partial mixing of this blood. (Giboney 1983, Duncan et al. 2004, Gournay 2011)

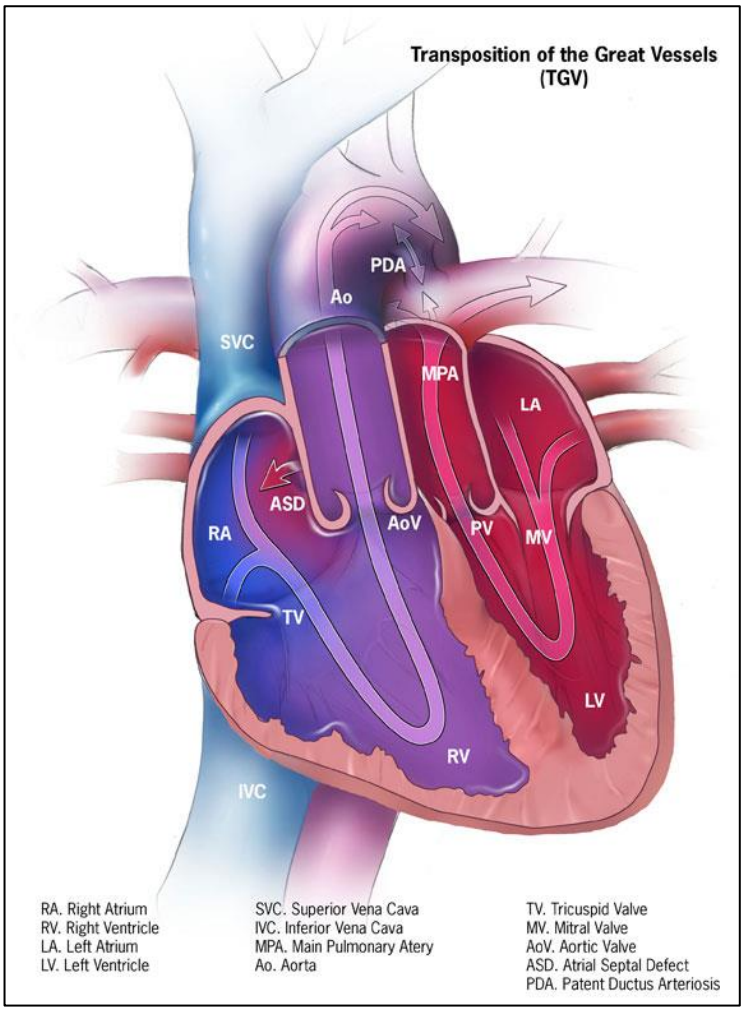

Figure 7 - Transposition of the Great Arteries (TGA) (Source CC0 1.0 Public Domain Dedication)

Transposition of the great arteries accounts for 5-10% of all cardiac malformations. If this condition goes untreated, 90% of children born with it will die within a year. 30% of these deaths occur within the first week. (Rodefeld et al. 2005)

1.5. Tetralogy of Fallot (ToF)

Tetralogy of Fallot (ToF) is a congenital heart condition which is a combination of a four different defects: ventricular septal defect, pulmonary stenosis (which involves the narrowing of both the main pulmonary artery and the pulmonary valve, the enlargement of the right

ventricular wall known as right ventricular hypertrophy), and a mispositioned aortic valve which spans both left and right ventricles. (*Figure 8*) The patient must suffer from at least 3 out of these 4 malformations to be diagnosed with ToF.

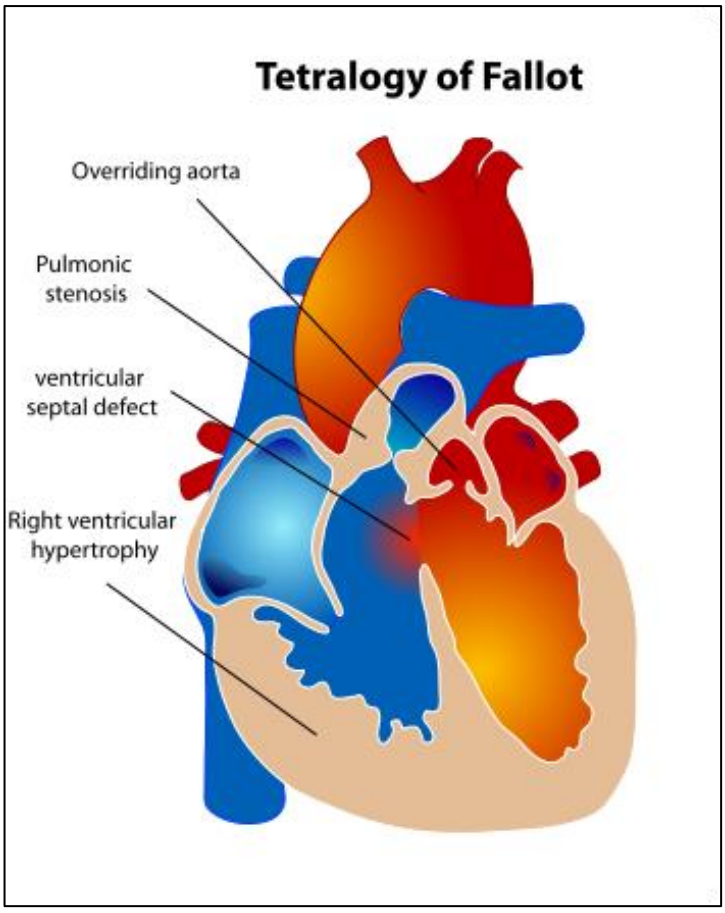

Figure 8 - Tetrallogy of Fallot (ToF) (Source CC0 1.0 Public Domain Dedication)

Surgical repair of tetralogy of Fallot show survival rates of 85% at 20 years. Also, at 5 years post surgery, 93% of patients no longer required revision surgeries. (Jonas 2009)

1.6. Hypoplastic Left Heart Syndrome

Hypostatic left heart syndrome is caused by failure of the left heart to fully develop and thus results in a smaller-than-normal left ventricle, underdeveloped mitral and aortic valves and

quite often, coarctation of the aorta. (*Figure 9*) Aortic atresia (underdevelopment of the aortic valve) and atrial septal defect may also be present with this condition. (Haw 2005)

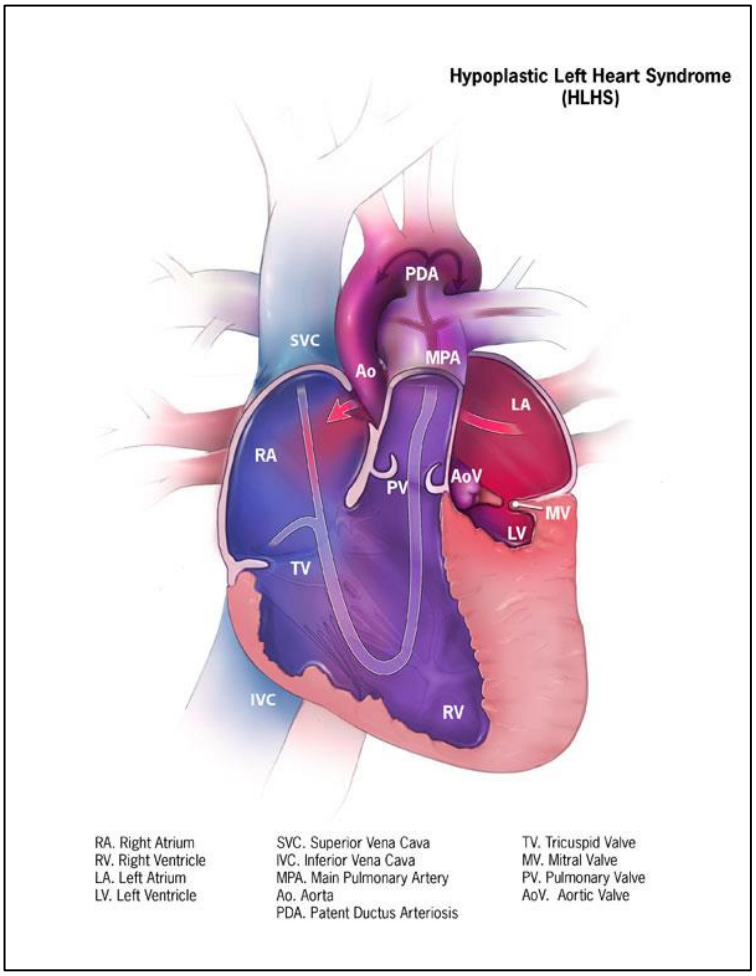

Figure 9 - Hypoplastic Left Heart Syndrome (HLHS) (Source CC0 1.0 Public Domain Dedication)

Hypoplastic left heart syndrome often goes un-noticed for the first 24-48 hours. The heart may remain functional while the ductus arteriosus remains open. However if this closes, it can lead to circulatory failure and death. (Haw 2005)

1.7. Truncus Arteriosus

Truncus Arteriosus is a form of congenital heart disease in which the main pulmonary artery and the aorta fail to separate during foetal development. This results in a large single arterial

trunk that supplies blood to the coronary arteries the pulmonary arteries and the systemic circulation. With truncus arteriosus, there is usually a ventricular sepal defect present at the base of this common vessel. Due to lack of separate pulmonary and aortic valves, an abnormal common valve takes their place. This disease means that the blood is mixed both within the heart itself and in this common blood vessel, sending both oxygenated and deoxygenated blood to both the lungs and the rest of the body. (Delius et al. 2005)

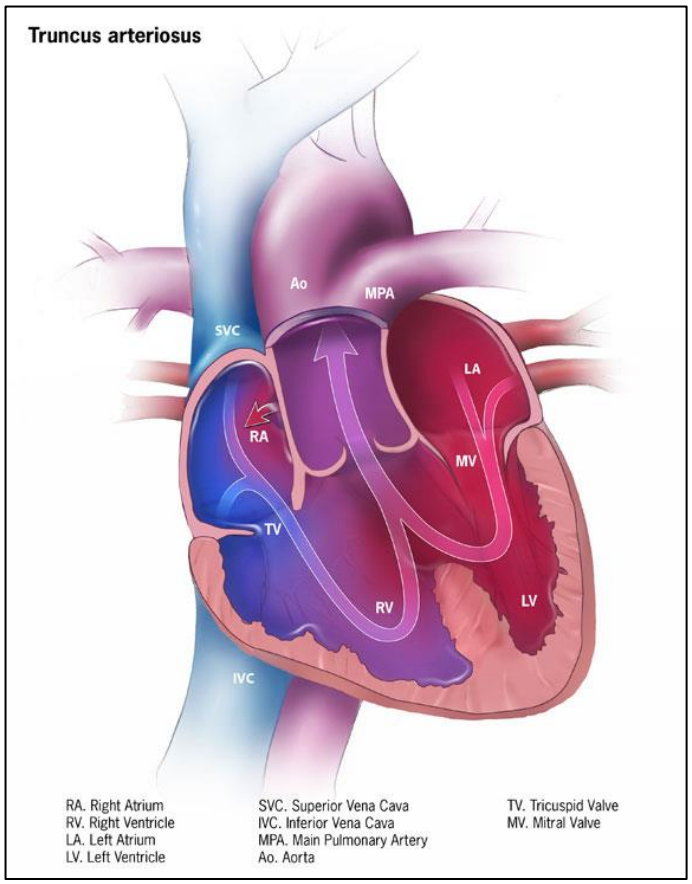

Figure 10 - Truncus Arteriosus (Source CC0 1.0 Public Domain Dedication)

While being one of the rarer forms of congenital heart disease (Jahangiri et al. 2000) it has a 10% survival rate within the first year if left untreated, half of these deaths occur within the first month, usually due to congestive heart failure. (Delius et al. 2005)

1.8. Pulmonary Atresia

Pulmonary atresia is a condition where the pulmonary valve is hypoplastic (under developed). In addition to this, the right hand side of the heart is also hypoplastic, and this has serious effects on the transportation of blood to the lungs. (*Figure 11*) Often patients who suffer from pulmonary atresia also present with ventricular septal defect. When this occurs, it is called PA/VSD (pulmonary atresia with ventricular septal defect).This means that there is mixing of blood within the heart and also congestion of blood on the right side of the heart. This condition consideribly increases the workload of the heart.

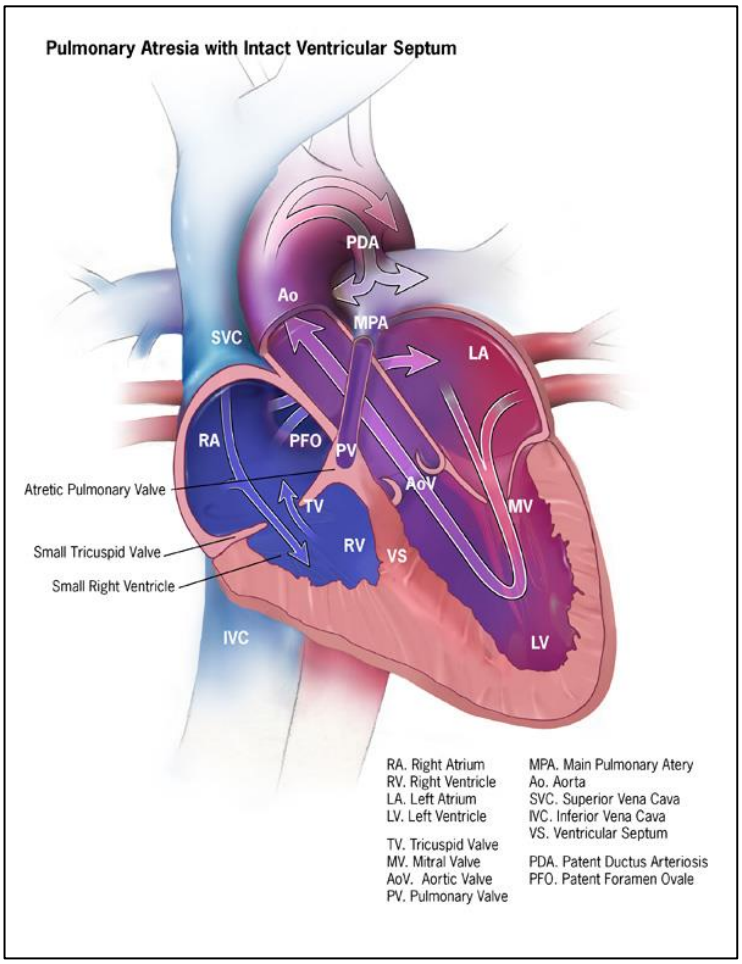

Figure 11 - Pulmonary Atresia (Source CC0 1.0 Public Domain Dedication)

1.9. Pulmonary and Aortic Stenosis

Pulmonary stenosis is defined by the narrowing of the pulmonary artery which thus restricts the flow of deoxygenated blood flow to the lungs. It is recognised when the cross-sectional area is less than $0.5cm^2$. (Monro 2005) (The average for a small healthy infant being around $3.5cm^2$. (Van Meurs-van Woezik et al. 1987)) This narrowing also affects the pulmonary valve and it severely hinders the functionality of the valve. Similarly, aortic stenosis, refers to aortic narrowing and accompanying valve dysfunction. This may cause the muscle in the left side of the heart to thicken to compensate for the pressure increase required to shunt blood throughout the rest of the body.

Chapter 2.

Congenital Heart Disease Repair Procedures Requiring the use of Conduits

2. Congenital Heart Disease Repair Procedures requiring the use of Conduits.

After numerous studies carried out in the 1940's, it was suggested that the pulmonary arterial pressure in animals could provide sufficient force to supply blood to the lungs and to the rest of the body. This led to a surge in experimental and clinical research and the development of a number of surgical procedures to treat patients with varying forms of congenital heart disease. Subsequently biological and synthetic conduits were used in many corrective surgery procedures for congenital heart disease, including conditions where reconstruction of anatomy is required to redirect the blood flow.

2.1. Surgical Procedures

2.1.1. The Fontan Procedure

The Fontan procedure has set the precedence by being one of the most successful procedures for congenital heart defects where only one functional ventricular chamber is present. (de Leval 2005) This means that there is a danger of the lungs being either inadequately – or over-supplied. The single ventricle also has to perform the workload of two ventricles. In 1971, Fontan et al developed this procedure for the palliative repair of tricuspid atresia (Fontan et al. 1971). The main aim of the Fontan procedure is to manipulate the remaining functional ventricle into pumping blood for both the systemic and pulmonary circulations. The procedure is designed to separate the oxygenated and deoxygenated blood by delegating the functional ventricle to deliver the oxygenated blood to the systemic circulation and ensure passive deoxygenated blood delivery to the lungs. This is achieved by connecting the veins returning blood from the body directly into the lung arteries instead of entering the heart, and allowing the single ventricle to eject the oxygenated blood back into the systemic circulation. (de Leval 2005)

Fontan connected the superior vena cava to the right pulmonary artery and the right atrium to the left pulmonary artery. Since then, there have been numerous adaptations and improvements of this procedure, which have significantly reduced mortality rates. However, the main principle of bypassing the right side of the heart and diverting the systemic venous return to the pulmonary circulation remained. Anastomosis-related complications such as thrombosis, valve dysfunction and major reoperation procedures are still a cause for concern. (Mavroudis et al. 2005)

The Fontan procedure is carried out in 2 stages. The Glenn procedure (also known as a Cavopulmonary anastomosis, or a Blalock-Taussing shunt, (See Chapter 2.1.2)), which connects the superior vena cava to the right pulmonary artery. This first stage can also be known as a Hemi-Fontan procedure. The second stage completes the total caviopulmonary connection by redirecting the blood from the inferior vena cava to the right pulmonary artery. This is known as Fontan Completion. (Migliavacca et al. 2003)

The Fontan circulation can be achieved using three different techniques, (*Figure 12*), atriopulmonary connection, lateral tunnel (intracardiac total cavopulmonary (TCPC) connection) and the extracardiac total pulmonary connection (TCPC).

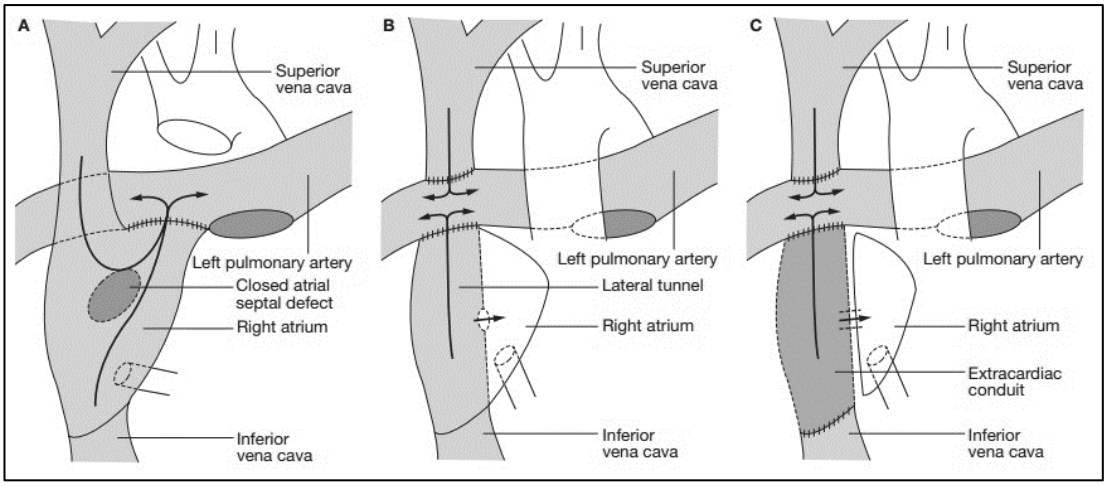

Figure 12 - The Fontan procedure, A) atriopulmonary connection, B) lateral tunnel, C) extracardiac total cavopulmonary connection (de Leval 2005)

Atriopulmonary connection involves isolating the right atrium from the rest of the heart to form a reservoir for the venous return blood. This is achieved by blocking off the atrioventricular valve and the pulmonary trunk. An anastomosis can then create the atrioventricular connection between the right atrium and the pulmonary artery. (Podzolkov et al. 1997)

Both the lateral tunnel and extracardiac total cavopulmonary connection (TCPC) procedures use an artificial conduit to redirect the blood from the inferior vena cava return to the pulmonary arteries. The difference lies with how they are implemented. The lateral tunnel passes the conduit through the right atrium itself, whereas the extracardiac TCPC places an external conduit on the outside of the heart to redirect the blood. (de Leval 2005)

The implantation of these conduits can however, increase the patients' blood pressure. To avoid this, the conduit can be fenestrated (the creation of a number of miniature holes) to relieve some of this pressure. This can cause cyanosis due to the lack of oxygenated blood and should eventually be sealed. (de Leval 2005)

The European Association for Cardio-Thoracic Surgery Congenital Database (EACTS), outlines the success rates for the various Fontan procedures. (*Table 1*)

Fontain Procedure used	Total No. of Procedures	No. of Deaths in First 30 Days	30 Mortality Rate
External TCPC (Non-Fenestrated)	415	15	4.36%
External TCPC (Fenestrated)	268	8	3.02%
Lateral Tunnel (Non-Fenestrated)	50	3	6%
Lateral Tunnel (Fenestrated)	90	5	5.56%

Table 1 - EACTS 2014 Data for Fontan Procedure

These data conclude that the external total cavopulmonary connection has the advantage over the lateral tunnel method, producing a lower mortality in the first 30 days, it also suggests that

fenestrated conduits reduce this percentage further in both procedures, however due to the difference in the total number of procedures this remains unclear.

2.1.2. Blalock-Taussing Shunt

Initially the Blalock-Taussing shunt, first used in 1944, was used in the repair of tetralogy of Fallot, where it utilised the patient's own subclavian artery to shunt blood from the pulmonary artery to the ascending aorta. The objective is to redirect the blood flow to the lungs.

The benefit of using the classic Blalock-Taussing shunt procedure is that it does not require a prosthetic conduit to redirect the blood and therefore allows the possibility of growth as the child grows. However, the procedures can be long and complex, and a high risk of post-operative upper arm ischaemia is present due to the redirected use of the subclavian artery which supplies blood to this region. (Ullom et al. 1987, Cameron et al. 2004, Yuan et al. 2009)

This method holds unpredictable results in infants due to the very small arterial anastomosis and the possibility of uncontrollable dilatation of the subclavian artery, which can lead to over circulation. As such, amodified Blalock-Taussing shunt was introduced, which replaced the joint between the subclavian artery and the pulmonary artery with a prosthetic anastomosis. (GoreTex) (Ullom et al. 1987). This modification simplified the procedure and did not sacrifice the subclavian artery. Also, the use of a prosthetic, ensured that there was no chance of dilatation and subsequent over circulation. However, patients were required to undergo revision surgeries to compensate for the increasing demand for blood flow associated with growth. (Cameron et al. 2004)

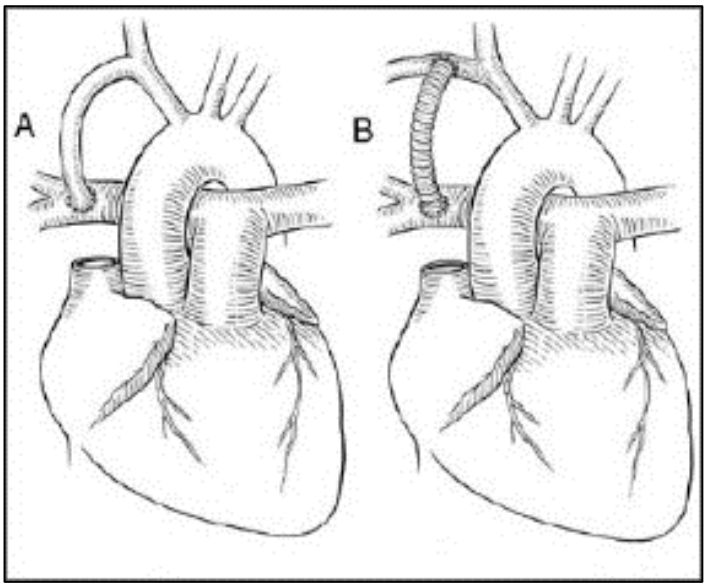

Figure 13 – A) Classic Blalock-Taussing Shunt, B) Modified Blalock-Taussing Shunt (Source: CC BY-SA 3.0, Author: Pezard)

This procedure is performed on patients experiencing cyanosis on its own or as part of a larger ongoing set of surgeries culminating in total correction, for example alongside the Norwood procedure (see Chapter 2.1.5) or as the initial stage of the Fontan circulation. (Cameron et al. 2004, Yuan et al. 2009)

The classic Blalock-Taussing shunt procedure involves thoracotomy which introduced complications regarding further cardiovascular reconstructions. The modified version eliminated this complication by being performed via a medial sternotomy, bringing with it advantages such as having clearer access to the pulmonary and systemic arteries. (Cameron et al. 2004)

EACTS reported a 30 day mortality rate for the modified Blalock –Taussing Shunt of 8.28% in 2014, which is actually an increase of 0.19% over the preceding 3 years. (EACTS 2014)

2.1.3. Central Shunt

A central shunt can connect the pulmonary artery to the ascending aorta. If the Blalock-Taussing shunt has failed or is simply not providing enough blood flow, a central shunt can resolve this. The patients' mammary artery can be used to achieve this or a prosthetic vessel is often favoured for smaller infants where the subclavian artery would be inadequate in the Blalock-Taussing procedure. (Yuan et al. 2009) Another advantage of the central shunt over the classic Blalock-Taussing procedure is that the subclavian artery remains untouched, and thus eliminates the risk of ischaemia. However, if a prosthetic conduit is used for this connection, it will also require further surgical replacement when the surrounding anatomy grows. (Yuan et al. 2009) The EACTS congenital database reports a 30 day mortality rate for the central shunt procedure of 12.35% in 2014. (EACTS 2014)

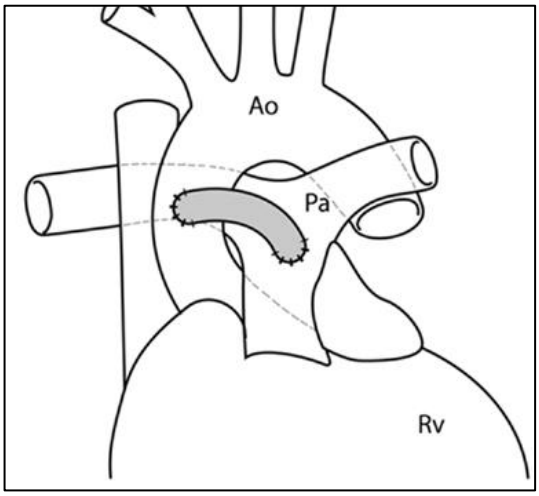

Figure 14 - The Central Shunt (Biglino et al. 2013)

2.1.4. Sano shunt

Also known as the 'Right Ventricle to Pulmonary Artery Conduit (RV-PA)', the Sano shunt was developed in 2003. (Sano et al. 2003) This involves connecting the right ventricle to the pulmonary artery, and is used in patients suffering from hypoplastic left heart syndrome. It

utilises the pumping action of the right ventricle to direct blood into the vessels of the lungs for oxygenation and therefore connects the pulmonary and systemic circulations. Typically, an artificial conduit is used to redirect the blood flow in this procedure, and a 30 day mortality rate of 5.98% was reported by EACTS in 2014.

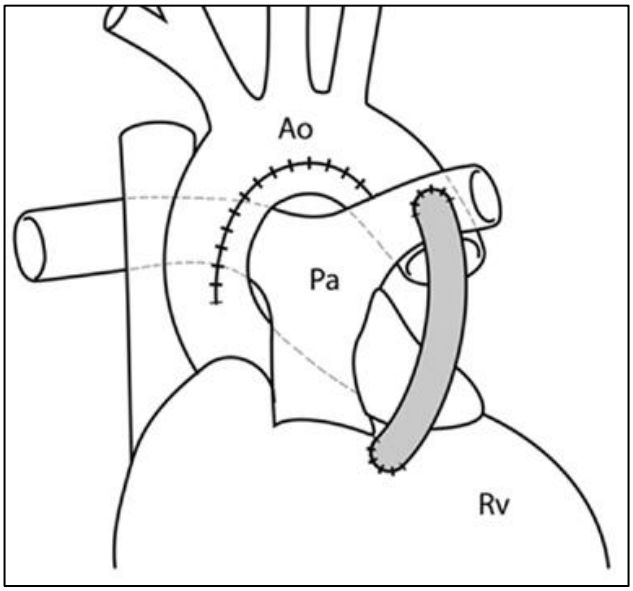

Figure 15- Sano shunt (RV-PA Shunt) (Biglino et al. 2013)

2.1.5. Norwood Procedure

The Norwood procedure is used to treat hypoplastic left heart syndrome, but can also be used to treat other congenital heart defects that result in the failure of one of the ventricles. Developed in 1981, this procedure aims to ensure adequate blood flow to the systemic circulation using a single ventricle. To achieve this, circulation to the lungs is artificially disrupted and the lungs are then supplied using an alternative route. It is a three stage procedure, wherein the first stage is a palliative procedure, performed in the early days of life as soon as the condition is recognised.

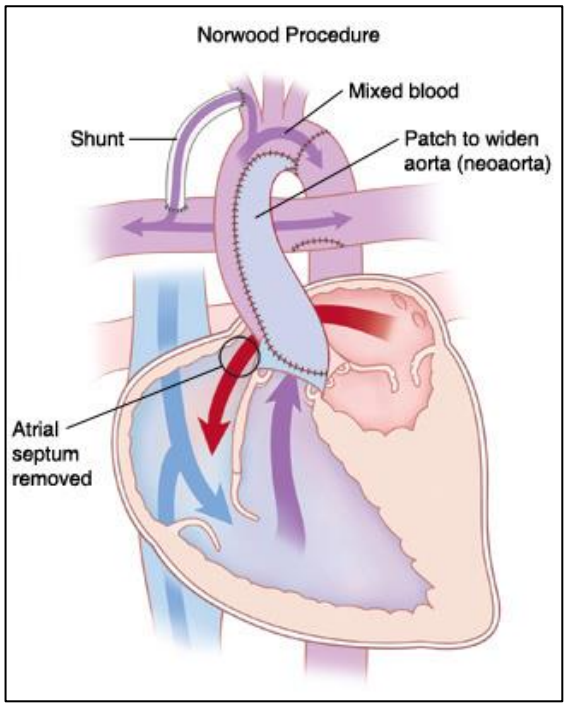

Figure 16 - Stage I Norwood Procedure (Chicago 2014)

This involves detaching the pulmonary artery from the heart just above the pulmonary valve, and the aorta is reconstructed using a homograph to incorporate the pulmonary valve, this feeds the blood from the right ventricle to the aorta. The disconnected pulmonary artery is tied off at the base and a shunt is then used to direct blood from the superior vena cava to the pulmonary artery for oxygenation. This can be done by using any of the Blalock-Taussing, central, or Sano shunt procedures.

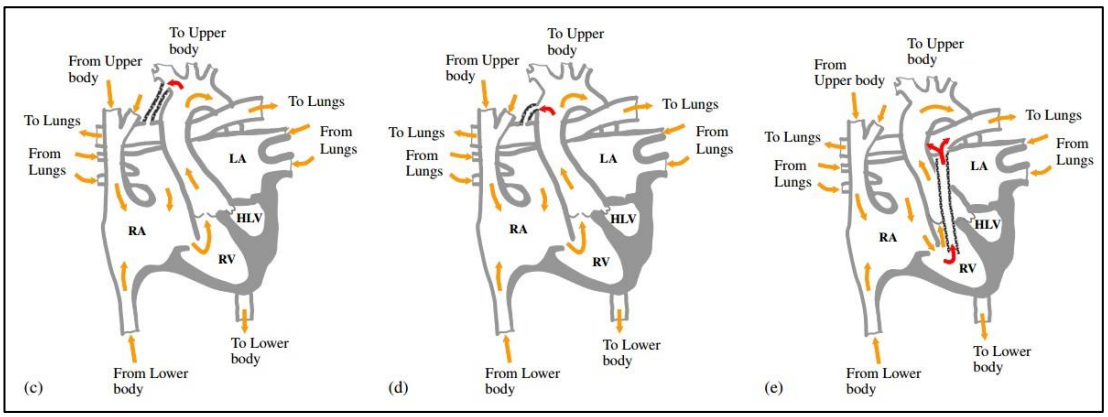

Figure 17 - Norwood Stage I with (a) Blalock-Taussing Shunt, (b) Central Shunt, (c) Sano Shunt

Stages II and III of the Norwood Procedure are carried out at around years 2 and 4, respectively. Stage II is used to match haemodynamic demand as the child grows, using an anastomosis between the superior vena cava and the pulmonary artery. Stage III involves the final correction with a lateral tunnel or extracardiac connection.

The stage I Norwood procedure has he second highest 30 day mortality rate of cardiac surgeries of 34.66%, second to only the ECMO (Extracorporeal Membrane Oxygenation) procedure which stands at 62.07%. The risk of mortality increases as the child undergoes the further 2 stages required for total completion. (EACTS 2014)

2.1.6. Hybrid Procedure

This is a palliative procedure often used in hypoplastic left heart syndrome. However, it has also been used to treat patients with tricuspid atresia and other forms of congenital heart disease with ventricular dysfunction. It involves using a self-expanding catheter nitinol stent to keep the ductus arteriosus open during the early days of life, to allow for the blood to flow through this channel, similar to the Blalock-Tausing shunt. It ultimately enables the blood to be pumped from the systemic to pulmonic circulation for oxygenation. Combined with the stent, an internal pulmonary atrial band is used to prevent over circulation, and a balloon atrial septostomy ensures adequate blood flow. This Hybrid procedure has a hospital mortality rate of 21.5%, which is significantly lower than the Stage I Norwood procedure. Additionally, since it does not require open heart surgery it is, in certain circumstances, an ideal alternative. This procedure can reduce the amount of further invasive surgeries needed for full corrective surgery. (de Leval 2005)

2.1.7. Ross Procedure

The Ross procedure describes a procedure to correct the anatomy where the patients' diseased aortic valve is replaced by their own pulmonary valve (the autograft), and the pulmonary valve is replaced by a valved homograft. This homograft was thought to have the potential for growth but transplant rejection can cause tissue calcification and thus inhibit growth.

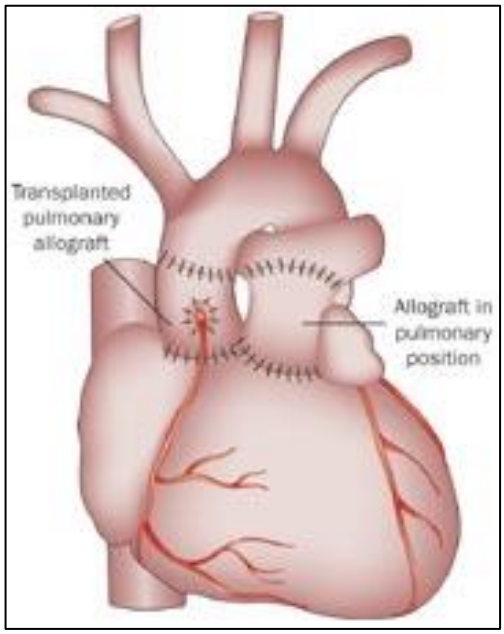

Figure 18 - The Ross Procedure (King 2009)

This procedure holds many benefits for the patient over a prosthetic aortic valve. The longevity of the pulmonary autograft outlives its synthetic counterparts that fail after a few years, and therefore reduces the mortality associated with revision surgeries. The use of autograft and homograft in this procedure, allows for the possibility of growth as long as calcification does not occur. Another benefit is that the patient does not need any form of anticoagulation drugs, which are used to stop thrombosis and blood clots forming around synthetic grafts. The Ross procedure has a 30 day mortality rate of 1.19%. (EACTS 2014)

2.1.8. Rastelli Procedure

The Rastelli Procedure was developed in 1969 and has been used to repair congenital heart conditions such as transposition of the great arteries and double outlet right ventricle. It can also be used in the first stage Norwood procedure, and to correct aortic atresia with ventricular septal defect. (Rastelli et al. 1969)

The procedure involves using a grafted patch (biological or synthetic) to redirect blood through the ventricular septal defect into the aorta and into the systemic circulation. A conduit is then placed from the right ventricle to the pulmonary artery to transport blood to the lungs for oxygenation. (Delius et al. 1995)

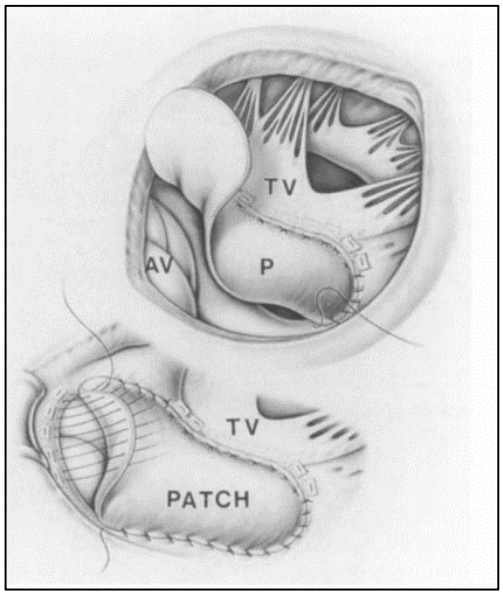

Figure 19 - VSD to aortic valve patch placement (Delius et al. 1995)

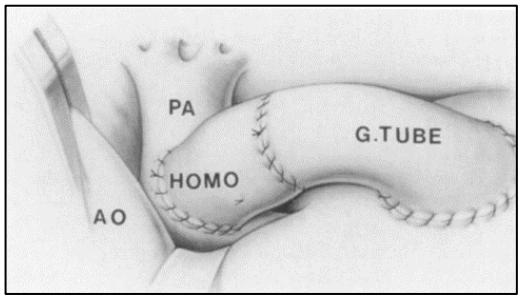

Figure 20 - RV to PV Homograft and GORE-Tex conduit (Delius et al. 1995)

According to the EACTS Congenital Database, the Rastelli procedure on its own holds a 30 day mortality rate of 11.22%. This procedure used with corrected TGA repair and Atrial Switch procedures reduces the 30 day mortality to 9.09%. (EACTS 2014)

2.1.9. Paediatric Coronary Defects

Coronary Artery disease can be either congenital (defects formed during the foetal development of the coronary arteries) or acquired as seen in Kawasaki disease. Coronary anomalies are rare but still require complex surgical repair. Depending on the type of coronary artery disease, bypass can be performed using a graft or anastomosis to reroute anatomy or reconnect vessels. (Mavroudis et al. 2004)

Chapter 3.

Vascular Prosthesis Employed in the repair of Congenital Heart Disease

3. Vascular Prosthesis Employed in the repair of Congenital Heart Disease

3.1. Vascular Prostheses

Implantable vascular conduits are used for the correction of many forms of congenital heart disease. They are used to replace or bypass existing damaged vessels or aid in the reconstruction of malformed anatomy. During the First World War, Alexis Carrel started work on developing the first artificial blood vessels, replacing natural blood vessels with glass and aluminium conduits. He later found that synthetic fabrics were most suited to this cause. (Advameg 2016) Replacement conduits can either be made from biological or synthetic materials, which have a myriad of advantages and disadvantages. As such, the 'Ideal' vascular prosthesis is yet to be created. One of the main issues surrounding vascular prostheses for use with congenital heart defects is their need for replacement over time, as they inevitably become stenotic as the child outgrows them.

3.1.1. Biological Materials

Biological grafts which are often used for vascular prostheses are split into 3 main categories, autografts, allografts and heterografts. autografts use a patient's own vein instead of the required conduit. Allografts use a donor's vein (usually deceased), and heterografts are a donor vein from another species (eg. Bovine). Autografts hold immunological benefits for the patient as the vein is less likely to be rejected. Both allograft and heterograft patients require immunosuppressant drugs in order for the donor vein not to be rejected. (How 1992)

3.1.1.1. Autografts

In 1944, Blalock used an autograft during the repair of tetrallogy of Fallot, joining the subclavian artery to the left pulmonary artery. (How 1992) The patient's great saphenous vein is often used as the replacement cardiac conduit as an autogenous graft in coronary bypass

surgery for treatment of Kawasaki disease due to its ideal size. (Mavroudis et al. 2004) However the internal mammary artery and iliac vein, along with the hypogastric artery may also be used as vascular grafts. The benefit of using the patient's own blood vessel is that there are no immunogenicity problems which would require the patient to have a constant supply of immunosuppressant drugs to avoid the risk of transplant rejection. The autograft also has the potential to grow with the child which reduces the need for any revision surgeries, and also does not require any anticoagulation drugs which may be required for synthetic conduits containing metal stents or integrated valves. (Elkins et al. 1994) Using these grafts is beneficial but can become problematic as the child grows and develop donor site morbidity.

3.1.1.2. Allografts

Allografts (also known as homografts), use a donor vessel for the vascular prosthesis. Cardiovascular allografts have been used clinically since the 1940's, and valvular allografts were first used by Gordon Murray in 1956 to replace the descending aorta. (Hopkins et al. 1991) Allografts originate from human donors, usually cadaveric tissue chemically preserved at low temperatures. Their preservation techniques are known to cause accelerated structural deterioration rates in infants and young children and thus require frequent replacement due to calcification and immune system rejection if the patient is not properly medicated. (Elkins et al. 1994) It was originally thought that chemical preservation of allografts ensured that immunosuppressant drugs were not necessary, but immune responses were subsequently reported. (Hopkins et al. 1991)

Advantages to allografts mean that the patient does not need to sacrifice a vein in their own body for prosthetic use. Like autografts they do not require anticoagulation drugs. (Elkins et al. 1994) Sterilisation is also an important issue, which has a beneficial effect on both disease transmission and graft longevity. Both gamma and ethyl-oxide sterilisation processes are effective for non-biological substances but can decrease the mechanical strength of the homograft. (Vang 2006)

3.1.1.3. Heterografts

In 1963, Norman Rosenberg developed vascular prosthesis from bovine sources. Otherwise known as a xenograft, they are typically harvested from bovine or porcine, but by definition it is a graft taken from a different species to that of the recipient. These prostheses share many disadvantages with allografts in which they can induce immunological and calcification issues. (Teebken et al. 2002) Calcification was addressed by Johnson et al in 1990, and they experimented with pre-treating the graft with an anti-calcification agent (ethanehydroxy diphosphonate). This proved successful in rats and sheep where the treated prostheses lasted significantly longer than the untreated alternative. (Johnston et al. 1990)

Immunological and biological barriers are still very much an issue with the use of xenografts. Hormoral rejection can occur either immediate (occurring within minutes or hours) or delayed which can occur weeks or months after transplantation. Another major issue is the risk of porcine endogenous retrovirus (PERV) which has been found to infect mice transplanted with pig islets. A study has also been carried out on human cells in vitro with positive signs of infection however no infection has been detected in humans transplanted with porcine xenografts in short term studies. No long term studies have been carried out on patients under immunosuppression so it is still unclear if this issue has potential to arise therefore it remains a cause for concern. (Le Bas-Bernardet et al. 2008)

Studies have been carried out involving gene transfer and inactivation techniques to produce genetically modified xenografts to counter these issues. These techniques involve reducing the expression of αGal (a gene expressed in all mammals except humans) in the donor tissue which can lead to endothelial damage, haemorrhage, fibrin distribution and microvascular thrombosis, Adapting the molecules for controlling coagulation and immune response, and modifying the RNA sequence to prevent PERV expression. (Le Bas-Bernardet et al. 2008)

3.2. Synthetic Materials

The first reported use of synthetic materials used for vascular grafts was in Columbia University, 1952, when Voohees et al used a Vinyon-N cloth tube to replace a diseased artery in a dog. (Thompson 2001) This material proved unsatisfactory in clinical applications initiating further investigation into possibilities for new synthetic vascular prosthetic materials. (Dennis 1987)

Nylon vascular prostheses were developed in 1955 by Stirling Edwards. Issues arose with these prostheses including collapse and kinking of the conduit due to positioning and anatomical pressures. This led Edwards, along with his associate J.S. Tapp, to design a crimping technique that would make the conduit more structurally sound and prevent any blockage. However, the nylon material did not cope well with this technique. (Thompson 2001)

Expanded polytetraflouroethyline (ePTFE), better known as Teflon, was considered a viable material due to its controllable node-fibril manufacturing process. This allowed the prosthesis to have a porous structure that would encourage tissue ingrowth. Many other vascular grafts are manufactured with a valour coating on the internal and external surfaces to promote further tissue integration. (Monahan et al. 2007) Manufacturing with external supporting rings gave the necessary structural support to prevent bending/kinking. (Tomizawa 2003) This material can be quite thrombogenic but can be carbon coated to decrease the chance of thrombosis. (Ballermann 1998)

W.L. Gore & Associates, Inc. developed their own form of ePTFE in the form of GORE-Tex. Its first reported use was as a lower-extremity bypass conduit in 1976, and continues to be one of the most popular materials for lower extremity and arterio-venous bypass grafting. (Kapadia et al. 2008)

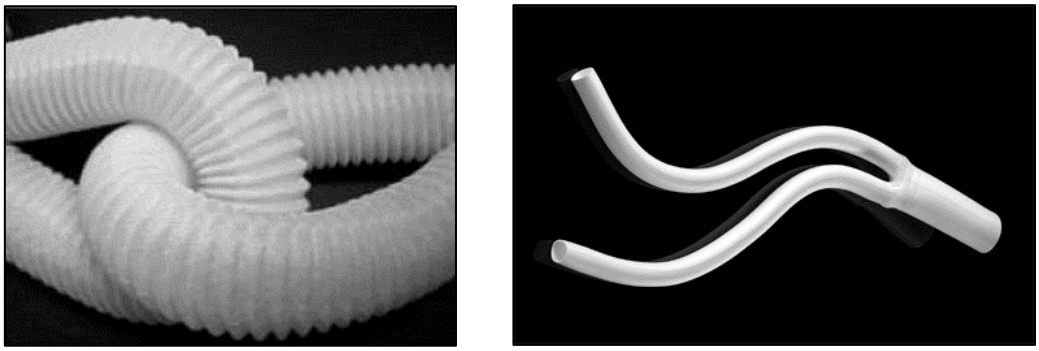

Figure 21 - Teflon and GORE-Tex Vascular grafts (Khlif et al. 2011)

During 1954, Michael E. DeBakey and colleagues collaborated with a textile engineer named Professor Thomas Edman to create the first polyethylene terephthalate (PET) graft, using a custom built knitting machine. This came to be known as Dacron, and was manufactured in a number of different specifications based on size and porosity. Dacron proved a popular choice with vascular grafts, retaining the majority of its tensile strength over time and only losing up to 20% during tissue integration during surgery. (Dennis 1987)

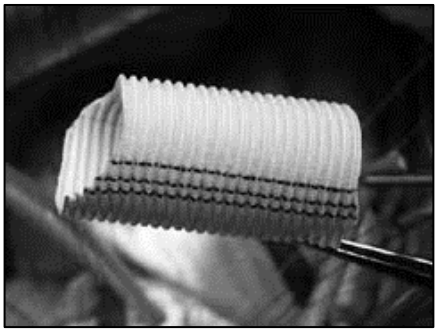

Figure 22 - Dacron Vascular graft (Svensson 2012)

The most common materials used in prosthetic vascular grafts are that of Dacron (PET) and ePTFE. Early *in vitro* studies suggested that dacron grafts were responsible for higher risk of infection and thrombosis, compared to ePTFE. This was only evident in the preclinical experiment, and there was no clear difference between the materials during clinical studies. (Yasim et al. 2006) These preferred materials both have the strength to withstand the pressure loads and mechanical forces *in vivo*, and only a small number of patients experience problems with fibre breakdown and rupture of these conduits. These prosthetics are less robust when

used to replace smaller diameter vessels. Their ridged walls cannot expand due to internal pressures in comparison to their native vessels, and along with the possibility of blockages caused by thrombosis make them only suitable for replacement of larger vessels. (How 1992, Ballermann 1998, Monahan et al. 2007) Thrombosis within the vessel is caused by a lack of endothelial cells lining the graft. The endothelium in a healthy blood vessel provides anticoagulation functions, and a lack of this layer causes a build-up of myofibroblasts that lead to stenosis and ultimately thrombosis. This may be moderated by applying a layer of endothelial cells to the inside of the graft before implantation. (Ballermann 1998)

Generally these configurations are suitable for vascular prosthesis in paediatric surgery that requires shunts with a diameter of around 5mm (such as the RV-PA shunt procedure discussed in section 2.1.4 where a PTFE conduit is used to connect the right ventricle to the pulmonary artery.)

3.3. Anastomosis

In the context of heart surgery this maybe the site at which a native vessel is connected to another, ie. coronary artery bypass graft of where an artificial vessel is used to join two structures creating a shunt. For example RV-PA shunt. In the latter case, there are two anastomosis sites, one at either end of the shunt. Regarding the cardiovascular system, it is the point where a heart vessel splits or branches of from another. An example of the velocity flow rates through an anastomosis is shown in figure 23.

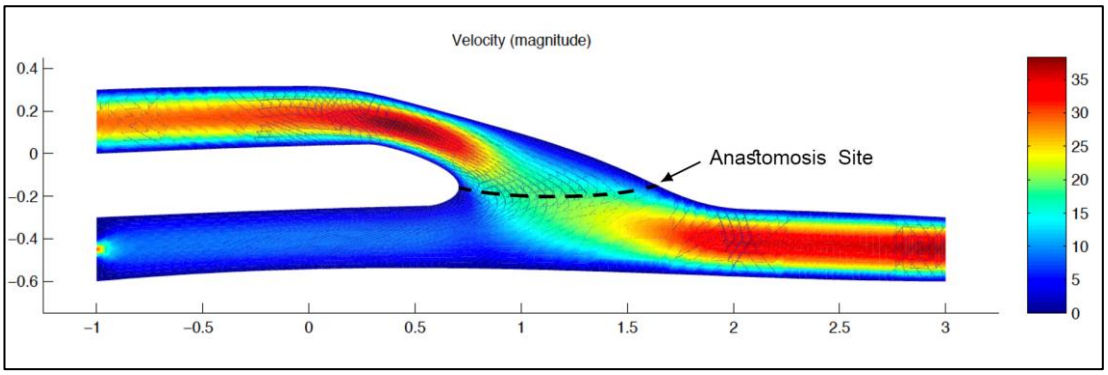

Figure 23 - Velocity Profile simulation of blood flow through an anastomosis (Quarteroni 2010)

This point of intersection between the vessels is an area of concern when it comes to the implantation of conduits, whether they are replacing an entire vessel, or just a small section. The body's natural reaction towards any kind of cut or rupture is to self-repair, and this is also evident in the anastomosis site. Once the vessel is cut and the conduit is sutured in place, scar tissue will form at the anastomosis site. This can cause haemodynamic problems within the vessel and may result in localised thrombosis and clotting – known as neointimal anastomotic hyperplasia (NIH). (Monahan et al. 2007) The extent of NIH increases with further review procedures. NIH usually occurs at the distal end of the conduit depending on the direction of flow and causes a narrowing of the conduit. This problem is predominantly found when using synthetic conduits and its narrowing along the anastomosis site is a major cause for graft failure. (Cole et al. 2002)

The difference in the mechanical properties between the vessel and the prosthesis can also cause a build-up of scar tissue. Due to the vessels natural expansion it can cause stress at the anastomosis causing excess scarring to occur, therefore it is crucial to use a prosthetic of the correct size to minimize scar tissue formation. (Cole et al. 2002)

Chapter 4.

The Growth Compensation Challenge

4. The Growth Compensation Challenge

4.1. The Problem

Congenital heart disease is one of the major causes of infant mortality in the United Kingdom and the United States. The repair procedures for these lesions are often fairly complex many involving the use of biological or synthetic conduits to replace existing anatomy or redirect blood. Though these provide a successful short-term solution, they are often subject to failure due to thrombosis and pannus formation causing intimal hyperplasia in the long term, requiring replacement or corrective surgeries. (Salacinski et al. 2001) A new technology is needed to reduce this need for corrective surgeries.

Repair of many forms of congenital heart disease requires the use of implantable conduits to reconstruct cardiovascular anatomy. Procedures used to correct hypoplasic left heart syndrome, for example, involve the use of 'End to Side' conduits through use of Blalock-Tausing shunt, central shunt, Sano shunt or a combination of the aforementioned to ensure adequate blood flow is provided to both the pulmonary and systemic circulations with the use of only one ventricle. 'End to Side' conduits are the most commonly used clinically. (Kapadia et al. 2008) Each of these procedures are described in chapter 2.

Though these conduits present an adequate short term solution, the influence of the anastomosis sites on graft patency can be significant and lead to graft failure even if the anastomosis is in itself adequate. For example, inclusive anastomosis can lead to turbulence further downstream.

Vascular grafts are currently not ideal. There are many problems associated with their use, in particular, the current inability for graft technology and their associated anastomoses to respond to growth, poses a considerable technical and clinical challenge. The result of this is the need to replace these devices as the patient grows. This is a challenge particular to paediatric surgery where the added complexities of somatic growth is present. The situation in

adult surgeries is less complicated as patients will receive their surgeries beyond the normal growth cycle.

To date, the approach to compensating for growth in children undergoing complex cardiac surgeries has been to be responsive to patient size - graft mismatch. This results often in multiple revision open heart surgery procedures in this patient cohort in during the period of infancy to adolescence. Growth continues beyond this and a legacy issue of graft implantation at adolescence, particularly in RV-PA shunt patients is an enlarged right ventricle and development of right heart failure. Although the aetiology of this condition is multifactorial, the mismatch between proportions of implanted grafts and the growth to adulthood and the associated cardiovascular development, plays a role in this legacy condition.

There are several other mechanisms of graft failure that are both related and unrelated to somatic growth but contribute to the problem, these include the body's natural reaction to trauma during operative procedures results in the build-up of fibrous tissue around the site of anastomosis. This build-up of scar tissue, thrombosis/pannus formation, calcification and lack of distendability, hinder the practicality of synthetic vascular grafts, requiring them to be replaced as the graft grows slower than the adjacent neighbouring anatomy.

4.1.1. Thrombosis and Pannus Formation

Although thrombosis is a natural occurrence, it can be more problematic when it affects synthetic vascular grafts. The narrowing of the graft due to either thrombosis or pannus tissue formation is determined using Doppler imagery to visualise the velocities at the inlet and outlet anastomosis. Stenosis occurs when the peak systolic velocity is more than double the normal inlet velocity. (Kapadia et al. 2008)

Thrombosis is common at the connecting site between the local biological tissues and the vascular graft (biological or synthetic), and results from the formation of platelets as a reaction

to tissue healing around an anastomosis site. These platelet deposits may protrude inside the vessel and disrupt the blood flow.

A study carried out by Tumaiuolo et al (2014), showed how platelet deposition inside the blood vessel affects the velocity of blood flow. Figure 24 shows that platelet numbers have a significant effect on the blood flow through the vessel. It can be seen that in extreme cases *(Figure 24c)* that the narrowed lumen creates an area of high velocity as the blood flows through the smaller diameter. The secondary effect is low velocity blood flow at the base of the thrombosis formation (note the dark blue area at the base of the platelet build up in Figure 24). This low moving or static blood may clot and cause further obstruction of the vessel or potentially break off and cause a blockage (embolus) elsewhere in the body (e.g. embolic stroke). (Tomaiuolo et al. 2014) Thrombosis can occur in bioprosthetic grafts but is more common in synthetic grafts. (Roudaut et al. 2007)

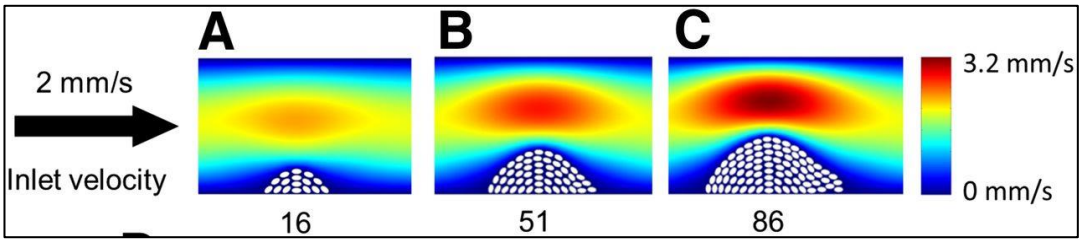

Figure 24 - Velocity profiles of blood through a thrombotic vessel. (Tomaiuolo et al. 2014)

Pannus growth differs from thrombosis in that it involves endothelial cells at the anastomosis rather than platelets. This is common with vascular grafts, however not as frequent as thrombosis, and can cause turbulence in the blood flow through the conduit. (Barbetseas et al. 1998)

Researchers have tried to combat this by using drug-eluting stents in their grafts to prevent the formation of thrombosis by eluting blood thinners such as paclitaxel. However the drugs contained within the stent soon run out and clot formation becomes more likely unless the material has become endothelialised. Recently, researchers at ITMO University in Russia have

developed a coating which promotes release of the body's natural fibrin clot dissolving enzyme plasmin to avoid this issue. (Chapurina et al. 2015)

Both thrombosis and pannus formation are natural occurrences common with healing after surgery. However, it is hard to determine to what extent these could occur and what effect they might have on the vascular blood flow through the vessel. In severe cases these reactions can cause severe intimal hyperplasia resulting in the thickening of the tunica intima, which obstructs blood flow. (Kapadia et al. 2008)

4.1.2. Calcification

Calcification is a serious problem when it comes to vascular prosthesis. The majority of the body's calcium supply is stored in the bones and teeth and any excess calcium is dissolved in the bloodstream and transported for excretion. However the build-up of calcium can occur in other areas of the body - this can be the part of the body's natural reaction to injury or a mechanism for fighting infection. Excess calcium around the surgical anastomosis site can restrict or block blood flow and lead to growth arrest by hardening the surrounding tissue.

A Study carried out by Park et al (2001) at the Yonsei University College of Medicine in Korea examined the magnitude of calcium deposits on 3 biocompatible polymers - Polytetrafluoroethylene (PTFE), silicone and polyurethane. The experiment involved placing a sample of each polymer in an incubator which was continually refreshed with a calcium solution via peristaltic pump, and the magnitude of calcium formation was measured up to 21 days. Their results show that throughout their experiment PTFE (in this case Teflon – an extremely common material for the construction of bioprosthetic vascular prosthesis) showed the highest build-up of calcification. (Park et al. 2001)

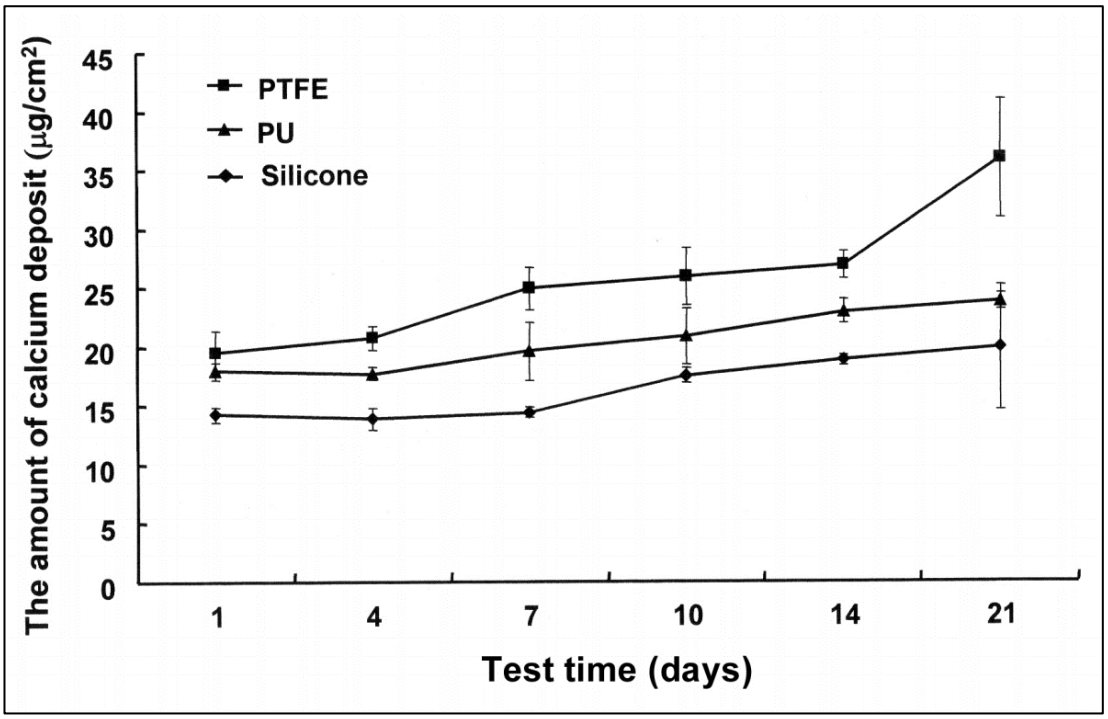

Figure 25 - Build-up of calcium deposits on Polytetrafluorethylene (PTFE), Polyurethane (PU) and Silicone over 21 days (Park et al. 2001)

They essentially show that excess calcium can accumulate quickly on vascular grafts impairing its vital mechanical properties and ability to grow with the surrounding anatomy.

The ideal vascular graft should mimic the behaviour an artery. (Castro et al.) These properties include mechanical strength, biocompatibility, and viscoelasticity and biostability. These may all be compromised by the body's immune responses to the implant. (Desai et al. 2011) The materials themselves also have their own limitations. For example, ePTFE graft commonly used in surgery have poor mechanical compliance, the ridged walls limit distendability and their lack of an endothelial cell lining can cause biocompatibility issues. However, the microporous luminal surface can be treated to become anti-thrombotic. Dacron grafts suffer from thrombosis and neo-intimal proliferation of tissue cells. (Desai et al. 2011)

4.2. The Ideal Solution

The problem of graft failure in children is a multiclausal challenge, however it is clear the development of an ideal graft deployed in the repair of congenital heart disease will have a number of particular characteristics if the challenge of somatic growth and graft durability is to be addressed.

These characteristics include:

1. ***Biocompatibility***
2. ***Ability to expand in response to haemodynamic need associated with somatic growth.***
3. ***Anastomotic interface that has the potential to expand in response to the haemodynamic need.***

Should these characteristics be addressed they will result in an ideal graft/anastomosis technology that will reduce the need for revision surgeries in a critically challenged cohort of children. However in developing these new characteristics, a number of additional challenges present themselves. These include:

1. ***A need to monitor the haemodynamics within the graft to perform the expansion rate.***
2. ***A need to communicate this information from the graft site to the outside world.***
3. ***A need to provide a mode of expansion for the graft and the anastomosis site.***
4. ***A need to provide power to the sensors and actuators required to carry out 1. 2. and 3.***

These are considerable technological, surgical and engineering challenges however the reward for achieving and overcoming these is considerable and could lead to a steep change in the treatment of children with complex congenital heart disease.

Chapter 5.

Thesis Objectives and Hypotheses

5.1. Objectives

The clinical challenge associated with the provision of a growth compensating anastomosis interface for conduit placement in children undergoing open heart surgery is clear and the provision of a technological solution to this clinical problem would be of considerable clinical benefit. In particular such a technology that will expand the anastomosis site in response to patient growth has the potential to reduce the need for multiple surgical interventions in a critical cohort of patients. The overall objective of this work is to develop a growth compensating anastomosis interface device that will recue the need for revision surgery in these children. In the absence of tissue engineered solutions to this problem this work will focus on the development of an electromechanical solution that will use motor driven technologies to effect the expansion of the anastomosis site at the point of conduit implantation. This approach raises a number of challenges, particularly with respect to providing power to the device, the site compatibility of the actuating device and determining the appropriate expansion cycle rate. The work will focus on developing a technological solution that addresses all of these challenges and in testing this under in-vitro and ex-vivo conditions. The work will utilise an iterative design and development approach to delivering the most suitable technological solution.

5.1.1. Objectives Summary

1. Design a small expansion mechanism with the potential to expand at an anastomosis site.
2. Develop a suitable encapsulation technique for the device and its components to maintain biocompatibility when in vivo, to stop any cross contamination between the device and the surrounding tissues.
3. Determine a plausible, minimally invasive method for supplying power to the device when implanted.

4. Test the mechanism under laboratory conditions to ensure expansion potential.
5. Implant test the technology under clinically mimetic ex vivo conditions.

5.2. Hypothesis

The hypothesis of this work is as follows:

It is possible to provide an electromechanical device solution to the challenge of anastomosis site expansion in response to somatic growth.

Chapter 6.

The Concept

6. The Concept

The concept design needs to take into account a number of different problems and variables such as implant site and driving mechanisms. The primary goal for the device is to expand with the growth of the surrounding cardiovascular anatomy to reduce the need for revision surgeries in conditions requiring conduit implantation.

6.1. Implant Site Considerations

A functional expanding ring required both a driving mechanism to increase the diameter of the anastomotic components thus providing an outward force acting on the surrounding tissues from device itself. The force exerted by the device will control the anastomosis expansion and exceed that of the force exerted on the device by surrounding tissue. The variation of potential tissue structures at implant sites would thus determine the force required for successful operation of the device. As such, selecting the correct driving mechanism is paramount for producing a successful working prototype.

6.2. The Cardiovascular System

6.2.1. Tissue Structures of the Cardiovascular System

The cardiovascular system consists of a sophisticated network of blood vessels that aid the blood transportation to the lungs and the rest of the body. Since they comprise a combination of different kinds of biological tissue, their mechanical properties vary.

6.2.1.1. Arteries and Veins

Arteries and veins are made up primarily of elastin and smooth muscle tissue. There are three distinctive tissue layers in the walls of both arteries and veins, the tunica intima (the innermost layer), the tunica media (the middle layer), and the tunica externa (the outermost layer) (*Figure 28*). The tunica media is comprised of smooth muscle tissue and is responsible for the dilation

of the vessel. As arteries and veins require different dilation capabilities, they contain varying amounts of this layer. The tuncia media of arteries contain more smooth muscle than the veins, enabling arteries to vasoconstrict and vasodilate in response to changes in blood pressure and blood requirements of the tissues they supply. Veins have a thinner layer of smooth muscle in the tunica media because they rely on the use of valves to prevent backflow of the blood as it returns to the heart. These valves are comprised of the endothelial cells that make up the tunica intima. The tunica externa is mainly comprised of collagen, and has an additional external elastic lamina in arteries. This layer performs anchorage, in that it provides a means for stabilising the vessels by attaching to organs. (Martini et al. 2009)

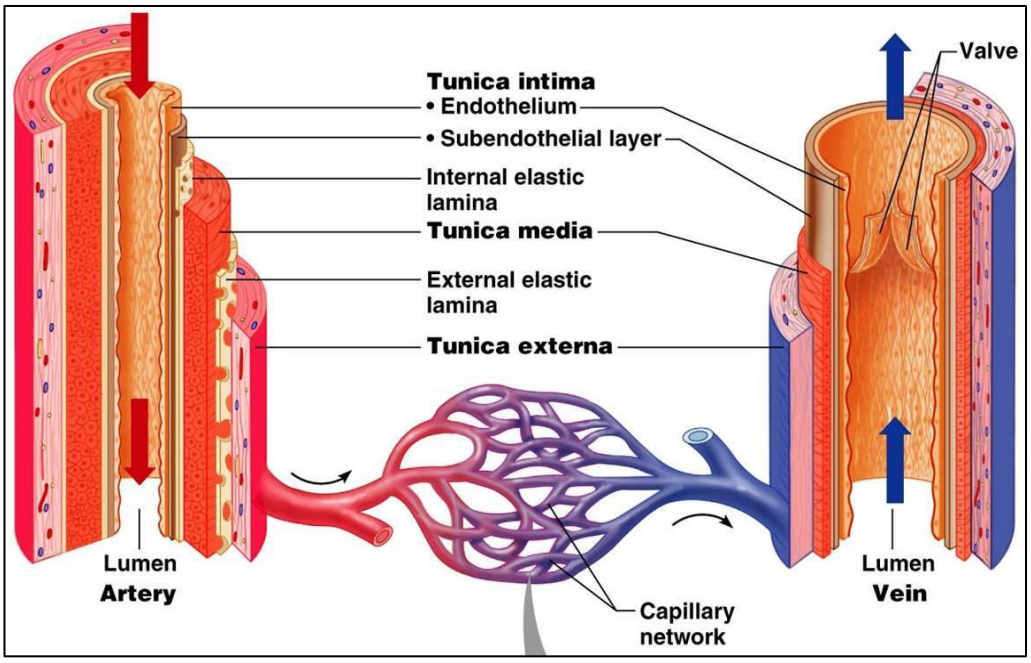

Figure 26 - Anatomy of Blood Vessels

The lengths and diameters of these blood vessels are not fixed; they can fluctuate depending on whether the heart is in the diastole or systole phase. *(See Chapter 6.2.2.)* This makes the mechanical properties of these vessels harder to determine.

If the anastomosis device is to adhere to a vessel, the internal diameter must match that of the vessel so as to minimise turbulence in the blood flow. The diameter of the pulmonary artery

can be calculated by relating the measurements to the body length of the new born child, according to the Centres of Disease Control and Prevention (CDC) this ranges between 46cm to 53cm in males and 45cm to 52cm in females. (Results as of 2010). (Prevention 2010, Prevention 2010) A study by Van Meures-van Woezik et al, concluded that the mean value of internal diameter for the pulmonary artery is 6mm in a child that is 40cm in length, and up to 10mm in a child that is 60cm in length. Therefore, the starting diameter of the proposed anastomosis device must be considered with this range in mind.(Van Meurs-van Woezik et al. 1987)

6.2.1.2. Ventricular wall

In some cases for the treatment of congenital heart disease, a conduit is connected to the heart itself, more often than not, the right ventricular wall. Like blood vessels, the heart wall structure comprises of three layers: the epicardium, myocardium and endocardium. The outer layer – the epicardium, is made from connective tissue similar to that which comprises the tunica externa in blood vessels. The myocardium is the smooth muscle layer of the heart wall, and its thickness is relative to the pressures involved during the cardiac cycle. The left ventricle has a thicker layer of smooth muscle because it is required to pump blood through the arteries to the rest of the body. The myocardium of the right ventricle is thinner because it only has to transport blood to the lungs for oxygenation. The inner layer of the ventricle comprises a layer of endothelial cells. (Martini et al. 2009)

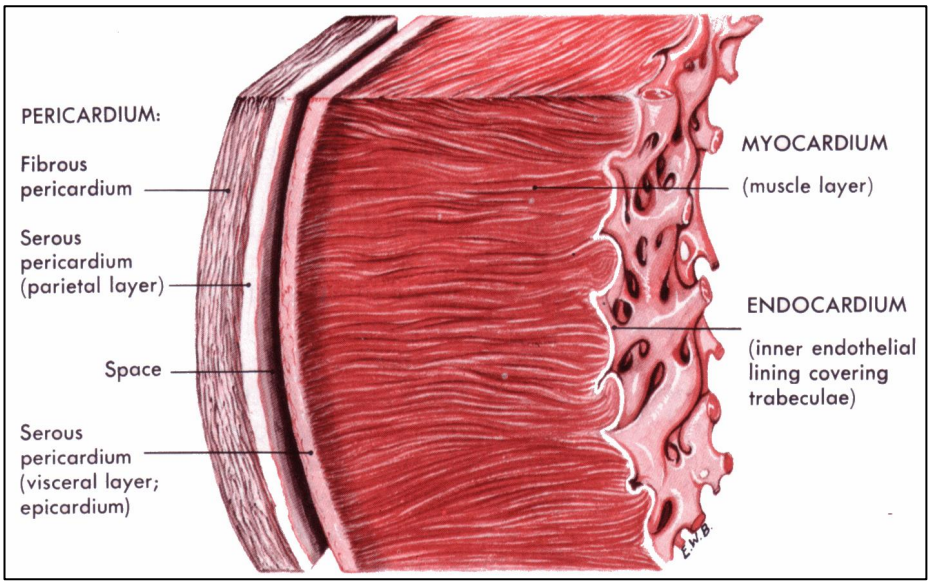

Figure 27 - Anatomy of the Heart Wall (Gallik 2009)

6.2.2. Cardiac Cycle

The cardiac cycle is the completion of one full heartbeat and includes two main phases, diastole and systole. Diastole refers to the relaxation of the muscles of the heart that allows the ventricles to fill with blood. Systole is when the heart muscles contract, squeezing the blood from the left and right ventricles into the arterial circulation and pulmonary artery, respectively. The ventricular wall thickness differs in the left and right ventricles, where the right side of the heart has less muscular tissue than the left because it only has to supply blood to the lungs for oxygenation and generally works against lower resistance. Therefore, there is a slight difference between the thickness of the left and right ventricular walls. (Martini et al. 2009)

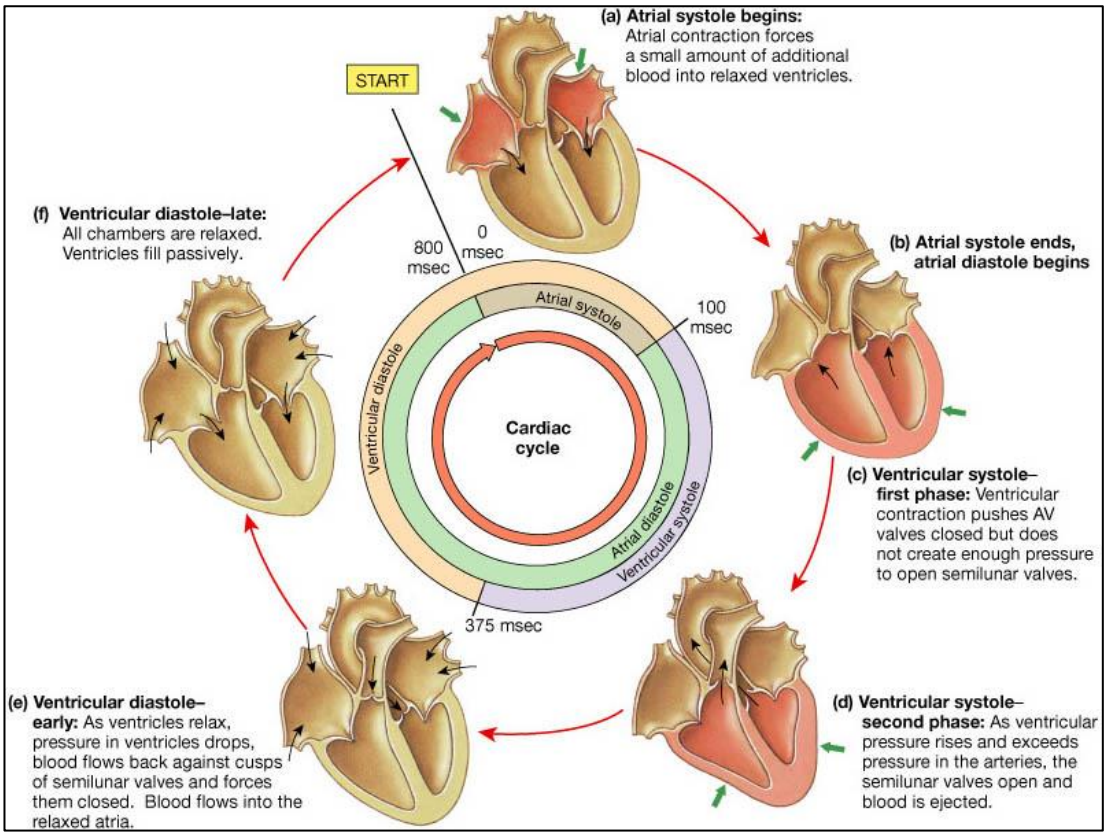

Figure 28 - The Cardiac cycle (Martini et al. 2009)

For a healthy new born child the average left ventricular wall thickness is around 5.4mm during systole and 2.5mm during diastole. The less muscular right ventricular wall ranges from 5.1mm during systole and 2.1mm during diastole. This small change in ventricular wall thickness is near negligible in the healthy postnatal heart. (Sutton et al. 1978) However, a child with congenital heart defects which involve the enlargement of one or both of the ventricular walls - such as conditions that require a RV-PA shunt *(see Chapter 2.1.4)* where a shunt redirects blood from the right ventricle to the pulmonary artery - this difference in ventricular wall thickness may be amplified. Therefore the force required for expansion would fluctuate dependant on the condition of the native anatomy and disease conditions.

It is this variety in tissue structure that make the design of a device like this challenging, but extremely beneficial for the repair of a number of forms of congenital heart disease. Therefore

the anatomy of these sites must be considered when designing a device for deployment under these conditions.

6.3. Force Considerations

The repair site and the surgical correction procedures are dependent on the type of congenital heart disease, for example, the RV-PA shunt procedure has two anastomosis sites that are connected by a conduit. One end of the conduit is attached to the right ventricular wall - a thick, smooth muscle structure - and the other to the pulmonary artery, which is a smooth muscle structure with a smaller wall thickness. The variety in anatomical structures and tissue properties make it difficult to predict how much force will be needed to allow for a smooth expansion of the anastomosis device.

If implanted into the ventricular wall, the device will need a comparatively larger force than if sutured to replace a malformed section of an artery, as the force needed to expand the latter will be significantly reduced.

The expansion performance of the device expanding with growth and/or pushing against resistive tissues will be affected by the presence of scar tissue at the intervention site. Scar tissue forms as a result of the bodies inherent repair process. Following tissue injury, vascular spasm reduces blood flow to a damaged vessel and this is followed by platelet plugging (an aggregation of platelets form a plug). A clot then forms containing red blood cells, macrophages (removing any debris from the wound site) and fibroblasts, which secrete collagen to the wound site which aid the repair of the damaged tissue. This remaining scar tissue is highly fibrous and does not have a normal blood supply. The random distribution and alignment of formed collagen proteins also mean that the tissue is much less flexible than normal tissue. (Hardy 1989)

It is unclear how much the scar tissue around the surgical anastomosis site will inhibit the devices' expansion, and the unpredictable shape, quantity and properties of the scar tissue

would vary from patient to patient. This presents a secondary and less predictive challenge in terms of device design and deployment.

6.4. Drive Mechanisms

In order to keep this technology as reliable as possible, and due to the longevity of the task it needs to undertake, the expansion mechanism should be kept as simple as possible to minimise the potential for failure. The expansion rate should be controlled to ensure that it is commensurate with the growth of the surrounding anatomy using either a passive or active drive mechanism. However, inadequate force is the major problem as it would result in failure to expand with the growth of the child. Therefore for testing purposes, the device will be implanted in vivo in the right ventricle, as this is expected to provide the greatest resistive force in the heart.

6.4.1. Passive Drive Mechanisms

The simplest method to expand the anastomosis would be to use passive expansion achievable using a coiled wire spring in which the relaxed diameter of the spring would match the final vessel diameter.

A major issue with this configuration is that the coiled spring must then be primed to reach the initial diameter for implant, with a view to harnessing the natural uncoiling force of the spring until it ultimately expands to its relaxed diameter.

The primed condition of the spring is where the outward force acting on the tissues will be at its greatest. The delicate healing tissues post-surgery may have potential to rupture and cause complete device failure. This issue inverts at the stage where the spring is almost completely relaxed, as the force exerted by the spring on the surrounding tissues will decrease as it approaches it relaxed state. In order for the anastomosis to expand, the force of the spring must be greater than that of the surrounding tissue. As the spring expands its outward force

decreases, and the two opposing forces will eventually converge. It would be expected that at some point before full expansion, the force of the tissue will exceed that of the spring, and fall short of its fully expanded mark. To get to the desired diameter, the spring must have a relaxed diameter greater than that of the final vessel diameter. However, this would result in greater forces present at the initial phase of expansion when the spring is primed. The inherent nature of using passive drive is that there would be no control over the expansion rate. This concern means that an active controlled drive mechanism must be incorporated.

6.4.2. Active Drive Mechanisms

The use of an active drive mechanism ensures that there would be complete control over the generated force and expansion rate of the device. This could be achieved by using either electroactive polymers which would expand to allow the device to expand under electrical stimulation of the ring material, or incorporating the use of a micro motor to drive expansion of the device.

6.4.2.1. Electroactive polymers

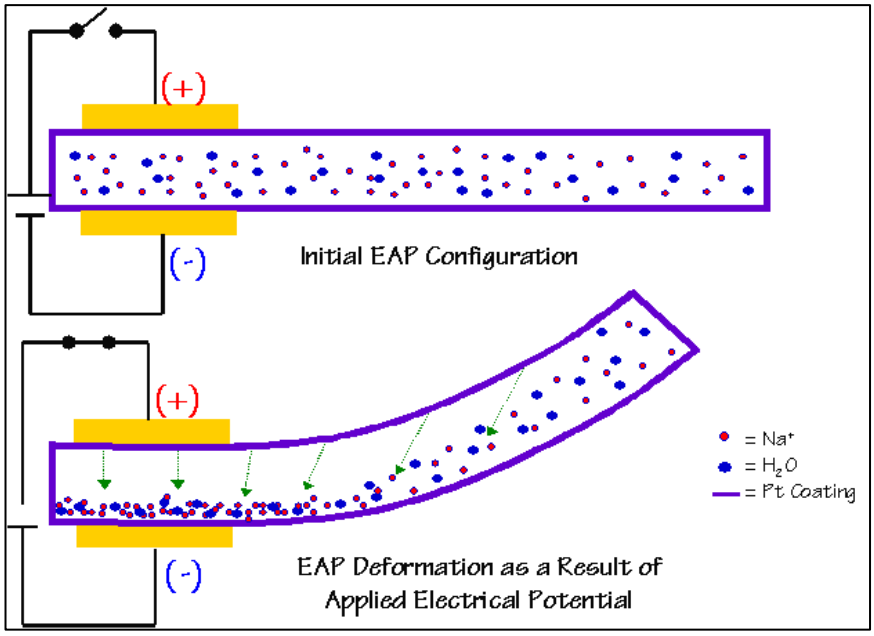

Figure 29 - Fundamentals of Electroactive Polymers (Deyle 2009)

Materials that can change their shape in response to an electrical stimulation are described as electroactive polymers. Electroactive polymers can be either electronic or ionic. Electronic electroactive polymers are influenced by a change in voltage and ionic electroactive polymers use the mobility or diffusion of ions within the polymer when electronically stimulated-(current). Electroactive polymer technology would be feasible to drive this anastomosis device, and its benefits include dramatically reducing the number of mechanically moving parts, and thus ensuring longevity of the drive mechanism. However, the amount of force these polymers can produce would be insufficient for the functionality of the device – an electroactive polymer can produce up to 40MPa of pressure but this application requires very small surface areas. Additionally an electroactive polymer needs a constant supply of power, and any drop or fluctuation in this would cause the polymer to return to its original form. For example, if the battery was to run out, the device would not hold its position, meaning it would return to its initial diameter and possibly cause tissue collapse and heart failure if the surrounding tissues are not strong enough to support themselves. (Bar-Cohen 2004)

This concept - a material changing its structure under an electrical influence - should not be over looked. If the material can deform when an electrical current is supplied then it should work in reverse, an electrical current will be generated when an external force deforms the material. This phenomenon will be explored when considering potential methods for powering the device. *(See Chapter 8.1.3.)*

6.4.2.2. Micro Motors

A mechanically elegant method of expansion would be to use a micro motor. This, connected to a control circuit, will ensure a smooth driving force to the anastomosis ring allowing for complete control of expansion configuration. However, the orientation of the motor and how it interacts with the ring may have major implications regarding driving power and the proportional outward force acting against the tissue.

DC Brushless Micro motor

In order to ensure device longevity, during long term implantation, the drive mechanism must have a limited number of mechanically moving parts as this would significantly reduce the chance of device failure through ‘wear and tear’. Motor technology in general contain a number of moving parts and rely on the contact of wire brushes to transfer the power from the battery to the coils inside the motor, which then generate a strong magnetic force and propelling he motor shaft. These brushes can degrade and cause the motor to fail. Brushless DC motors use coils mounted on the inside of the motor housing and power is supplied to them one at a time. The motor shaft is polarised and turns with the excitation of each coil. The contactless mechanism makes it ideal for this device, eliminating one potential risk of failure over the brushed motors. (*Figure 30).*

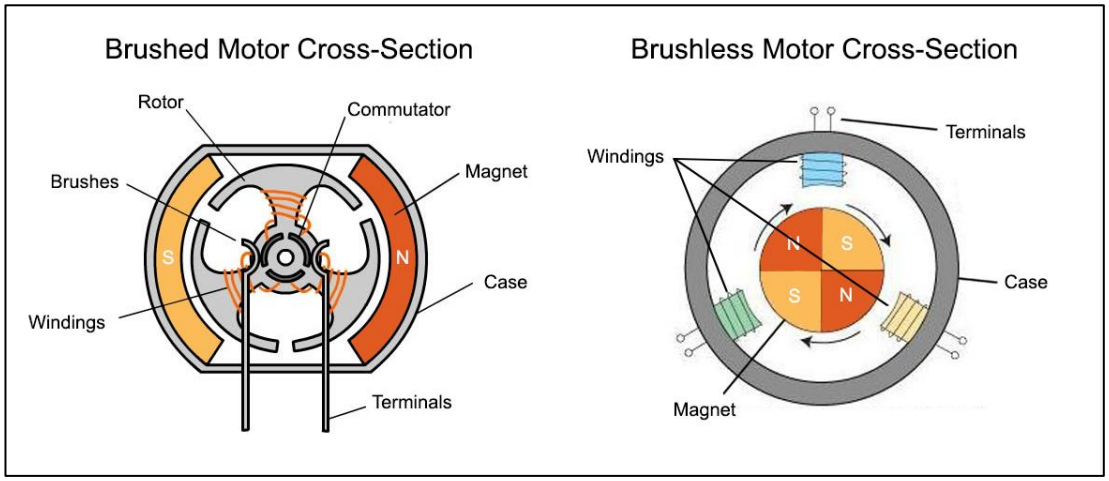

Figure 30 - Brushed Vs Brushless Motors

A simple way of increasing torque from a motor is adding a gearbox, which reduces output shaft speed (rpm) while gaining a significant increase in torque. It is important in this device to gain the maximum torque possible out of the motor without causing damage to the motor itself. Micro motors were selected that had a reduction gearbox as the primary method of increasing torque.

Using a reduction gearbox would attain maximum torque from the motor and would be directly proportional to the pushing force of the anastomosis ring. This would mean mounting the motor perpendicular to a coiled expansion strip and using a spur gear to drive the expansion strip outwards. *(Figure 31a.)* However, it is possible to gain a higher driving torque on the expansion strip without requiring more power from the motor through the use of a linear actuator. This will increase the torque of the motor further providing a greater linear force pushing the expansion strip out. This also facilitates a reduction in the speed of the motor while maintaining a high pushing force. *(See Figure 31b.)*

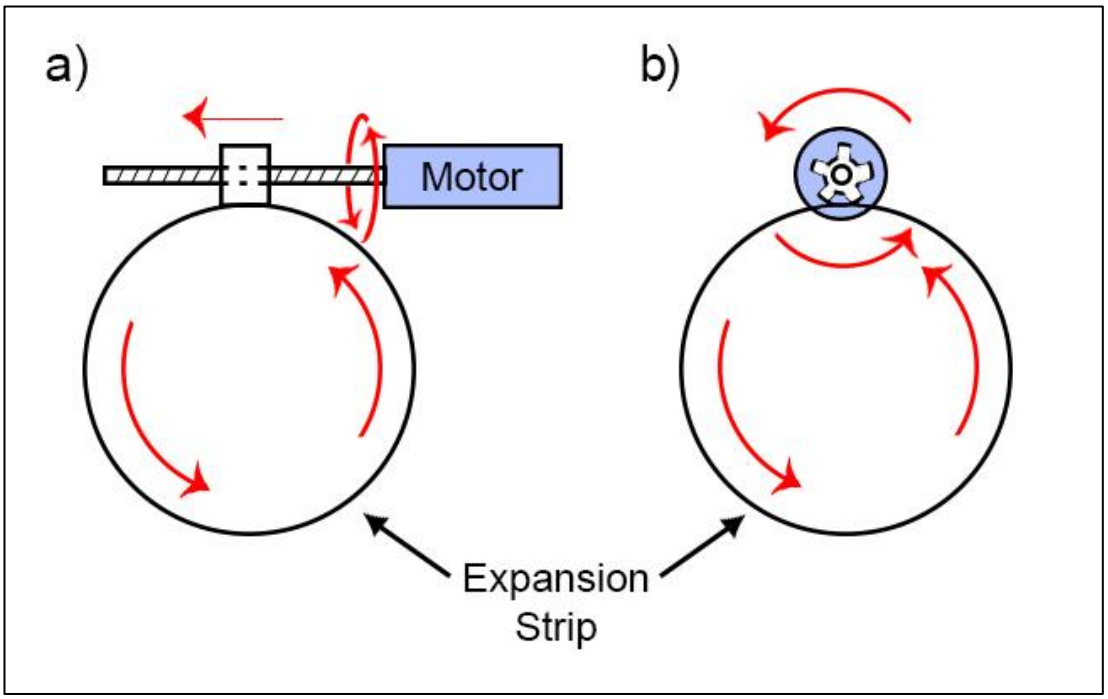

Figure 31 - Actuator Vs Spur Gear: a) actuator-strip interaction, b) spur gear-strip interaction

Piezoelectric Motors

Piezoelectric (also known as ultrasonic) motors incorporate the use of piezoelectric materials to drive the motor. The piezoelectric effect is when a material subject to a mechanical stress produces an electrical charge. It can occur naturally in monocrystalline materials such as Rochelle salt, however the effect is very small. Polycrystalline ferroelectric ceramics, such as

lead zirconate tintanate (PZT), produce larger voltages when subjected to the same mechanical stresses. This is one of the most common ceramics used in piezoelectric motors. (GmbH 2012)

Instead of constructing the strip from an electroactive polymer as discussed in the previous section, the material is incorporated into the motor itself, and can then be used to mechanically expand an external anastomosis ring by applying an electrical charge to the material and using its deformation to manipulate its expansion.

Piezoelectricity describes a materials ability to generate a voltage in response to a mechanical stress. A potential difference (voltage) is generated between 2 opposing surfaces of the material. This is known as the direct piezoelectric effect. Inversely, when a voltage is applied to these surfaces, it causes the material to deform. This is known as the indirect piezoelectric effect. It achieves this due to the electrical charges present in the materials structure. When at rest, (no mechanical stress or voltage applied to the surfaces) the positive and negative charges within the material cancel each other out. However, when a current is applied, an imbalance of these charges and depending on what direction the current is flowing determines whether the material will elongate or compress. Through the use of a high frequency alternating current, can cause the material to vibrate at ultrasonic speeds. (Nanomotion 2008)

This piezoelectric effect can be reversed, meaning that if a voltage is applied to that material it will produce a stress on the surfaces, unbalancing the charges within its structure (similar to the action of electroactive polymers).

Piezoelectric motors can be either rotary or linear actuators. The linear actuator is more simplistic than the rotary motor and involves the use of a single piece of piezoelectric material with a contact foot attached. When a charge is applied to this material, it causes the material to deform and change in the current causes it to relax again. This alternating current cycle causes the ceramic to move in a snake like motion, with this motion the foot moves in an elliptical fashion, essentially ‘walking’ along the surface of an object. (Repas 2008)

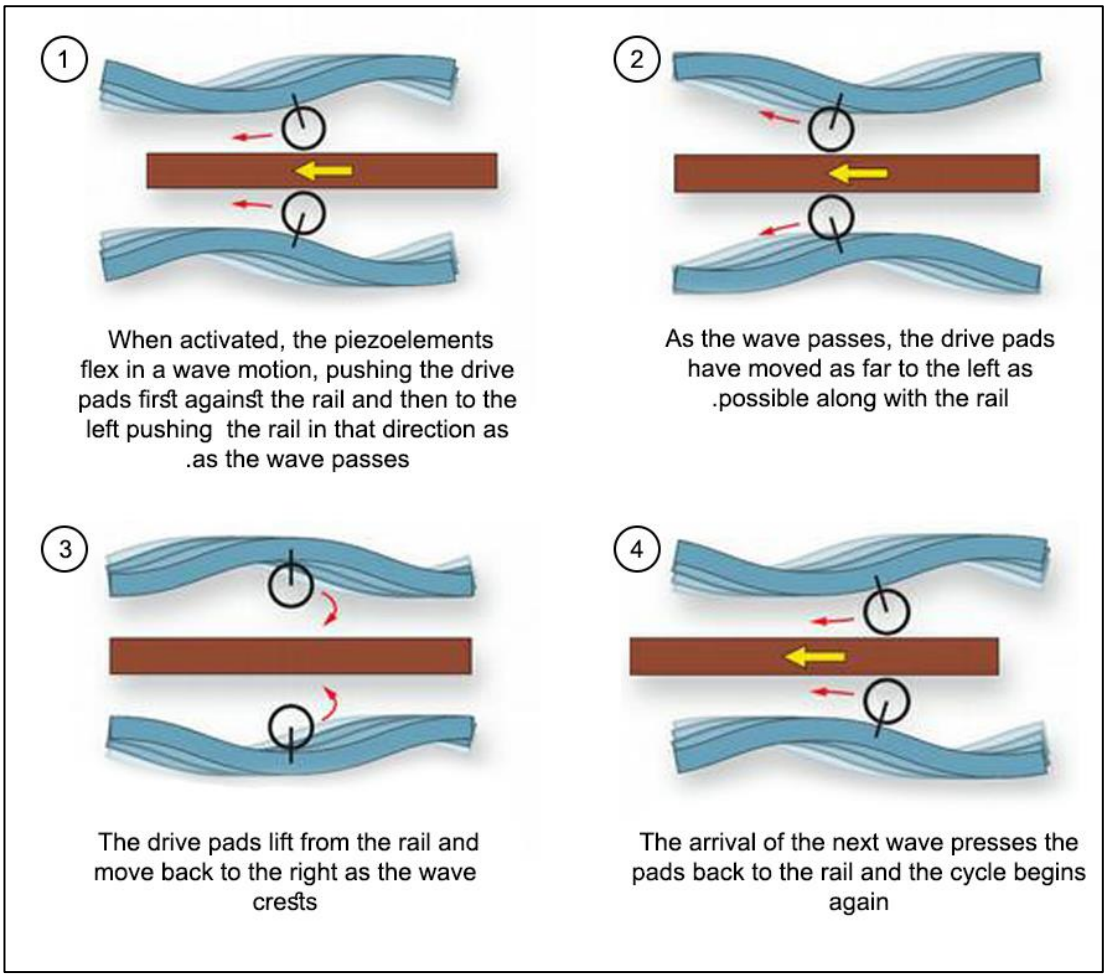

Figure 32 - Elliptical movement of Linear Piezoelectric Actuators (Repas 2008)

Rotary piezoelectric motors work by using a segmented ring of piezoelectric ceramic (called the stator) with a rotor mounted on the surface sharing the same rotational axis. By using the same principal as the linear actuator, when a charge is applied to the stator, the amplification and repetition of the elliptical micro-deformations within the stator causes the rotor to turn. (Bar-Cohen et al. 1998)*(Figure 33.)*

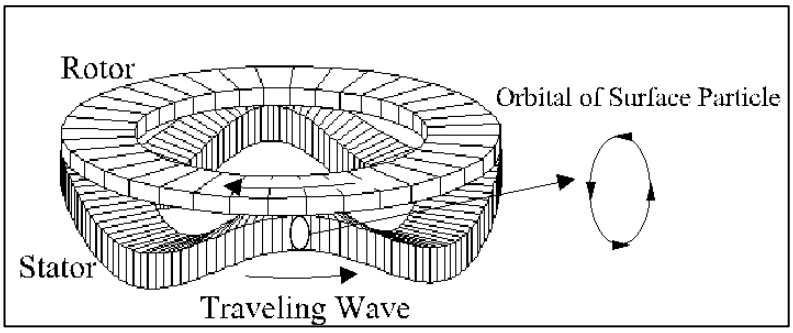

Figure 33 - Rotary Piezoelectric Motor (Bar-Cohen et al. 1998)

The use of a piezoelectric motor as a driving mechanism would be ideal for ensuring the devices longevity as it would potentially incorporate only one moving part, however the complications would arise when trying to incorporate it successfully to expand the anastomosis ring, such as friction coefficients between the driving surfaces.

Active drive mechanisms definitely hold more benefits over a passive drive system, even though they require more power, but eliminate many of the risks and uncertainties that hinder the passive drive mechanism. Therefore concept developments were made around how to manipulate the use of micro motors to achieve the desired functionality of the device. These concepts are discussed in the next section.

6.5. Proof of concept model.

In order minimise power requirements, concept designs were based on the idea of using a single drive mechanism for expansion.

The proof of concept model will function over the higher range of initial diameters based on the diameter of the pulmonary arteries in infants - starting at an initial diameter of 10mm *(as discussed in Chapter 6.2.1.1.)* and to determine whether it is possible to expand a coiled stainless steel strip to double its diameter. If necessary, this initial diameter can be reduced in further stages of the design process, to cater for anatomy where a smaller initial anastomosis

diameter is required. Complete control of the expansion is necessary and must allow for either a slow and controlled continuous expansion or using periodic expansion cycles.

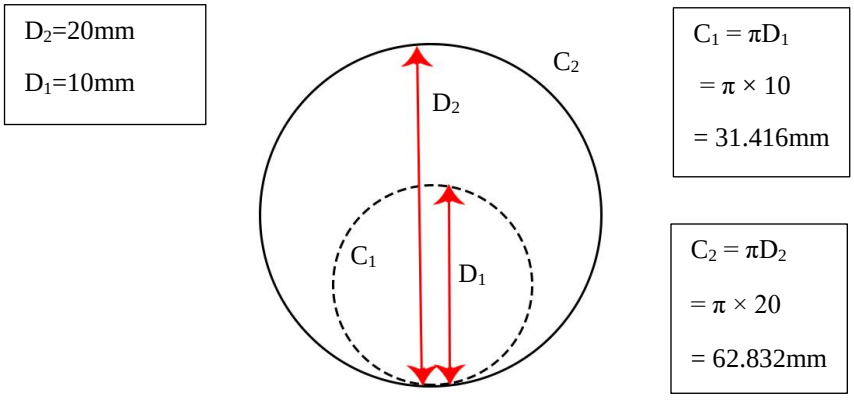

Figure 34 - Circumference calculations

When the strip expands to double its size (diameter from D_1 (10mm) to D_2 (20mm)) the circumference will also double, therefore and increase in circumference length of 31.42mm is needed to reach the desired size. To achieve this while retaining a single point of expansion, the strip must be coiled double, to ensure the same length is available to expand out from the strip. Double the diameter, double the circumference.

6.5.1. Basic Concept

Various designs or micro motor-powered device were considered before deciding on the optimal method to fabricate.

6.5.1.1. Concept I (Actuator – Single point)

A linear actuator holds a number of benefits in driving force of the micro motor. *(See Chapter 6.4.2.2.)* An actuator can be mounted to the drive shaft of a small micro motor and the distal end would adhere to the surface of a stainless steel strip. The motor would cause the actuator to lengthen and in turn, the strip is then pushed out from its pre coiled position increasing the diameter of the device in a controlled movement. *(Figure 35.)*

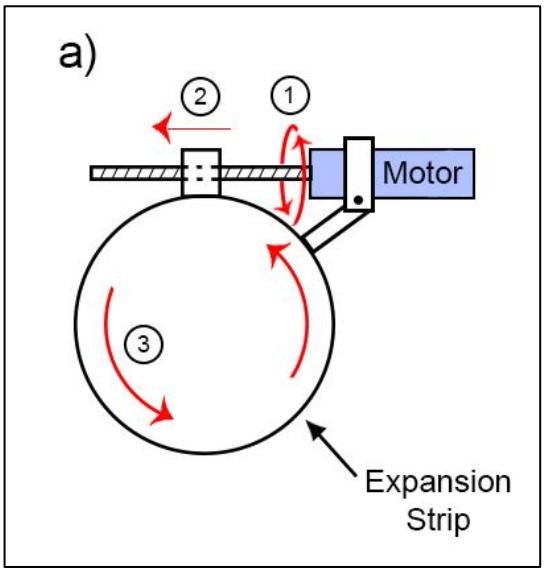

Figure 35 - Concept I - Actuator (Single Point): (1) Worm attached to the motor shaft rotates; (2) Nut fixed to the strip surface moves away from the motor; (3) Coiled strip unwinds and expands.

Pros

The simplicity of this expansion method makes it a valid contender for the long term implantation. All vital parts of this method are secured in place and the only moving part in the drive mechanism is the motor itself. With the end of the actuator adhered to the strip eliminates any chance of slipping between the motor and the strip, maintaining complete control of the device throughout expansion.

Cons

A downside to this concept is the length of the actuator needed for this expansion. For this concept, the devices expansion is directly proportional to the length of screw needed. This means for an increase in circumference of 30mm the length of the actuator must also be 30mm. In addition to this, the motor would be situated in line with the actuator, which would increase the overall length of the device significantly, thus deeming it impractical for this purpose.

6.5.1.2. Concept II (Actuator - Multiple points)

This would take the basic principles from the previous concept of the linear actuator, and instead of expanding the full length along one actuator shaft, it would divide the length between multiple shafts positioned at certain distances around the circumference. However this would involve a complex gearing system and/or multiple drive points. In order to overcome this, instead of a solid strip, the strip would be made up of a lattice structure. If rolled out flat and compressed, all that would be required is to pull the two initial corners of the lattice towards each other, expanding the lattice along the perpendicular axis of the actuator. This would result in the increase in circumference being spread over a number of sections. *(Figure 36.)*

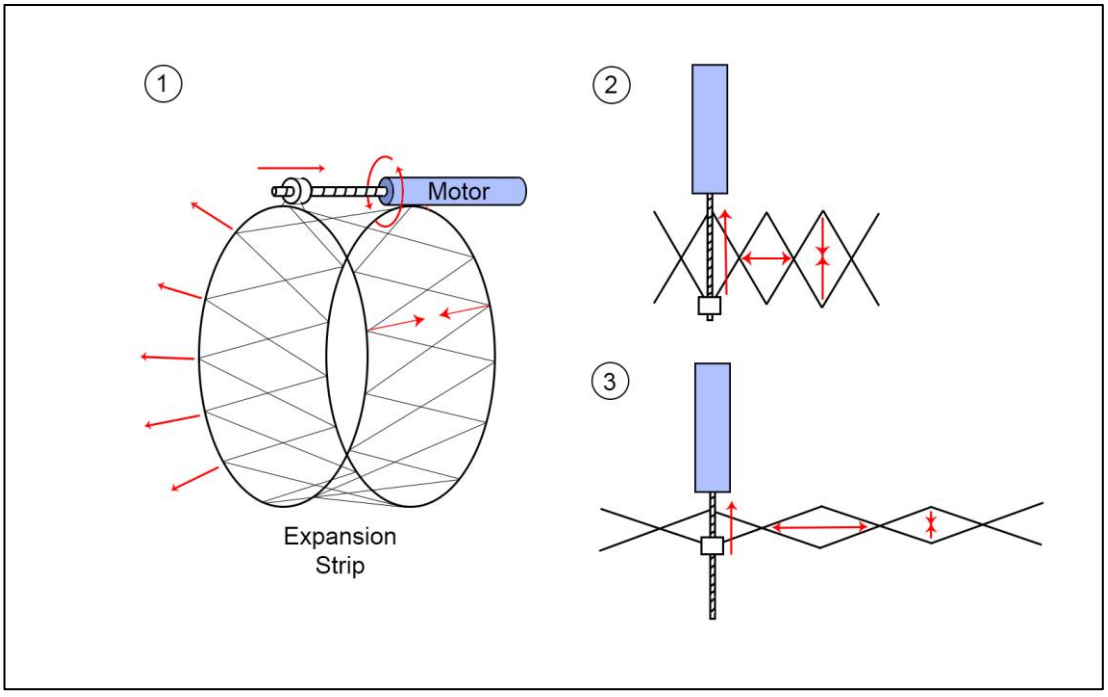

Figure 36 - Concept II (Actuator Multiple Points): (1) Fully assembled device; (2) Lattice structure at small diameter; (3) Lattice structure at final diameter, structure has been elongated.

Pros

Due to the lattice structure, the actuator only has to move a small amount to have a big effect on circumference and thus the diameter of the device. This results in the actuator type would result in a much smaller overall size for the device, a potentially key benefit.

Cons

The complex lattice structure could cause problems if not manufactured correctly. As such, there is a higher chance of mechanical failure. Multiple moving parts and pivot points would make encapsulating the device to make it biocompatible and protect the device mechanics difficult without interfering with its operation. An inner/outer mounted solid strip would make this encapsulation easier, although this may impede upon the movement of the device. This may be resolved by using a flexible skin covering the entire structure rather than a mounted strip. This configuration was not taken forward due to many perceived difficulties that might negatively impact on performance once encapsulated and implanted.

6.5.1.3. Concept III (Spur Gear)

This concept proposed the use of a spur gear attached to a micro motor. The gear would interact with grooves on the surface of a thin flexible stainless steel strip and the gear would allow the strip to expand smoothly without losing traction. This is important because there is only one point of contact between the gear and the strip, so any slip with the interaction between these two parts could cause device failure. *(Figure 37.)*

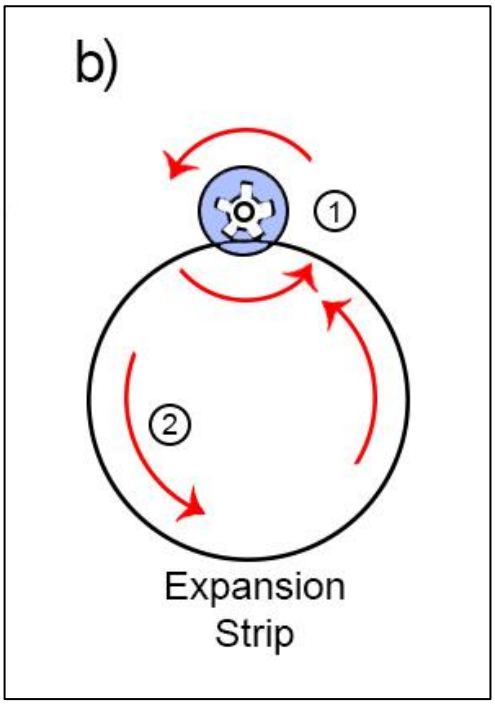

Figure 37 - Concept III (Spur Gear): (1) Spur gear attached to the motor rotates; (2) Interaction between the gear and the strip causes it to unwind and expand.

Pros

There are few mechanical moving parts so theoretically fewer failure modes and enhanced durability. Good interaction between the worm gear and the strip would ensure smooth controlled expansion of the strip. By using only one point of expansion/contact, the device would be easier to encapsulate than that of the lattice structure discussed previously.

Cons

Good contact between the gear and the strip is the crucial issue that would definitely determine its efficiency. Alignment of both motor gear and grooves on the strip are fundamental as misalignment could slip the gear out of the grooves. Another downside is that motor would require a high torque to move the strip using this method. The perpendicular positioning between the expansion strip and gear means that a lot more torque is required than when using a linear actuator *(Chapter 6.4.2.2.)*

6.5.1.4. Concept IV (Worm Gear)

Since a linear actuator would be too large for the device's purpose, the basic principle could be applied to a different technique. This method would combine the basic principle of the linear actuator with that of the spur gear. Knowing that you can get more axial force out of the motor when using a linear actuator, compared with the torque needed for the spur gear to move, the worm gear of the linear actuator could be used to push a fixed point along the shaft.

However if you remove this fixed connection and make the gear interact with an expandable strip through the use of corresponding grooves rather than a fixed point, this provides the higher axial force of the linear actuator and the interaction with grooves on the strip allows for a shorter worm gear to be used. Thus we would expect a reduction in the size of the device without compromising on reduction of power. *(Figure 38.)*

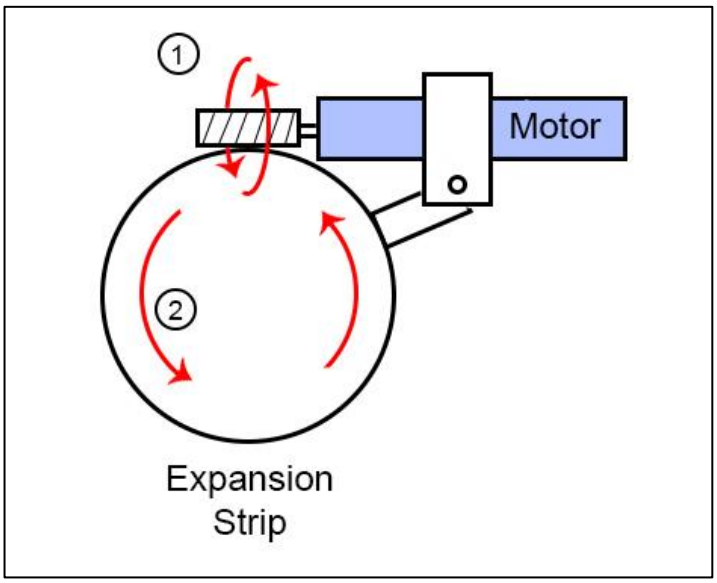

Figure 38 - Concept IV (Worm Gear): (1) Motor rotates worm gear mounted on the shaft; (2) Worm gear interacts with grooves on the surface of the strip causing the strip to unwind and expand.

Pros

The worm gear would allow for reduction in size while maintaining a high enough axial force to expand the strip. The interaction with the strip will hold the device at the current diameter securely and allow for complete control over the devices' expansion rate.

Cons

One of the potential problems with this mechanism, similar to that of the spur gear concept, is the interaction between the strip and the worm gear. Alignment of these parts is even more challenging - any slippage would cause the device to expand rapidly.

6.5.1.5. Concept V (Ultrasonic/Piezoelectric)

This concept involves the use of an ultrasonic motor to drive the strip expansion. A linear ultrasonic motor would be mounted perpendicular to the expanding strip. Housing would hold the motor in place on the strip and springs positioned on the inside of the strip between the strip and housing would allow the strip to maintain secure contact. As the motor runs it will guide the strip though the housing allowing for the expansion.

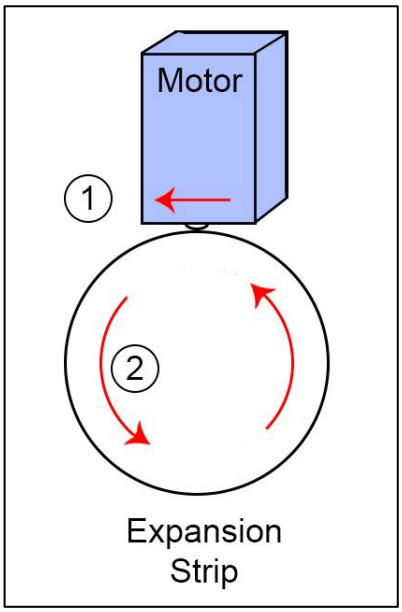

Figure 39 - Concept V (Ultrasonic/Piezoelectric): (1) Motor foot walks along the surface of the strip; (2) Strip unwinds and expands.

Pros

Depending on the power of the motor, the overall size of the device would remain fairly small with only one part protruding. Ultrasonic motors consume less power than that of a DC brushless motor, therefore reducing the main power consumption drastically. With correct mounting, the motor would be able to hold the strip securely in place. With only one active moving part in the system it is less likely to fail when working over a long period of time.

Cons

Power/size ratio of these ultrasonic motors might not be adequate for this situation. Complex programming is needed to run these motors effectively. Complex housing system is required to ensure the strip stays securely in place when device is dormant.

6.5.2. Concept Summary

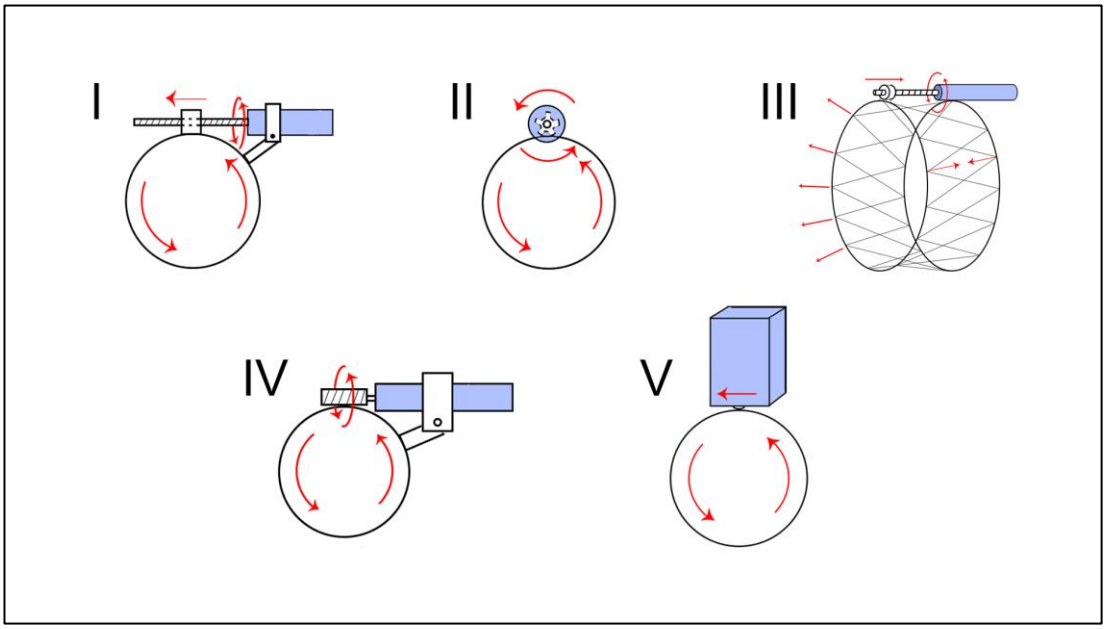

Figure 40- Concept Summary

Concept	***Type***	***Pros***	***Cons***
I	Actuator – Single Point	• Few moving parts • Secure interaction between expansion strip and motor shaft	• Large overall size
II	Actuator – Multiple Points	• Reduced overall size • Small actuator travel distance • Low torque motor required	• Complex Lattice Design • Lots of moving parts • Difficult to encapsulate

III	Spur Gear	• Few moving parts • Secure interaction between expansion strip and spur gear	• Alignment issues • High torque motor required
IV	Worm Gear	• Reduced overall size • Secure interaction between expansion strip and worm gear • Low torque motor required	• Alignment issues
V	Ultrasonic/Piezoelectric	• Lower power over DC motors • Hold strip securely • Smallest	• Low power may not be sufficient • Complex housing required

Table 2 - Design Concept Comparisons

6.5.2. Concept Selection

To proceed, two concepts will be looked into further. One using a DC brushless micro motor and the other an ultrasonic motor driven system. Concept I involves a linear actuator, and even though it would be the most efficient way of expanding the device, it is compromised by its potential large size. The second method involving the linear actuator (Concept II) would be ideal for this application - however in practice, the complex lattice structure could prove to be mechanically unstable. As a result of this, Concept III and IV were investigated further to produce a ***proof of concept prototype***.

6.6. Challenges

Having selected two configurations for the device, there are a number of application specific challenges that have to be addressed in the design plans. These include:

i. Bio-compatibility
ii. Implant Site
iii. Power
iv. Sensing, Monitoring and Control

6.6.1. Bio-compatibility

For any foreign device or structure that is intended for implantation, it is essential that it is be biocompatible. Ideally any device that is implanted into the body should not be perceived as ‘’foreign’’ by the host. This defines complete biocompatibility. This state is rare, and some degree of bio-incompatibility is the norm. In accepting this consensus, it is essential to take steps to limit the degree of device/host interaction. In the case of the proposed device, which is constructed for a variety of tissue contacting materials, steps must be taken to ‘’mask’’ relatively incompatible materials such as metal surfaces, control wires etc. with a more biocompatible coating.

Crucially, such a coating must not impair the functionality of the device. The coating of the crucial moving parts such as the expansion strip needs to be flexible, elasticated and strong to expand with the device. Our approach to achieve this is further discussed in Chapter 7.8.3.

6.6.2. Implant Site

As discussed in Chapter 6.1, the implant site for this device can have a number of different mechanical properties depending on the clinical application and disease. In addition to this, the implant site impacts significantly on the overall size and shape of the device. Space is limited inside an infant’s chest, so keeping the entire system as small as possible is essential.

The site of the control systems and the power supply required to drive and control the system all depend on accessory size. If these are small then they can be integrated within the device itself, although they may have to be placed close to the device. Subcutaneous implantation may instead be necessary if they are unsuitable for implant in the chest.

6.6.3. Power

One of the main concerns of this device is power requirement. Electronic devices that are implanted within the body tend to currently be for very low powered applications such as drug dispensing, pace making or monitoring systems and these are either powered with a battery positioned transcutaneously, or recharged wirelessly with induction coils positioned above and below the skin. *(Figure 41.)*

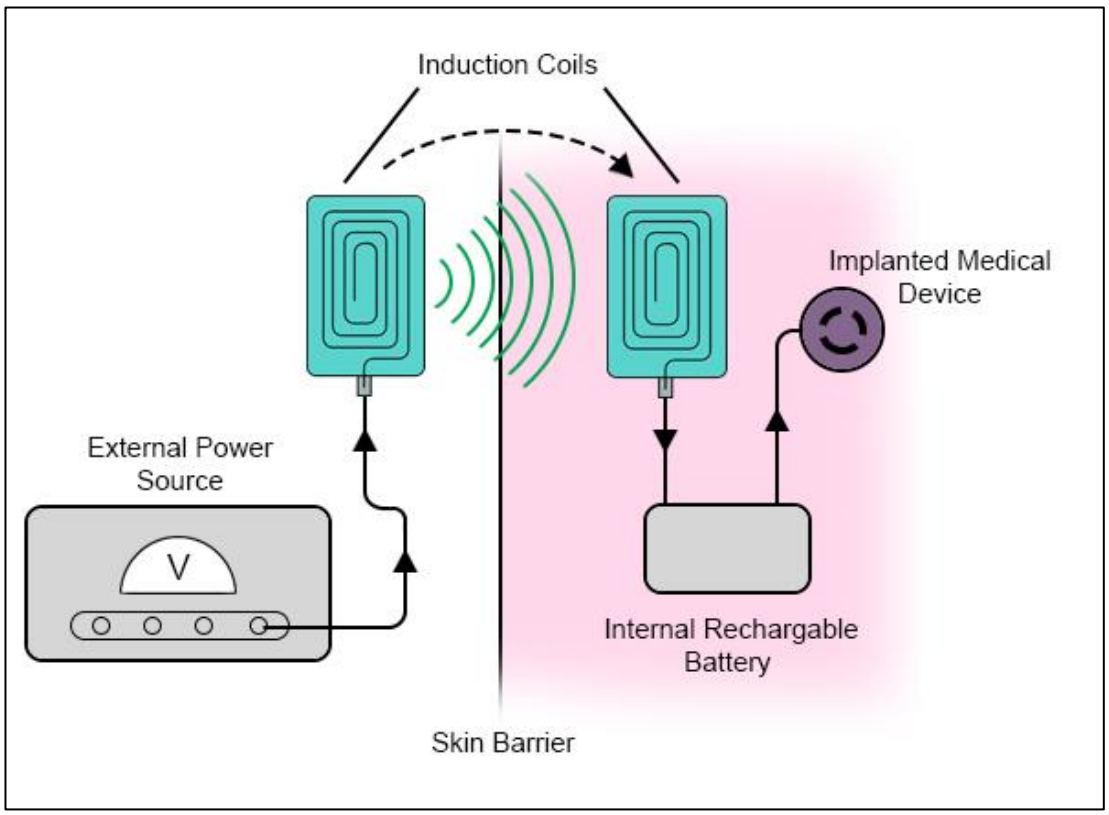

Figure 41 - Transcutaneous Induction Charging

Ideally the proposed device would be powered by energy harvesting from the body itself. This would prove beneficial as it would not require an invasive procedure to replace drained batteries nor would it need to be recharged through the skin. It would be a totally independent device that would constantly top up its battery from energy sources such as, movement of body parts, body heat or energy created by chemical reactions within the body. These options will be explored in Chapter 8.

6.6.4. Sensing, Monitoring and Control

Controlling the device is the key to its success. The final device will be functional for a duration of around 12 years. This means that since the circumference of the device will on average be increasing only 3mm per year, it is important that the expansion is kept under control. This may seem an extremely small amount but variation in this could cause ruptures in the surrounding tissues and be catastrophic for the patient. A simple control circuit should be enough to keep the device within the correct expansion limits, and a solid interface between the strip and the drive mechanism is required to ensure control is maintained at all times.

An example of where monitoring and control of the device is essential is blood pressure. It is important for the device to maintain correct blood pressure throughout the growth of the child, if the device expands too quickly, the child will experience low blood pressure causing hypotension in the vessel. A slight drop in blood pressure may not be a cause for concern but if it drops significantly, there may be severe heath consequences.

On the other hand, if the device was to expand too slowly, it would effectively cause mechanical stenosis in the vessel. This stenotic lesion and associated haemodynamic conflict can damage the cells in the inner lining of the connected artery. This may cause the walls of the artery to become thick and stiff in a condition called atherosclerosis, where dietary fats enter the blood stream through the damaged cells. This is an undesirable and potentially life threatening consequence of inadequate expansion control.

Therefore, a feedback mechanism will need to be in place which monitors the child's status and determines the desired blood pressure and adjusts the device accordingly.

In addition, failsafe's should be in place to ensure the correct expansion is given for the growth of the patient. This ideally would involve a feedback system to assess the flow of the blood through the anastomosis and its current diameter. To reduce the need for invasive alterations the device should have an external wireless control, allowing for the devices standalone controller to be over written if required.

These concerns will be addressed further in the iterative design developments throughout the following chapters.

6.7. Summary

The concept design needs to take into account a number of different problems and variables such as implant site and driving mechanisms. The primary goal for the device was to expand with the growth of the surrounding cardiovascular anatomy to reduce the need for revision surgeries in conditions requiring conduit implantation.

In order for the device to perform as intended, all of these variables will be considered to find the most efficient design. 5 concepts were considered for the device, discussed in *Chapter 6.5.* and summarised in Table 2, where concept designs III (spur Gear) and IV (Worm Gear) were selected for further development.

- **i.** Bio-compatibility
- **ii.** Implant Site
- **iii.** Power
- **iv.** Sensing, Monitoring and Control

The above challenges will have a major impact on the final form factor of the device. These challenges and their limitations are discussed throughout this work.

Chapter 7.

Concept Development - 1st Iteration (Mechanism Design)

7. Concept Development – 1st Iteration (Mechanism Design)

As discussed in the previous chapter it was concluded to develop and test the feasibility of two configurations of the proposed R.E.A.D. device. These are:

1. **Concept III – Spur Gear**

   Pros – *Few moving parts*

   Secure interaction with expansion strip

   Cons – *High torque motor required*

   Alignment issues

2. **Concept IV – Worm Gear**

   Pros – *Few moving parts*

   Secure interaction with expansion strip

   Lower torque motor required

   Cons – *Alignment issues*

With the initial intention of developing a spur gear design *(Concept III mentioned in Chapter 6.3.1.3.)* it was important to test the feasibility of this concept in its simplest terms – the feasibility of using a motor with spur gear to interact with and expand a stainless steel strip. An early concept sketch of this expansion mechanism is shown in figure 42.

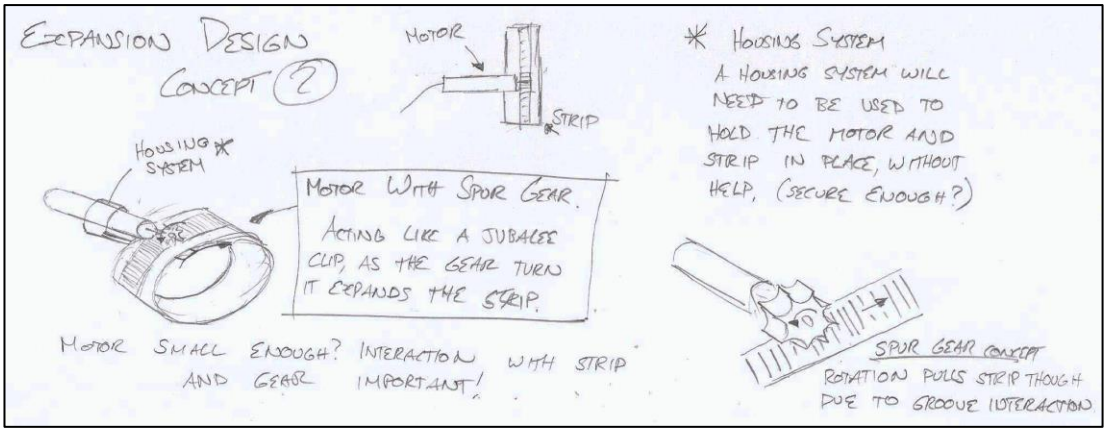

Figure 42 - Early Concept Sketch of Spur Gear Design

7.1. Early Concept Feasibility

A simple rig was constructed by attaching a DC brushless micro motor (with spur gear attached) to a small block of wood with a coiled 10mm serrated stainless steel strip anchored to the block separately and the grooves aligned with the motorised gear. An additional steel strip was used to hold the strip against the motor to allow the gear to remain in contact throughout strip expansion.

Figure 43 - Early Concept Feasibility using wooden block

When running this set up, the motorised gear expanded the strip, and confirmed feasibility of this expansion mechanism. This small proof of concept test also highlighted the two main considerations for this configuration: motor positioning in relation to the strip, and the need for material to hold the strip against the gear securely. This pilot work highlighted the position of the motor in relation to the expandable strip as a potential concern at the implant site. The motor would have to be positioned or even attached along the length of the graft hindering its distendability significantly. *(Figure 44.)*

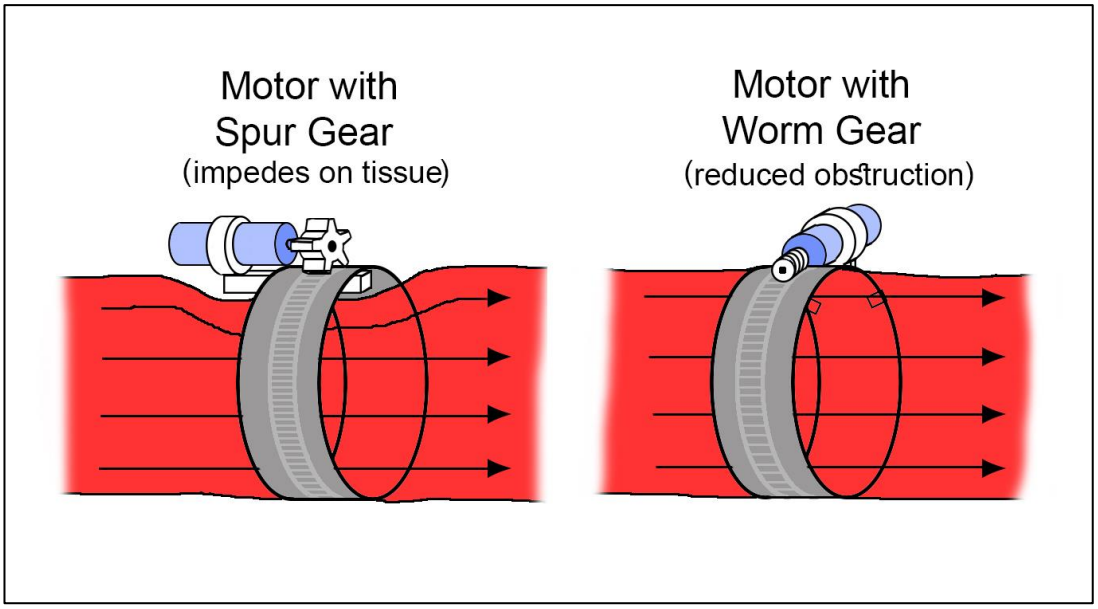

Figure 44 - Spur Gear Vs Worm Gear

This test provided evidence of the need for secure interaction between the strip and the gear as it showed that any slight force would dislocate the strip from the motor and cause it to lose traction, which led to the immediate and forceful expansion. Once re-secured the motor and spur gear effectively hold the strip in position and prevents the strip from uncontrolled expansion. Further device development was aimed at optimising this beneficial configuration.

7.2. Motor Selection

The motor had to maintain a small profile to allow the device to be fully implantable without impeding growth of the surrounding anatomy, and also powerful enough to drive the strip to full expansion.

Motors were sourced from MAXON Motor UK Ltd (Berkshire, UK). For the first design iteration the MAXON Motors EC6 *(see APPENDIX I for full technical Specification)* which had the option of an integrated planetary reduction gearhead, with reduction ratios ranging from 3.9:1 to a desirable 854:1. This higher gear ratio allowed the motor to output a lower speed with greater torque while maintaining a high motor speed. This reduces the possibility of the motor stalling or burning out when attempting to output slower speeds directly from the motor shaft without a gearhead. The addition of a gear head increased the overall length of the motor from 25mm to 46mm from base to the tip of the motor shaft.

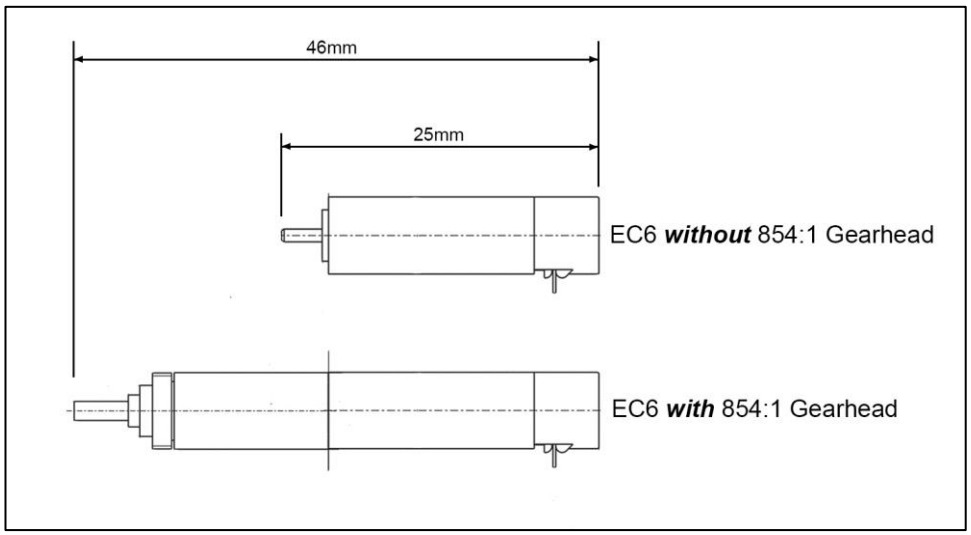

Figure 45 - EC6 Size Comparison with and without Gearhead

However, for the enhancements they provided allowing for the slow expansion and controlled movement, this size increase was justifiable for the first design iteration. The main design

characteristics of the MAXON Motors EC6 are listed in the table below compared to the EC4 motor *(Discussed in Chapter 10)*

Motor	Operating Voltage	Max Continuous Torque w/o Gearhead(mNm)	Gearhead Ratio	Max Continuous Torque w/ Gearhead (mNm)
EC6	6	0.251	854:1	30
EC4	6	0.219	280:1	2

Table 3 - Micro Motor Gearhead Comparison

The power required to expand the strip was not yet determined, for the first iteration. The EC6 was chosen for its torque, power requirements and option for a high reduction gearheads. Smaller profile motors (such as the EC4 *(Figure 46)*) were tested once proof of concept testing was performed for with the EC6.

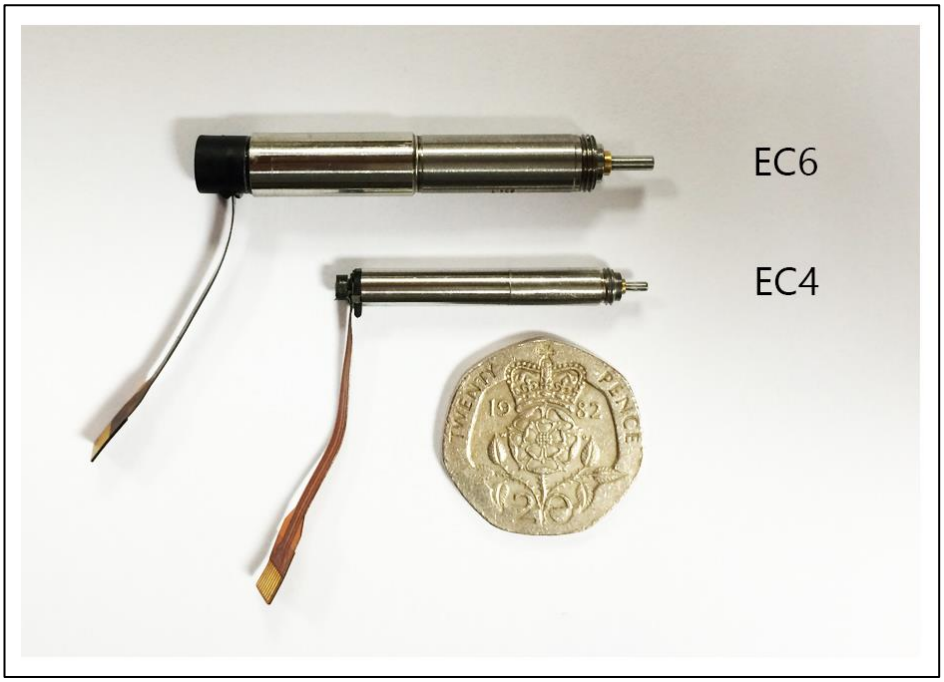

Figure 46 - Size comparison of MAXON Motors EC6 and EC4

Technical data for these motors is available in APPENDICIES I and IV.

7.3. Gear selection

Although a spur gear was used to test the basic concept, a worm gear was selected for the first iteration *(Concept IV in chapter 6.5.1.4.)*. This method incorporates the basic idea of the linear actuator *(discussed in Chapter 6.5.1.1.)* while maintaining a smaller profile initially. This is shown in Figure 47.

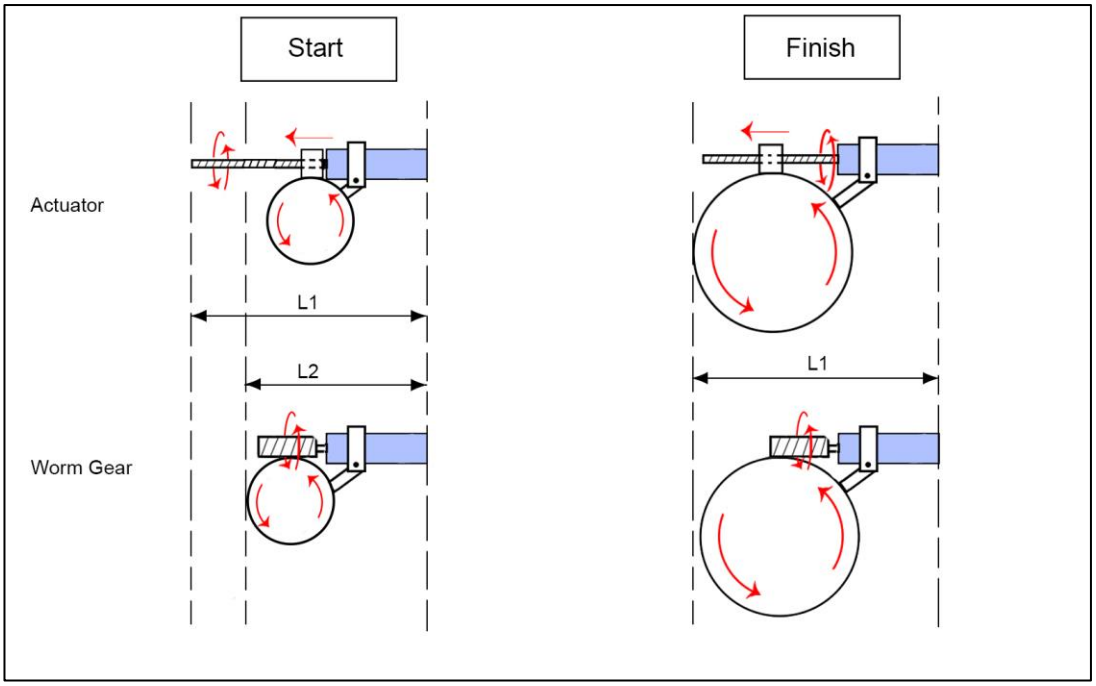

Figure 47 - Actuator Vs Worm Gear: Initial and Final Size Comparison

The use of a worm gear to control the strip allows for the motor to be placed tangential to the strip allowing a linear axial force application to the strip rather than the tangential force applied with the use of the spur gear, which relies on the torque of the motor to expand the strip. The use of this worm gear also adds an additional speed reduction to assist the integrated reduction gear head of the micro motor.

Worm gears are capable of reducing the speed of expansion further while being able to keep the speed of the motor relatively high and can provide more axial force to aid strip expansion.

The extent to which a worm gear reduces motor speed further depends on the lead angle - this is the angle that the tooth of the worm gear revolves around the shaft (the smaller the lead angle, the more rotations on a given length of screw). Therefore the motor shaft needs more rotations to move the corresponding gear a certain linear distance. When the angle is larger, fewer turns are needed, meaning it would take a shorter duration to travel the same distance at a constant motor speed.

The worm gear is constructed using 1.4104 full hard stainless steel. This material has good mechanical properties and easy machinability, which is important when manufacturing such small high precision parts. (Edelstahlwerke 2007) Accurate machining allows for improved traction between the thread of the worm and the serration of the strip throughout the duration of expansion. For this technology, it was necessary to reduce the speed of the motor while keeping the worm as small as possible. A pitch angle of 4.76 degrees was chosen so that the thread can attain as many revolutions as possible in the smallest space provided. This allows the motor to move extremely slowly to enable small and precise expansion without placing excessive stress on the motor.

The output linear force (F_{gt}) of this system can be calculated using the following equation to calculate the axial force produced by the worm gear:

$$F_{gt} = F_{wt}\left(\frac{cos \propto_n \cdot \cos(\gamma) - \mu \sin(\gamma)}{cos \propto_n \cdot \sin(\gamma) + \mu \cos(\gamma)}\right)$$

(Beardmore 2013)

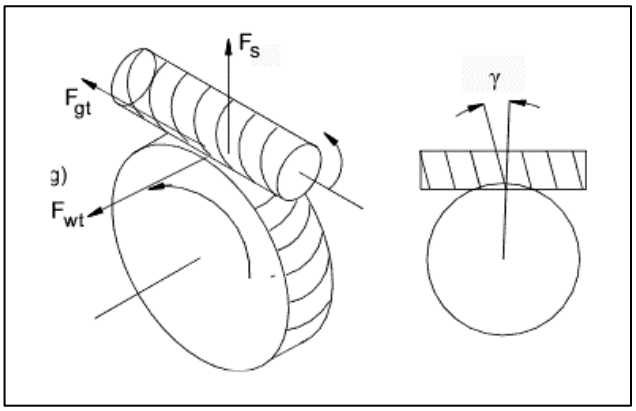

Figure 48 - Worm Gear Force Diagram (Beardmore 2013)

Where α_n is the normal pressure angle, 20°

γ = Worm gear lead angle, 4.76°

μ = Friction coefficient for Stainless steel 1.4104 in dry conditions: 0.78

F_{wt} = Tangential force on worm:

$$F_{wt} = \frac{2 \times M_1}{d_1}$$

Where M_1 = Worm Torque (Nm) = 0.06Nm

d_1 = Pitch diameter of worm = 2.4mm

$$F_{wt} = \frac{2 \times 0.06}{2.4}$$

$$= 0.05\text{N}$$

Substitute values into original equation:

$$F_{gt} = F_{wt}\left(\frac{cos \propto_n \cdot \cos(\gamma) - \mu \sin(\gamma)}{cos \propto_n \cdot \sin(\gamma) + \mu \cos(\gamma)}\right)$$

$$F_{gt} = 0.05\left(\frac{cos20 \cdot \cos(4.7) - 0.78\sin(4.7)}{cos20 \cdot \sin(4.7) + 0.78\cos(4.7)}\right)$$

$$F_{gt} = 0.099N \; or \; 99mN$$

This outwards force is only significant at the later stages of expansion. The primary expanding force of this device was the energy stored in the stainless steel strip itself. The output linear force was secondary to the gears capability to control the natural tendency of the coiled strip to expand.

The use of a worm gear not only allowed for further reduction of the motor speed, (meaning that the motor will draw less power) but also allowed the motor to be mounted perpendicularly to the direction of the conduit/vessel. As such, the device would not interfere with the action of the conduit. Pressure exerted on the conduit longitudinally may potentially impair the conduits ability to distend.

Worm gear specification can be viewed in APPENDIX II.

7.4. The Expansion Strip

The expanding strip of the device was made using precision cut strips of stainless steel. (TECAN ltd, Dorset, UK) In order for the strip to interlock with the drive mechanism, the strip was etched with narrow grooves to accommodate the teeth of the worm gear. These grooves were made as deep as possible without penetrating through the strip itself.

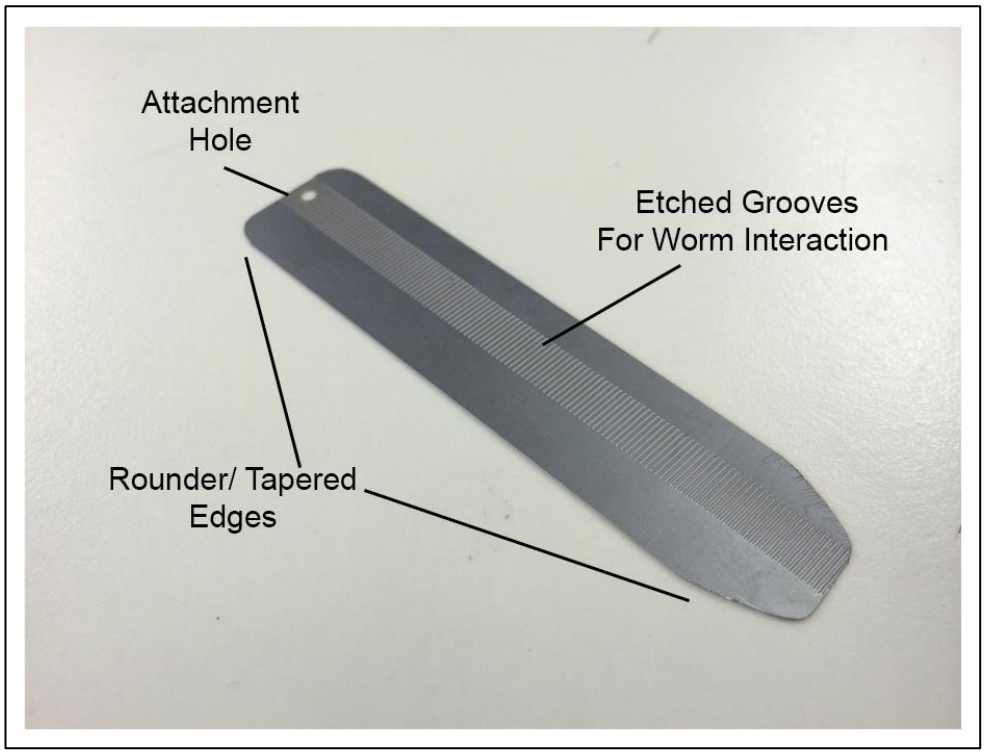

Figure 49 - Etched Stainless Steel Expansion Strip

7.4.1. Strip Metallurgy

One of the principal methods for inducing mechanical properties in a metal is through the method of manufacturing. Stainless steel can be annealed and full hard, and these are distinguished by their stiffness properties. Annealing steel is a method of reducing stress within the steel, where the temperature of the steel is brought well above its recrystallisation point (around 500°C). This allows for the steel to soften and therefore become easier to manipulate. Annealed stainless steel therefore loses its 'springiness', and when bent it will not spring back to its original shape. In contrast, full hard is 'cold worked' to strengthen its properties and will retain a certain amount of 'spring'. (Higgins 1968) This 'spring like' property was necessary for this device and would be the primary force in the expansion of the strip and work in concert with the force generated by the motor and gear. This also helps the strip maintain its circular shape throughout the expansion of the device, allowing for minimal disruption to the blood flow.

316 stainless steel was used for the strips. 316 is a specific code created by the Society of Automotive Engineers (SAE) and refers to the second most common Nickel-chromium steels. The first being 304 Grade stainless steel. The difference between the two is that 316 contains molybdenum for added corrosion resistance. Its properties also include high stress and resistance and has been used on other bodily implants such as knee and hip replacement. (Keegan et al. 2007) Stainless steel contains over 10% chromium (316 Grade with around 16%) and this is what gives it a protective barrier when it comes in contact with air or water. In contrast, the iron contained in other forms of steel lacking this chromium content, will corrode and form a layer of rust on the surface. (ArcelorMittal 2010) To get the variations in mechanical properties of stainless steel it can be treated in different ways such as heat treatment using tempering, where the steel is heated until read hot and either hammered or pressed and cooled rapidly, for example a blacksmith hardening a horse shoe. 316 stainless steel however is an austenitic steel which cannot be hardened using heat, instead it is cold rolled under extremely high pressures to achieve the full hard qualities. (Higgins 1968)

7.4.2. Strip Testing

A number of different strips were produced by TECAN (Dorset, UK) with varying dimensions including thickness, width, and length along with different steel stiffness's. This allowed for testing to optimise strip configuration. All of these elements are related to the strips mechanical properties.

The strips were designed so that the surface grooves were offset, allowing for some of the strip to sit inside the orifice of the tissue allowing it to apply the outward pressure as it expands. The strips tested had the following specification:

	Length (mm)	Width (mm)	Thickness (mm)
Strip 1	80	18	0.16
Strip 2	80	18	0.18
Strip 3	80	18	0.2

Table 4 - Stainless Steel Strip Dimensions

In order for the gear to interact with the strip, a series of grooves of minimum depth required for the gear to function were etched into the surface. The strips themselves are already very thin so removing any more material from the etching would result in the strip becoming less pliable. So this removal of material determined strip thickness and width. The etched grooves did not penetrate through the entire strip (which would, in theory, provide the best interlocking solution between the strip and the gear) as it would cause complications further down the line when encapsulating the device. Device encapsulation is discussed in Chapter 7.8. The strip surface was therefore etched deep enough to give the strip as much traction without penetrating through the strip entirely.

Testing was carried out on the strips to determine the outward force that they would apply to the surrounding tissues (the expansion force). This was carried out using the Electroforce Systems Group (Minniesota, USA) Electroforce 3200 load frame system.

The Strips were tested for expansion force by mounting them onto a platform and coiling them down to an initial diameter of 12mm, and held at that diameter using a small clamp. They were then mounted into the Electroforce 3200 and a 450N load cell was positioned just touching the surface of the strip *(Figure 50.)*

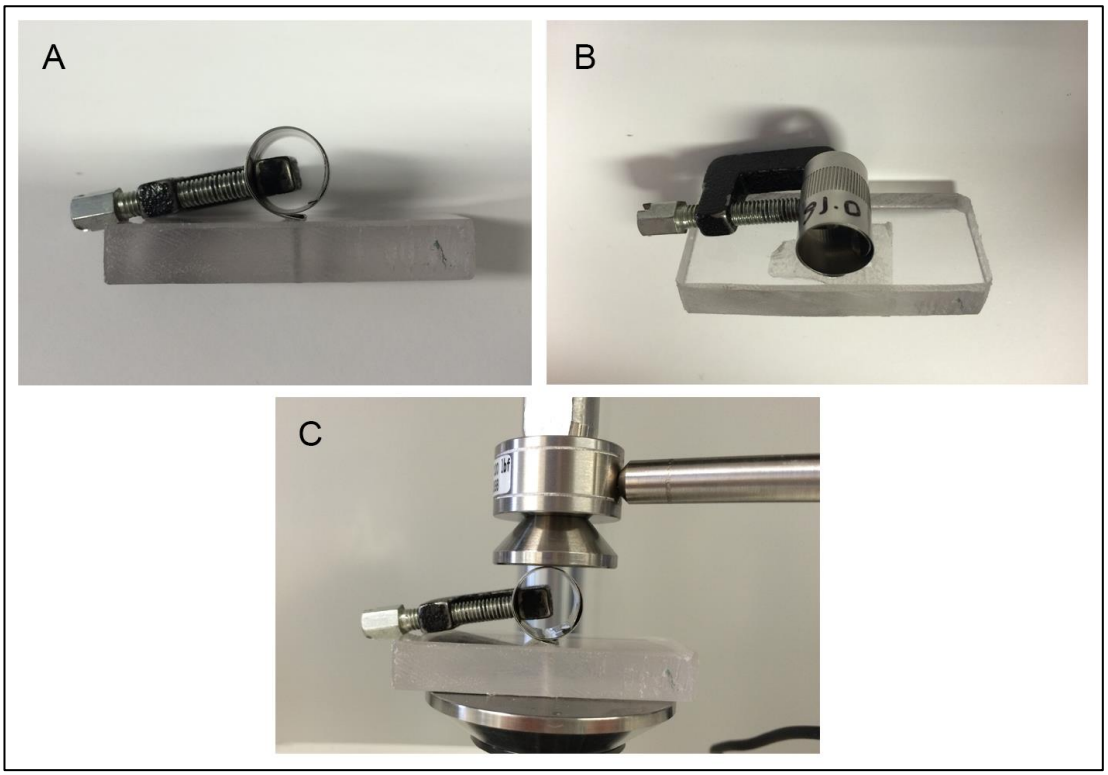

Figure 50 - Strip Testing, A.& B. Clamped strip on support, C. Clamped strip in position touching force plate

The clamp was then released allowing the strip to push up against the load cell, and a reading was taken, the plate then retracted upwards to allow the expansion of the strip. The expansion force of the strip was then measured through the systems maximum range of 5mm from 12mm reaching a final coiled diameter of 17mm. Two identical strips were tested for each size, one used (been pre coiled and expanded during testing of device) and one unused (coiled only for the purpose of these force tests). This was to determine if there was any significant difference in strength between the two.

A total of 43 readings were taken over the course of 25 seconds expanding each strip from 12mm to 17mm. Each strip was tested 3 times and the results plotted.

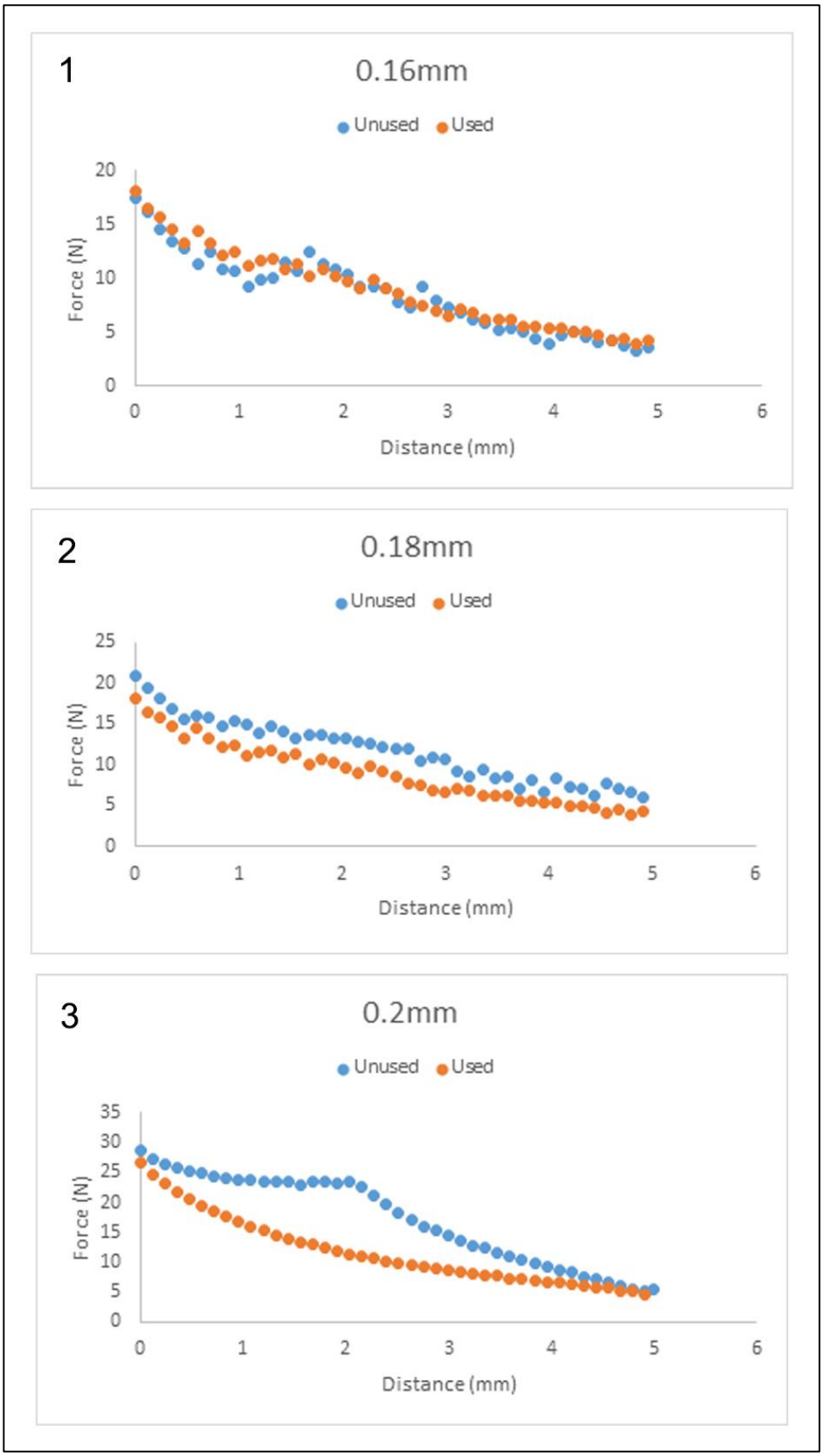

Figure 51 - Graphs obtained from Strip Expansion Testing

It can be seen from graphs 1 and 2 in Figure 51 that the data obtained from these tests experienced noise associated with the etching on the surface of the strip catching on the screw which secured the strip to the testing platform. This catching causes natural plateau then sudden drops, this is clearest in graph 3 where the unused 0.2mm expansion strip experienced only a single catch whereas the others encountered multiple. This would not be the case for the final device as the expansion strip would be positioned clear of this screw.

The important values to observe from these experiments was the initial and final readings, representing the maximum and minimum forces at the beginning and end of expansion respectively. These represent the highest and lowest forces acting on the tissues by the expansion strip alone. The assumption can be made as seen in the data obtained with the 0.2mm thick strip (which produced the least amount of noise) that the force decreases as the strip expands as would be expected. The maximum and minimum force values obtained by these tests are recorded in the table below.

	Max (N)	**Min (N)**
0.16 unused	17.54	3.54
0.16 Used	18.11	4.26
0.18 unused	20.85	5.96
0.18 Used	20.77	3.36
0.2 unused	28.3	5.34
0.2 Used	26.79	4.63

Table 5 - Strip Expansion Forces

One may assume that the optimal strip would have most force at the end of the expansion range. However, if a high force still remains at the end of the cycle, the force at the beginning must also be higher, shown in Table 5. Having such a high force at the initial stages could result in over-powering the drive mechanism and rupturing the connected tissue. Another

downside to having an excessively large initial force is that it makes it more difficult to coil the strip down to its starting diameter. It can also be seen from the results that strips lose their strength the more they are used, so it makes sense to use a strip only once to obtain the best results.

As a result of these data, an unused 0.18mm strip was chosen for these early tests, if the expansion produced an excess of force the strip thickness used could be reduced to 0.16 and vice versa if there was too little force then the expansion strip could be increased to 0.2mm.

7.5. Aluminium Housing.

An aluminium scaffold was created to combine the motor and strip. An aluminium scaffold comprised 2 main sections: 1. A main housing to hold the motor in position which was secured using a grub screw through the side of this housing and 2. A hinged arm to hold the strip. Aluminium is an ideal material for this housing as it is strong and lightweight. Another benefit of using aluminium, especially in this first iteration stage, is that it can be easily altered during manufacturing and testing to provide the most efficient prototype. These parts were connected using a stainless steel pin, allowing freedom of movement between the two parts. The addition of a torsion spring at this pivot point allowed the strip to be forced up against the worm gear securely but also to accommodate for any movement which may occur during the devices expansion. *(Figure 52.)*

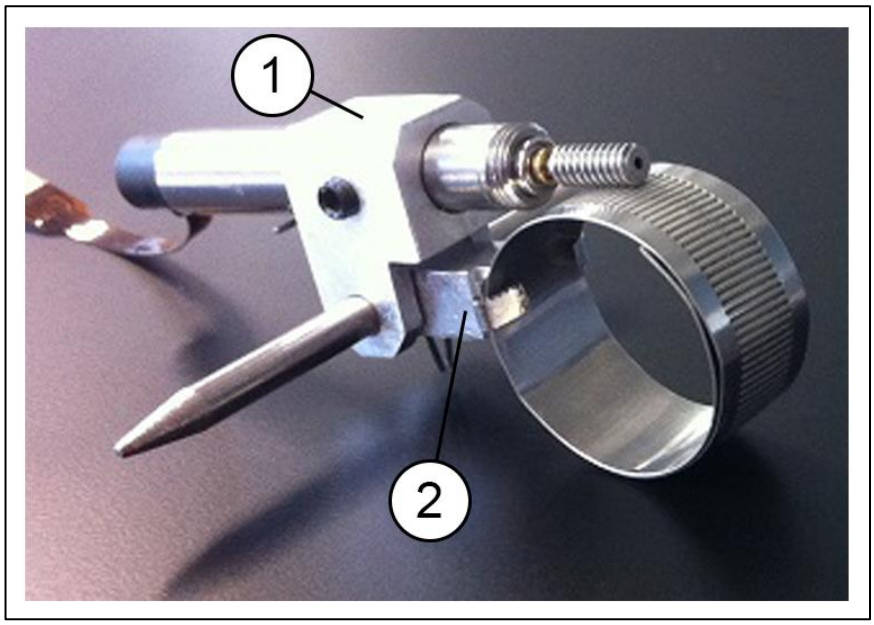

Figure 52 - 1. Main Housing, 2. Hinged Arm

7.6. Spring Selection

Another variable tested for this prototype was the strength of the spring used for the aluminium housing. In order for the strip to remain in contact with the worm gear, it was held in place by a sprung arm. The strip was attached to the arm at one end and the coil pushed up against the worm holding it in place. The spring had to be strong enough to hold it in position but also allow for movement to accommodate the strips expansion. For this iteration, a single torsion spring was secured in place by a 3mm pin, pushing against both the main aluminium section and the support arm of the strip. However, this did not provide sufficient force to hold the strip against the worm securely so an additional spring was added. Calculations for the force produced by these springs were not calculated at this time, however these calculations were carried out for the second iteration to find equivalent effective spring solutions.

7.7 Protective cover

The exposed drive mechanism of the device could prove troublesome when it came to implantation as the motor shaft, worm gear and strip surface required protection from the biological tissues of the implanted surroundings and may be affected by inherent humidity in the chest cavity. Even though the device was coated in silicone, this would affect the drive mechanisms function, potentially leading to device failure. A hard shell was designed to encase the vital moving parts of the device to prevent blockage or jamming. This cover was 3D printed.

7.7.1. Introduction to 3D Printing

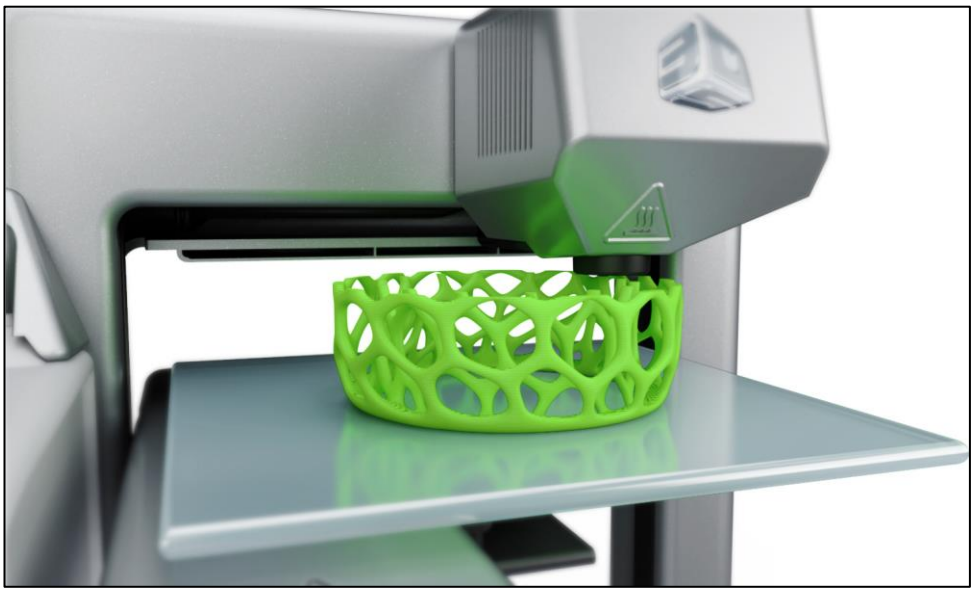

Figure 53 - Example of Fused Deposition Modelling (FDM)

3D printing (also known as ‘additive manufacturing) is a modern manufacturing technique that allows for quick production of complex 3 dimensional parts, models and prototypes directly from digital files.

It works by slicing the CAD model into layers, the thickness of these layers determines the resolution and how true the model will be to it digital counterpart. This resolution is completely

dependent on the printer that is being used. There are a number of different techniques used for 3D printing depending on the resolution and material desired.

7.7.1.1. Fused Deposition Modelling (FDM)

Fused Deposition Modelling (Also known as Fused Filament Fabrication) creates 3D models by feeding the desired material filament through a heated nozzel onto a build platform, printing each layer one on top of the other to form the 3D object. Depending on the printer, either the nozzle or the build platform moves vertically to apply the next layer.

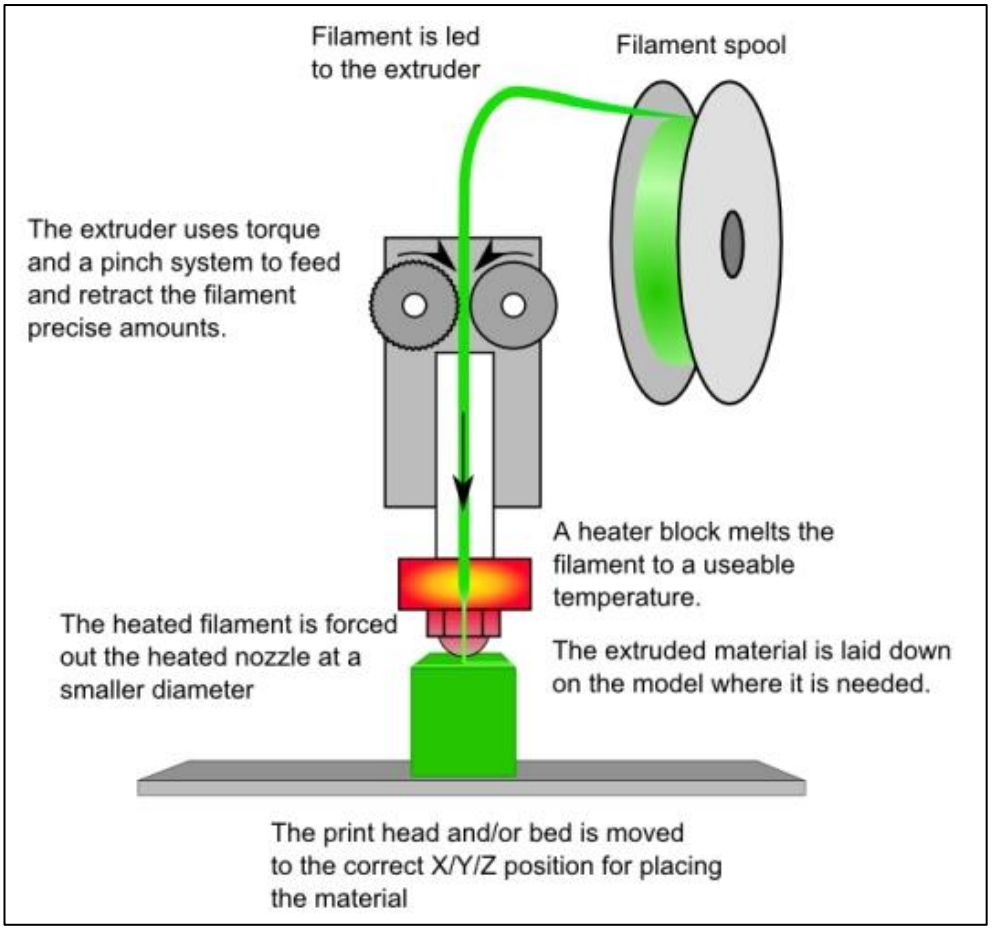

Figure 54 - FDM 3D Printing Process

This method is generally the cheapest and most basic form of additive manufacturing and is used to construct models from ABS, PLA or polycarbonate. It can be used throughout the design process from early prototype manufacture to final end use parts. Support structures for

this method are created at the same time as the part and can be tricky to remove. (Sculpteo 2010)

7.7.1.2. Selective Laser Sintering (SLS)

SLS models are created from sintered powder particles, a layer of powder is spread onto the build platform and a laser scans the cross section of the object onto the surface, sintering the powder together. This means it forms a solid object by heating the powder with the laser fusing them together without causing the powder to liquefy. Similar to that of FDM, once a layer is complete, the platform moves down and another layer of powder is spread across the surface and the process repeats until the final object is created.

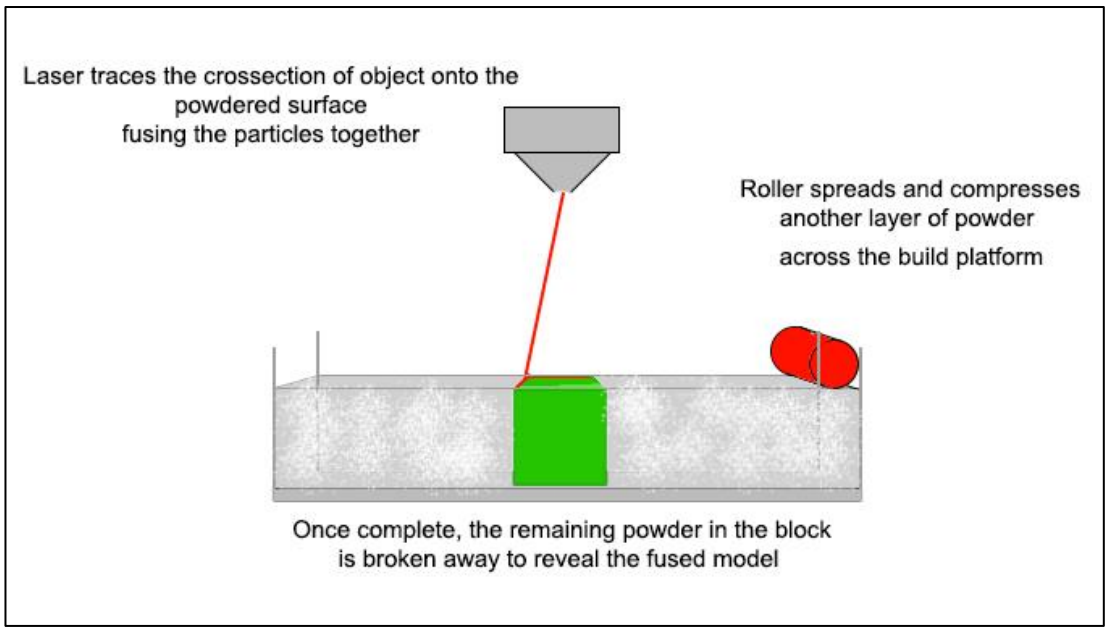

Figure 55 - SLS 3D Printing Process

This method of printing does not require a support structure as the residual powder of the previous layer supports any layers on top, because this support remains in its powder form it is easy to remove and makes it a perfect printing process for models that require moving parts. (Sculpteo 2010)

7.7.1.3. Stereolithography (SLA)

Stereolithography is a 3D printing process, which uses a liquid resin that can be cured by UV light. In contrast to that of FDM and SLS, the build platform used is submerged upside down in a vat of liquid resin. An ultraviolet laser then scans a cross-section of the model through the resin onto the baseplate, thus causing the resin to cure. The build platform is then lifted, allowing the surrounding uncured resin to flow under the previous layer repeating the process for the second layer and so on until the model is complete.

This method is excellent for producing models at higher resolutions than that achieved using fused deposition modelling. (Sculpteo 2010)

7.7.1.4. Digital Light Processing (DLP)

Digital light processing utilises the same process as stereolithograpghy, the main difference however is that it uses a standard projection light instead of a UV laser to cure the silicone. This process also projects the entire cross-section layer onto the build platform at once allowing for significantly reduced build times compared to that of SLA. (Sculpteo 2010)

7.7.1.5. Direct Metal Laser Sintering (DMLS)

The technique used to produce parts using selective laser sintering *(see Chapter 7.7.1.2.)* can also be used to create objects out of materials like stainless steel and aluminium. The laser is used to sinter metal particles, which then fuse and form the solid model. Parts created using this method are extremely durable and favoured for easy replication of machine parts along with parts used in the motor and aerospace industries. Post processing of these parts for example achieving a smooth surface, is time consuming. (Sculpteo 2010)

7.7.1.6. PolyJet technology

PolyJet 3D printing is a technique created by the company Stratasys (Minnesota, USA). This technique prints a layer of liquid resin onto the build platform similar to that of an inject

printer for printing documents. This layer is then cured using UV light and proceeds to the next layer. The fine droplets of resin used for this method allow each layer to be extremely thin providing high-resolution models with relatively quick turnaround. Where support material is required, a liquid gel can be printed with each layer, which can be easily removed. (Stratasys 2015)

7.7.2. Sheath design

The design for the sheath was manufactured using the Stratasys EDEN350 3D printer. In conjunction with using Object studio software, the EDEN350 uses the companies own PolyJet method of printing *(Chapter 7.7.1.6.)* to produce high-resolution models in a semi-transparent ABS polymer.

The cover design and 3d printed cover are shown below.

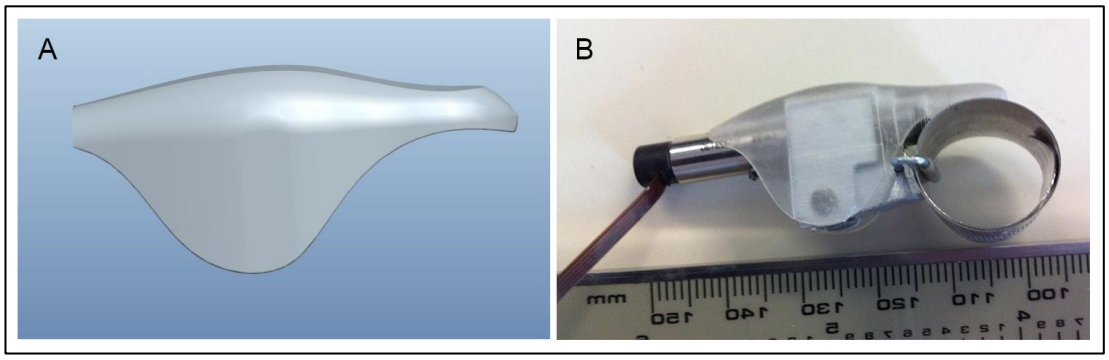

Figure 56 - A. Hard Sheath CAD design, B. Printed sheath in position on the device.

7.8. Tissue Integration

7.8.1. The use of Sewing Rings

Sewing rings are commonly used on a number of cardiac implants such as replacement heart valves and conduits. They allow the devices to be secured in place using conventional suture. They are often made from a porous fabric material such as Dacron, allowing for a strong

durable connection of the tissues with high biocompatibility, as blood and tissue can easily integrate with the fabric.

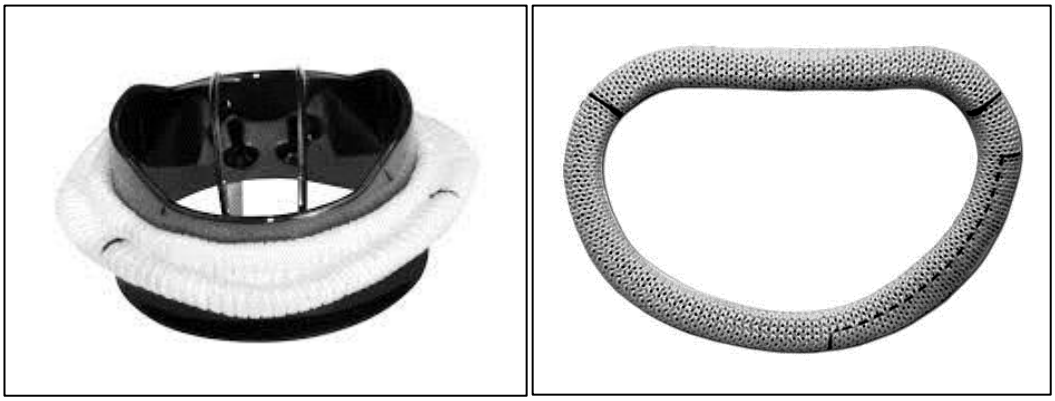

Figure 57 - Examples of Dacron sewing rings (Stojanovic 2013)

For the purposes for the first device iteration - focusing on the implant site of the ventricular wall, the device included a double sewing ring on the edge of the expandable strip. This allowed for one ring to be positioned on the inner surface of the wall and the other on the outer surface. The sutures penetrated all three layers, effectively sandwiching the cardiac tissue between them. This is depicted in *Figure 58.*

Because there is a fair amount of force exerted when the device is expanding there needs to be a secure join between the tissue and the rings, more so than with heart valves, the stresses on their surrounding tissues is fairly minimal, however this device is producing a large force to the tissue and needs to be held securely to them. This means the connection between the rings and the device would have to withstand all applied forces. The two options for adhering the rings to the device would be to either create them separately, joining them after using a bonding agent, or to integrate them with the rest of the silicone coating for the device. The latter would provide a more mechanically sound result due to there being no joins or weak points in bonding.

7.8.2. Suturing technique

The device was be sutured in place using a simple interrupted suture technique. This type of suture is beneficial over the simple running suture due to the space restrictions and complex shape of the device with the added bonus of having a greater tensile strength than a simple running suture.

To simplify the suturing further, a custom suture tool was designed using CREO 3.0 design software, and printed using the same EDEN350 3D printer as discussed in Chapter 7.2.2. This comprised of a long slim handle that held 2 parallel needles connected by a common thread, they would be lowered through the orifice of the device, shown in Figure 58A. The handle was then lifted piercing, the tissues and both sewing rings from the distal side and tied off on the outer ring. *(Figure 58B.)*

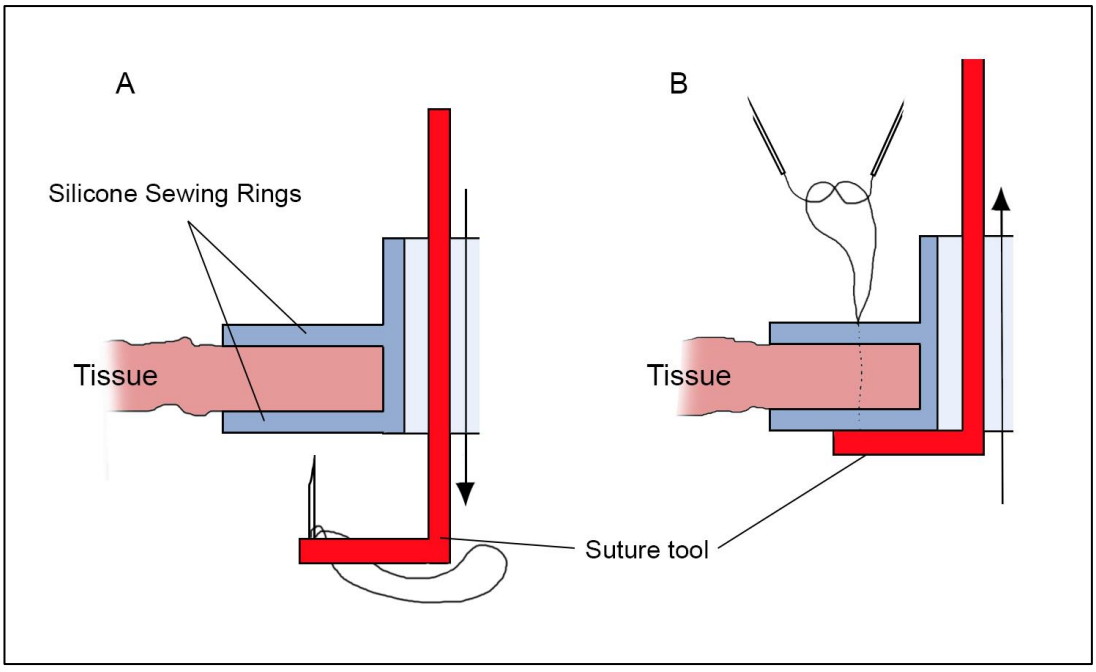

Figure 58 - Suturing method for securing device. A. Primed suture tool lowered through orifice, B. Suture tool pierces sewing rings and tissues with needles tied off.

A number of these tools were prepared with 2 needles prior to surgery. *(Chapter 9)* This removed the need to 'reload' the tool each time in order to make the next suture. This saved time and reduced the complications that could occur during an already complicated surgical procedure. Figure 59 shows the CAD design for this suture tool depicting the needle placement and the final printed tool with needles loaded.

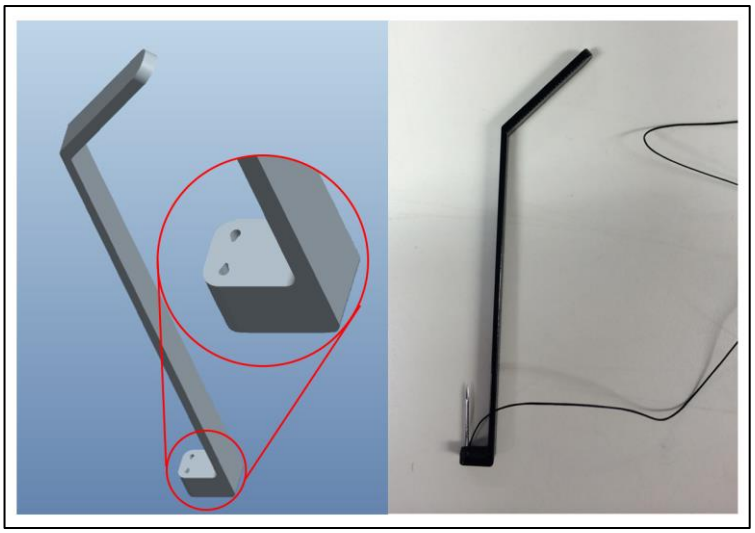

Figure 59 - CAD design of suture tool showing needle positioning

7.8.3. The use of Silicone in Medical Devices

For the proposed device to be fully biocompatible it was considered appropriate to coat in a layer of silicone. This provided a barrier between the surrounding tissues and the drive mechanism itself, eliminating any cross contamination between the two. The hard protective sheath protects the device from external forces and solid tissues interfering with the mechanism of the device but there is nothing stopping contaminants such as blood seeping in under the sheath and coagulating hindering the devices functionality.

Silicones have been used for a number of medical applications since the 1940's and their material properties such as hydrophobic qualities, low surface tension and stable structure were considered promising for blood coagulation purposes. Testing carried out by Jaques et al (1946), initiated exponential growth in silicone use in medical applications. (Jaques et al. 1946,

Colas et al. 2004) Also in 1946 silicones were first used as implantable medical devices when Dr Frank H. Lahey used silicon for a bile duct repair procedure. Silicone's biocompatibility, elasticity and chemical stability, make it ideal for long term implantation. (Lahey 1946)

Medical grade silicone is that which has been approved for a number of medical applications, these can be broken down into 3 categories: External, short term implantation (up to 30 days) and long term implantation (over 30 days). The difference between medical grade silicone and medial grade silicone is the way that it is produced. In order for the silicone to be FDA approved for medical devices it needs to be manufactured in strict sterile clean conditions. When silicone is produced normally it produces a toxic hydrogen chloride gas. For medical grade silicone, however, the chlorine is replaced by non-toxic acetic acid. The silicone must then comply with the regulations outlined in the ISO standard - ISO 10993-10, biological evaluation of medical devices.

Medical grade silicone elastomers are used across many medical disciplines including orthopaedics. Silicone joints for the hand were developed during the late 1960's and use for smaller joints for the bones in the feet soon followed. Early metallic knee implants also utilised the benefits of implantable silicone functioning as a shock absorber between the joint surfaces.

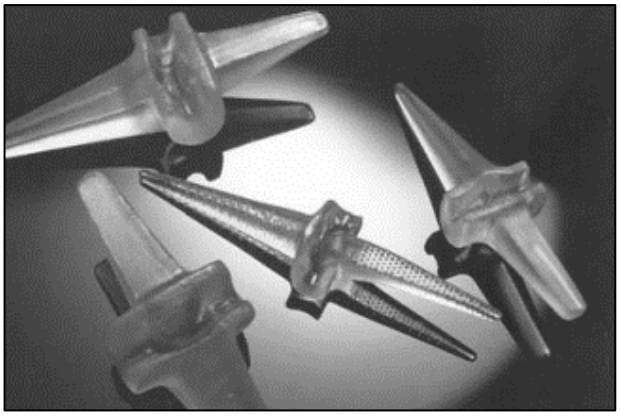

Figure 60 - Silicone hand Joints (Colas et al. 2004)

Silicones currently are best known for their use in catheters and shunts. The elastic and hydrophobic properties make it the ideal material for tubing used in bypass systems, and used

as a protective barrier for both surrounding tissues and device internals. An example of this is the latex Salastic Foley catheter, with a thin silicone coating on both external and internal surfaces to aid with biocompatibility. Silicone elastomers are highly beneficial to the creation of medical devices due to its adjustable curing conditions. (Thomas 2007) See table below.

Silicone Materials	***Key Physical Characteristics and Performance***	***Medical and Pharmaceutical Applications***
Fluids • Polydimethylsiloxane • Organofunctional siloxane - Silicone polyether - Silicone alkyl wax	• Spreadability, film-forming • Diluent, dispersing property • Substantivity • Controlled occlusivity • Hydrophobicity • Lubricant property • Emulsifying property	• Siliconization of needles and syringes • Medical device lubrication • Excipients for topical formulations • Skin protecting composition • Drug carrier
Compounds • Silica + polydimethylsiloxanes	• Antifoam • Diluent, dispersing property	• Antiflatulent (APIs)
Gels (unreinforced elastomers) • Cross-linked polydimethylsiloxanes	• Softness • Resilience • Tackiness • Transparency • Adjustable cure conditions: from ambient to elevated temperature • Foamable	• Cushioning material • Gentle adhesive for skin (soft skin adhesive) • Wound interface (nonadherent wound dressing, foam dressing) • Soft matrix for drug release
Elastomers • Cross-linked polydimethylsiloxanes • Reinforced with silica • Various cure system: radical, hydrosilylation, condensation	• Rubbery property • Mechanical resistance • Adjustable modulus • Adjustable cure conditions: from ambient to elevated temperature • Adjustable cross-linking conditions • Foamable • In-situ film-forming	• Soft and resilient material for medical device • Recognized biocompatibility for human implantation (e.g., pacemaker) • Medical adhesive (sealant) • Film-former
Pressure sensitive adhesives (PSAs) • Silicate resin in polydimethylsiloxanes	• Tacky material • Adhesion to skin and various substrates (e.g., plastic films) • Substantive film-forming	• Temporary fixation of devices on the skin (e.g., wig, catheter) • Film-former • Transdermal drug delivery system

Figure 61 - Correlations between Silicone Materials, Performance and Applications (Thomas 2007)

7.8.4. Encapsulation Methods

The two methods of encapsulation of the device were investigated; dip coating and injection moulding. Both methods could coat the device immediately or be used to create a removable silicone cover that would slip over the device and then be sealed.

For the initial encapsulation tests, three different silicones were tested from the Smooth-on Ecoflex series (Pennsylvania, USA), each with different shore hardness of 50, 30 and 10. Higher the shore hardness suggests stiffer polymer, resulting in a greater force required to stretch it. In contrast, a lower shore hardness will provide an easier stretch but may be more likely to rupture. It is unclear if this silicone is safe for short or long term implantation. The company state that it has been ISO certified for skin irritation and sensitisation (ISO 10993 – 10). It is for this reason why it was chosen for the first stage implants only where the mechanics of implantation were being tested. The silicone selection would be re-addressed for the second iteration, where a more acceptable silicone was chosen.

7.8.4.1. Dip Coating

The simplest way to ensure full silicone coverage over the device was to dip coat it. This involved lowering the device into a beaker of silicon until fully submerged, then removing and suspending the coated device in the air until the silicone has set.

A number of issues came as a result of this method. Due to the silicone being in its liquid form once removed from the beaker, it gravitated towards the distal end of the device before solidifying, resulting in an uneven coating.

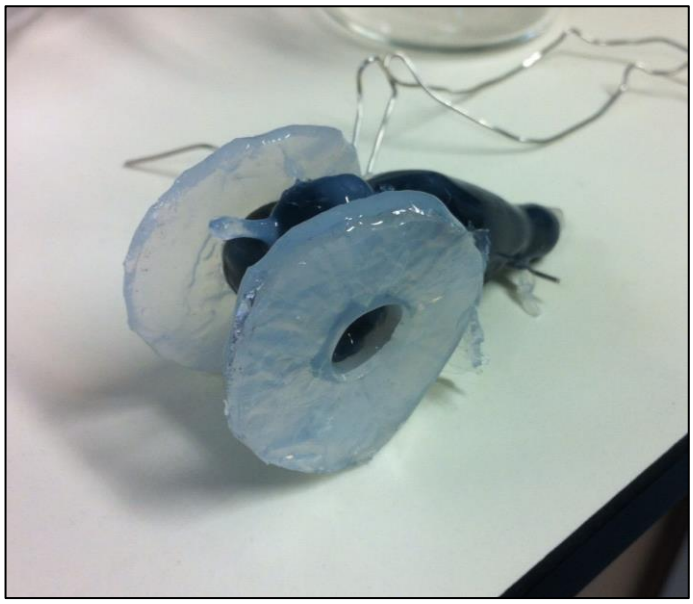

Figure 62 - Dip coated dummy device with attached sewing rings

7.8.4.2. Injection Moulding

Failure to evenly distribute silicone using dip coating motivated the need to injection mould the device. Advantages to this method would be that it would maintain a controlled even coating of silicone over the entire device during curing and also that the sewing rings could be created at the same time as the rest of the covering, eliminating the weak points that would have been created with dip coating the device.

The injection mould process was used through all iterations of the device. The process of creating the mould was complex and required computer modelling of the device and then creating the mould block around it. Due to the complex shape of the device the mould block had to be split in a way that allowed the device to be removed in one piece without any stress being applied to the silicone that might cause it to tear. Each piece of block was designed to be removed smoothly to leave the silicone intact. The delicate cap of the motor and its cable would protrude from the top surface of the mould to be coated after. The hole which the silicone would be injected into, (also known as the runner) was positioned on the top surface leading directly into the mould cavity. The figure below shows the CAD model of the device

and the protective sheath. This was used as the base model for the mould to be created. To ensure an even coating of silicone was applied the model was scaled by 5% and then removed from the mould block creating a cavity within which the motor can sit and allow the silicone to flow around the outside.

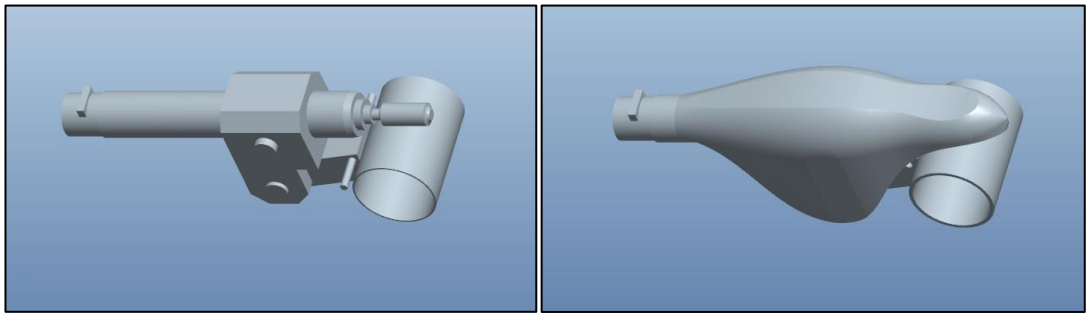

Figure 63 - CAD design of drive mechanism with printed sheath for use in mould creation.

The mould was 3D printed using the same clear ABS mimic material used for the protective sheath which would allow any problems, for example, air bubbles to be seen once the silicone had been injected. To add additional reinforcement the sewing rings, sections of Dacron were positioned on the sewing cavity so they would be encapsulated during injection.

The device was then positioned inside the mould and sealed and secured using an array of flexible straps and the 2-part silicone mixture was then injected through the runner in the top surface where the motor cap and cable was exposed. The mould was left to cure for 24 hours.

Once the silicone had set, the mould pieces were carefully removed, and any excess trimmed.

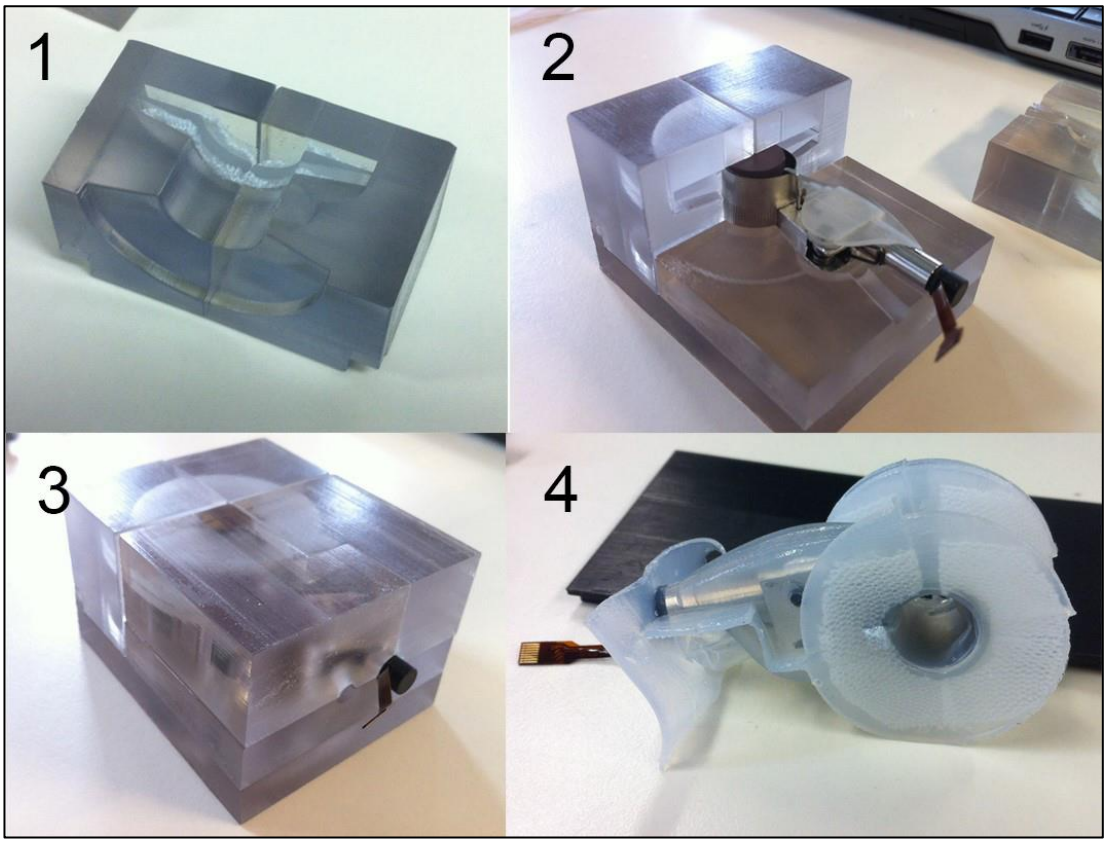

Figure 64 - 1. Mould block with Dacron pieces positioned in the sewing ring cavities. 2. Device positioned inside open mould, 3. Device fully enclosed within the mould, 4. Silicone coated device once removed from mould (not trimmed)

Once the device was removed and patched, the short motor cable was inserted and sealed into a junction allowing for the motor cable to be extended and coated manually brushing with the same 2 part silicone that was used for encapsulation leaving the ends of the cable free to be connected to the control box.

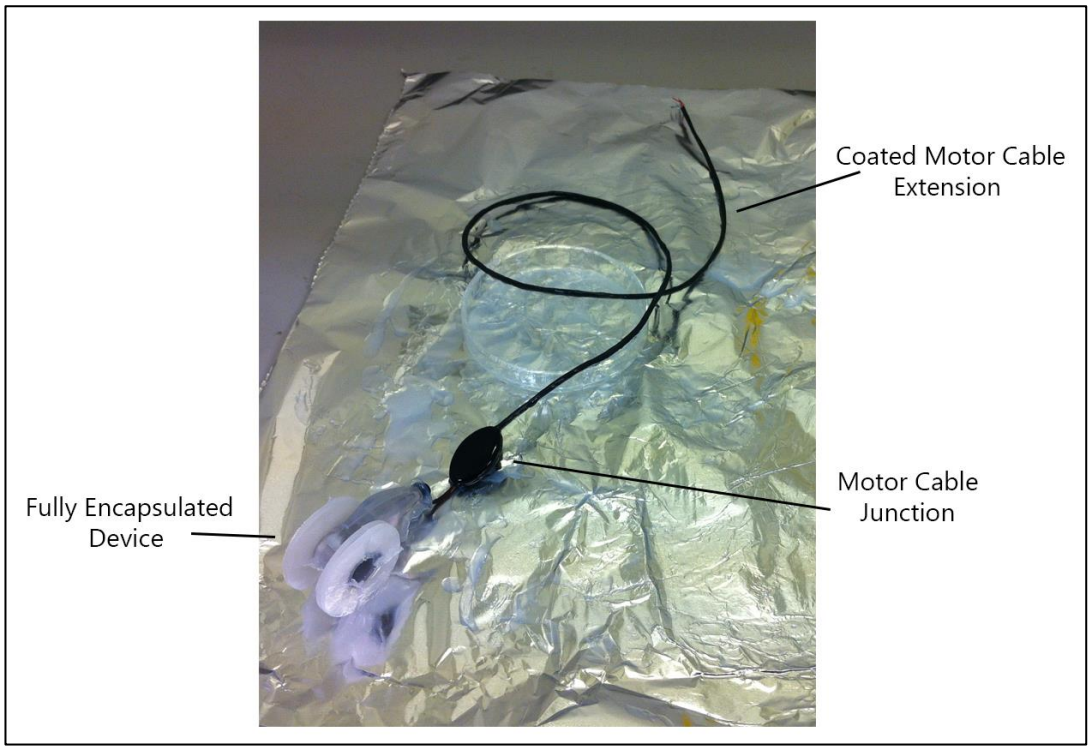

Figure 65 - Final 1st iteration silicone coated with cable extension.

Chapter 8.

Power and Control Systems

8. Power and Control Systems

8.1. Powering implantable medical devices.

Implantable medical devices are used for a number of applications, not only in the treatment of a number of cardiovascular diseases, but also in drug delivery systems for patients suffering from conditions such as diabetes. Though the applications and functionality of implantable devices are widespread they often require constant monitoring and control, and such features require a reliable and consistent power source to remain functional. In recent years, developments in implantable power have evolved beyond simple battery solutions, into areas such as energy harvesting and transcutaneous induction charging of implantable devices with the aim of developing a completely independent reliable power source for low powered implantable technologies.

8.1.1. Implantable Batteries

Batteries convert stored chemical energy into electrical energy and are used widely across all portable electronic applications. Batteries contain at least two or more electrochemical cells and electricity is produced as a chemical reaction between these cells. Implantable batteries allow for continuous monitoring and functionality of implantable devices without any external intervention. (Bock et al. 2012)

Although the majority of these chemical reactions are converted to electrical energy, some of that energy will be lost to the surroundings as heat. It is important that the implantable battery has an operating temperature that is within the range of the human body (around 37 degrees) and does not heat up to a level that damage surrounding tissues.

Batteries come in two different forms; *primary* and *secondary* batteries. Primary batteries are also known as dry cells. This is due to the fact that the chemical reactions that take place within the battery are non-reversible, and electrolytes are contained within an absorber. This is unlike

secondary batteries, which contain free or liquid electrolytes. This means that if the battery is connected to a power source in reverse to its discharge polarity, the chemicals within revert back to their original form allowing the battery to be used again. Primary batteries are generally less expensive and have higher capacities than secondary batteries. However the downside is that they need replacing once the battery has depleted. Therefore, primary batteries are not ideal for a minimally invasive implantable device. The smaller capacities of the secondary rechargeable batteries are a more viable option, as there are ways of replenishing the batteries without the need for complicated replacement strategies.

8.1.2. External Charging of Implantable Batteries

A popular form of charging implanted devices is through the use of wireless energy transfer. This can be done transcutaneously through the surface of the skin using induction coils also known as ‘near field’ or through the use of radio waves which can transmit power deeper within the body, ‘mid/far field’. (Culbertson 2015)

An electric field can be produced by passing an electric current through a coil of wire. The idea of induction charging involves a secondary coil of wire that is positioned within this electric field essentially converting the magnetic energy back into current.

This principle of wireless energy transfer was realised by Michael Faraday in 1825 when he conducted an experiment using a coil of wire and a magnet. He observed that as the magnet passed close to or through the coil an electrical current was produced. However, if the magnet remained stationary the current would stop. (Roche 1987)

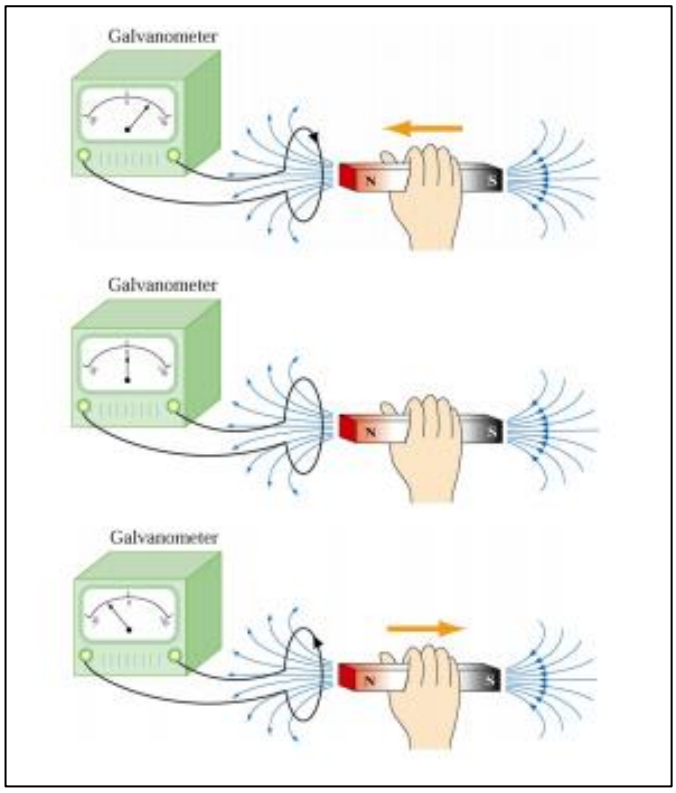

Figure 66 - Michael Faradays' Wire Coil and Magnet Experiment

From this, Faraday conducted another experiment; 'The Iron Ring Experiment' which involved a coil of insulated wire wrapped around one side of a soft iron core. *(Figure 67)* This coil was connected to a battery interrupted by a switch. A secondary coil of wire was positioned around the other half of the core and connected to a galvanometer. The rationale for this experiment was that when connected to the battery, a steady current created in the coil intensified by the iron ring would be strong enough to produce a current in the secondary coil when the switch was close. He observed that when the switch was closed, there was a sudden spike of current recorded on the galvanometer which quickly returned to zero. This relates back to the stationary magnet in his first induction experiment which produced no power when the magnet was stationary. The magnet had to be moving in order to produce a reading. The small spike when the switch was closed was the increase in current before it reached a steady state, therefore it was clear that an alternating current would produce better results. (Al-Khalili 2015)

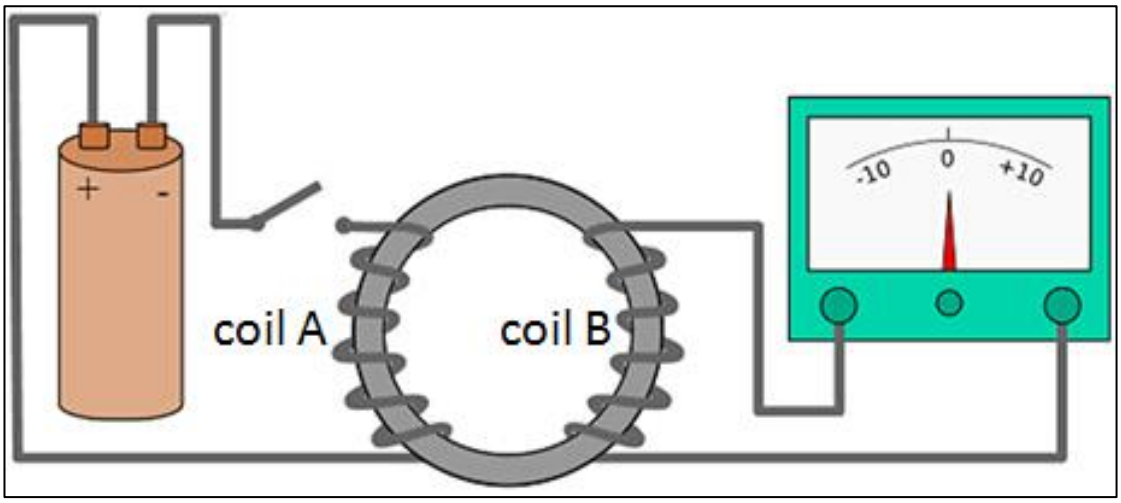

Figure 67 - 'The Iron Ring Experiment'

Wireless charging of electrical devices is becoming more common in modern day technologies, including devices such as wireless electric toothbrushes and mobile phones. They take advantage of this practice by allowing their internal batteries to be charged without the need of direct cables. Wireless charging of implantable devices is currently used in devices such as cochlear implants and cardiac pacemakers, where a primary coil is connected to a charging source and positioned on the surface of the skin and the secondary coil resides within the body. A main factor in the efficiency of wireless charging of implantable devices is the distance between the primary and secondary coils and the nature of the physical matter that separates them. The presence of tissues such as muscle and bone between the primary and secondary coils may reduce the strength of the magnetic field if positioned deeper within the body. (Culbertson 2015)

The use of induction charging eliminates the need for high capacity primary batteries to be used for implantable medical devices. Smaller capacity secondary batteries can be used and ‘topped up’ when needed.

8.1.3. Energy harvesting

Energy harvesting techniques hold a number of benefits over primary implantable batteries and induction charging as it collects the energy to recharge a secondary battery from its surroundings, whether that is heat produced by the body, chemical reactions within the body or kinetic energy produced by bodily movements. All these sources of energy can be harnessed and converted into electrical energy to recharge a battery, this eliminates any need of outside intervention as it is its own self-contained system.

8.1.3.1. Thermoelectric Energy Harvesting

Thermoelectric generators are used to harvest energy from temperature gradients. The amount of the power harvested is (in an ideal system where no energy is lost to the environment) directly proportional to the magnitude of the temperature gradient. (Snyder 2008)

The idea of generating electricity from a temperature gradient is a simple one, discovered by T.J. Seebeck in 1831 who twisted 2 wires of different materials together and altered the temperature at one end. It was noted that with this change in temperature caused a current to flow in the circuit. The output voltage generated increased proportionally to the temperature gradient. (Sterntech)

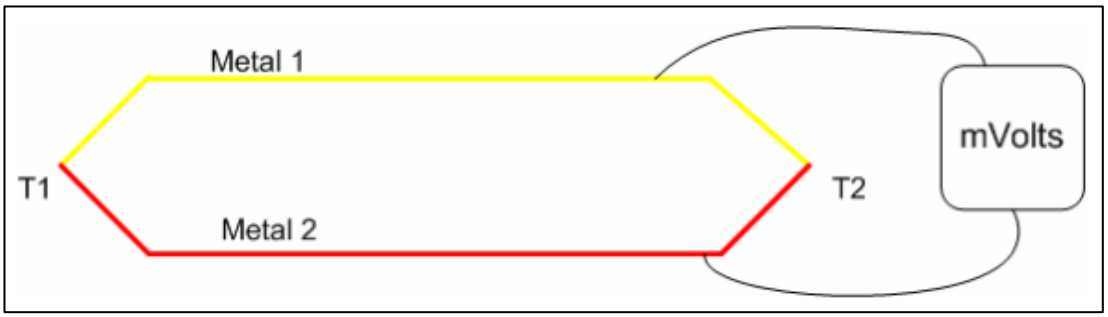

Figure 68 - T.J. Seebecks' Thermocouple Experiment (Sterntech)

For the idea of using thermoelectric generators for harvesting energy for implantable medical devices, it is important to look at the temperature gradients that are produced within the body (to utilise these harvesters most effectively, a significant temperature gradient is required.).

The normal core temperature of the human body is around 36-37°C. Although the body self regulates this core temperature to remain constant however the peripheral temperatures can change vastly depending on the environment. (Sue et al. 2012, Sircus 2013) Figure 69 below shows how temperatures of the human body differ depending on room temperature. It can be seen that the body experiences the highest temperature gradients when subject to colder conditions, even at a normal room temperature, the temperature of the torso remains fairly consistent throughout. The cooler temperatures occur in the distal aspects of the limbs. The difficulty is to obtain the most from an implanted thermoelectric generator would need to position one end of the probe in the core area where the highest temperature is recorded and the other in the cold temperatures of the distal limbs.

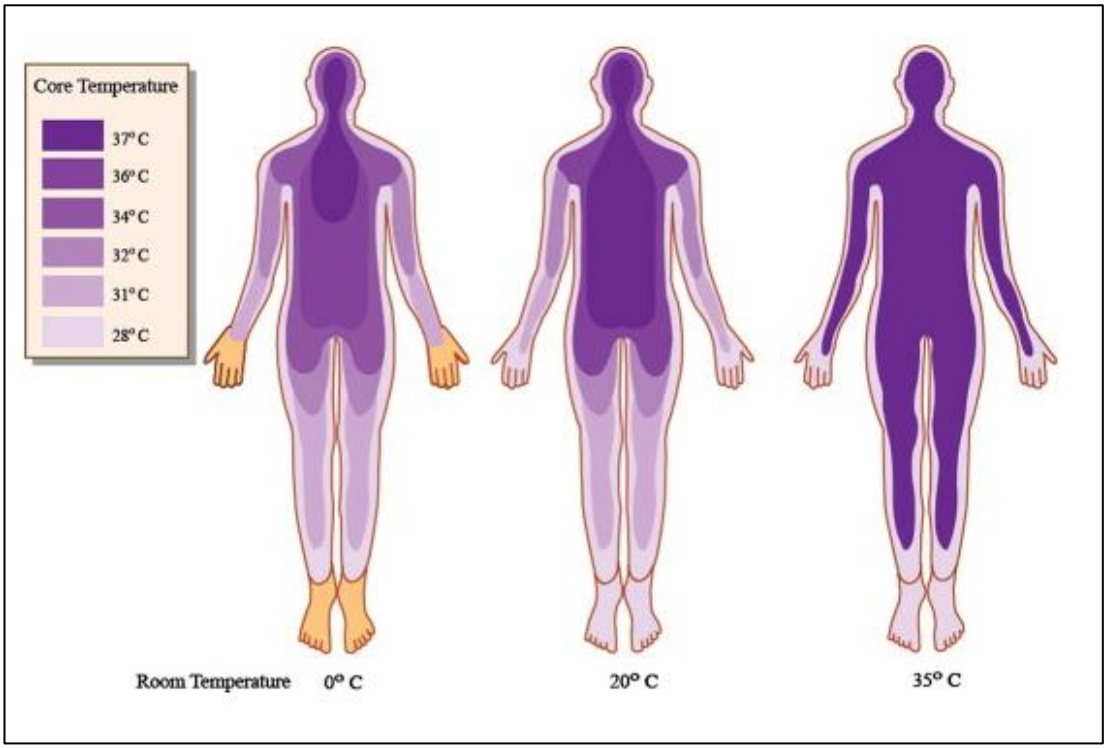

Figure 69 - Temperature Gradient of the Human Body (Sircus 2013)

Thermoelectric generators are commercially available for use in temperature monitoring systems for electrical and mechanical applications where power generation needs are fairly small. However, these generators can be bulky in size. The company Perpetua Power Source Technologies Inc. (Oregon, USA) have attempted to resolve these limitations and have designed a flexible, thermoelectric generator patch patented TEGwear. Compared to other commercially available thermoelectric generators, the flexible nature of this patch would allow it to be implanted easily into the body without causing tissue damage or patient discomfort, which would most certainly occur with the larger, more ridged industrial generators.

Unfortunately, a single TEGwear generator of size 14mm x 13mm only generates 5.2mV per 1°C. That means that for a temperature difference of 9°C (The max temperature gradient depicted in Figure 71) 25 TEG's would be required to produce the output voltage of 1.2V (the same voltage produced by a regular AAA battery) resulting in a surface area of 70mm x 65mm. As appealing as this is, the downfall for this technology is that the temperature gradient is needed, across the thickness of the patch which is only 2.1mm. This is impractical for the device.

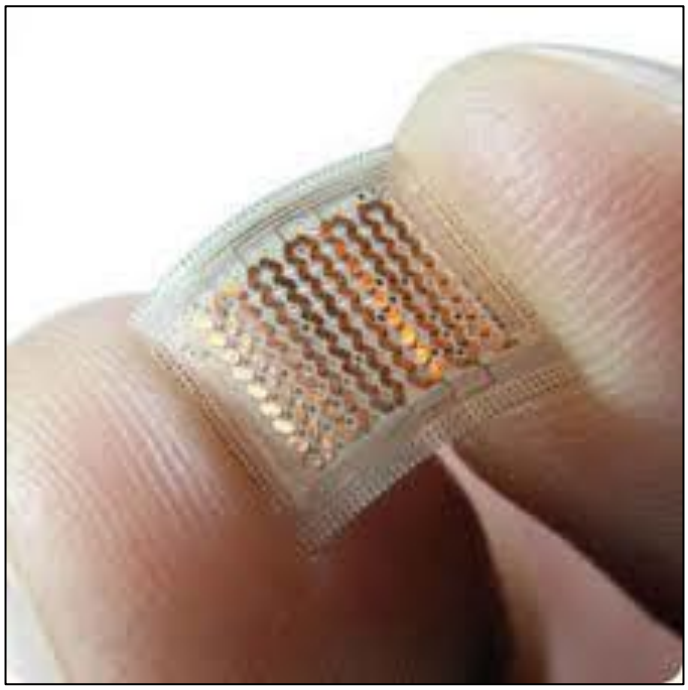

Figure 70- TEGwear Thermoelectric Generator

8.1.3.2. Biological/Chemical Energy Harvesting

There are a number of chemical energy sources found within the body. With the use of a micro-biofuel energy harvester, the chemical reactions within the body hold a lot of potential for harvesting this energy for use with implantable technologies. For example, micro-biofuel harvester using a glucose oxidase based anode and cytochrome cathode has been proven to produce an electric current, through glucose stores within the body. (Davis et al. 2007) These chemical energy harvesting devices are generally used for low powered sensors and would fail to provide enough power for this application.

8.1.3.3. Piezoelectric Energy Harvesting

Piezoelectric energy harvesting utilises the same principles of a piezoelectric motor *(discussed in Chapter 6.4.2.2.)* only in reverse. This means that instead of a piezoelectric/ ultrasonic motor which uses a voltage applied to a piezoelectric polymer or ceramic causing it to deform, a voltage can be generated by the deformation of a piezoelectric polymer or ceramic. This allows for kinetic movement from environmental sources such as natural vibrations and muscle movement to be stored to power certain electrical components.

There is an abundance of kinetic energy produced by both *voluntary* and *involuntary* muscle movement within the body. Voluntary muscle movement includes activities such as walking or arm movements. These movements however, are not a reliable and consistent source of movement so utilising this type of movement, the energy produced could be best stored up and used as needed rather than a continuous supply.

Involuntary muscle movements are those originating from the cardiovascular and respiratory systems along with others that are in constant motion. These provide a steady source of energy that can be used for technologies that require a more consistent source of power. For example,

cardiac muscle is in a constant state of motion throughout a person's lifetime and therefore this makes it an ideal source to harvest energy.

An example of harvesting energy from cardiac muscle was demonstrated by Zurbuchen et al (2013) who utilised the mass imbalance oscillation generator (found in commercially available automatic wrist watches) to harvest the mechanical energy of the beating heart. (Zurbuchen et al. 2013)

Like that of the cardiovascular system, the respiratory system (including the diaphragm) are generally in motion throughout a lifetime. The lungs and diaphragm provide a steady state of low frequency high amplitude oscillations where the volume inside the ribcage can increase to around 70% with each breathing cycle. (Mengeot et al. 1985) Whereas the airways encounter high frequency, low amplitude vibrations as air passes though.

One of the most common materials used for piezoelectric energy harvesters is lead zirconate titanate (PZT) which can be found in devices such as ultrasound transducers, piezoelectric motors and actuators. It is a ceramic with strong piezoelectric properties, which make it ideal for structural monitoring because of its capability of detecting small vibrations. However, as with all ceramics, this material is very brittle, and it would be hard to use for harvesting energy within the body without impeding the function of internal structures and tissues due to its regitity. Some manufactures however are claiming to produce 'flexible' PZT materials which are investigated in Chapter 8.2.

Research into another piezoelectric material is proving more hopeful in the advancements of a flexible energy harvester - zinc-oxide (ZnO) nanowires. Wang et al (2006) focused on harnessing the piezoelectric and semi conductive properties of ZnO by creating arrays of nanowires; when deformed these nanowires produce an electrical current. (Wang et al. 2006) This technique was advanced by Qin et al (2008), where nanowires were grown around strands of Kevlar. A gold-coated strand of this material was then wound round a single uncoated strand

and pulled along its surface. The nanowires rubbed over one another to produce the electrical current. (Qin et al. 2008) *(Figure 71)*

More recently, in 2014, Khan et al took this idea further and grew ZnO nanoneedles on a conductive fabric to overcome the flexibility issue that stunted the PZT generators. (Khan et al. 2014) This kind of fabric would prove beneficial to this application as its flexible properties would conform to the anatomy, harvesting energy from bodily movement without impeding functionality.

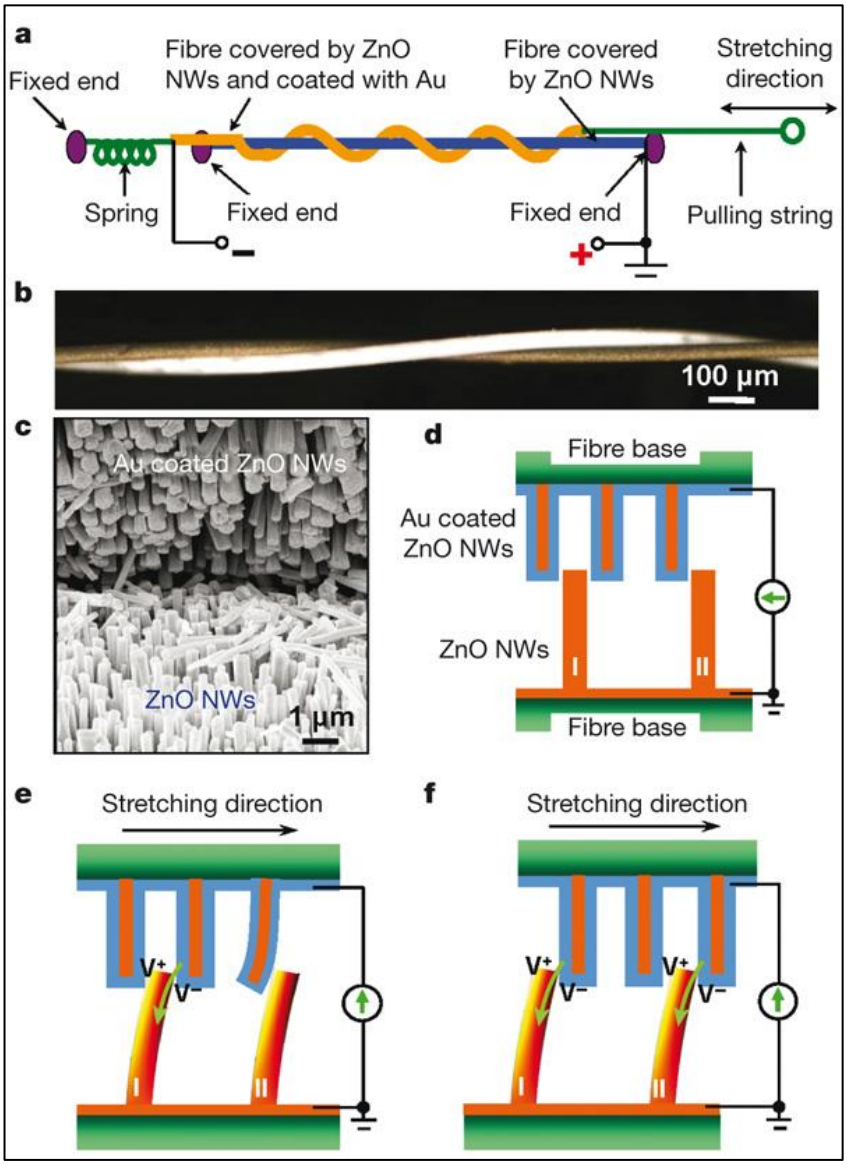

Figure 71 - ZnO Nanowire Experiment (Qin et al. 2008)

Developments in piezoelectric generators have grown rapidly over the last 10 years although the new technologies are still in their research phase and not yet commercially available. Therefore a closer examination in to materials that are currently on the market was conducted as to whether or not current technologies would be acceptable for powering this device.

8.2. Feasibility report of readily available piezoelectric material.

In order for piezoelectric material to be a viable solution for powering this device the specification must be as follows:

I. **Flexibility** - Flexible enough to conform to the human anatomy without impairing function of the anatomy.

II. **Power Output** - Produce a high enough DC voltage and continuous current to charge a battery*.

III. **Size** - The harvesting device must be small enough for implantation onto ideally the diaphragm or other similar locations inside an infant's body in constant motion.

***** *Battery selected for this study is a Quallion (California, USA) implantable rechargeable lithium-ion battery (QL00370B) Specs: 410mAh, 3.6V. This was chosen due to its small size and current uses in medical device applications, boasting long life, ultra-high safety and reliability.*

8.2.1. Material Technical Information

A commercially available 'flexible' microfiber composite was chosen for this feasibility study which was 'SMART MATERIAL Micro fibre composite. Originally invented by NASA, these were then made commercially available by SMART MATERIAL in 2002, and they are used for many applications such as actuation, sensor modules and energy harvesting.

These MFC's are made up using rectangular PZT fibers sandwiched between layers of polyimide film. Electrodes are attached to the film in an integrated pattern allowing the voltage to pass to and from the piezoelectric fibers. *(Figure 72)* If the MFC is bent or distorted it produces an electrical potential. However the magnitude of this potential is based on how much the MFC is distorted. This can then be used on structures to sense small vibrations or bending/torsional stresses. If the magnitude is large enough it should be able to produce enough energy to power small electronic devices. This process is also reversible, which means that if a voltage is applied to the MFC then it can act as an actuator.

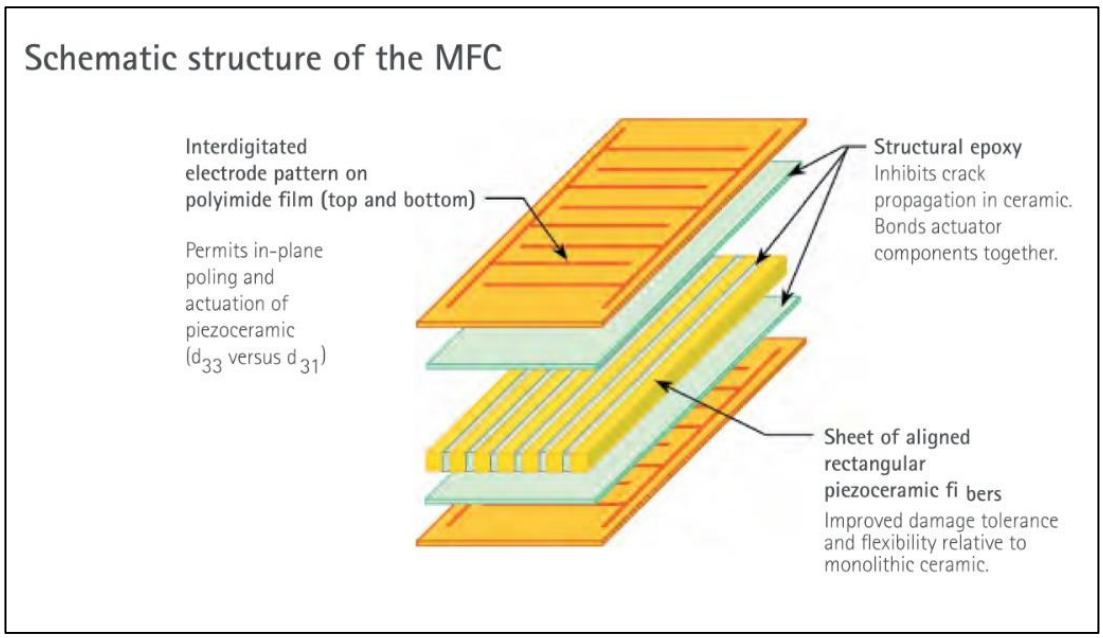

Figure 72 - Schematic from Smart Material MFC Brochure

8.2.2. Flexibility

For this study, flexibility of this material is important in being able to conform and move freely with the anatomy to which it is attached. Manually handling the material suggested that it may not be flexible enough for this application. However after a short time of 'wearing in'

involving bending the material back and forth, it became more compliant but still may be too ridged to attach anywhere without impairing the anatomy.

In order to try and overcome this stiffness, it was proposed that the polyimide film was removed from the active area of the MFC and then replaced with a thinner, more flexible coating of silicone. However it was found that the electrodes had been printed onto the underlying surface of the film, meaning it was impossible to remove the film without harming the electrodes. It was also discovered while taking the MFC apart that the fibres inside were quite brittle, suggesting that the MFC (though described as flexible) was not intended to be bent excessively. During the 'wearing in' of the MFC, the material was bent at a tighter angle, thus fracturing the fibers within the material. The fractures may reduce the performance of the MFC due to the damaged fibers.

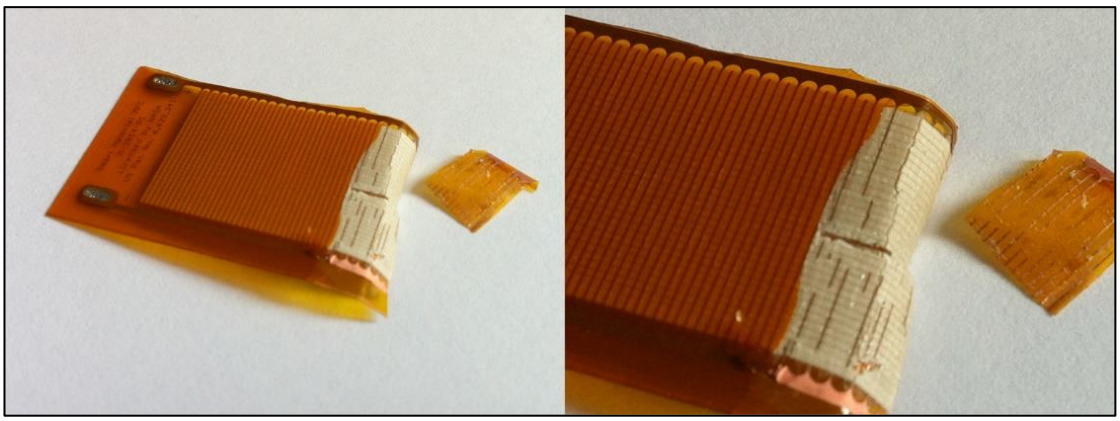

Figure 73 - Damage Caused to PZT Fibers inside MFC

8.2.3. Power Output

In order to investigate the energy output of the MFC, a mechanical model was designed to simulate the low frequency oscillations of the diaphragm. This comprised of a silicone membrane stretched across a wooden o-ring and a high torque, Crouzet motor with gearbox, to reduce the speed down to imitate that of a breathing cycle. Attached to the motor shaft was

a custom prop positioned perpendicularly underneath. *(Figure 74)* An MFC with surface area of 85x28mm was attached to the silicone membrane of the model. As the motor rotated, it caused the prop to push the silicone membrane up and deform the MFC. The oscillating frequency of the diaphragm was dependent on the motor speed. Two different frequencies were examined using a digital oscilloscope providing a read out of both minimum and maximum voltages along with the DC average.

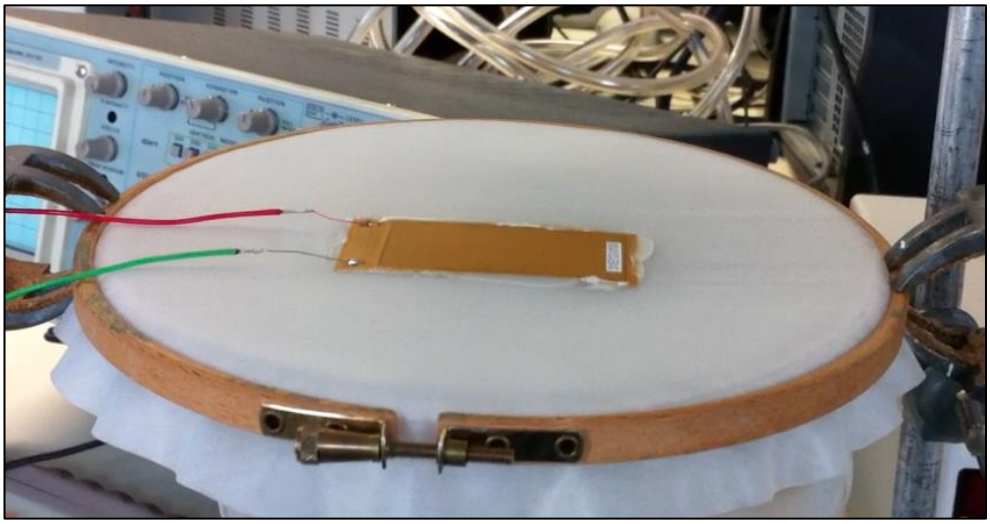

Figure 74 - Smart Material Piezoelectric Generator on Silicone Diaphragm Test Rig

The results obtained from this experiment are detailed in the table below.

Oscillating Frequency (Hz)	**Maximum Voltage (mV)**	**Minimum Voltage (mV)**	**DC Average (mV)**
0.45	8724	-5292	163.6
0.36	7866	-5102	298.7

Table 6 - MFC output Voltages

The data showed that with a low operating frequency the MFC is capable of producing up to 8.7V. Since the MFC is in constant movement, this maximum voltage is produced when the

MFC is in mid phase (maximum displacement). Due to this constant movement a range of voltages are produced and the DC average value is recorded. It was found that the **lower the oscillating frequency the higher the DC average**. This value will be the one used for the battery charge calculations to follow.

Figure 75 shows oscilloscope trace depicting clearly when the MFC is at maximum displacement. It can also be seen that even the small vibrations of the diaphragm are producing noise, which indicated the sensitivity of the MFCs. This could mean that the placement of the MFC does not have to be on a low frequency structure but could instead be attached to a structure that is subject to small vibrations, such as the throat.

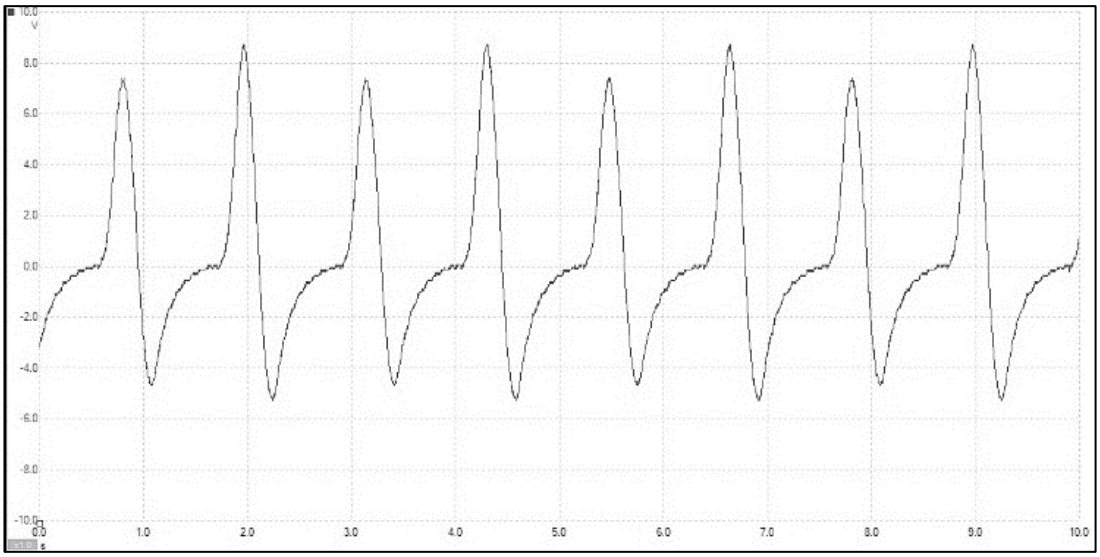

Figure 75 - Electronic Ocilloscope Trace of Smart Material Piezoelectric Generator

In order to be capable of charging the battery, the material needs to be able to produce a voltage equal to or slightly higher than that of the battery (in this case 3.6V). Taking in to consideration **the average DC voltage produced by the material is only 299mV this value is much lower than what is needed to charge the 3.6V battery.** The only way to achieve this value at these low frequencies would be by adding additional MFC's in series. However, more MFCs would

unacceptably increase the surface area of the technology. The MFC quantity was then calculated to asses this feasibility.

8.2.4. Size

Calculation for **number of MFC's required**:

$$No.of\ MFC's = \frac{V_{Battery}}{V_{MFC}}$$

$$= \frac{3.6}{0.299}$$

$$= 12.04\ \therefore \mathbf{13}\ \boldsymbol{MFC's}$$

It would take 13 MFC's to produce the required minimum voltage required to charge the battery. **Since 1 MFC has the surface area of 23.8cm^2, 13 of these MFC's would be 309cm^2, which is an excessive dimension for this application.**

Another issue with using MFCs to charge a battery is the current required. The time it takes to charge a battery is dependent on the amount of current that there is in the charging circuit; i.e., the less current there is the longer it will take to charge the battery.

To calculate the current required to charge the battery depends on 2 variables; the battery capacity and the length of time allocated to charging the battery.

In this case the battery capacity is 410mAh, and the assumption of this calculation is that the battery is running for 1 full day every 2 weeks. The continuous current needed to charge the battery can be calculated as follows:

Number of hours for full charge:

2 weeks = 336 hours

1 day = 24 hours

Maximum time for full charge (MTFC) = 312 hours

Battery Capacity (BC) = 410mAh

CRC (Charge Rate Current) = to be determined

Therefore, continuous current needed to charge battery (Assuming 0% efficiency loss):

$$MTFC = \frac{\left[\left(\frac{BC}{CRC}\right) * 10\right]}{10}$$

$$CRC = \frac{\left[\left(\frac{BC}{MTFC}\right) * 10\right]}{10}$$

$$CRC = \frac{\left[\left(\frac{410}{312}\right) * 10\right]}{10}$$

$$= \mathbf{1.314}\boldsymbol{mA}$$

This means that for the battery to reach full charge, it needs to have a constant current of at least 1.314mA. This is entirely possible because in order to produce a current for charging the battery a small resistance (EMF) will need to be applied. This will be present in the chargeable battery and should not need to be in the external circuitry. This theory has been examined by applying small load resistors into the circuit (10Ω - 390Ω). Adding the **10Ω** resulted in

minimal drop to the average DC output voltage (299mV to 255mV) while generating a current of around **20-24 mA** more than enough needed for this application.

A possibility may be that the voltage output of the MFC will decrease when the EMF resistance is introduced into the charging circuit, meaning a larger number of MFCs would be required to reach the minimum charging voltage of 3.6V.

8.2.5. Review of the use of Piezoelectric Technologies

Flexible piezoelectric technology is very much still in its infancy when it comes to energy harvesting and the technology that is commercially available is unsuitable for this application (requiring a total surface area of 309cm^2 to produce the constant DC voltage required). Also the maximum voltages produced may be too high and cause damage to the battery. In Summary;

- Flexibility of MFCs are poor for this application. However they are extremely sensitive so possible to position on a variety of locations.
- They produce a small DC average output voltage; large number of MFCs required to meet voltage needs.
- Current depends on the EMF of battery or external resistance.
- Maximum voltage may have detrimental effects on the battery (possible damage/ reduced efficiency).

8.3. Understanding of wireless energy transfer

Since it may not be feasible to power the device using energy harvesting techniques, it would be beneficial to look further into recharging the battery in another minimally invasive way. This could be achieved through the use of induction charging *(discussed in Chapter 8.1.2.)* and involves the use of an induction coil connected to the implanted battery and positioned just below the skin. Another external coil is placed externally when charging is required, and this would allow the battery to be charged wirelessly without the need for replacing the battery. It is not a completely independent solution like that of energy harvesting but it does not require any additional surgeries in order to replace the batteries when needed.

In order to obtain a further understanding of this charging method, a simple induction circuit was fabricated and tested to see how possible it was to transmit power wirelessly.

8.3.1. Induction Power Transfer Experimentation

In order to obtain further understanding of near field induction power transfer, a small experiment was carried out to examine the strengths and weaknesses of using this as a viable non-invasive energy charging solution for the proposed device.

Firstly, a simple test was carried out using commercially available induction coils. (RS,UK), the primary circuit coil was made of thick copper wire wound in a single layer on a steel plate. A magnet was positioned in the centre of this coil in order to enhance the magnetic field that would be produced by the current flowing through the coils. A 0.022µF capacitor was placed in parallel between the coil and a function generator. This function generator was set at 15kHz, providing the sinusoidal current needed to produce a magnetic field.

The secondary circuit consisted of a matching coil and capacitor set-up, with an LED was attached to each end *(Figure 76).*

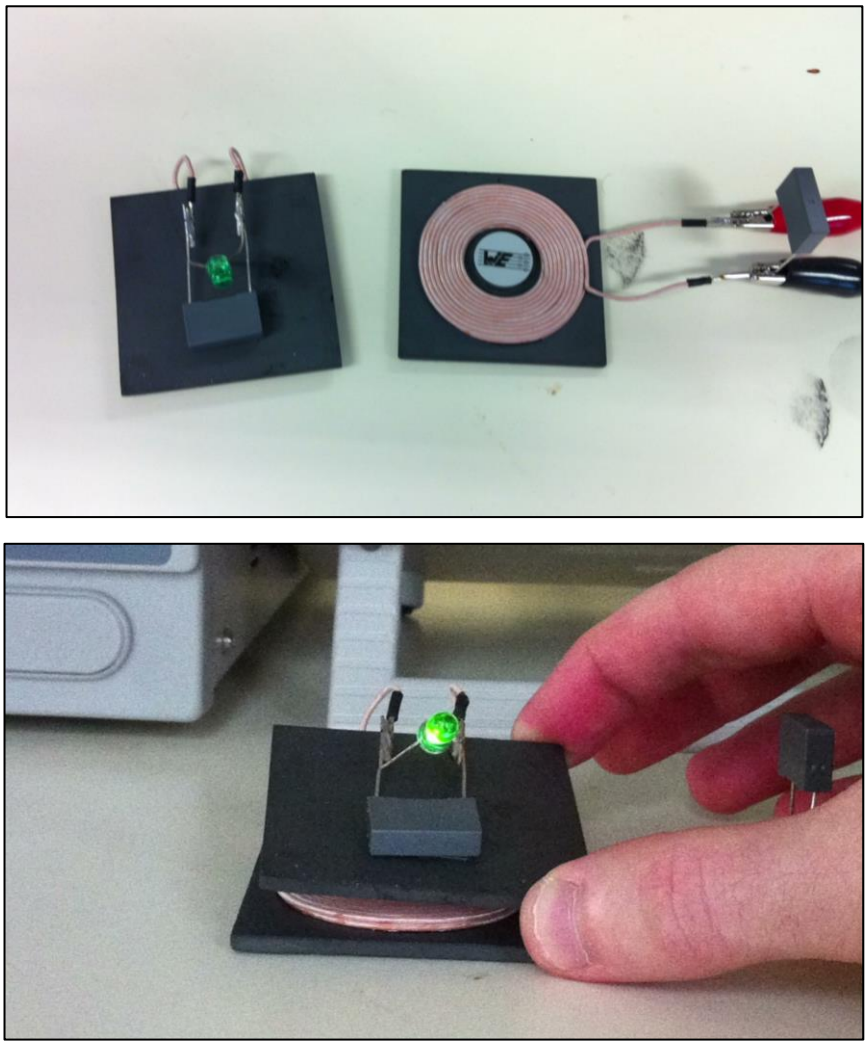

Figure 76 - Commercially Available Induction Coil Testing

When the system was switched on, the stand alone secondary coil was positioned above the primary coil and the LED illuminated, when the gap between the coils decreased, the LED brightness increased, this shows that the closer the coils are to one another the more efficient the power transfer is. It was also observed that when the secondary coil was moved left and right over the primary, the LED brightness altered. This gives a visual representation of the magnetic field. From this it can be seen that positioning also plays a large part in the efficiency of induction wireless power transfer.

The experiment was then repeated with ‘home made’ coils. This was to examine if a difference in size and wire turns would affect the power transferred. These were constructed out of

0.56mm insulated copper wire. The primary coil consisted of 200 turns of wire at 120mm across, and the secondary 100 turns at 70mm across. The rest of the experimental set up remained the same.

The results were similar to that of the industry manufactured coils, the alternating brightness of the light mapped out the magnetic field. The size of the coils was not as important as first imagined, therefore a larger coil can be used externally as the primary coil, producing a larger magnetic field and a less invasive coil subcutaneously to sufficiently transfer the power. The larger magnetic field from the primary coil will give more room for error when positioning against the secondary.

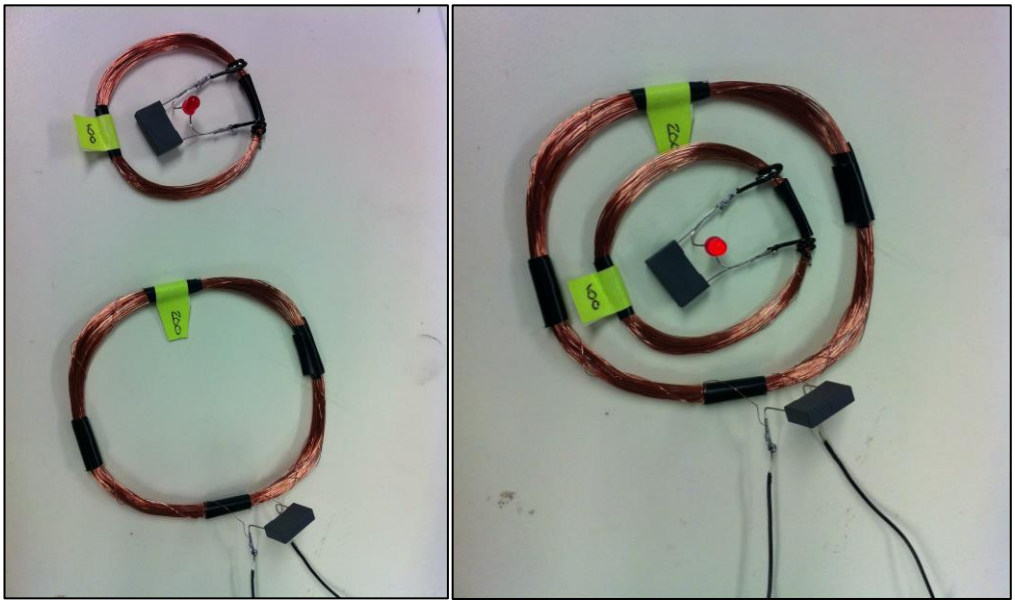

Figure 77 - Hand Made Induction Coil Testing

8.4. Power Selection

From both piezoelectric and induction theory and testing it was decided that the best method for powering/ recharging the implantable device in the long-term would be induction charging. Current technologies in piezoelectric materials are not sufficient enough to accommodate the requirements for this device, not just power generation but conformability for implantation.

For short term prototype testing, the focus will be on the expansion of the device rather than the functionality of the charging system and therefor high capacity batteries will be used and located externally to allow the device to be powered throughout the short term experiments without the need for recharging or replacement. However in the future, promising developing technologies like the piezoelectric fabrics could indeed prove beneficial.

Induction charging is an established technique for implantable medical devices and although imperfect, wireless power technologies exist commercially and are simple to design and manufacture. Further testing would be required to determine if the power required for this device would be safe for wireless transfer as it is currently only used for low powered implantable devices (3V pacemakers being the highest). Possible damage to tissues by heat production from these coils could be an issue when using larger currents and voltages.

8.5. Control System

The final device being developed in this project has an active life cycle of 12 years. It is clearly impractical to test the device over that length of time, and therefore an accelerated test was be carried out over a period of 30 days. During these 30 days the device expanded for 30 seconds each day until it reached day 30 where it would have reached full expansion. A control system was designed to achieve this schedule.

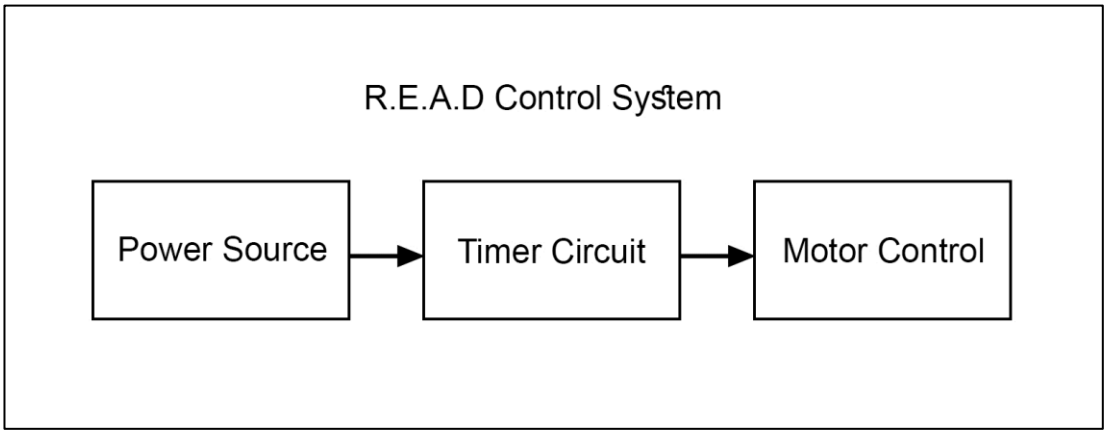

Figure 78 - R.E.A.D Control System

8.5.1. Motor Speed and Control

The MAXON Motors EC6 came with its own motor control board which was used alongside a custom time circuit. This would mean that the motor speed and direction could be set and controlled, either on or off, by the attached timer. Initially a number of variables had to be determined. Firstly the input speed of the motor, which could be reverse calculated from determining the overall distance the strip needed to be expanded.

Then, the expansion distance had to be calculated. The device would function from an initial diameter of 12mm to a final diameter of 20mm. This means a change in circumference of 25.13mm (the length of strip that passes through the worm gear.)

Calculations for the input motor speed were as follows:

Distance travelled per day

$$Travel\ distance = \frac{distance\ of\ travel}{number\ of\ days}$$

$$= \frac{25.13}{30}$$

$$= 0.838mm/day$$

Distance travelled in 1rpm = axial pitch of the worm gear = 0.628mm

Therefore:

$$1rpm = 0.628mm$$

Then

$$1.33rpm = 0.838mm$$

Since it has to cover this distance in 30 seconds per day

$$rpm = \frac{1.33}{2}$$

$$= 0.665rpm$$

Therefore, the output speed of the motors 854:1 gear box needs to be 0.665 rpm, and the output speed of the motor needed to allow this is 568rpm.

The initial motor control board provided by MAXON motors to use in conjunction with testing the EC6 motor was the EPOS2 24/2 positioning controller, which could also be used for a number of MAXON branded motors. (APPENDIX IV) This was then programmed though USB connection using MAXONs' own EPOS2 software. A new profile was made for this iteration, entering the required details using the EPOS2 software's 'Setup Wizard'. Information entered corresponded to the model of motor that was being used, in this case the EC6. This allowed for the motor controller to run its own optimising and tuning tests which checked that all the components such as the hall sensors were functioning correctly. The details required for this tuning possess were as follows:

- EC Motor
- Hall Sensor
- Max Speed: 40000 rpm
- Nominal Current: 265 mA
- Max Output Current: 314 mA
- Thermal Time Constant: 0.2 sec
- Number of pole pairs: 1
- Max following error: 2000 qc

These values along with other motor information can be found on the manufactures data sheet in APPENDIX I.

Once tuning was complete, the motor speed calculated was entered into the software and stored onto the internal memory of the motor board. This allowed for the motor and controller to be run independently of the MAXON programming software when a connection is made between ports 1 and 8 on the controller board. A manual activation switch was connected in-between these two ports so that the motor system could be activated for testing independent of the timer control circuit which will later be discussed.

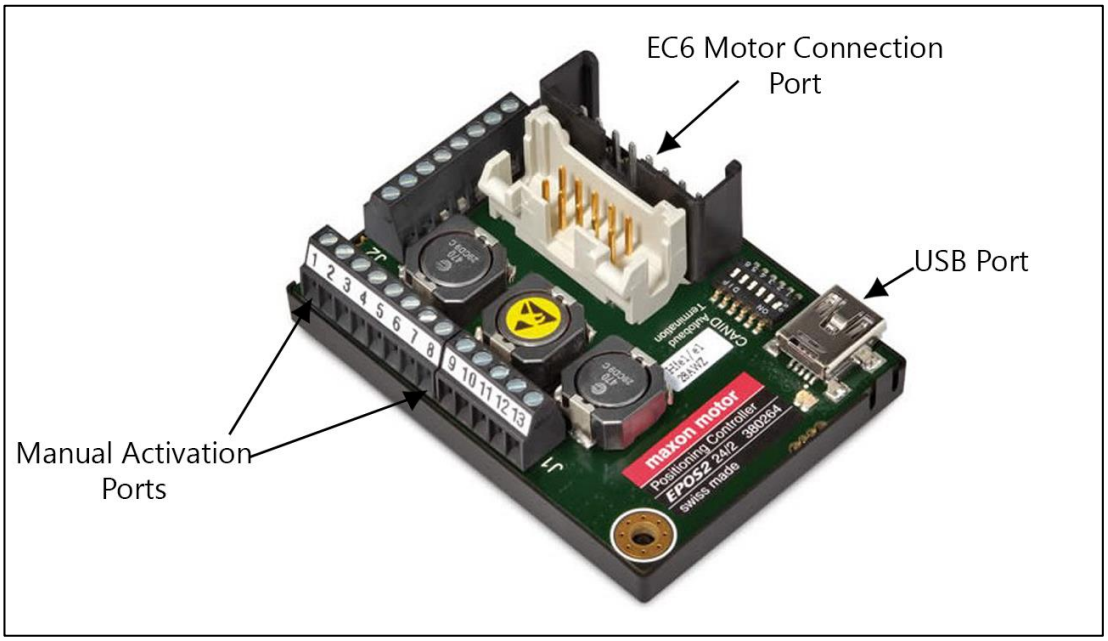

Figure 79 - EPOS 24/2 Motor Positioning Controller

8.5.2. 1st Iteration Timer Circuit

Now that the motor had a set speed the timer circuit could be designed. It comprised of a CD4060BC 14-Stage binary counter used in conjunction with a 555IC timer. The binary counter would determine the length of time the motor wasn't running for (ie 24 hours) and the 555IC specified the 'ON' time for the motor. The binary counter relayed the time, doubling

its value until it reached 86,016 seconds. This was close enough to the 24 hours (86,400 seconds) and once reached it activated the 555 timer which closed the parallel loop for the motor controller allowing it to run for 30 seconds before switching off and the process would be repeated.

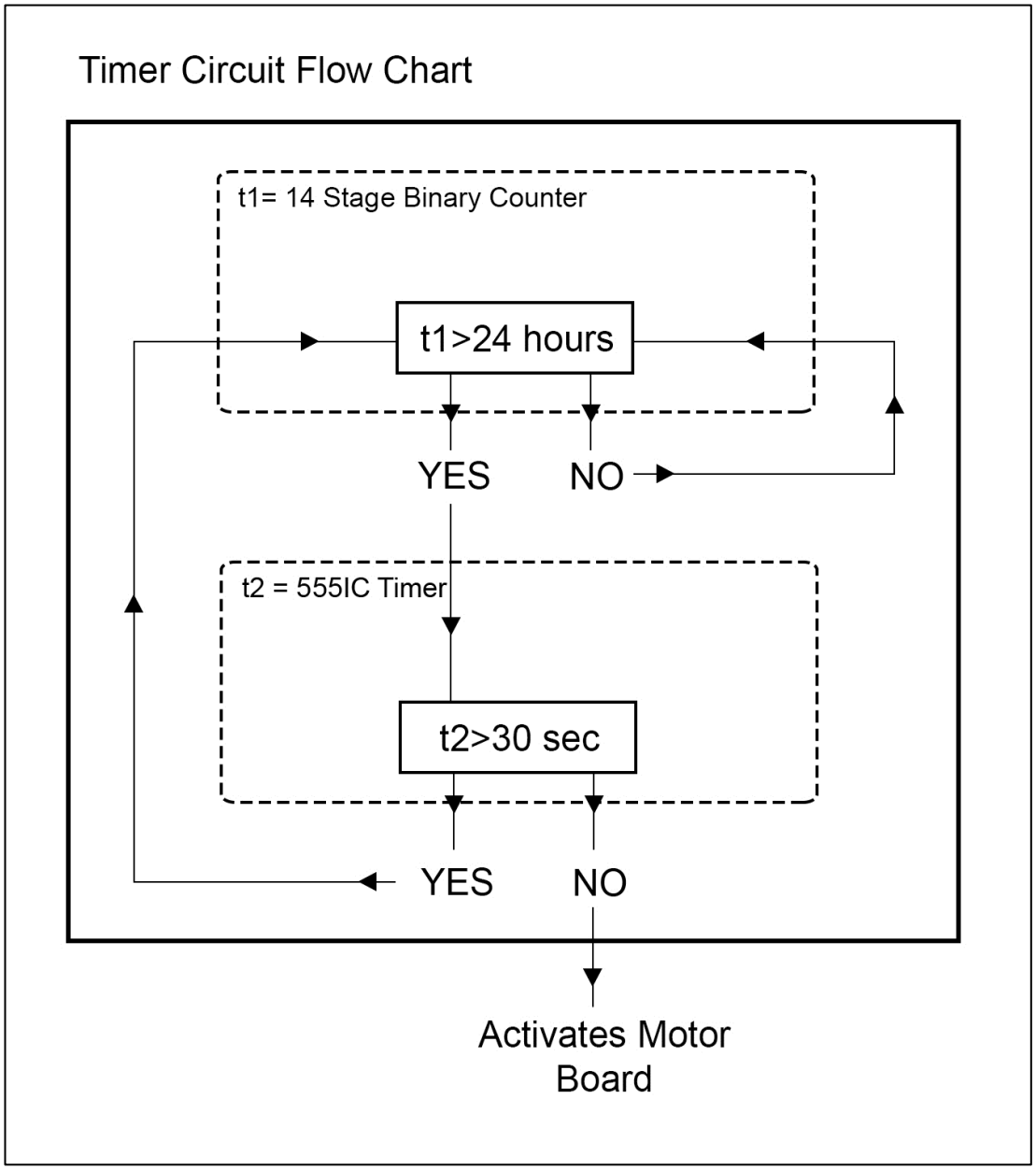

Figure 80 - Timer Circuit Flow Chart

These components were housed alongside the battery pack in a custom designed box that would be mounted on the back of the animal during the testing procedure. The control box contained the battery pack, charging terminals for easy recharging of the batteries without having to dismantle the box, the timer circuit and the motor circuit. The motor cables were to be fed percutaneously through the skin at the animal testing stage and screwed into an externally mounted terminal feeding through to the motor control board once the device had been implanted and the whole system activated by a switch mounted on the side. A manual motor activation switch was housed inside for testing purposes. *(Figure 81)*

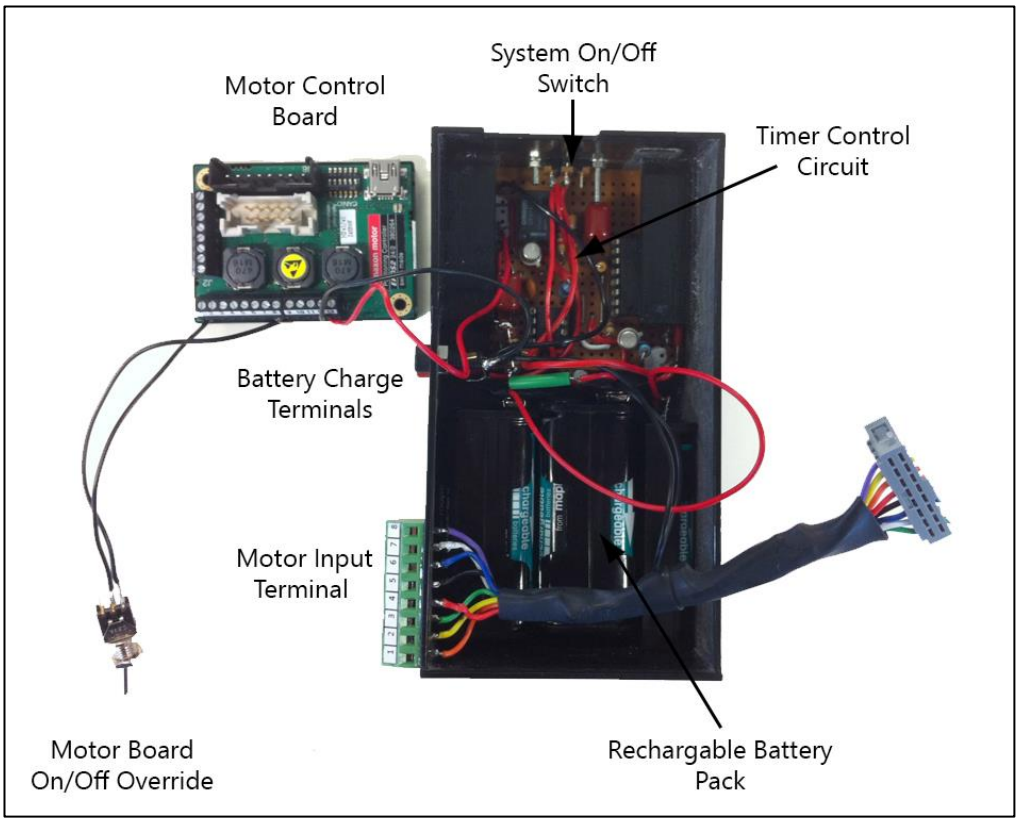

Figure 81 - First Iteration R.E.A.D. Control System

As the box was being positioned externally, the dimentions for the controller was not a constraint, so the batteries selected for the control box were 10 x 1.2V high capacity rechargable AAA batteries. These provided a total output voltage of 12V with a capacity of

950mAh. This is more than sufficient to power the motor controller operating at voltage of 12V (minimum operating voltage of 9V).

Chapter 9.

1st Implantation Series

9. 1st Implantation Series

The purpose of the first implantation, using cadaveric animals, was to determine any potential impediments that would need to be addressed for implantation in the live animal models. This procedure will test the implantation techniques while also examining device size and positioning limitations.

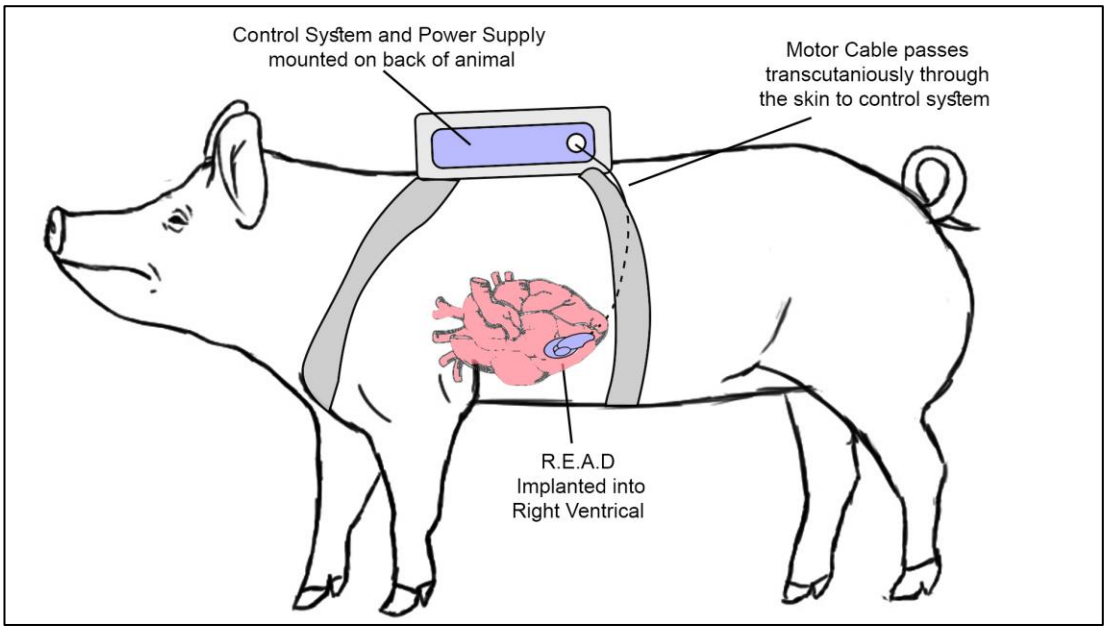

Figure 82 – Device implant location

9.1. Device Implantation

This study was carried out on a 12kg, male, landrace pig cadaver. The device would be implanted into the wall of the right ventricle, with the power and control cables passed transcutaneously to a backpack where the power supply and the device circuitry is housed. This is shown in figure 82 above.

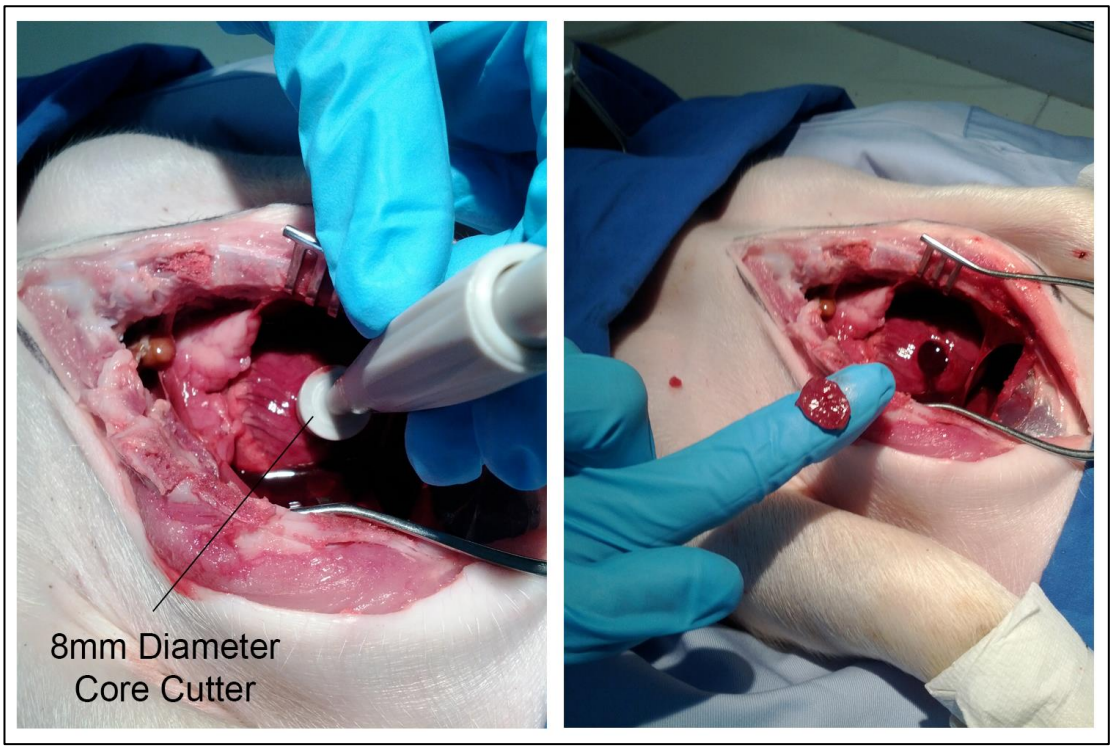

Figure 83 - Preparing the Right Ventricle for Device Implantation using 8mm Core Cutter

Once the sternum was cut, the chest was clamped open the heart required preperation for implantation of the device. This involved cutting an 8mm diameter hole in the right ventricle. This was achieved using an 8mm Harris Uni-Core cutter (Ted Pella, Inc, CA, USA). This cutter is used to cut and retrieve samples from tissues and specimens. This was important because it allowed the hole to be cut but also prevent the cut tissue from entering the ventricle which would be difficult to retrieve. This is shown in Figure 86.

In preparation for inserting the device into the right ventricle, the exterior sewing ring was removed along with the ring that would be placed on the inner wall of the ventricle. This made the device easier to insert in to the orifice created by the cutter and removed the obstruction of the outside sewing ring which would have reduced visibility of the suturing area. As a result of this increased visibility, the suture tools that were developed to aid in securing the device were not needed.

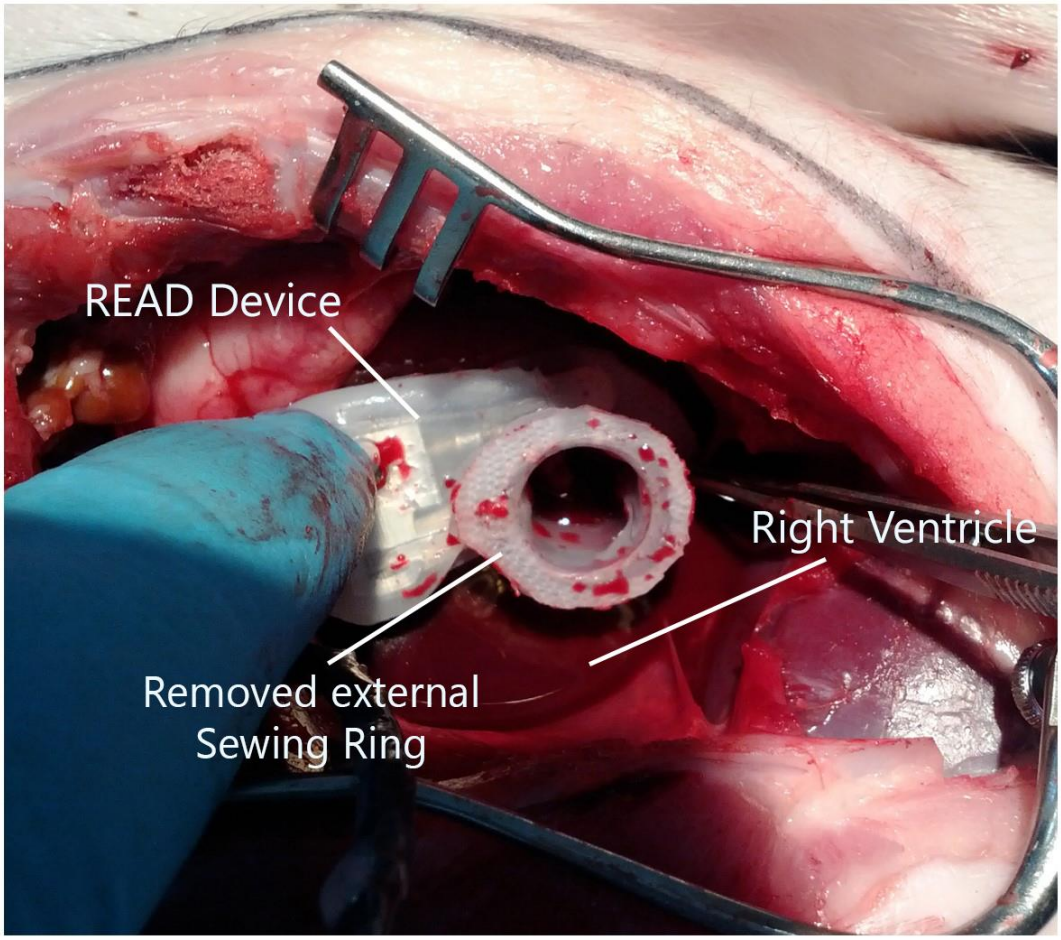

Figure 84 - Trimmed Device being sutured into place into the Right Ventricle

Once the sewing rings were removed, the device was sutured in place using 8 interrupted sutures. Once the device was sutured into place in the ventricle, it was clear that the device itself was too large for the application, this is depicted in Figure 84 where the device takes up a too much space within the chest cavity. If this device was implanted in live animal models, the chest would need to be closed, and with a device this size it would rest on the inner surface of the chest cavity. The proposed technology would be attached to either end of an implantable conduit and if the device remains this large, it would be impossible to attach a conduit to this device and have it function correctly without being impeded by the anatomy.

One area that was overlooked by the development of this first iteration which was made clear by this implantation that the orifice through the device would need to be blocked off. Since

these implantations are solely to test the expansion mechanism, the orifice which allows the redirection of blood flow through the conduit would need to be sealed. This could be done either by sealing the orifice off once the device had been sutured in place or have the device pre-sealed before implantation which would result in a change to the suturing technique as there would be no route to lower the pre-loaded suture tool.

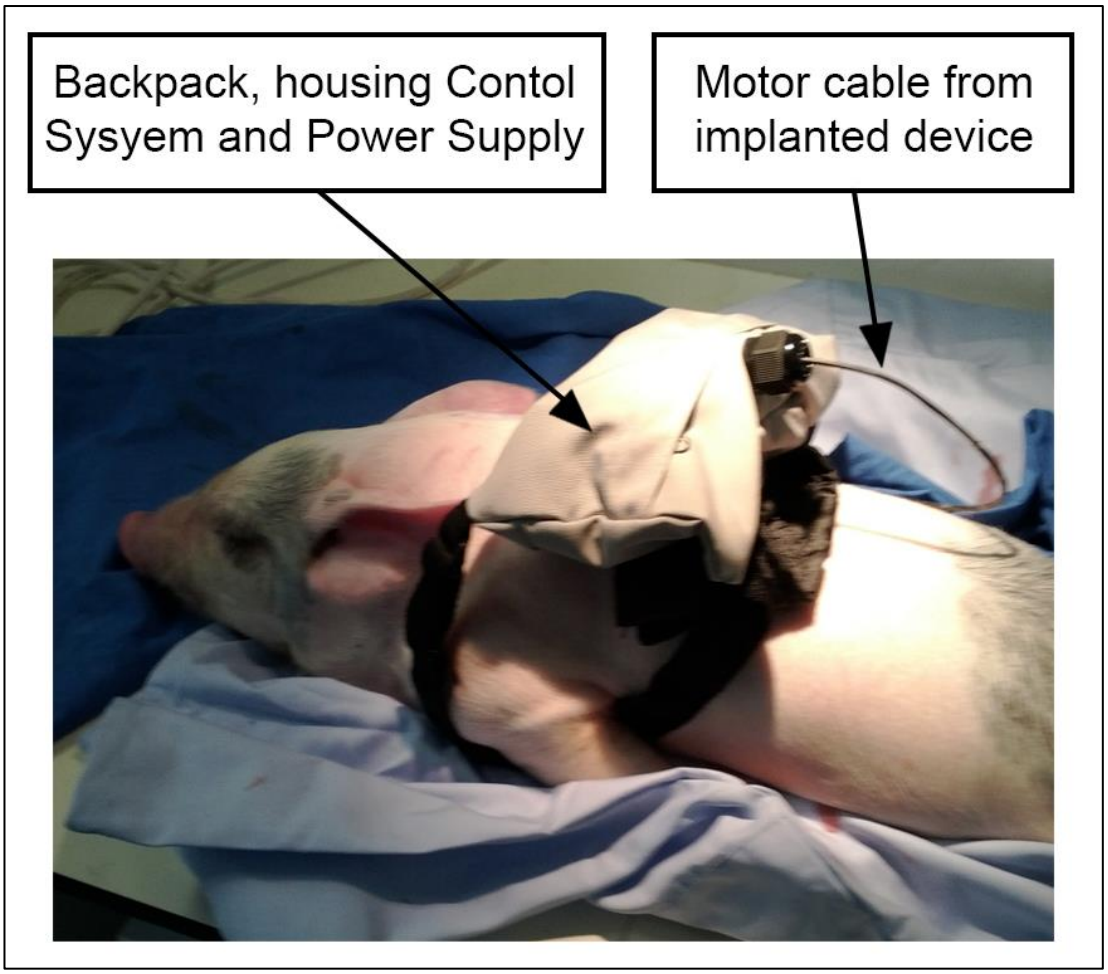

Figure 85 - Control System and Power Supply connected via cable through the skin to the implanted device

Another issue that emerged from this first implantation procedure was having the cable from the device fed through the skin to the power and control mechinisums placed in a pouch on the back of the animal. *(Figure 85)* It can be seen that the pouch is too large and combersome for the animal. Loose fitting straps and cabling would be vunerable to the everyday activities

of the animal and would be prone to being pulled and damaged, which would result in device failure and potential death.

At this stage a decision was taken to modify the technology, with emphisis on the following:

- The size of the active elements of the technology.
- Better approach to power and control cable rooting.

Chapter 10.

Concept Development – 2nd Iteration

10. Concept Development - 2nd Iteration

It was clear from the first iteration that device size was a concern. The second iteration of the device focused on reducing the size and weight of the device while maintaining optimal functionality. The basic design principle remained the same with the use of the worm gear to expand a stainless steel strip. The main focus was on miniaturising and optimising this design.

From the first iteration a number of components would be redesigned and adapted to improve device delivery. These components parts are detailed in *Figure 86.*

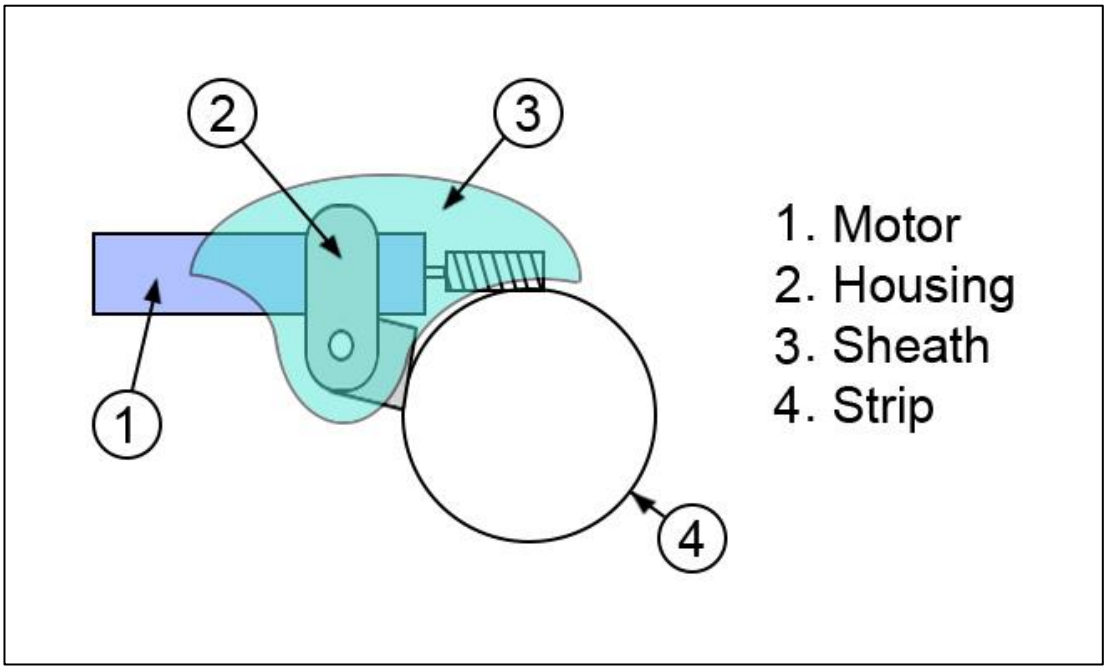

Figure 86 - Device components

10.1. Motor Selection (New Gear Head)

To reduce size, the existing EC6 motor which was used in the previous iteration was replaced with that of the smaller and lighter EC4. This motor utilised the same software and controller hardware of its predecessor, and benefits include reduction of the physical size and weight of the device. The motor had a smaller integrated gear head at 280:1. This reduced value would

be taken into consideration when the motor was programmed. *(see Chapter 10.7.2.1.)* Motor information found in APPENDIX IV.

10.2. Housing Design

By mimicking the design of the previous iteration, the aluminium housing which held the motor and arm that supported the strip which were manufactured by hand in the previous model were custom designed for this model. This would allow for easy replication of the device instead of hand cutting/filing and machining each part individually. Using CREO 3.0 CAD design software (PTC software, Massachusetts, USA) the basic design resembled that of the previous iteration with a main body, holding the motor and a pivoted arm that held the strip. *(Figure 87)*

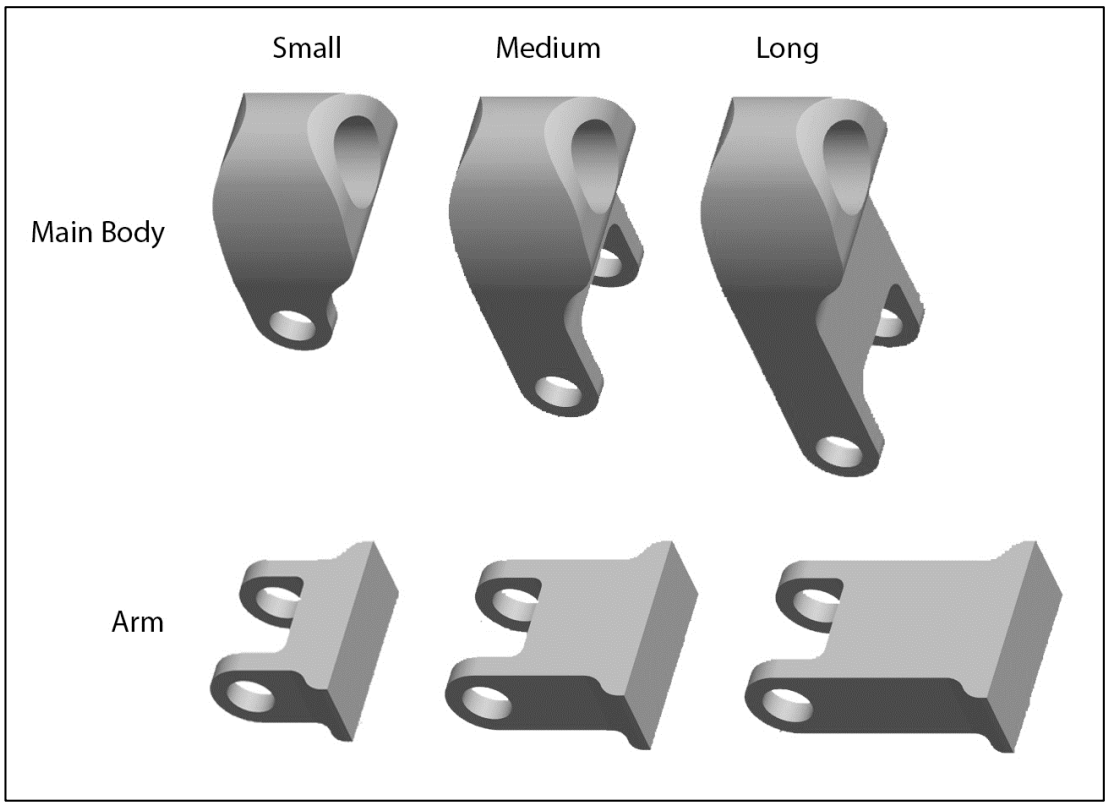

Figure 87 - Aluminium Housing Design

To obtain the optimal configuration, the parts were designed with 3 different leg sizes, to examine how effectively each combination held the strip onto the worm. The length of each

part was labelled as small, medium and long, at lengths of 3, 8 and 12 mm respectively. Combinations of each were assembled, making a total of 9 different iterations.

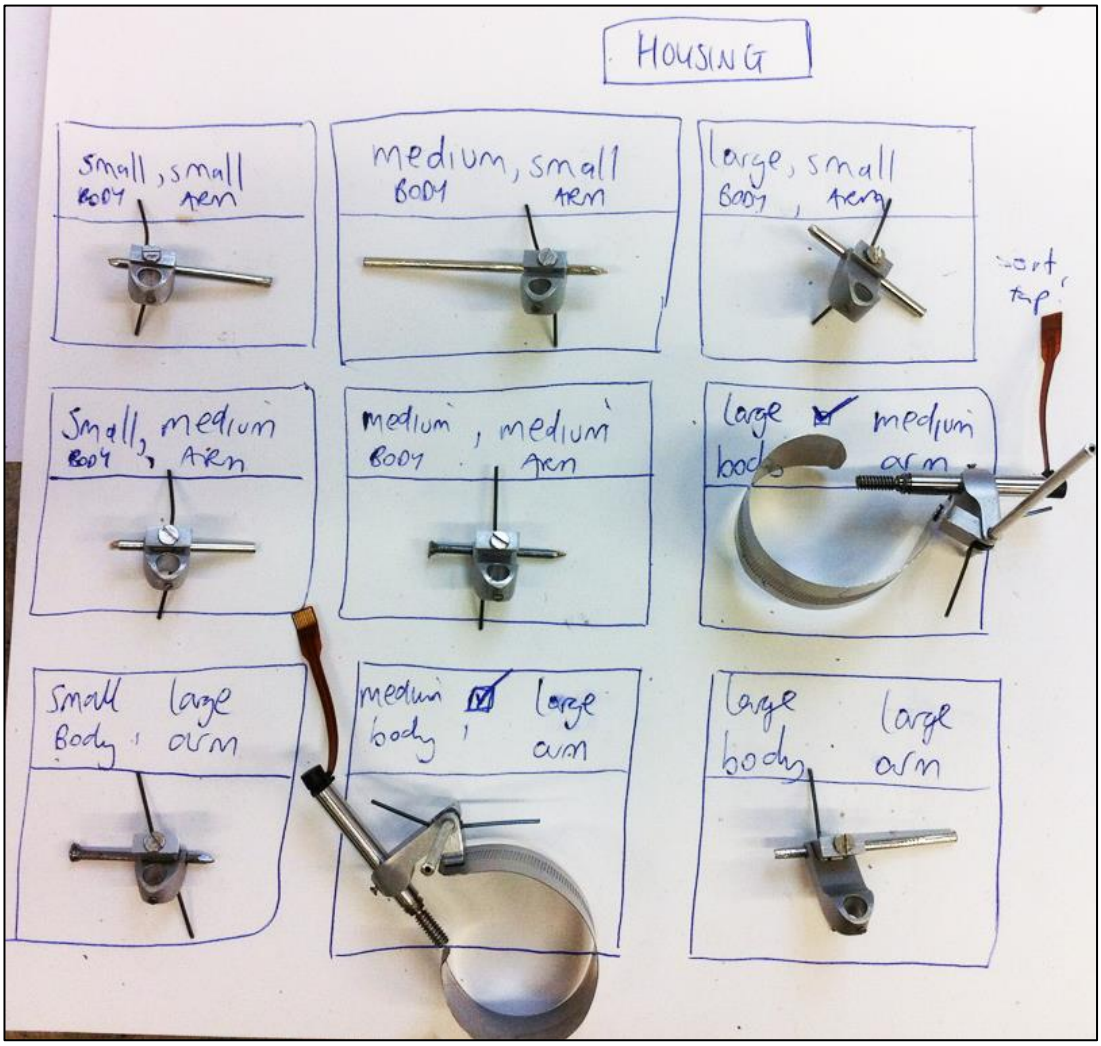

Figure 88 - Housing Testing to determine which held the strip securely most effectively.

It was decided that the combination of medium-medium would be used for this device. Other combinations either would not hold the strip securely, or deformed the strip making the device larger than desired. The medium-medium configuration held the strip in position successfully while keeping the desired small form.

10.3. Strip and Spring Selection

The strips used for this design did not change although, slight alterations had to be made to their shape by chamfering the corner to reduce the amount of excess strip material when it attached the arm. However, the spring used to pivot the main body and the arm had to be modified to take the new smaller structure into consideration. The torsion springs used previously were too large to fit in between the legs of the housing, and the legs themselves could not support the previous 3mm pin, so custom designed springs were manufactured for this purpose.

To obtain the highest force from a torsion spring there are two main variables to take into account: the thickness of the wire and the number of turns forming the spring. The previous device used 2 x 3 turn springs in order to achieve a force of 40mN. However, with the new smaller profile there was less space to work with so the thickness and/or number of turns would have to be altered to achieve the same result with a single spring. Manufactured by Irvine Springs (Ayrshire, UK), a number of springs were chosen and their force output studied with a mixture of different wire thicknesses ranging from 0.508mm to 0.71mm and either 1 or 2 coil turns. These were tested to determine which one would be adequate.

The force of each spring was manually calculated using the following formula:

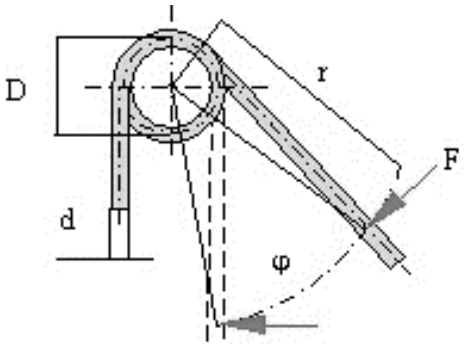

$$F = \frac{\pi}{32} \times \frac{d^3}{r} \times \sigma$$

Where:

F = Force (N)

d = wire diameter (mm)

r = distance from the centre to where force is being applied (mm)

D = Mid diameter of coil (mm)

n = Number of active turns

E = Modulus of Elasticity (MPa)

φ = angle of deformation (degrees)

σ = Bending Stress

To calculate the Force applied by the spring, first the bending stress (σ) must be calculated using the formula:

$$\varphi = \frac{2D\pi n}{Ed} \times \sigma \times \frac{180}{\pi}$$

The spring force of the smallest wire diameter of 0.508mm and 2 is calculated below:

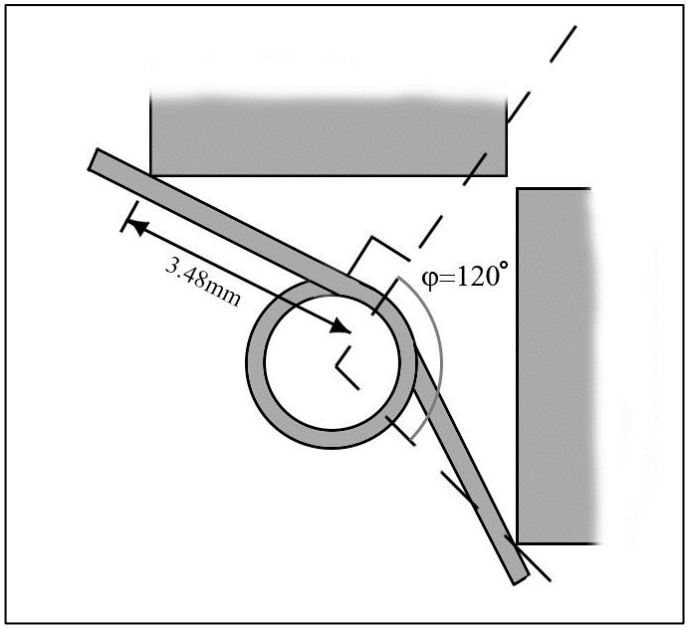

Figure 89 - Spring Positioning Diagram

Where:

φ = 120°

D = 2.608mm

n = 2

E = 207 MPa (value for spring Steel)

d = 0.508mm

r = 3.48mm

Note: The modulus of elasticity (E), deflection angle (φ), and the leg length (r) remained the same for all springs.

To find the bending stress (σ) can be found using the formula below:

$$\varphi = \frac{2D\pi n}{Ed} \times \sigma \times \frac{180}{\pi}$$

$$120 = \frac{2 * 2.608 * \pi * 2}{207 * 0.508} \times \sigma \times \frac{180}{\pi}$$

$$120 = \frac{32.77}{105.2} \times \sigma \times 57.30$$

$$120 = 0.312 \times \sigma \times 57.30$$

$$120 = 17.88 \times \sigma$$

$$\sigma = 6.71$$

Sub this value into original equation for Force:

$$F = \frac{\pi}{32} \times \frac{d^3}{r} \times \sigma$$

$$F = \frac{\pi}{32} \times \frac{0.508^3}{3.48} \times 6.71$$

$$F = 0.098 \times 0.038 \times 6.71$$

$$F = 0.024N$$

The force calculated for the spring of diameter 0.508mm with 2 turns is 24mN.

Table 7 shows the specification and calculated force values using the same method for all the springs tested. The force was also calculated for the original springs to match which springs gave the same output force. This value was a total of 40N for the 2 springs combined.

	Wire Diameter (mm)	Number of Turns	Mid Diameter (mm)	Bending Stress, σ	Force (mN)
1st Iteration	**0.6**	**3**	**4.1**	**3.37**	**20**
2nd Iteration	0.508	2	2.608	6.71	24
	0.508	1	2.608	13.42	49
	0.61	2	2.71	7.77	49
	0.61	1	2.71	15.52	99
	0.71	2	2.81	8.71	88
	0.71	1	2.81	17.44	176

Table 7 - Calculated Spring Properties

Circled in red in the table above depicts the values closest to the original value of 40N from the previous iteration. However, when tested these springs were incapable of providing the force needed with the new housing system so the spring with the next highest output force was selected for this iteration. (*Circled in green in Table 7*)

10.4. Sheath Design

Initially the sheath design was similar to that of the first iteration, allowing for protection of the worm gear and motor from the silicone and the forces from the environment that could disrupt the motors function. This remodified sheath was again designed using CREO 3.0 and printed in the same material as the previous.

The original design had the sheath and motor held in place with the use of a small grub screw through the side of the aluminium housing, which was tightened to secure the motor in the

desired position. The protruding part of the grub screw held the 3D printed sheath in place. This had to be re-addressed with the new smaller design as there was insufficient material on the side of the aluminium housing to hold a thread. Instead a small m1 hole was positioned at the top of the housing and countersunk slightly to accommodate an m1 countersunk screw. This maintained the devices low profile and the countersink allowed for the sheath to be held in place firmly.

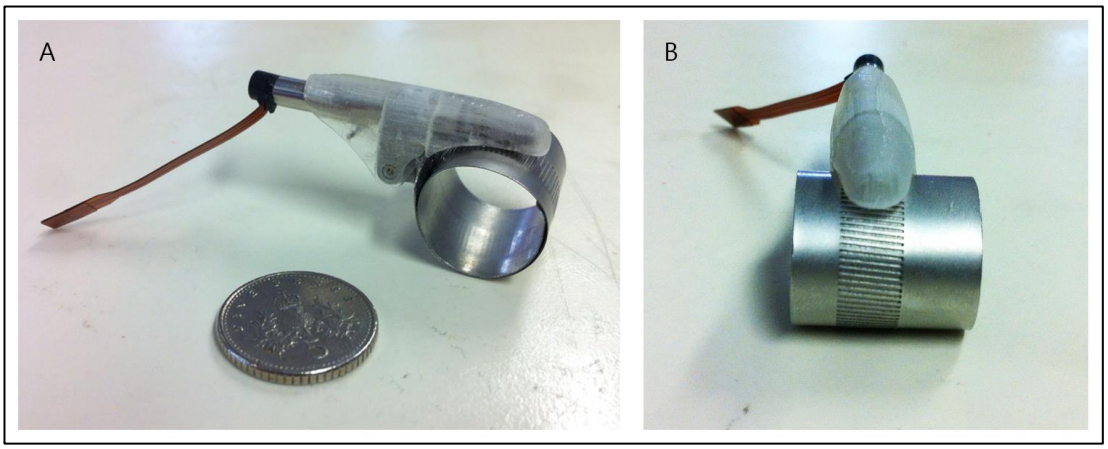

Figure 90 - Sheath Design and Device Size Comparison

10.5. Early Bench Tests (Lateral Travel)

Once assembled, the device functionality was tested. The device was suspended in tweezers and held elevated from the table. The motor was then powered to see if the device functioned as desired. It was observed however, during testing of the device mechanics that the worm gear experienced lateral travel along the grooves of the strip. This meant that the strip itself was twisted abnormally and caused the worm to lose grip on the grooves and this resulted in the strip slipping. This is not favourable as if the device slips or jumps it could rupture the silicone coating and damage surrounding tissues.

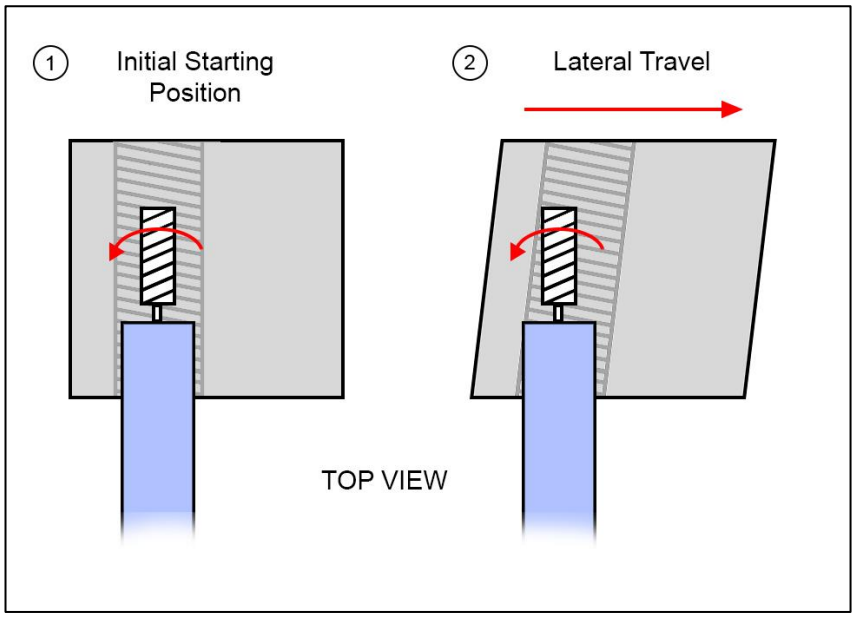

Figure 91 - Worm Gear Lateral Travel

This phenomenon occurred because the strip was allowed to rotate at the fixed point on the aluminium arm. On the previous iteration this was prevented with the use of a small wire loop emitting from the arm and wrapped around the layers of the coiled strips to ensure that they were retained. *(Figure 92)*

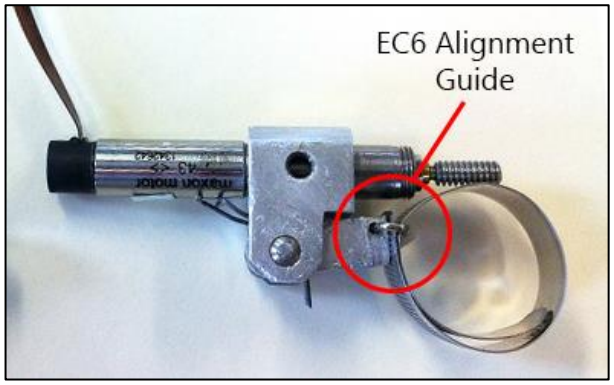

Figure 92 - EC6 Alignment Guide

Size constraints of this iteration precluded the use of this additional modification, so another solution had to be considered.

A guide / feed-though would need to be constructed, and due to the lack of space and practicality of putting the guide where it was previously, this component was incorporated into the sheath, looping round the point where alignment was most crucial at the worm gear / strip interaction site. This would also aid in holding the strip in place, reducing the likelyhood of traction loss on the strip.

It was originally thought that the guide would be a closed loop around the worm and the strip. This would prove problematic when it came to construction of the device as threading the strip though this loop would be complex. The guide was designed taking the form of wings which would clip over the edges of the strip allowing some flexibility in assembly and positioning. *(Figure 93)*

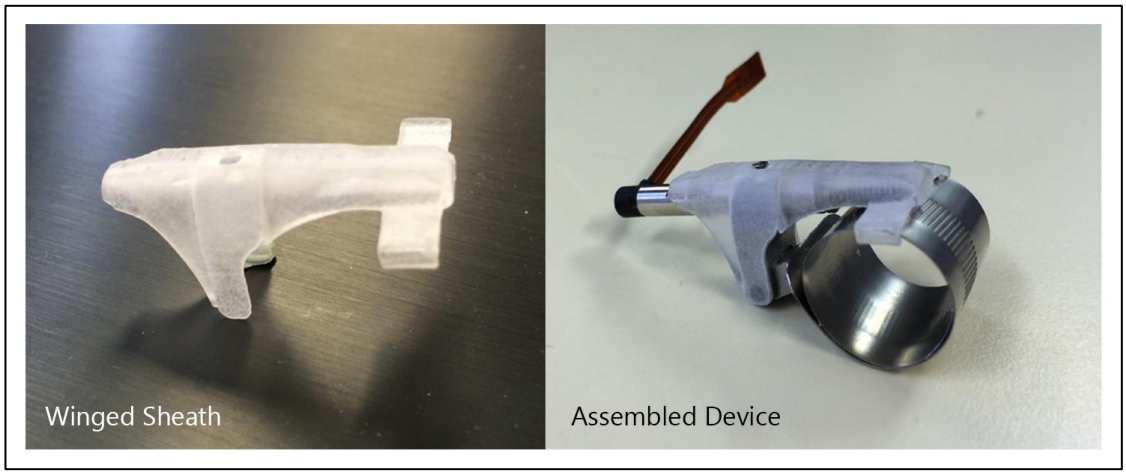

Figure 93 - Sheath Design with Alignment 'Wings'

These new sheaths were printed in the same material as previous and proved successful in resolving the alignment issue. However the material was fragile, and if too much force was applied to clip the wings around the strip, they had a tendency to snap. Thus, the same design was printed in aluminium, but when it came to assembling the device, they had no flex in the wings and they could not be secured over the strip. Finally we returned to utilise the printed plastic material with additional care in assembly.

10.6. Device encapsulation

The device required complete encapsulation in a biocompatible material to ensure minimal device/tissue interaction. This required the construction of encapsulation moulding tools to facilitate this process.

10.6.1. Mould Design

As with the previous iteration, injection moulding was used to provide a coating of silicone around the entire device. *(as shown in Chapter 7.8.4.2.)* The mould was once again designed using CREO 3.0 software.

The mould was then printed in the same ABS as with the previous design on the Stratasys EDEN350 3D printer. Mould tests were carried out using this mould, repeating the same process that was used with the previous iteration by reinforcing the sewing rings with Dacron strips *(see Chapter 7.8.4.2).* Because of the poor production quality the parts did not securely link together, which left gaps and caused silicone to leak. Also, the silicone did not adequately cure, and the mould was tested a further 3 times with the same result. It was thought that chemical composition of this mould material prevented the silicone to cure fully, and investigation into other mould materials was carried out. *(see Figure 94)*

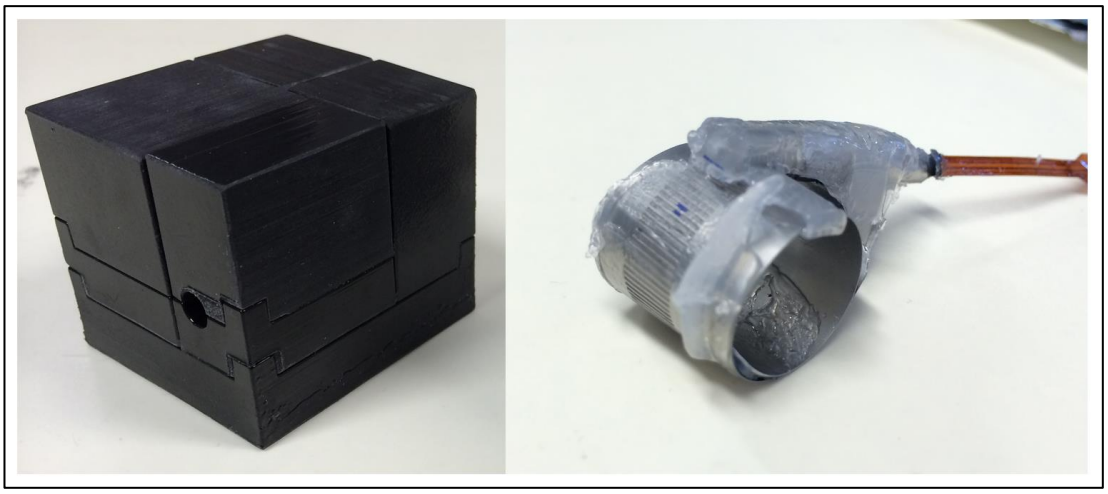

Figure 94 - First Device encapsulation test, resulting in uncured Silicone

The unacceptable outcome of the black-ABS like material mould printing meant that a different material had to be considered. It was then printed in a semi-transparent ABS like material which was polished post printing. This made the material fully translucent and would allow for the coverage of silicone to be seen from the outside of the mould to determine if there were any regions where silicone was not reaching. The presence of air bubbles contributed to this phenomenon during testing.

Air bubbles were predominantly located at the outermost regions of the sewing rings. This material also failed to ensure adequate silicone curing, so other 3D printing materials were considered.

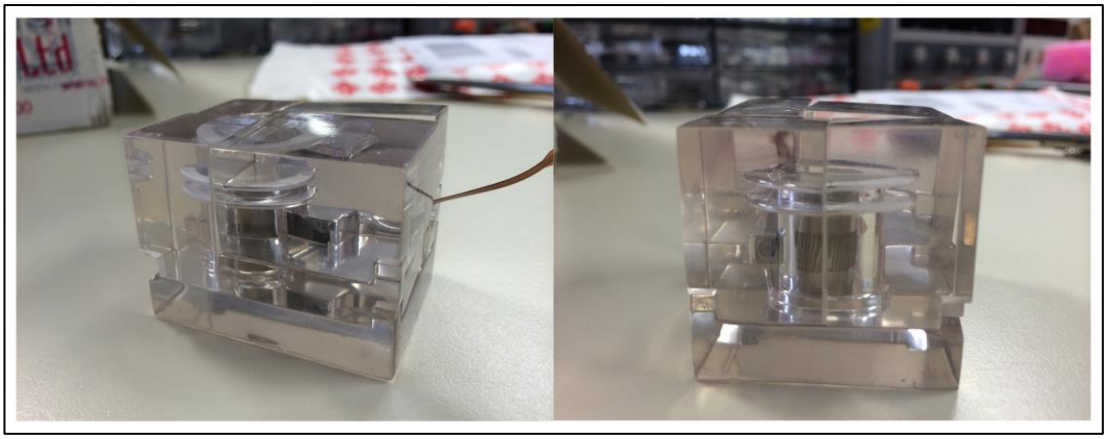

Figure 95 - Device inside acrylic polished mould

3D printing was outsourced to 3D Alchemy (Shropshire, UK), who have expertise in materials for injection moulding applications. The recommended material was Veroblue full cure which was printed using stereolithography (SLA). Regarding resolution, this was printed in 16 micron layers to ensure a highly accurate build. Their professional servicesallowed the prototype to undergo a number of post printing stages. These were: support removal, cleaning in a weak sodium hydroxide solution to facilitate the removal of any residual support material, additional UV curing, hand finishing to remove any evidence of build layers with a slight

abrasive, and then coating with a general purpose cellulose primer to act as a barrier between the mould material and the silicone.

To ensure optimal development, moulds were also ordered in stainless steel and aluminium form Fine line Prototyping (Minnesota, USA), both these moulds were printed using DMLS *(detailed in Chapter 7.7.1.5.)* with a resolution of 20 microns. Due to costings and time constraints only the aluminium was post processed to a smooth surface finish. As a result however, the aluminium mould parts lacked a tight fit when assembled. All three material moulds were tested to create a silicone encapsulated device. The aluminium mould (due to its poor fit) allowed silicone to escape through the cracks during the injection process, and this was also observed with the Veroblue mould but to a lesser extent. The stainless steel mould provided the best results, with a minimal amount of silicone leaking through the mould parts. The rough surface acted as a barrier reducing the leak and providing a more uniform coverage all round. Figure 96 shows all of the mould materials that underwent the testing process.

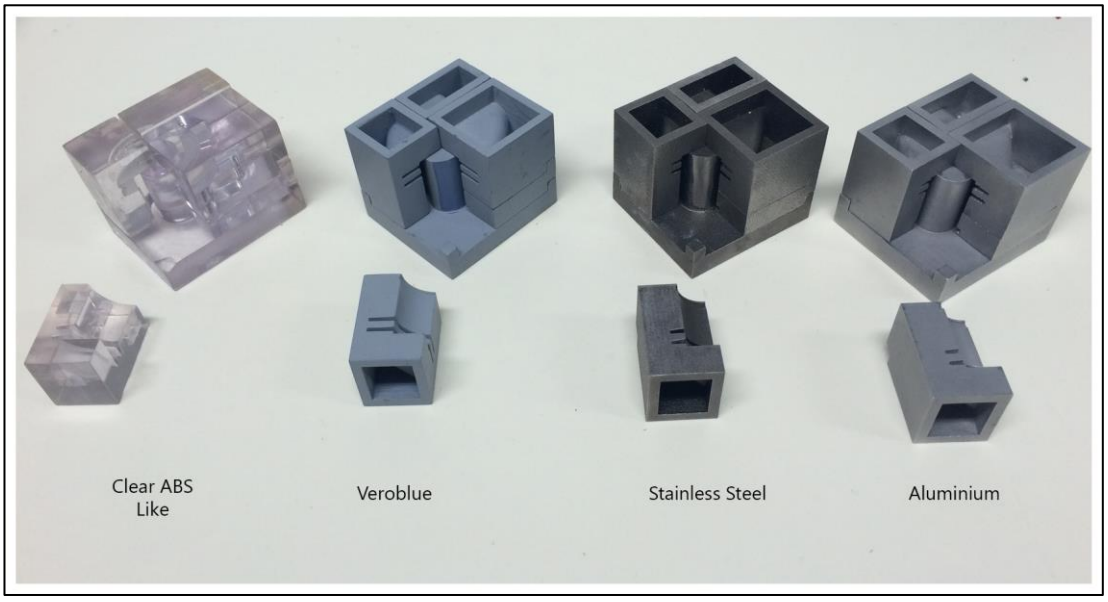

Figure 96 - Selection of moulds in various materials

Once the device was encapsulated using the stainless steel mould, it was important to inspect the device underneath the winged sheath to ensure no silicone entered the gear mechanism. To

do this the silicone coating was removed from the test device, and the sheath lifted partially. It was found that silicone had entered under the brim of the sheath and caused it to cure and jam the worm gear.

To resolve this, silicone grease was placed in the gear/strip interaction area to prevent liquid silicone entering during the injection moulding procedure. *(Figure 97)*

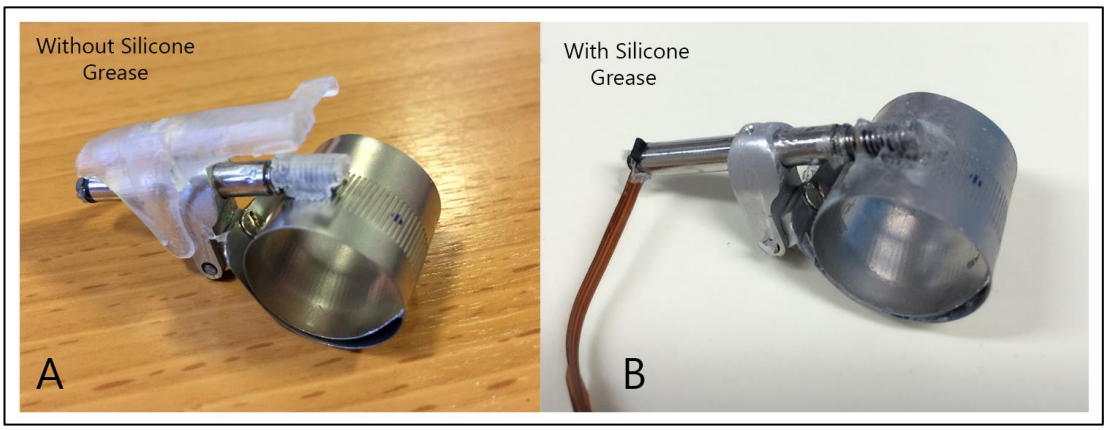

Figure 97 - Device blockage, with and without silicone grease

This grease would stay in a gel form allowing the worm and strip to move freely within it and remain functional. Figure 97A shows the build-up of silicone under the sheath without the use of grease compared to the site where grease was applied (Figure 97B). All experimental work was subsequently performed using the stainless steel mould with silicone grease application.

10.6.2. Silicone Selection

Since the device was intended for animal testing, a medical grade silicone had to be chosen for short to long-term implantation, The silicone used up to this point stated that it passed ISO standards for irritation and sensitisation, although it did not state that it was acceptable for use in short or long term implantable devices.

10.6.3. Sewing Ring Alterations

Late feedback from the previous surgery suggested that a single sewing ring was advised. Pre-implantation bench testing of the suture tool concluded that placement of a single sewing ring would be an optimal configuration. Difficulty arose in the needle-threading technique for a considerably smaller device and the inability to access the underside of the sewing rings.

To minimise the likelihood of tearing the sewing rings during surgery, further reinforcements were made to the sewing ring by including an additional layer of dacron attached to both sides of the silicone ring. The suture locations were reinforced further with the use of pledgets. These are small soft pre-punched PTFE polymer pads were purchased from Covidien commercial ltd (Fareham, UK) of dimension 3mm x 7mm x 1.5mm, 8 of which were positioned evenly around the circumference of the sewing ring acting as a guide for the suturing. Such materials are commonly used with suture secured implantable devices.

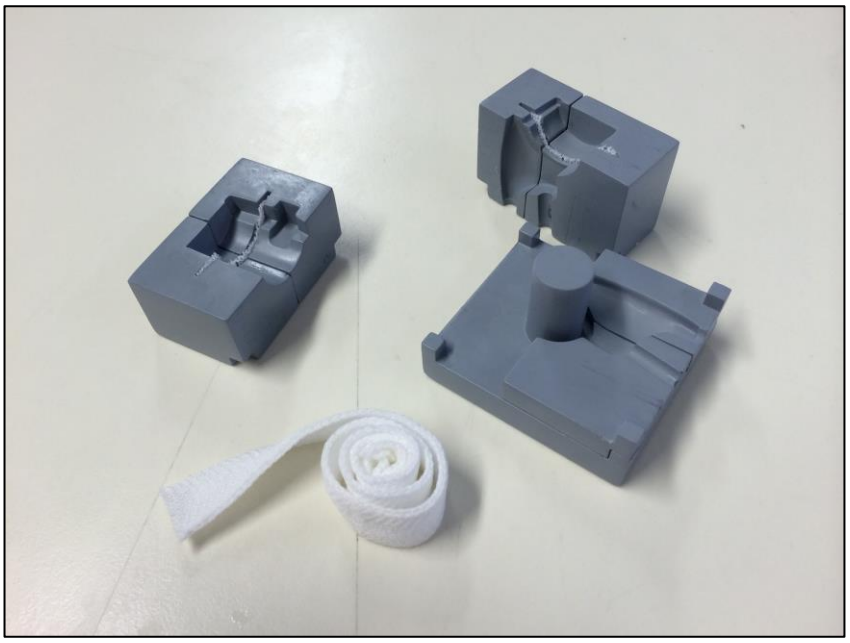

Figure 98 - Final single ring open mould, with Dacron

10.6.4. Silicone Conduit Cap

Initial testing of this device was to determine the feasibility of the size and expansion of the device under conditions that represent the highest challenge for the conduit. It is because of this that the device was implanted into the wall of the right ventricle in line with common clinical practices in the event of RV-PA conduit implantation. This would emulate the stresses and forces it would be subjected in a real life clinical situation. Because the focus of this work

was on the expansion device, there was no need for an attached conduit to the device. The orifice of the device was therefore sealed to prevent exsanguination. A silicone cap was used and adhered to the inside of this orifice.

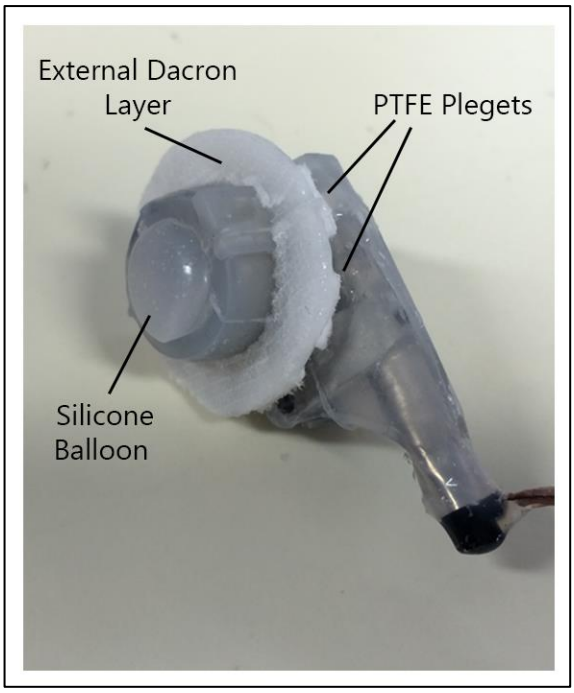

Figure 99 - Final implantable expansion mechanism with balloon, external Dacron layer and plegets adhered

10.7. 2nd Iteration Control and Power

It was crucial to miniaturise the power and control system for this iteration, as the previous system was too large for implantation. Previously the entire system *(Chapter 8.5.2.)* was housed in one box and was held in a pack on the back of the pig. This proved to be highly impractical for this application so steps were taken to miniaturise the control system and to make it more manageable and secure.

The power and control systems were then designed to be implanted subcutaneously so that the animal could not interfere with any cabling. Therefore, it was important for these items to have as small a profile as possible.

The previous box contained 3 main items: The batteries, motor controller and the timer circuit. The aim was to reduce the size of each of these components individually and house into two separate boxes.

10.7.1. Miniaturised Control Board

The motor board used in the previous iteration was the EPOS 2 24/2, which was a generic test board for a number of MAXON branded motors. The advantage was that you could connect a number of different motors to the board for testing as it was universally compatible with their motors. MAXON provided a smaller motor board for a more permanent and specific use once the motor had been selected. This board was the EPOS 36/2.

This board had similar functions as the previous EPOS2 24/2 however instead of designated connections for each motor, it provided solder pins to allow the motors to be hardwired, which in turn reduced the size of the board considerably.

This board connected to the PC through RS232 connection though an evaluation board, which allowed the board to be programmed using EPOS2 Studio software.

The output motor speed was determined using the same method as the previous iteration *(Chapter 8.5.1.)* which depended on the expansion rate and the motors integrated gearbox.

As the EC4 reduction gear box was 280:1 compaired to the EC6 gearbox 854:1 the output rpm of the motor before the gearbox would need to be around 4x less than that of the EC6. Running the motor at such low speeds could stall the motor as there would not be enough power being supplied to the motor to overcome its inertia. To resolve this, it was decided to run the motor at a much higher speed and change the variables on the timer circuit side of the system to accommodate this. (Therefore, instead of running the system on a preconceived time duration

(30 seconds a day) the calculations worked out the time the motor would need to function dependant on a constant motor speed in order to keep the speed high.)

The motor speed selected was an output of 1500rpm. This value was selected to keep the motor speed fast enough so there was no possibility of stalling when trying to expand the device. From this it could be calculated that the output of the integrated 280:1 gearbox was 5.35rpm.This speed would provide enough power to prevent the motor from stalling during operation.

The rate of device expansion would again be over a duration of 30 days, the device would function from an initial diameter of 12mm to a final of 20mm. This means a change in circumference of 25.13mm (the length of strip that passes through the worm gear.)

Calculations for the input motor speed were as follows:

Distance travelled per day

$$Travel\ distance = \frac{distance\ of\ travel}{number\ of\ days}$$

$$= \frac{25.13}{30}$$

$$= 0.838mm/day$$

Distance travelled in 1rpm = axial pitch of the worm gear = 0.628mm

Therefore:

$$1rpm = 0.628mm$$

Then

$$1.33rpm = 0.838mm$$

Time taken to travel 0.838mm at a speed of 5.35rpm:

$$time = \frac{1.33}{5.35}$$

$$= 0.24min$$

$$= 14.4\ seconds$$

10.7.2. New Smaller Timer Circuit (Coding)

With the addition of the new smaller motor controller it was also considered to be beneficial to try and miniaturise the timer circuit. The previous iteration used two through-hole timer ICs. These were replaced by a smaller, simplified custom designed microcontroller board, which would, in turn, provide more accurate programming of the timer.

The configuration of this board is shown in *Figure 100.*

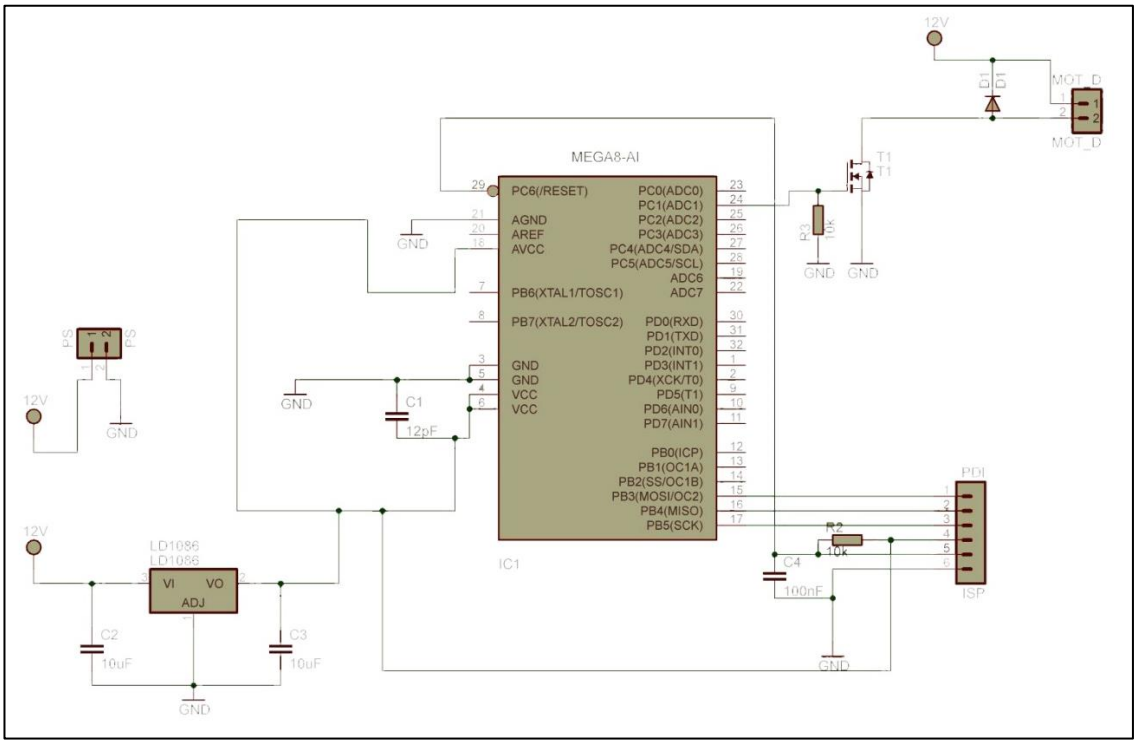

Figure 100 - Timer circuit schematic

The board could then be programmed via PC interface using Atmel Corporation (California, USA) Atmel Studio coding software. The code used is shown in Chapter 10.7.2.1.

10.7.2.1. Timer code

Firstly it must be noted that the timer IC used on this board is only accurate for around 5 seconds, a little. With this in mind the first section of code defines the function of a ‘day’.

```
// global variables to count the number of overflows
int x=0;
int y=0;
int dayloop=0;
int dayloop2=0;

void day () // day=86400 sec. In 5 sec intervals = 17280 = 120x144
{
	for (y=0; y<=119; y++)
	{
		for (x=0; x<=143; x++)
		{
			_delay_ms(5000);
		}
	}
}
```

The ‘day’ function splits the day into 5 second intervals. It is then split into two separate section and counts 144 of these 5 second intervals 120 times. This means there are 17,280 intervals that make up the 24 hour day.

```
int main(void)
{
	// connect led to pin PC0 and set to output to 0000 0001
	PORTC |= (0<<PORTC1);
	DDRC |= (1 << 1);
```

The initial state of the controller output is set to off. This means that the there is no voltage being supplied to the controller, ensuring the motor does not start as soon as the power to the timer circuit is supplied.

```
	// loop forever
	while(1)
	{
		for (dayloop=0; dayloop++)
```

```
                {
                        day();
                }

                for (dayloop2=0; dayloop2++)
                {
                        PORTC |= (1<<PORTC1);
                        PORTC |= (1<<PORTC1);
                        _delay_ms(4400);
                        _delay_ms(5000);
                        _delay_ms(5000);
                        PORTC &= ~(1<<PORTC1);
                        PORTC &= ~(1<<PORTC1);
                        day();
                }
        }
}
```

The ‘day’ function defined previously, is then called. Once the timer has reached the end of the day function, the output of the controller is set to ‘on’ for a total period of 14.4 seconds as calculated in section 8.7.1. Once this time has elapsed, the controller gates the power to the motor board again initiating the day function again. The final timer PCB layout was designed and outsourced for assembly to Newbury Electronics Ltd (Berkshire, UK), who were able to surface mount the components reducing the size of this board significantly.

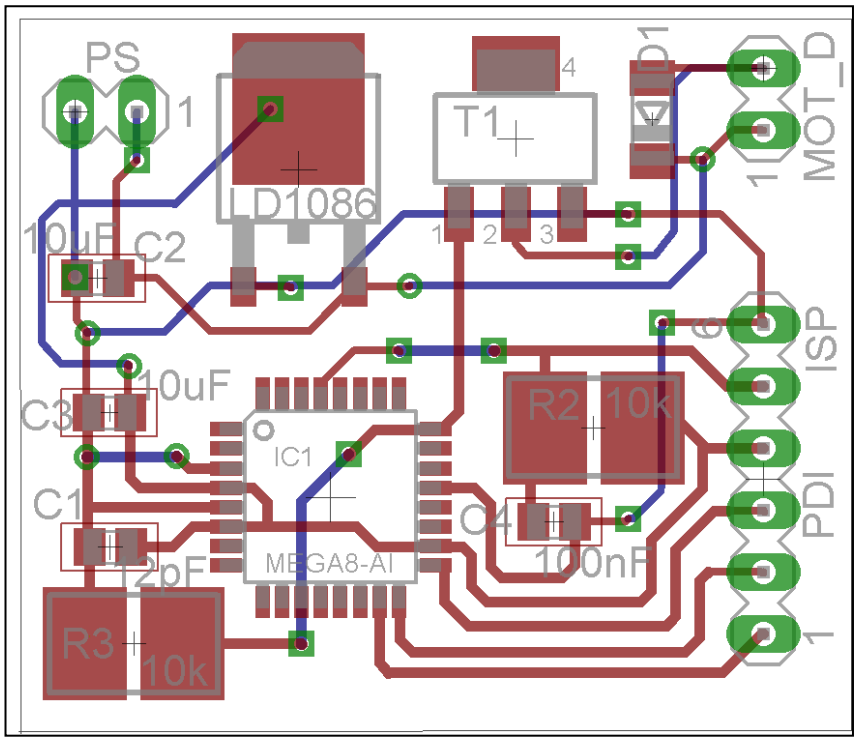

Figure 101 - Timer circuit board layout

10.7.3. Overall Reduced Power

There was significantly less power consumption with this new configuration. When activated, the timer board consumed 10mAh, which was a significant improvement over the previous iteration which used 100mAh, allowing the batteries to last longer before they require recharging. Even though the motor has the same operating voltage as its predecessor, the new EPOS2 2/36 motor controller could run at the slightly lower voltage of 10V, resulting in a reduced power over all.

The new power source for this system was three 1100mAh, 3.7V mobile phone batteries (Part number: PDA91016) purchased online at: www.allbatteries.co.uk (Solihull, UK), which replaced the 10 x AAA batteries used for the previous iteration. These readily available mobile phone batteries have an integrated regulation circuit which is something that most implantable

medical batteries lack. The regulation circuit prevents the batteries from overloading when connected to each other, and protects the attached external circuitry from irreversible damage. If medical batteries had been used, a regulation circuit would need to have been added which would have increased the size of the system overall.

To house these batteries, 2 different designs were created for the battery boxes, The first stacked the batteries on top of one another which produced a more box like appearance and the other stacked them in a pyramid fashion giving a longer length in total but reducing the height significantly, the second option was chosen for implantation as there was less of a protrusion formed when implanted subcutaneously.

The motor controller board and timer board were packaged together in a control box and the power source was housed separately. This significantly reduced the size for implantation. A casing was designed for both the 2/36 and the 2/24 boards, these are depicted below, due to its size, the 2/36 case was favoured, and be used for implantation.

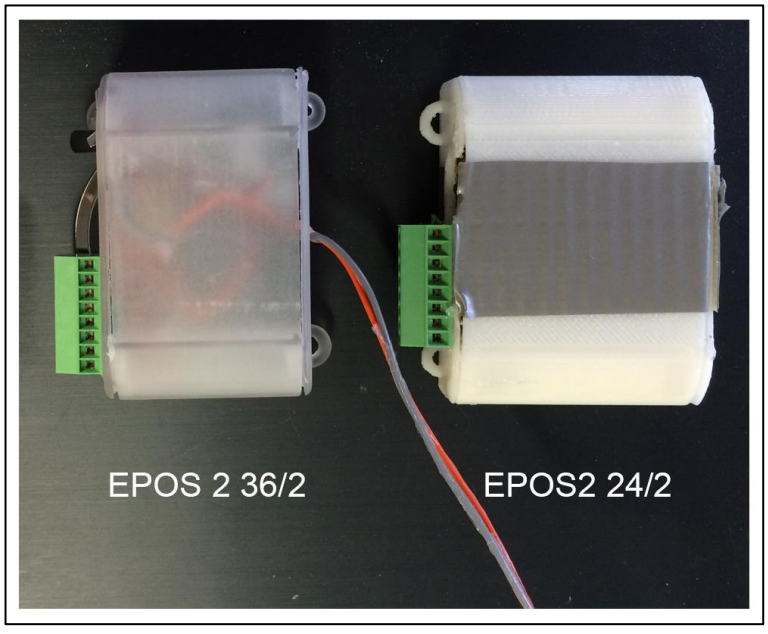

Figure 102 - EPOS2 24/2 vs EPOS2 36/2 control box size comparison

The cables, control box and battery box were coated in the same silicone as encapsulation. The EC4 had the same 8 individual motor cables as it predecessor so the same manual terminal was used for connecting the motor to the motor control box, and the ports sealed off with silicone. The completed device is shown in Figure 103.

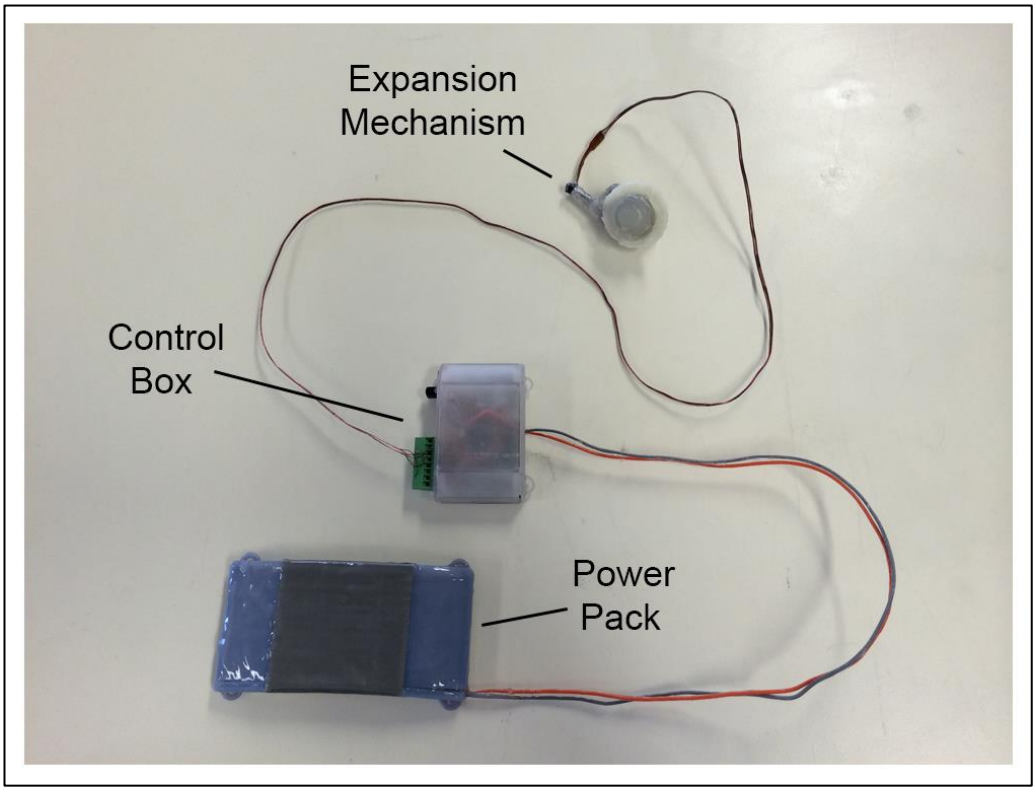

Figure 103 - 2nd Iteration final implantable device

10.7.4. Sterilisation

Sterilisation is important for implantable medical devices. Sterilisation aids in preventing infection at the implant site by removing/destroying any harmful contaminants from the devices surface. There are a number of methods used to sterilise medical devices. Depending on the characteristics of the device, it is important that the correct method is selected, especially when the device contains electronic components. (Crow 1993, Lerouge 2012)

The degree of sterilisation is defined using the term ‘security assurance level’ (SAL). This is the probability of finding a single organism on the device after sterilisation. For medical devices or products that only come in contact with the skin, the SAL required is 10^{-3}. For implantable medical devices the SAL is reduced to 10^{-6}. (Block 2001, Lerouge 2012)

10.7.4.1. Steam Sterilisation (Autoclave)

One of the most effective ways to destroy/remove microorganisms is heat. Heat causes the proteins and enzymes to coagulate. This coagulation can be increased with the presence of moisture, and this moisture can penetrate materials and fabrics quicker than air, which ultimately spreads the heat more effectively. (Rutala et al. 2008)

The autoclave system, invented by Charles Chamberland in 1879, utilised this principle and uses pressurised steam to achieve sterilisation. The chamber is sealed and steam is then forced into the chamber at high pressures. This is quick and regarded as one of the most dependable methods used for sterilisation today. (Maxim Integrated 2010)

This method is extremely effective on medical devices that can withstand high temperatures (maximum of around 148°C). This however, is not suitable for devices with batteries. Due to the high pressures and heat involved, the efficiency and lifetime of batteries can be significantly reduced. Additionally the moisture can cause any mechanical lubricants in the device to break down. (Maxim Integrated 2010)

10.7.4.2. Ethylene Oxide (ETO)

An alternative method is ethylene oxide sterilisation. This is a chemical method that can operate at much lower temperatures than the autoclave system (around 60°C). (Maxim Integrated 2010)

The process of ETO consists of 4 stages, where the first is the evacuation and dehumidifying stage. This is where the devices are placed in a chamber where all air and moisture is removed. Secondly the ethylene oxide gas is introduced, and this gas can either consist of 100% ethylene oxide or a combination of a gas stabiliser such us chloroflourocarbon (CFC) at a ratio of 12%. (Rutala et al. 2008) The devices are then exposed to the gas for a specified length of time depending on the amount of sterilisation required. The gas is then evacuated and the chamber is cleansed with air through a number of washes until no toxic gas remains. While this method may be beneficial for electronic components operating at this low temperature. (Maxim Integrated 2010)

10.7.4.3. Gamma Sterilisation

Another low temperature method of sterilisation is through the use of gamma rays. Using the gamma radiation produced by cobalt-60, it is a fast an effective method of sterilising medical devices. As this does not require a pressurised chamber or high temperatures, this makes it ideal for batteries. Gamma radiation sterilisation is mainly used in industry for bulk sterilisation purposes. (Rutala et al. 2008)

Items are introduced to a field of high gamma radiation, the level of gamma radiation is calculated so that each item receives the correct amount as the conveyor continuously moves through the field. The exposure to this radiation penetrates deep into the materials disintegrating any microorganisms present.

The benefits of this method are that it is fast and effective. However, this method can be extremely costly, and the radiation can also effect semiconductors and polymers that are present in integrated circuits so care must be taken when determining the dosage. (Maxim Integrated 2010)

10.7.4.4. Sterilisation Selection

The sterilisation method chosen for this device was Ethylene oxide. This allowed for the vital electronic components to be preserved which could be damaged by the high temperatures of Autoclave or possibly damaged by the radiation used with Gamma sterilisation.

In preparation for Ethylene oxide (ETO) sterilisation the expansion mechanism and its control system were sealed in separate autoclave sterilisation pouches and delivered to Anderson Caledonia (Bellshill, UK) who specialise in infection control and have Both Autoclave and ETO sterilisation equipment onsite.

Once sterilised, the device component remained in their packaging until needed for the second implantation surgeries.

Figure 104 - Packaged and Sterilised R.E.A.D.

Chapter 11.

2nd Implantation Series

Chapter 11. 2nd Implantation Series

11.1. Background

The object of this series of experiments was to implant the new device, designed for clinical deployment in children receiving conduit implantation for the correction of cardiac lesions affecting the RV outflow tract, in an animal model. These experiments will prove the clinical efficacy of the device to be assessed prior to possible future clinical implantation.

11.2. Brief Protocol

We planned to carry out these procedures in 6 piglets as a pilot study with the objective of following the animals progress for a period of up to 3 months post-surgery, at which point the animals would be sacrificed and the devices harvested to investigate the impact of the device on host tissue and device integrity. The experimental procedure is highly complex and briefly follows the following condensed plan:

- Induction
- Intubation
- Anaesthesia & Analgesia
- Ventilation
- Chest opened
- Cannulation of Aorta and RA
- Initiation of Cardiopulmonary Bypass (CPB)
- Deep Hypothermic Arrest
- Device implantation
- Rewarming
- Cessation of CPB
- Implantation of Control and power systems

- Chest closure
- Recovery

11.3. Experimental Procedure

11.3.1. Setup of the Implantable Technology

The technology employed in these studies comprised;

1. The R.E.A.D. device

2. The Control System

3. The Battery Pack.

The control system was set up in such a way that the READ device would expand from 12mm to 20mm over the duration of 30 days (expansion rates are calculated in Chapter 10.7). The battery pack, control system module and interconnecting wires were all coated in silicone to enhance biocompatibility. Once coated, the entire apparatus was packed and Ethylene Oxide sterilised. The sterile device package was then considered to be suitable for implantation.

11.3.2. Surgical Procedure

The animals were sedated prior to surgery with Zoletil 100 (6-8mg/kg) and Atropine (0.03mg/kg) prior to surgery. Anaesthetic induction was achieved using Propofol (1mg/kg) prior to intubation. The animals were then intubated, using Xylocain as a local anaesthetic for the trachea. The animals were then connected to the ventilator. A Fentanyl patch was then placed on the neck of the animal, secured with Tegaderm. A pulse oximeter and ECG leads were then applied to the animals to effect monitoring of vital functions. All surgical sites (cut-down areas for fluid transfusion and pressure monitoring) were flushed with Bupicacain 0.5% as local analgesia. To prevent respiratory complications during and immediately post-surgery

250mg of Methylprednicolone was administaered I.v and further Fentanyl bolus injections (10-20microgr/kg) delivered as required. When the animals were ready for CPB a continuous infusion of Hynovel (midazolam), Fentanyl and Rapinivet (propofol) as a continuous neuroleptanalgesic. The neuroleptanagesic protocol was continued as the animals recovered from the surgical procedure whist monitoring pain withdrawal reflex as a marker of anaesthetic depth.

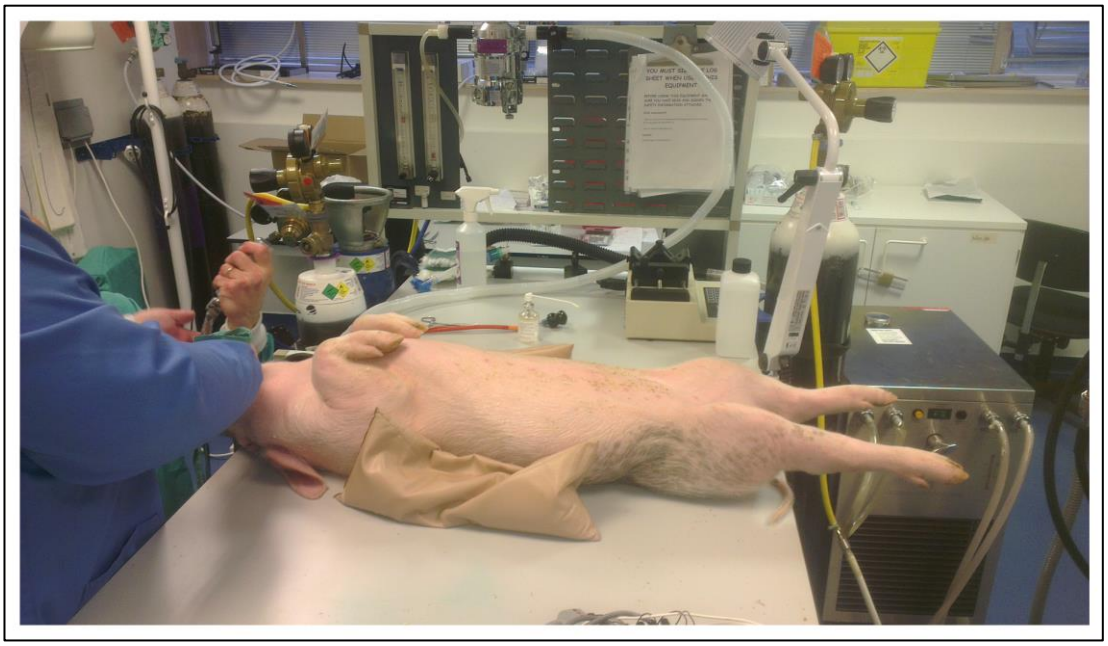

Figure 105 - Initiating Anaesthetic

The animals were placed supine on the operating table and arterial and venous cannulae and temperature probes were introduced to facilitate physiological monitoring and drug delivery. Once stable the animals were draped and the sternum divided at the mid-line. (*Figure 106*). Diathermy was utilised to ensure haemostasis. The pericardium was divided to expose the heart, heparin administered and cannulae positioned in the ascending aorta and into the right atrium via the right atrial appendage. A single two stage venous cannula was employed for venous drainage purposes.

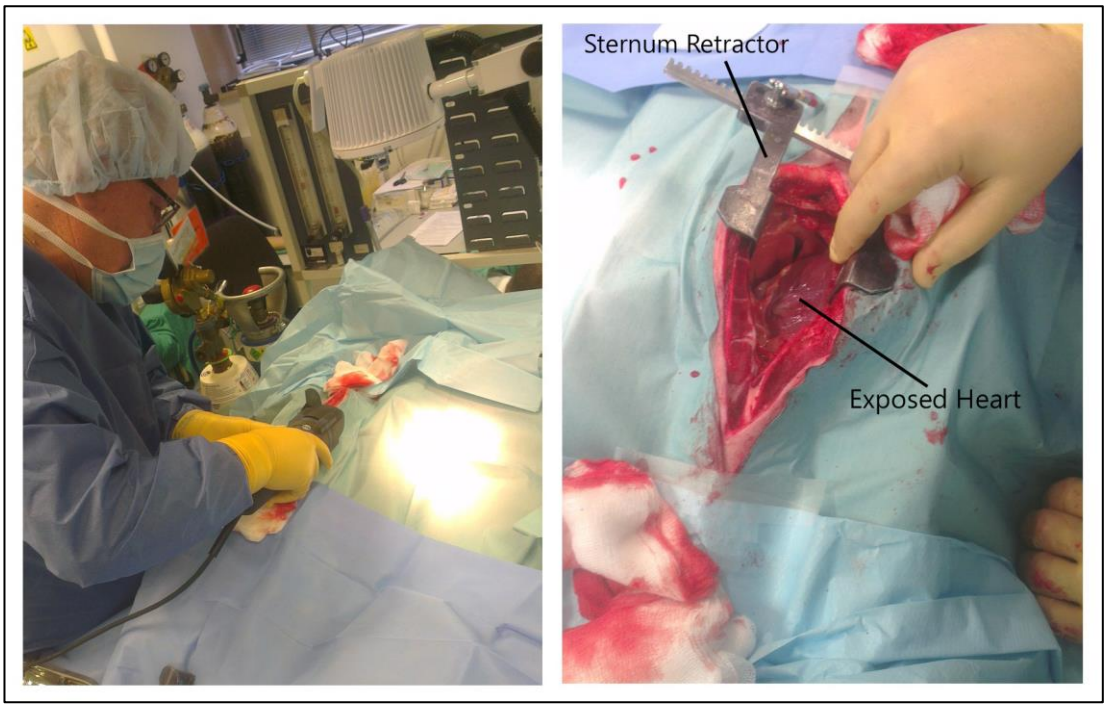

Figure 106 - Cutting sternum to reveal Heart

Once the cannulae were in introduced, the animal was connected to the Heart/Lung machine which consisted of a Stockert roller pump for arterial return, a Maquet Oxygenator, Pall EC 3 arterial line filter and interconnecting PVC tubing throughout. Suction was provided by a second tier of roller pumps feeding a Sorin Paediatric cardiotomoy reservoir.

11.3.3. Circuit Prime

The CPB system was primed with a solution consisting of:

- Calcium Chloride (4.7 w/v) 1ml/litre prime
- Mannotol (20% w/v) 2.5ml/kg with a maximum of 100ml
- Sodium bicarbonate (8.4 w/v) 20ml (or sufficient to correct BE at 1ml/mmol/l.)
- 1000ml of 50/50 Ringer's/Gelofusine
- Heparin 5-7 iu/ml of prime solution.
- ACT maintained at >480 seconds

11.3.4. Maintenance of CPB

Once the animal was stable, cardiopulmonary bypass was initiated at a reference flow rate of 2.4 x BSA (approx. 100ml/min/Kg) and maintained at a level that was adequate to maintain an arterial/venous balance of >60mmHg throughout the procedure. Top-up reservoir volume was used when absolutely necessary, generally when flow was reduced to below 2.0 x BSA, in the form of Ringer's solution. Oxygenator gas flow was maintained at an FiO2 80% at blood/gas flow ratio of 1:1 using a Sechrest Blender and was adjusted in response to intermittent blood gas analysis results. Activated clotting time (ACT) was maintained in excess of 480 seconds throughout using a Hemachron Mini system for monitoring purposes, with additional Heparin administered as required when Hemachron results were below optimal values.

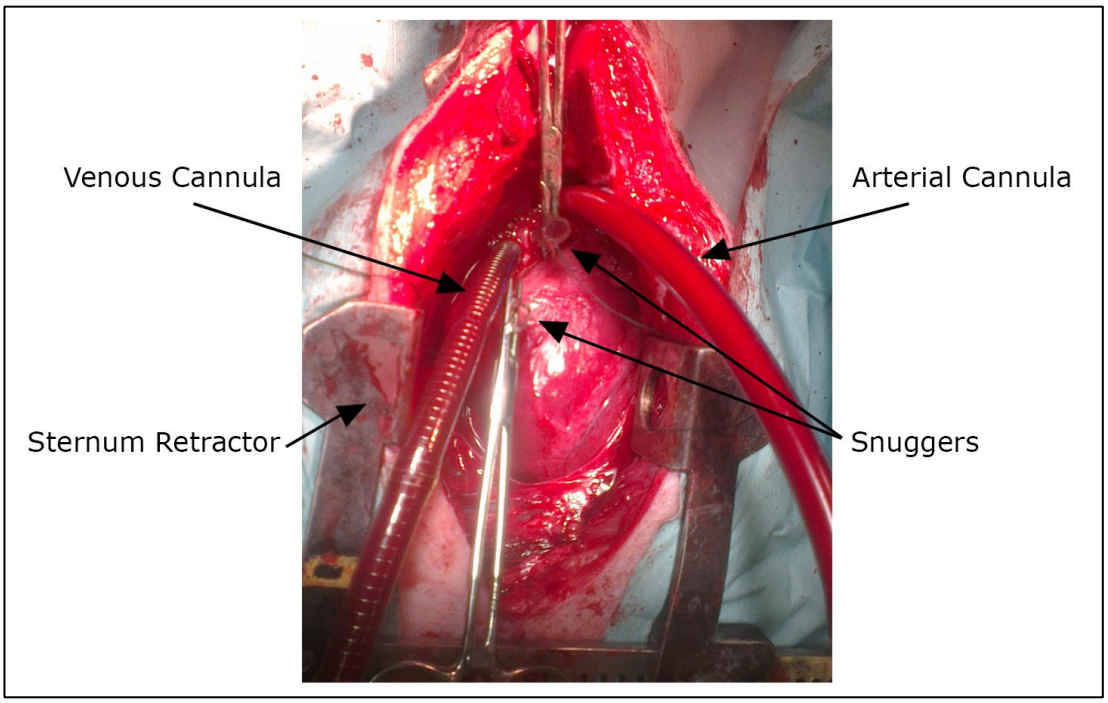

Figure 107 - Successful Cannulation of the heart.

11.3.5. Cooling Procedure

The animal was immediately cooled to 25°C (core temperature) at which point perfusion was reduced to around 50%. The aorta was cross clamped and cardioplegia administered.

Cardioplegia was achieved using a St Thomas/ ice cold Ringer's solution mix (at a ratio of 15ml St.Thomas's solution/400ml ice cold Ringer's solution.) A 400ml initial dose was followed by 100ml/20-30 minutes during cross clamp period and topical cooling with ice cold saline at 20 minute intervals. Animal temperature was further reduced to 12 degrees and perfusion was reduced to "trickle". This period of circulatory arrest was monitored and the head was packed in ice to provide a level of cerebral protection.

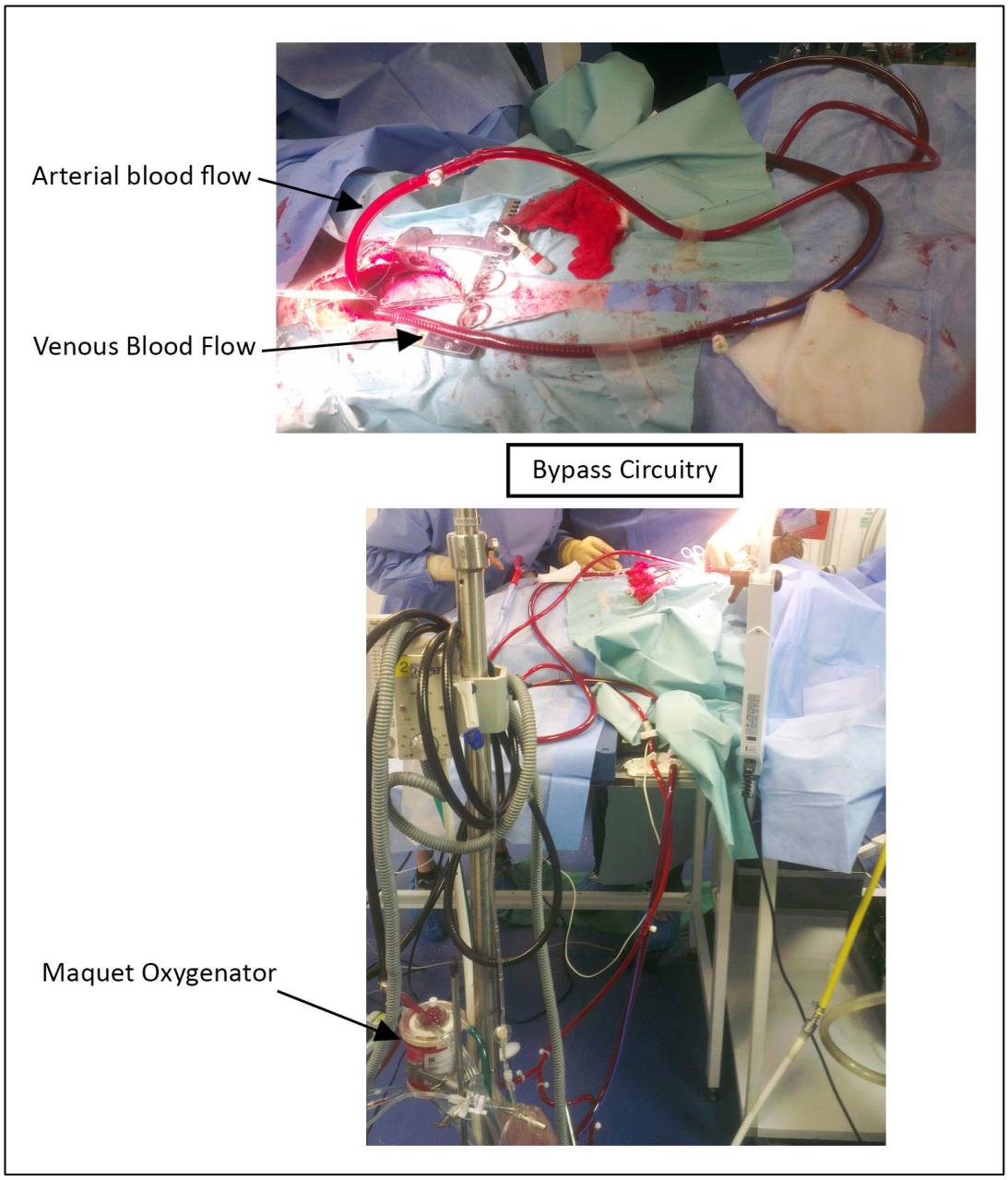

Figure 108 - Bypass Circuitry

11.3.6. Device Implantation and Revival

Once the period of circulatory arrest was initiated the R.E.A.D. device was implanted into the right ventricle after excision of a ring of RV tissue. The device was secured using interrupted 3.0 sutures and tissue glue. This assembly was permitted to set for 5 minutes, after which the heart was de-aired and CPB was re-started. Rewarming of the animal was then initiated.

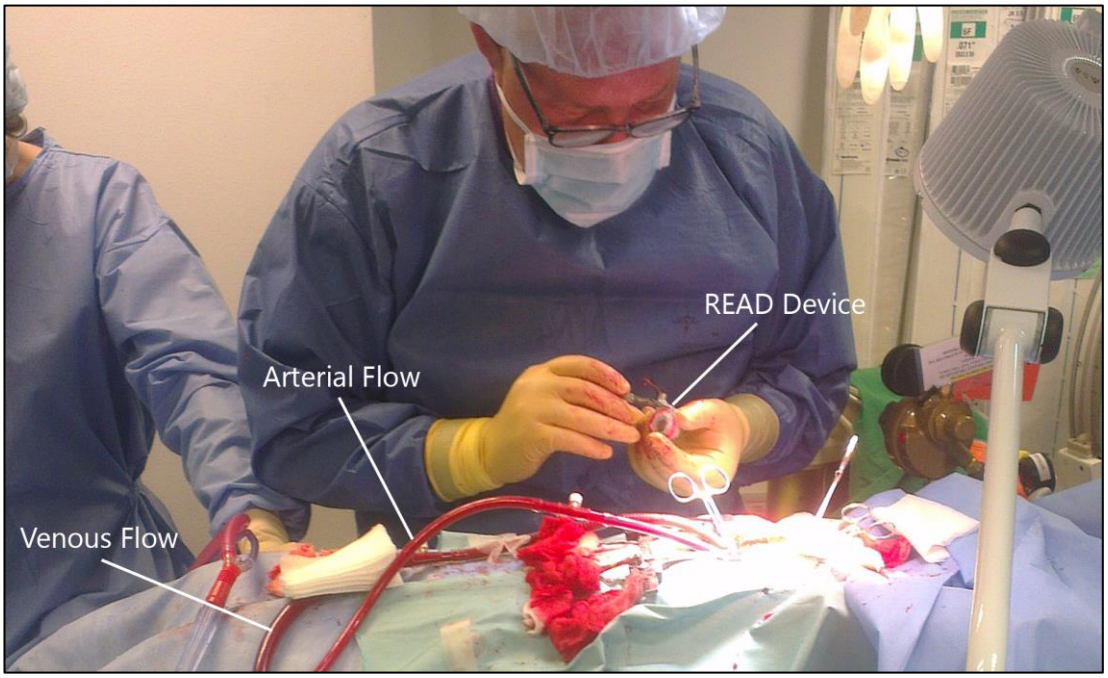

Figure 109 - Device Preparation

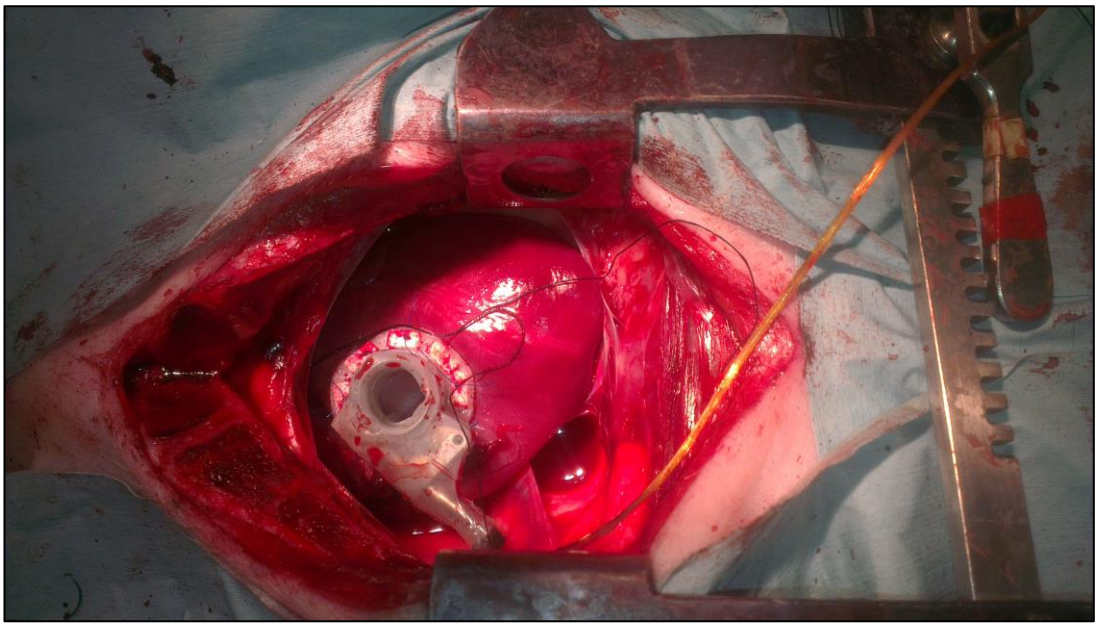

Figure 110 - Implanted device into right ventricle

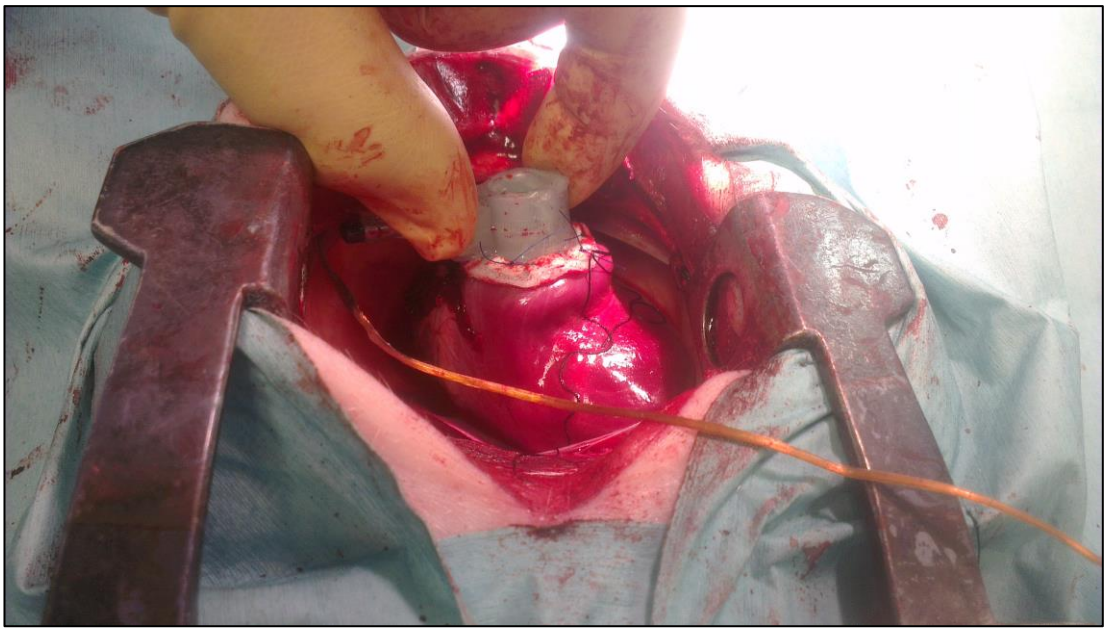

Figure 111 - Pulling device to test security of sutures

Once normal circulation rates were established, core temperature was raised to 30 degrees, the aortic cross clamp was removed and rewarming recirculation continued until deep core temperature reached normothermic levels (37°C). The heart was monitored for recovery of normal rhythm and once this was established, either spontaneously or with the assistance of defibrillation, a period of recirculation was established for 20 minutes, or until the peripheral

temperature reached normothermic levels. If the heart spontaneously converted to sinus rhythm, CPB was reduced over 10 minutes and de-cannulated. If no spontaneous conversion, then defibrillation was performed to return to sinus rhythm to initiate off CPB.

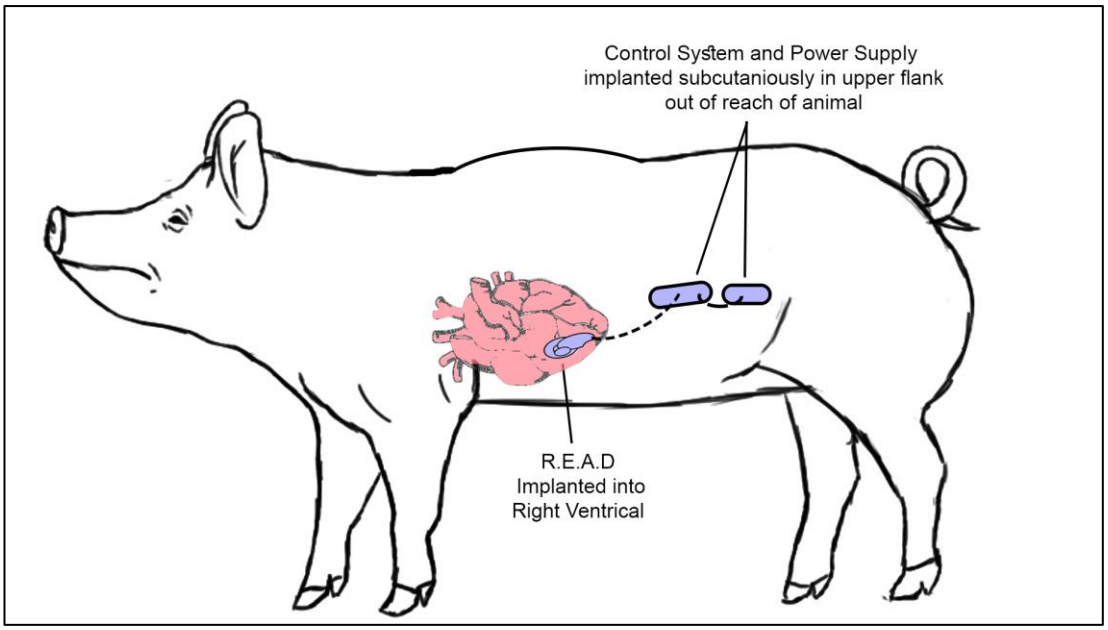

Figure 112 – Device implant location

Whilst normal circulation was underway, the control cables, battery pack and control system were positioned subcutaneously on the upper flank of the animal *(Figure 112).* Once these were in place, the device was activated and chest closure initiated. The chest was closed using sternal wires and the muscle and skin closed using running sutures. Once the chest was closed the animal remained on ventilation, with fluid balance maintained and any electrolyte imbalance corrected. The venous and arterial pressure monitoring lines were maintained during the period prior to transfer to recovery. Once the animals were stable, they were transferred to a recovery room and monitored for level of consciousness and pain levels and a recovery analgesic protocol initiated. Pain relief was given as required based upon monitoring of pain indicators (respiration rate, heart rate, sweating) until there were no enduring signs.

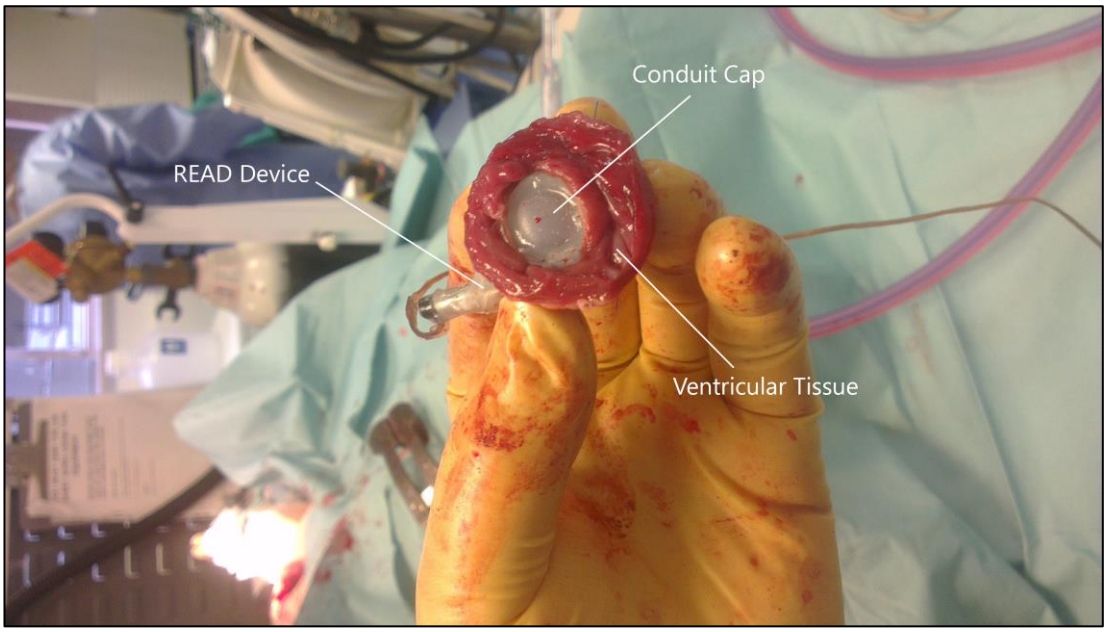

Figure 113 - Device removed tissues still attached, shows seal of the device

11.4. Outcome of the Pilot Study

In all, 6 procedures were carried out between Feb and April 2014. These procedures were not successful as the long term objectives of the study were not achieved. There were a number of experimental failures at varying stages of the procedures and these are explained in the table below *(Table 8).*

Procedure Number	Outcome	Comment	Remedial Strategy
1	Terminate	Surgical Error – Right Atrium Torn leading to Haemorrhage.	Consult paediatric cardiac surgeons at GoS and review RA cannulation approach.
2	Terminate Device deployed	Procedure was good, CPB initiated and DHA reached but device was not compatible with RV. Animal rewarmed and procedure terminated.	Redesign the device using only one sewing ring and buttressed interrupted suture placement with fibrin glue coating.
3	Terminate	Unusual anatomy, right heart rotated towards back of chest. Difficult to secure cannulae leading to Haemorrhage, terminated.	No strategy.

4	Terminate Device deployed	Animal exhibited arrhythmia and very unusual cardiac "hypersensitivity" to touch . Anti-arrhythmic drugs, adrenalin and KCl administered, but no change and animal developed terminal VT-VF.	Review temp data to determine whether this was associated with hyperthermic episode. Animal was normothermic throughout.
5	Anaesthetic Death	Initial difficulty with intubation;subsequent problems with ventilation and associated equipment leading to accidental exposure of the lungs to high pressure gasses leading to suspected massive lung damage. VT-VF. Procedure did not progress to surgery. Anaesthetic death.	Review procedures and equipment.
6	Terminate	Induction, anaesthetic and ventilation unproblematic. Surgical procedure progressed well, purse string sutures placed with no difficulty. Animal developed spontaneous uncontrollable VT/VF. Animal did not respond to anti-arrhythmic drugs, adrenalin or defib.	Stop all work and think whole strategy through.

Table 8 - 2nd Implant Study Results and Comments

11.5. Learning Outcomes and Proposed Way Forward

This series of experiments did not lead to the anticipated deployment of the devices or the required long term recovery of the animals. However, a number of very important lessons were learned through this experience;

(1) The device was redesigned after experiment 2 where it was apparent that the double sewing ring design was not compatible with the implantation procedure. A new single sewing ring design was developed rapidly and was successfully deployed in a further experiment. This is the design that will be employed in future work as it is both easy to deploy and secure after placement.

(2) There was frequent occurrence of arrhythmia in animals leading in some cases to VT/VF and, in one extreme case, ballooning of the heart whenever touched. This led to the termination of 2 procedures and may have played a part in the problems encountered in animal 5. We have looked into this, through a review of the literature and it would appear that a prophylactic approach to the administration of anti-arrhythmic drugs, as employed by some other investigators may help with this issue. In addition, we consulted a specialist veterinary anaesthetist with experience in open-heart surgery in swine, both in terms of the anaesthetic protocol and the equipment employed.

(3) Damage to the right atrium during cannulation that led to the termination of 1 procedure and combined with unusual anatomy led to the termination of another, has been addressed. Consultation with paediatric cardiothoracic surgeons familiar with the highly fragile RA tissue in children led to a new approach to RA cannulation through the RA appendage. This worked well in subsequent procedures and has resolved this issue.

We gained considerable knowledge from these experiments that will guide this research going forward;

1. We can establish CPB in this model.

2. We can deploy our device.

3. A new approach to cannulation of the RA is required and has been successfully employed.

4. A new Phase 3 device will be developed in response to this experience and this will considerably enhance the prospect of success in future experiments.

Chapter 12.

Concept Development – 3rd Iteration (Piezoelectric/ Ultrasonic)

12. Concept Development – 3rd Iteration (Piezoelectric/ Ultrasonic)

Piezoelectric ultrasonic motors (PUM's) offer significant benefits over brushed and brushless micro-motors. They are known for their high positioning accuracy, in the range of tens of nanometres. Due to their few moving parts they are a lot simpler in design than brushless motors, and this simplicity reduces the chance of motor failure. The principal on how piezoelectric/ultrasonic motors work is discussed in Chapter 6.4.2.2.

Although there are different variations of piezoelectric ultrasonic motors, they are all based on the principle of deformation of piezoelectric ceramics - most commonly PZT (Lead Zicorite Titinate.)

As discussed in Chapter 6.4.2.2, Piezoelectric ceramics generate an electric current when deformed. Conversely this can be reversed causing the ceramic to deform when subjected to an electrical current and this mechanism was utilised for the prototype for the ultrasonic motor concept. Piezoelectric motors.

The ability for the piezoelectric motor to securely interact with the strip was of prominent concern. The motor uses a piezoelectric foot that constantly and rapidly bends and straightens when it is subjected to an electrical current. When the deformation bends the piezoelectric material, there is a point during the cycle where the material is not in contact with the strip. A strategy had to be developed to compensate for this.

12.1. Motor Selection

The motor selected for this iteration was the Nanomotion EDGE motor purchased from Heason electrics (West Sussex, UK). This Reduced the power weight and size considerably compared to the previous DC brushless motors. *(See Figure 114.)* Data sheet provided in APPENDIX V.

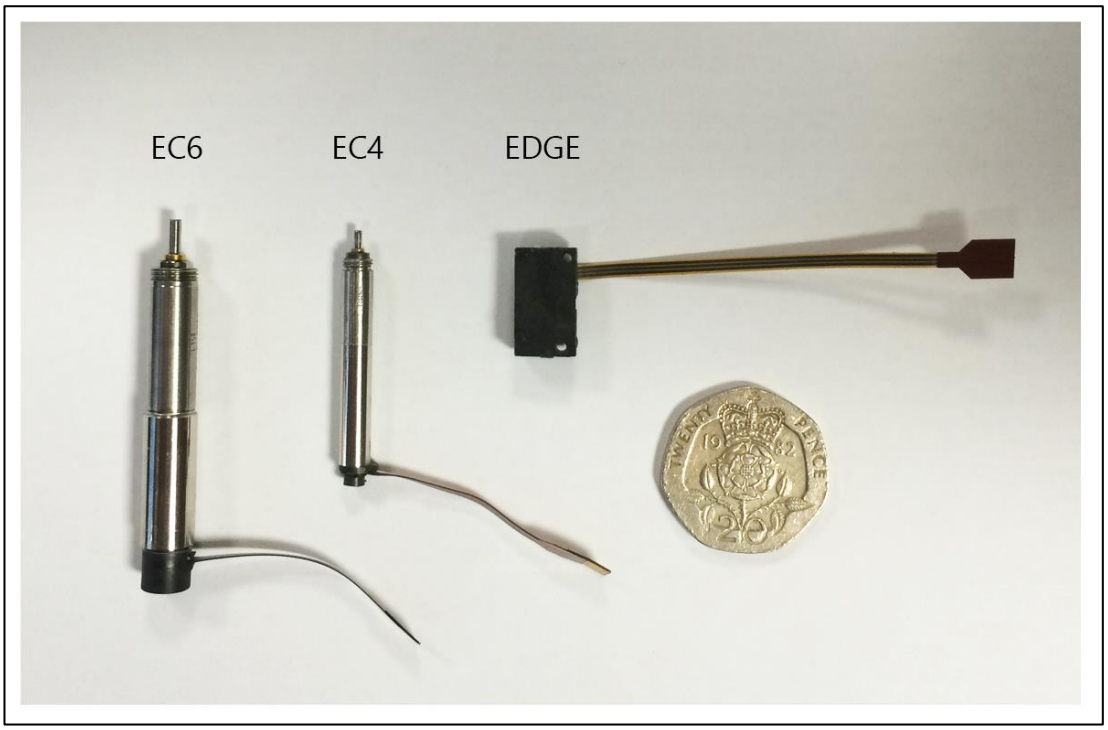

Figure 114 - EC6, EC4 and EDGE motor size comparison

Drive System	Length (mm)	Weight (g)	Power Requirement (V)
EC6 (Brushless)	52	9	12
EC4 (Brushless)	37	6.1	10
EDGE (Piezo)	**25**	**4**	**6**

Table 9- Drive Mechinism Properties Comparison

12.2. Concept Considerations and Restraints

12.2.1. Positioning

Due to the shape of the motor body, there was more flexibility with regards to the motor orientation and its interface with the strip. The motor itself is small and low profile and it did not require the addition of a bulky housing unit to maintain contact with the strip.

Motor positioning was considered to optimise function and profile. There are 2 ways in which the motor could be mounted to the strip. Option A *(Figure 115A below)* positions the motor directly above the strip (piezoelectric foot pointing towards the centre of the coiled strip.) Option B positions it perpendicular to the strip so that it can be flush with the top to the conduit. *(Figure 115B below)*

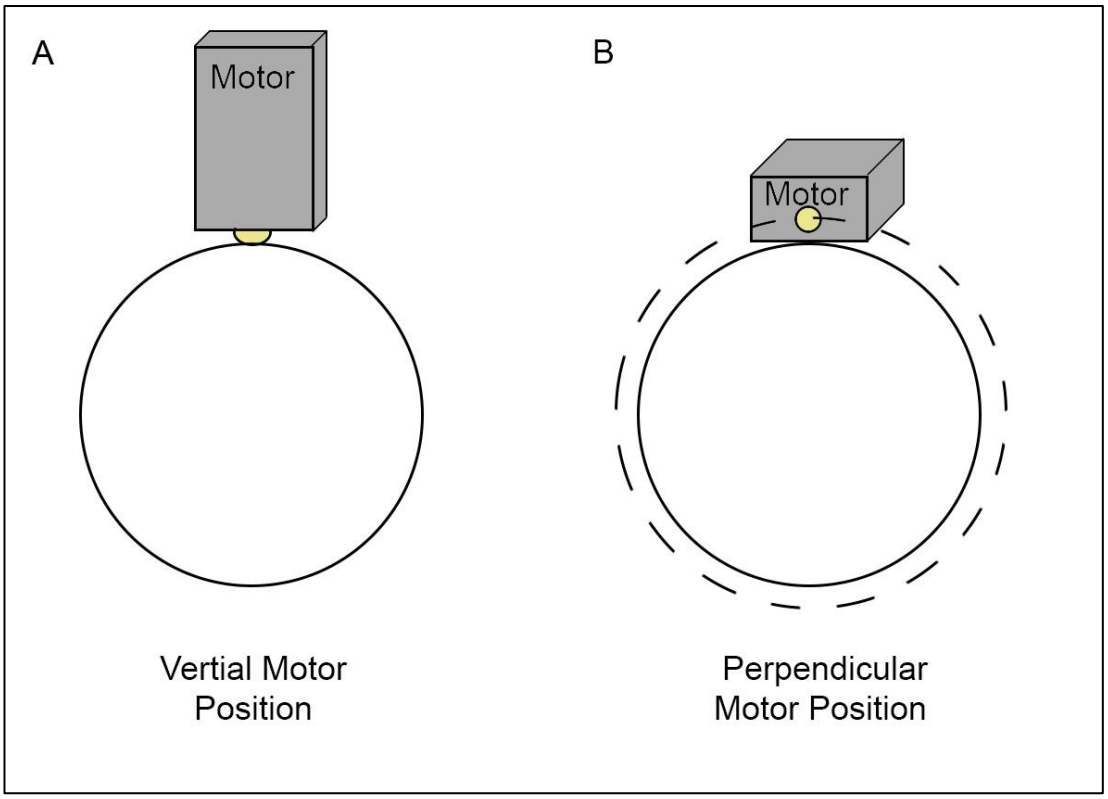

Figure 115 - EDGE motor position options, A) Directly above expansion strip, B) Perpendicular to expansion strip (require strip modification)

Option B would be less intrusive with regards to its effects on adjacent anatomy and reduce the profile of the device considerably. However, in order for the device to function the strip requires a raised section for the motor to interact with due to the positioning of the piezo foot. This additional contact surface is depicted by a dotted circle in Figure 115B.

The motor also requires a specific material with the correct friction coefficient to move and function correctly. These motors are designed to interact with hard ceramic tiles, rings or disks.

For the proposed application it is not possible for the strip to have material properties as it needs to remain flexible.

12.2.2. The Strip

A raised strip of ceramic would be needed on the surface of the strip for the piezoelectric foot to interact with. However ceramics are known for their hard brittle material properties. Due to the orientation required for the motor placement, the flexible ceramic sheet would need to be flexible in all 3 axis. This requirement is depicted below.

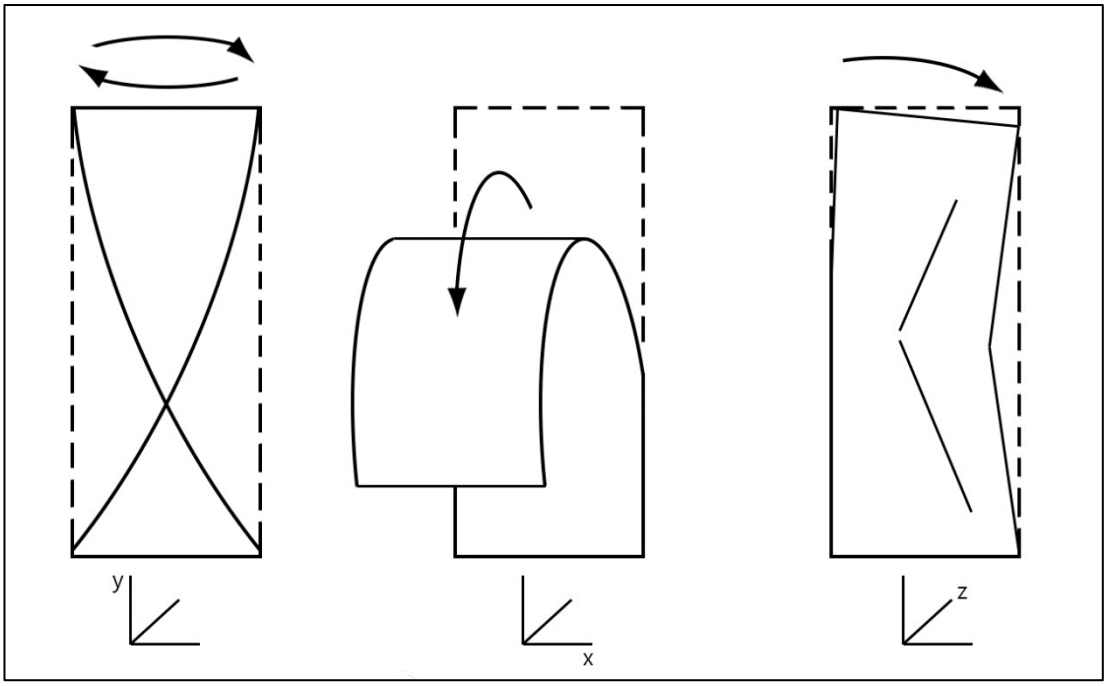

Figure 116 - Bending of ceramic sheet

You can bend the strip freely around the x axis, this is the natural way for the sheet to flex. You can even twist the sheet round the y axis creating a cork screw, but if it is bent around the z axis, the strip will buckle on itself and twist to accommodate this movement. This is influenced by the width of the strip. If the strip was as wide as it was thin (almost thread like) you would be able to bend it round all axes without noticing the deformation. For this application, the ceramic coating needs to be extremely thin in order to maintain its flexibility

but also wide enough for it to interact with the motor foot. This was not considered to be feasible.

Another possibility was to coat the strip in ceramic paint. Ceramic paints are used in the automotive industry for cosmetic and insulation purposes. Ceramic components exist in some exterior paints to protect against stretches and scuffs due to its high wear resistance. It is most beneficial when used in motorsport applications. On car engine components such as exhaust manifolds and turbo chargers ceramic coating help protect sensitive components from excessive heat which reduces risk of engine overheating and fires.

Typically ceramic paints are used on hard surfaces such as car body work steels and plastics. Our proposed method would involve flexion of the strip, so this method would crack and flake the coating if deformed too much, resulting in device failure.

To relate, each motor is designed to interact with a highly polished surface to allow for the maximum amount of friction as the motor moves along. As you cannot polish the thin surface needed to coat the strip without damaging it and so a paint coating technique would not be feasible.

The first preliminary designs for the ultrasonic motor relied on some kind of coating on the strip for it to interact with, however since this is not possible, another approach will have to be considered.

12.2.3. Motor Interaction and Drive Mechanism

To allow the piezoelectric foot of the motor to interact with a highly polished ceramic surface, a ceramic disc was mounted between the motor and the strip. If positioned correctly, the motor can be used to rotate the disc and expand the strip, either through friction or an integrated gear and notch mechanism.

Whether through friction or gearing, the positioning distances of the three components is critical. If using a friction drive between the disk and the strip, there would need to be sufficient force between them to hold them securely when stationary and enough friction to drive the strip when expanding. The motor would need to be positioned at the correct distance from the ceramic disc. If positioned too closely, the piezoelectric foot would not be able to straighten fully thus failing to complete its movement cycle effectively stalling the motor. The ceramic disks were purchased from Nanomotion, the providers of the ultrasonic motor. They are small 10 mm diameter discs with highly polished surfaces on all sides to correspond with the foot of the motor. With an inner diameter of 4mm allowed for a small bearing to be secured providing smooth rotation of the disc. Figure 119 below shows the testing platform built to test the integration between the piezoelectric motors and the disk. The motor could slide along a groove allowing for the motor to be positioned to apply different forces on the disk to determine optimal performance. It was found that a distance of 0.5 mm between the edge of the disk and the motor body allowed optimal disc movement.

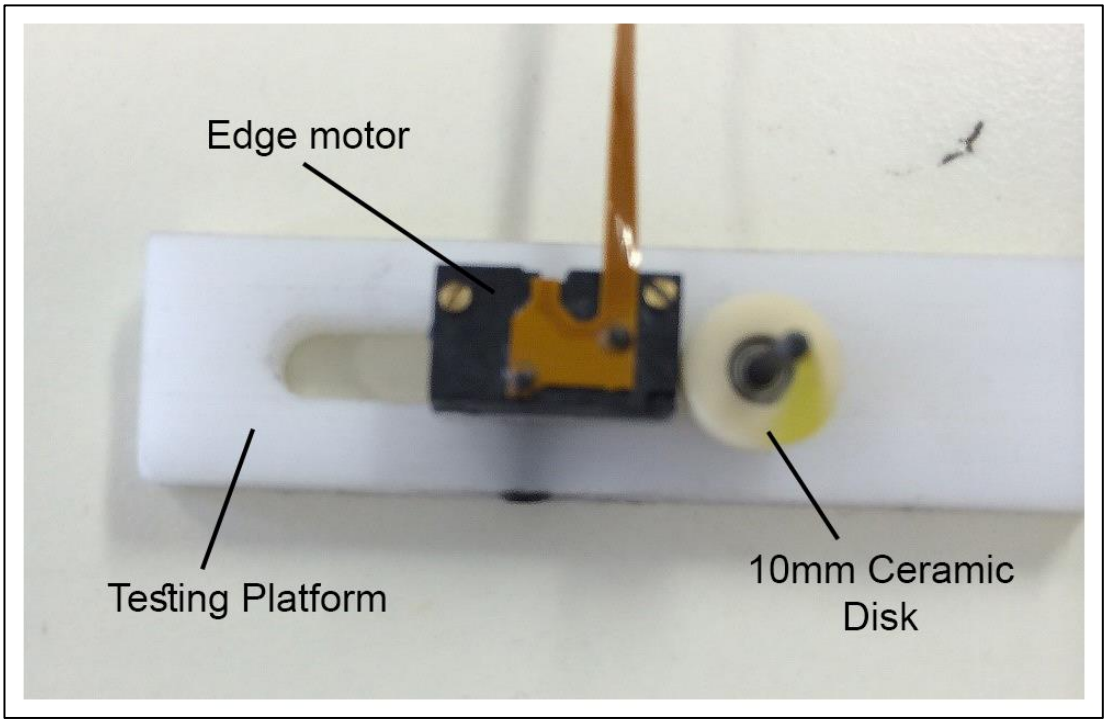

Figure 117 - Motor Testing Platform

The alternative to this friction drive is the gear-notch method. This would involve the mounting of a small spur gear on the top surface of the ceramic disk, whereby the teeth of the gear will correspond to notches along the ridge of the strip. This would mean there is no need for a high friction force connecting the disk to the strip.

Another issue to take into consideration with the strip is how it will be secured in place. In order to minimise the profile of the device it was designed to prevent the strip from overlapping as was seen in the thin stainless steel strip for the spur gear design. The addition of this raised ridge will make it difficult to double up on itself when rolled to its desired starting diameter. This could be done by having a slit in the strip just behind the ridge to accommodate the overlapping strip material. There were concerns that this configuration would be difficult to efficiently coat in silicone for implantation procedures.

12.3. Piezoelectric Prototype 1

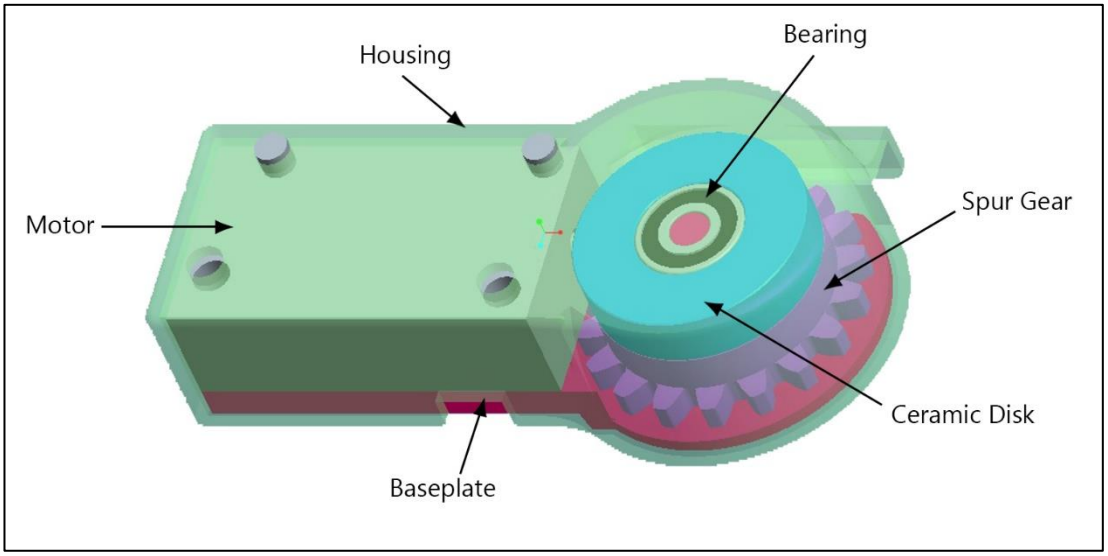

Figure 118 - CAD Design of gear/notch drive mechanism

The initial configuration for this concept involved using the spur gear mounted on the underside of the ceramic disc *(Figure 118)* in which the motor turns the disc and gear. This

gear will interlock with a raised section on the strip, with the motor providing drive to expand the strip which is guided through an inlet on the housing section of the device.

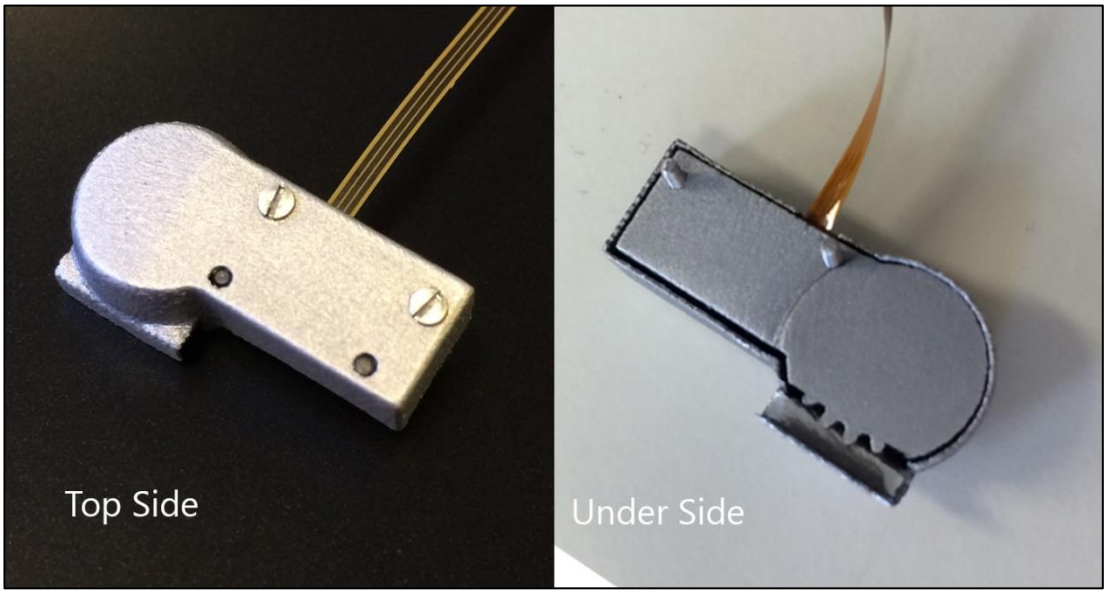

Figure 119 - Printed and assembled gear notch design

12.3.1. Strip Design

Unlike the worm gear concept, it is not possible to use a stainless steel strip for this design. For motor orientation, there needs to be a ridge on the strip to allow for the gear to interact with it. If a stainless steel strip was used, a flexible strip of some other material would need to be mounted to its surface. This unnecessarily complicates the design. If the adhesive that bonds the ridge material to the steel strip fails it could detach from the strip causing device failure, if the friction drive mechanism was chosen, it would be likely to become damaged under the stresses of assembly. Ideally the ridge and strip should be all in one piece, constructed of a flexible plastic, for example, the nylon used in a conventional cable tie. This means it could be possible to custom design the strip with regards to what drive mechanism is selected and have it 3d printed to a precise specification. This custom strip was 3D printed in a strong flexible material, TPU 92A-1 which was available from Materialise On-Site (Leuven,

Belgium), which allowed it to bend while maintaining control of the strip without the join between them which could prove problematic.

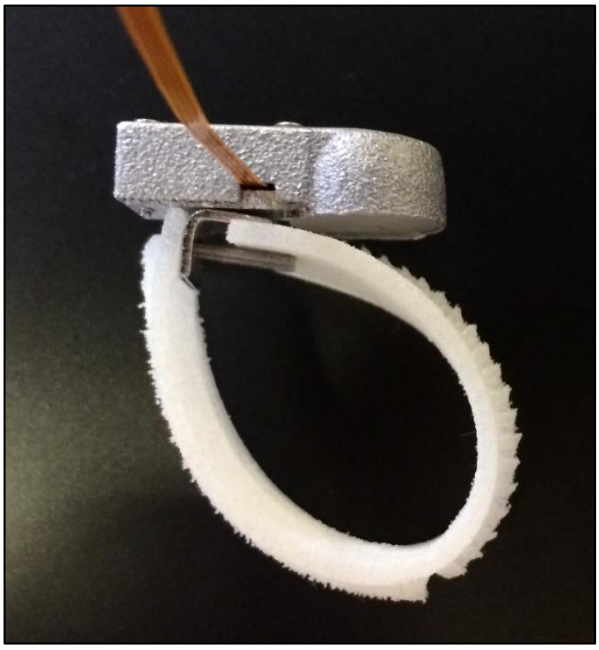

Figure 120 - Gear/notch design with 'flexible ceramic' strip

After construction of this prototype, when tested on a straight ridged strip, the motor mounted and interacted adequately with the teeth on the strip. However, when the flexible strip was attached and coiled it was clear that the expansion force of the strip was too strong for the motor to hold it in place. The friction between the foot of the motor and the disk was too low. It was also noted that the strip did not maintain a circular form when coiled *(Figure 122).* Another method had to be considered.

12.4. Piezoelectric Prototype 2.

To use the force applied by the motor to restrict the elastic properties of the expansion strip, in essence, to use the motor as a controlling mechanism working against the natural spring property of the coiled strip. This method uses the piezoelectric motor as the drive mechanism was coupled with the actuator concept described in Chapter 6.5.1.1. The previous concern was that due to the screw thread being attached directly to the motor shaft, and the length of screw

needed to expand the strip would make the device far too long. However, with the use of a piezoelectric motor, the screw thread can be positioned underneath the motor, essentially doubling back on itself. The disk would be mounted perpendicular to the motor, with the screw shaft passing through the centre of the disk. Similar to the worm gear concept, this reduces the amount of force needed to turn the disk and significantly reduces the likelihood of the device 'slipping'.

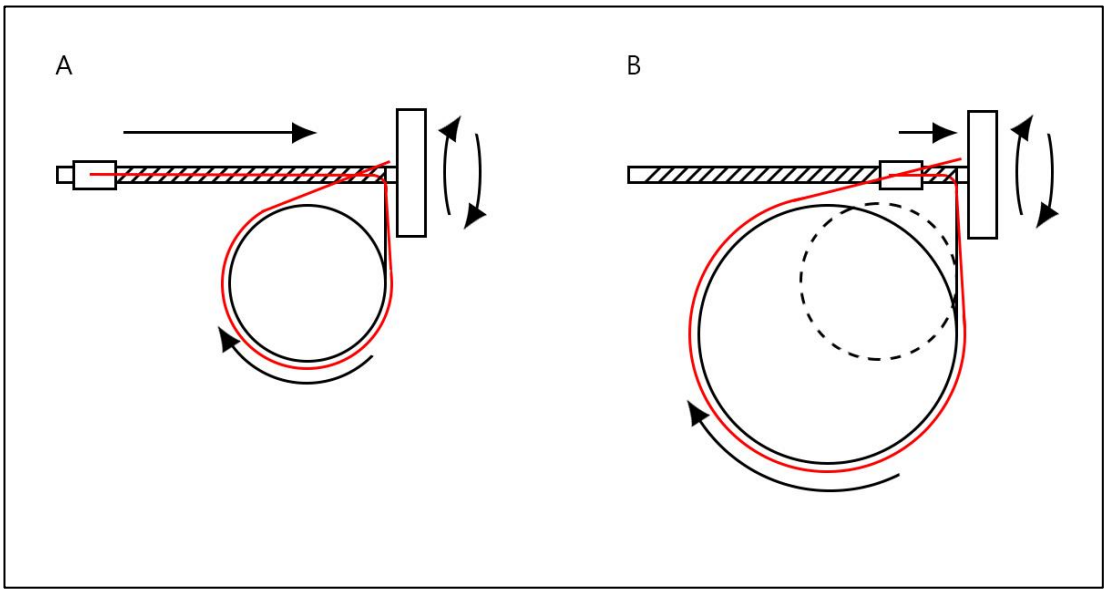

Figure 121 - Wired Actuator Expansion Design (Wires depicted in red)

A stainless steel strip could be used for this prototype, though the exact specification of the strip had to be carefully considered. It had to be strong enough to exert adequate force on the tissues but also had to be coiled to the initial 12mm diameter.

A small manual prototype was built from brass to demonstrate the new mechanism, this is shown in Figure 121. The red block represents where the motor would be positioned in relation to the strip and a white plastic disk is used to represent the ceramic disk which will interact with the motor.

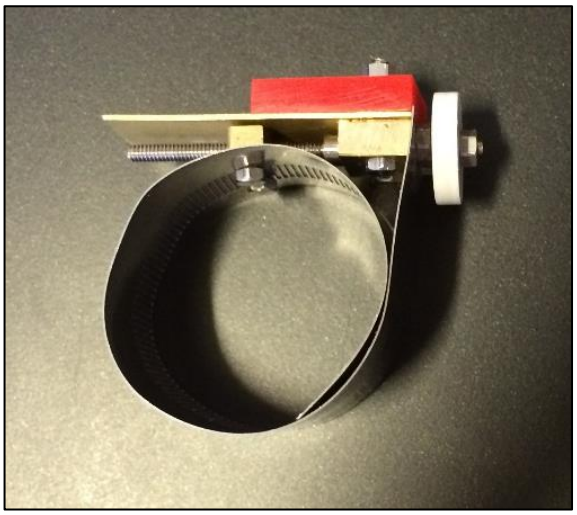

Figure 122 - Brass Prototype of actuator concept

Initially it was thought that the strip could be attached directly to a moving component threaded on the shaft (called the shuttle) with the point of contact moving away from the disk, expanding the strip. In practice, the strain on the thread, and the motor deformed the strip when it reached larger diameters. The length of the thread was determined by the increase in circumference of the strip, which calculated in Chapter 6.5. to be 25.43mm. An additional 5mm was added to the thread length so that the shuttle was not right on the edge of the screw thread.

To resolve this deformation issue, the strip was detached from the shuttle and wires were used to control its expansion. This allowed the strip to maintain its shape and, with the use of bearings allowed the shaft and disk to rotate smoothly along its entire length. As the screw turned, it slackened the wires holding the strip coiled, which allowed the strip to expand smoothly.

A functional prototype was built for bench testing. It was important for the wire to remain in line with the threaded shaft because any misalignment would create added friction between the shuttle and the thread. This meant that the wire had to pass along the central axis of the mechanism *(depicted in Figure 123).*

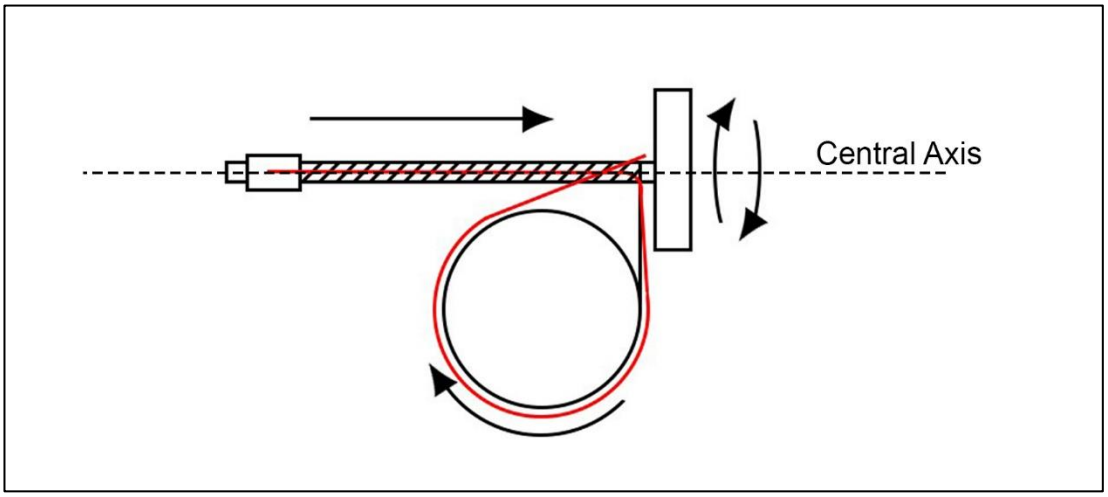

Figure 123 - Wire and Shaft alignment through central axis

The wires would run through a base onto which the motor was to be positioned and continue round the strip. However, one end of the strip has to be secured to the front of the base. This posed an issue with the wiring of the mechanism. If the wiring was to remain following the central axis, they would naturally fall behind the strip, since this concept used the wires to control the expansion they would need to be positioned on the outer surface of the strip. Two solutions were tested for this prototype, option A being to cut a hole in the strip to allow the wires to pass from the inside of the strip to the outside and option B was to move the attachment point of the strip into the base, rather than on the surface to allow the wires to flow over the top and down the front of the strip. These solutions are shown in Figure 124 and 125.

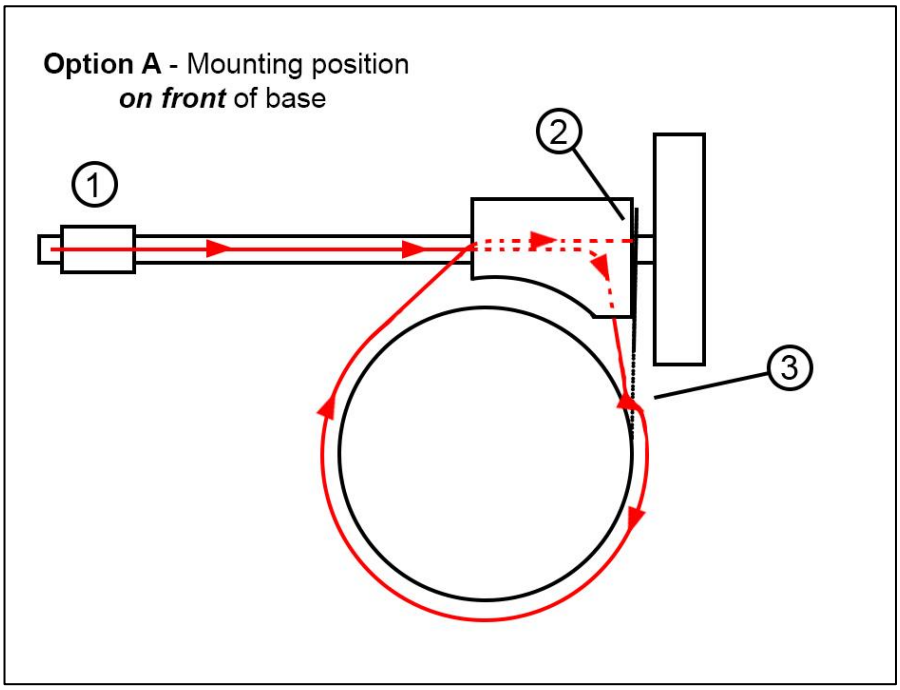

Figure 124 - Strip Position A - 1) Shaft rotates causing shuttle and wires to move along central axis, 2) Wires decend before passing the strip, 3) Wire feeds through a hole in the strip from back to front and continues round the outsidee of the strip

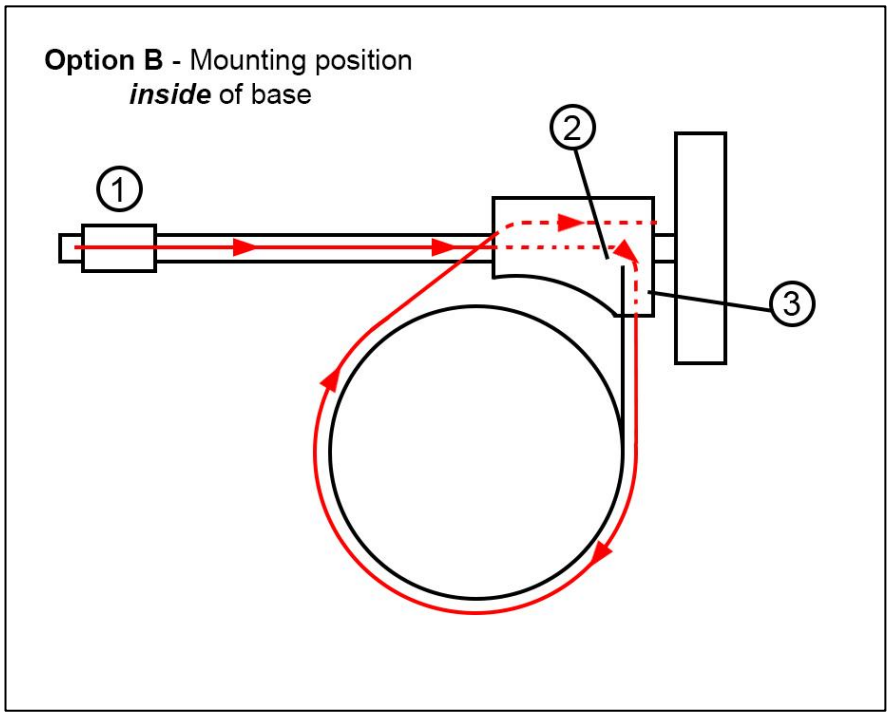

Figure 125 - Strip Position B - 1) Shaft Rotates causing shuttle and wires to move along central axis. 2) Wires continue along central axis and flow over the top of the strip. 3) Wire continues over the outside of the strip

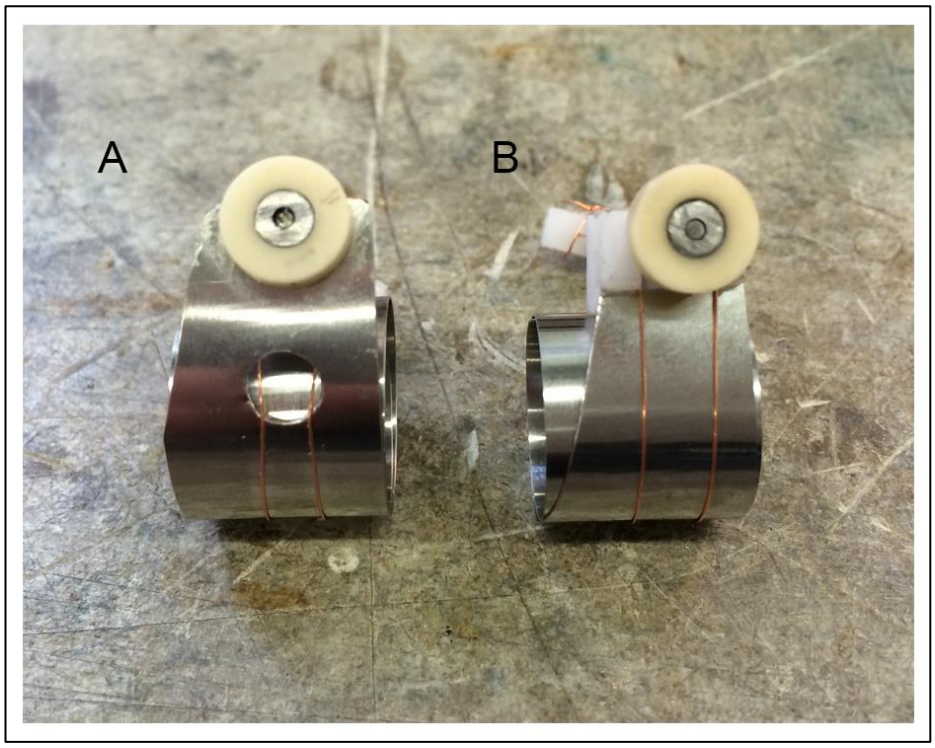

Figure 126 - Configurations A and B Built

During initial tests of these mechanisms, it was observed that in option A, the wire would scrape along the edge of the cut hole and would sever the wire during expansion. Therefore option B was favoured and developed further.

Figure 127 - Final strip and wire configuration

The base for the motor was then modelled and printed using the EDEN350 discussed in Chapter 7.7.2.The final motor base is depicted in Figure 127.

This method of expansion proved to be successful and a sheath had to be designed to encapsulate the expansion mechanisms as in previous methods. This sheath is shown in Figure 128, with the mechanism position within the sheath and the fully enclosed device. The mechanism and the sheath combined made the device smaller in length than previous iterations. This, coupled with the reduction in power by 50% gave the device a profile close to the final design. The device was then encapsulated and integrated with the sewing rings. *(Figure 129)*

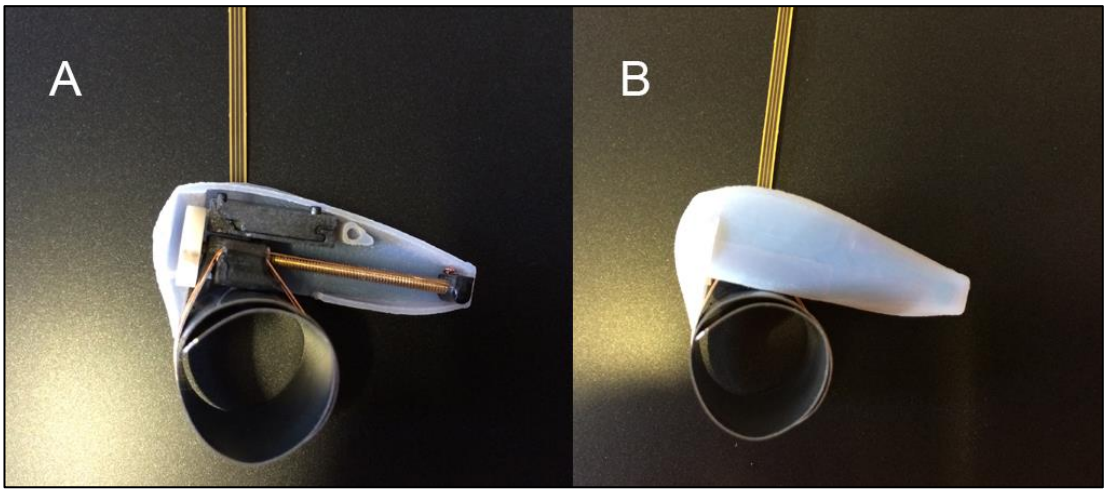

Figure 128 - A) Final device mechinism positioned inside the 3D printed sheath. B) Fully sheathed device ready for silicone encapsulation

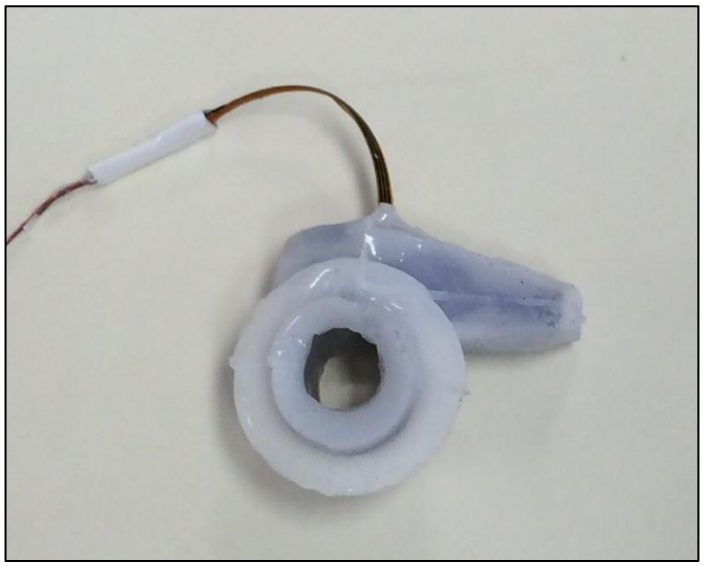

Figure 129 - Final silicone coated piezoelectric device with sewing ring and Dacron

12.6. 3rd Iteration Power and control

12.6.1. Motor board

Piezo electric motors generally use less power than DC brushless motors. Similar to the MAXON motors, its speed is determined by a separate microcontroller board. The microcontroller for the Edge motor was approximately half the size of that used for the second iteration which proved beneficial. Size comparisons are shown in Figure 130.

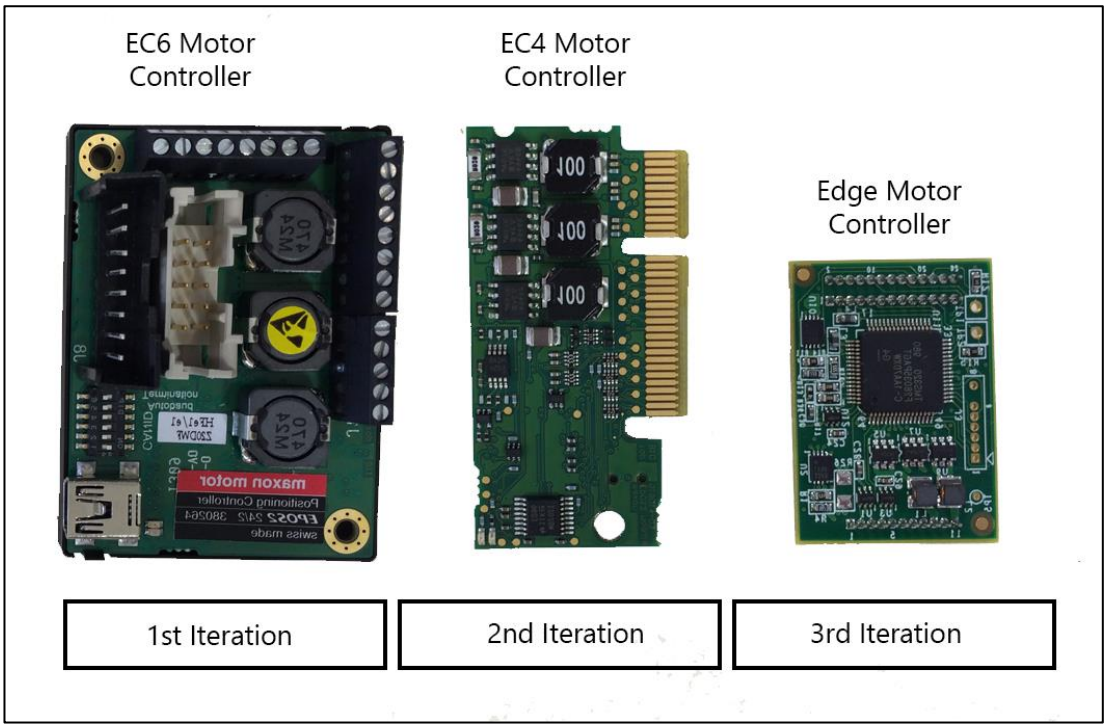

Figure 130 – Motor Controller Size Comparison

12.6.2. Timer Circuit

The timer circuit had to be reprogramed to accommodate this new motor. To do this, the motor was positioned on the testing platform as described in Chapter 12.2.3. The motor itself has a fixed operation speed. This was connected to the microcontroller programmed though RS232 cable to the PC, using Nanomotion's supplied software that came with the motors. The motor was programmed to run constantly when power was applied, which would then be controlled via the external timer circuit. It was important then to determine how many revolutions of the disk were needed to expand the device fully. As this is a time controlled mechanism, the time was recorded for the motor to revolve once. Due to the motors high speeds, footage of this testing platform was taken using the slow motion camera capabilities of the iPhone 5S, recording at 120fps. A 2 second clip was examined and it was noted that the motor turned the disk at a rate of 7 full turns within this time. Therefore the disk turned at a constant rate of one turn every 0.29s.

In order to expand the strip fully the shunt had to travel the full length of the thread which involved 62 turns of the screw thread over a 4 week period. The initial schedule was the same as previous iteration involving the device expanding for 1 day a week for 4 weeks, resulting 15 turns a day however, with the piezoelectric motor, this may put the motor under stress as they are generally used for short quick precision movements, and the 4.5 seconds of constant 'on' time may cause the motor to fatigue quickly. To resolve this, the 'on' period was further subdivided throughout the course of the week resulting in running at 2.2 turns a day. Although this was beneficial for the mechanism, it did not allow much time for the tissues to heal, allowing only 24 hours between each expansion period for recovery. It was then decided that the implantation period would be extended for a further 4 weeks, allowing a 7 day period of recovery time between a full week of expansion.

The coding for the timer circuit had to be amended accordingly for the motor to run for 638ms (2.2turns) every day for a full week every second week.

The altered motor coding section is shown below to accommodate this change.

```
for (dayloop2=0; dayloop2<=6; dayloop2++)
{
        PORTC |= (1<<PORTC1);
        PORTC |= (1<<PORTC1);
        _delay_ms(638);
        PORTC &= ~(1<<PORTC1);
        PORTC &= ~(1<<PORTC1);
        day();
}
```

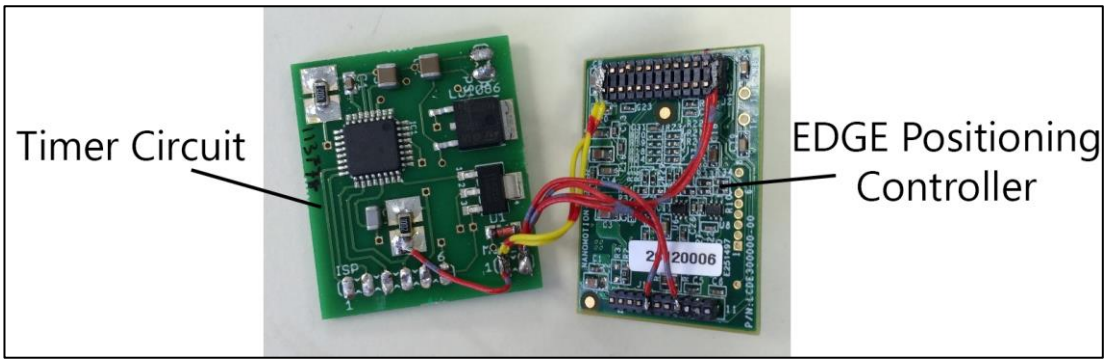

Figure 131 - EDGE Positioning Controller wired to timer circuit

The previous motor cable that was used for the MAXON motors had 8 wires within it, these wires needed to be attached one by one to the appropriate connecter on the side of the control box. With these piezoelectric motors, the cable only includes 4 wires, meaning a simple 4 pole 3.5mm jack connector could be used on the end of the cable and still be small enough to thread through any tissues. It also would reduce complications when connecting the device to the control box during surgery. Figure 132 shows the final control box used to house the microcontroller for the motor and the timer circuit , with the 3.5mm socket located on the side and the end of the motor cable with the 3.5mm jack connection.

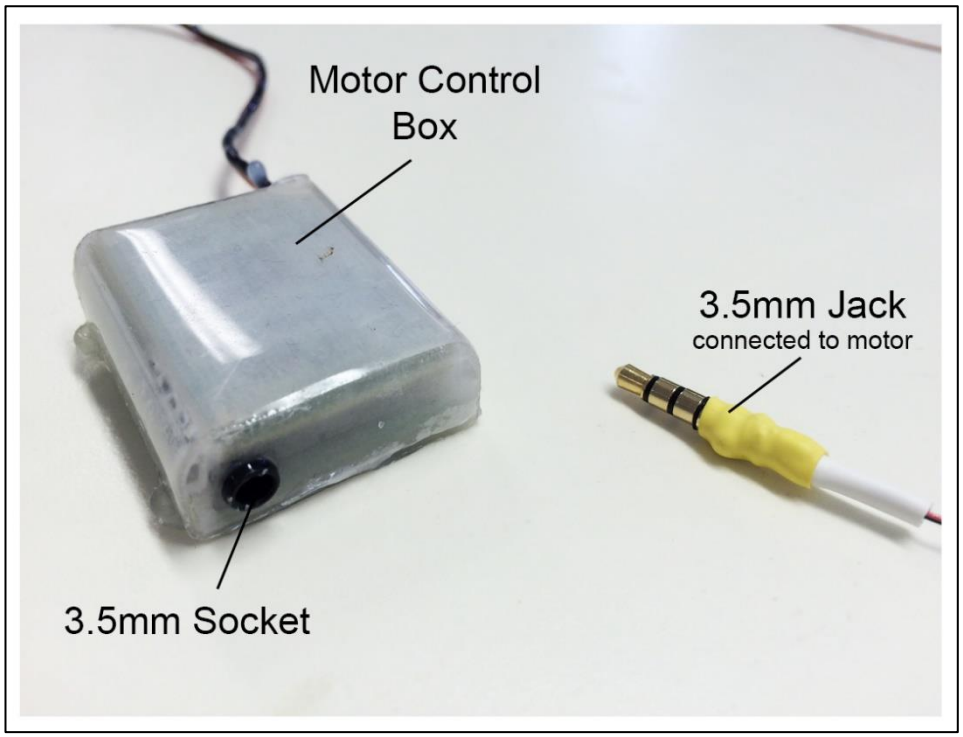

Figure 132 - 3rd Iteration Control Box with 3.5mm Jack and Socket connection

Since there was a further reduction in power needed by the new motor board and drive mechanism, the size of the power supply could be reduced further. Using three, CR247 3V coin cell batteries purchased from RS components (Northants, UK) produced well over the 6V required for this new control system. Their high capacity of 1000mAh would allow them to last the duration of the scheduled implantation. This new smaller power source also allowed for a smaller battery box, compared to that of the rechargeable phone batteries used in the second iteration.

The final coated device and control system is shown in Figure 133.

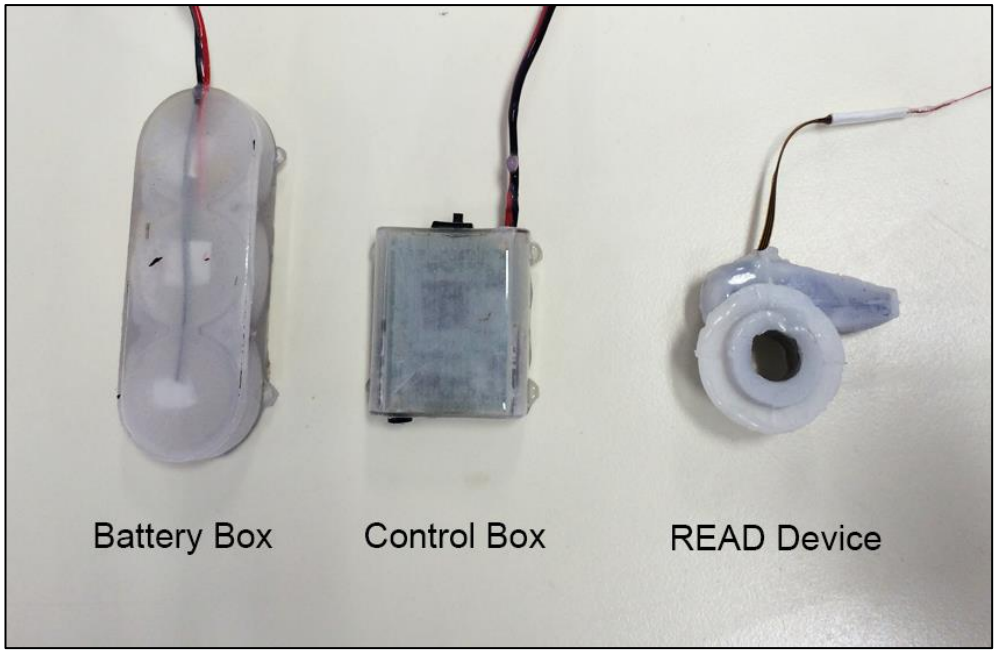

Figure 133 - 3rd Iteration final device ready for sterilisation

Chapter 13

3rd Implantation Series

Chapter 13. 3rd Implantation Series

13.1. Background

Following on from the second series of implant studies, a second series of implants were under taken at the experimental procedures facility at the University of Kirikkale in Ankara, Turkey. This facility was utilised due to their experience with implantation of cardiovascular devices and their strategic link to the University of Strathclyde. This revised combined technology was deployed in these animals in which the power and control elements were designed to be fully implantable subcutaneously to avoid the potential issue of infection and dislocation associated with the backpack solution employed in the earlier procedure. *(Figure 112)*

13.2. Brief Protocol

This aspect of the study employed the same study protocol as that of the previous series of experiments carried out at the Unievrsity of Strathclyde. *(Chapter 11.2.)* The advantage of performing these experiments at the University of Kirikkale in Turkey was that this centre is fully equipped to perform complex porcine experiments involving cardiopulmonary bypass supported invasive cardiac procedures. The equipment available is mimetic of modern clinical practice and eliminated the equipment related technical challenges that were apparent in the Strathclyde Unievrsity phase of the project.

13.3. Outcome of the Study

The pre-programmed READ devices (expanding from 12mm to 20mm in diameter over an 8 week period) were implanted as outlined in Chapter 11. 3 animal experiments were carried out in total and all survived the procedure through to recovery. One animal died of non- device related complications in the first week post-surgery, the remaining 2 animals survived through

to the planned experimental termination point of 12 weeks post-surgery. The details of the animal's clinical course is shown in Table 10.

Animal Number	Pre Weight (kg)	Weight at Termination (kg)	Complications	Comment
1	19	67.6	None	Uncomplicated course, device recovered
2	21	65.2	None	Uncomplicated course, device recovered
3	18.5	18.5	Died on Day 5 of respiratory failure	Unrelated to procedure

Table 10 - Basic clinical course and associated observations of study animals.

All animals were weaned from pain control and fluid transfusions over the first 3 days post-operation and all gained weight as expected of healthy animals. The third of the series of animals died on post-operative day 5 due to respiratory issues of unknown aetiology. It was suspected that pulmonary embolization was the route cause of this death, but there was only scant evidence of embolic deposition in the lungs with no apparent oedema present. The remaining 2 animals survived the 12 week post-operative course and grew significantly during this period, both gaining over 300% in body weight (animal 1 - 356%, animal 2 - 310%).

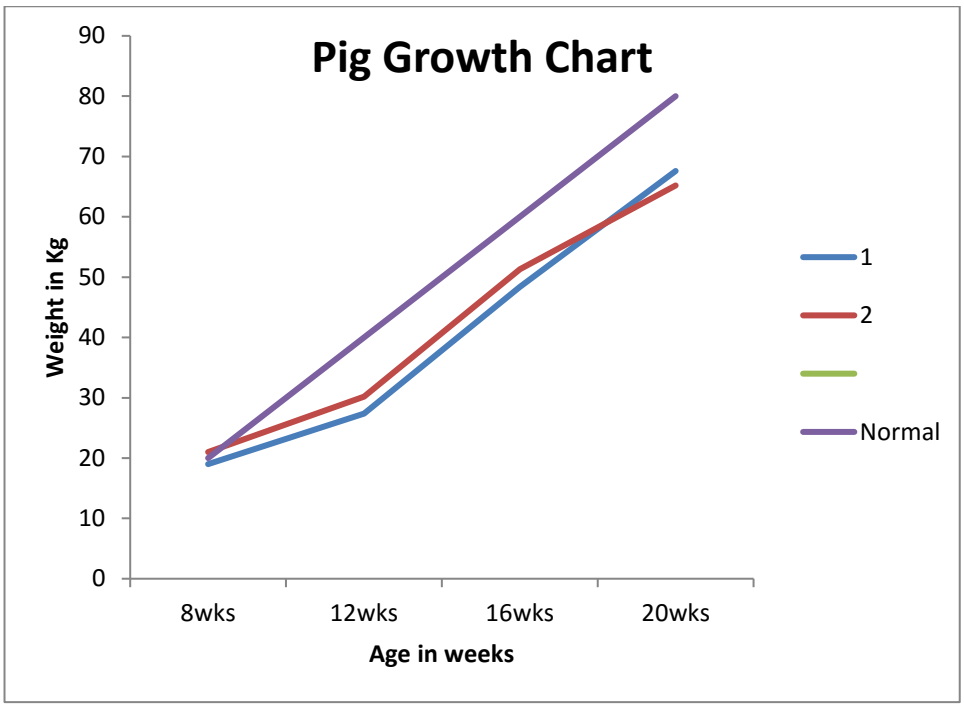

Figure 134- Pig Growth Chart

The weight gain profile for both animals over the experimental course can be seen in Figure 135, where the weight gain in the experimental animals is compared to expected normal growth (Carr 2016), using this as a marker of recovery from the procedure.. It is clear from these data that the growth rate of the experimental pigs was not normal and falls somewhat short of normal expectation. The first 4 weeks after the procedure were associated with a low weight gain compared to normal profiles, probably associated with the recovery from the highly invasive procedure. Beyond week 4, weight gain followed a normal pattern, suggesting a complete and uncomplicated recovery from the procedure

Both animals were sacrificed at 12 weeks and the READ devices recovered for inspection. In both cases is was found that the devices were rooted in the right ventricle with no apparent issues associated with the device/tissue interface, the devices were secure and uncluttered by tissue ingrowth. It was however clear that expansion of the READ devices as planned had not taken place. In both cases the devices were precisely the same diameter as they were at implant. Inspection of the power and control lines did not suggest technical failure in terms of control

or power supply, however, in depth testing of these was not carried out at this remote site. The battery packs and associated control and power delivery wires were intact and appeared not to have been negatively impacted by the implantation process or duration.

13.4. Summary Outcome of Second Phase of Animal Studies

The surgical procedures carried out in this second phase of implantation were all successful. All animals survived the surgical procedure and implantation of the devices. One of these died on the 5th post-operative day of complications unrelated to the device itself. The remaining two animals survived to the point of explantation, gaining weight at a sub-normal rate and recovering with normal social activity. 12 weeks after the operative procedure the animals were sacrificed and the devices harvested. Upon inspection of the devices there was no apparent expansion of the anastomotic region. There was breakdown of the electrical cables connecting the device to the power and control systems but no evidence of rejection of any of the components. There was some tissue ingress into and around the implant at the ventricular level with no clear orifice intrusion or impediment.

The results of this aspect of the work is on one level disappointing insofar as there was no evidence of expansion of the anastomotic device, but encouraging insofar as the integrity of the devices was maintained and there was no evidence of mechanical impediment or rejection of the devices. Critically, the devices were tolerated well by the animals all the through to explantation and appear to have little or no impact on the animals themselves. The clinical observations did not suggest at any time that there was any haemhorrage associated with the implantation, other than the normal drainage associated with open heart surgery. In this regard the devices were clearly deployable and apparently safely positioned in the hearts of the test animals. The major issue encountered was the apparent lack of functionality of the devices. It is difficult to determine the underlying reasons behind this, but the most likely cause is a disruption in power supply associated with the breakdown of the power and control cables, most likely due to mechanical disruption at the time of implantation. The expansion devices

appeared to be intact, but these are handled somewhat differently from the other components of the system during deployment. The expansion devices are implanted through an open chest into a lesion created in the ventricle of the animal, whereas the cables and the control and battery pack are “tunnelled” under the skin with considerable force. It is our belief that it is during these tunnelling processes that the integrity of these components were challenged leading to a power and/or control function disruption. Shorting of either cable component would without doubt lead to a disconnection between the control and power system and the expansion aspect of the device. These unfortunate circumstances make it difficult to determine the success of the devices in performing their primary function, but the successful implantation would suggest a genuine potential for success should the cabling problem be resolved.

Chapter 14.

Conclusions and Discussion

14. Conclusions and Discussion

In this work, the objective was to develop an electromechanical solution to the need for anastomosis site expansion in children who have had cardiac repair carried out requiring conduit implantation. The solution to this clinical problem has the potential to minimise further interventions and revision surgeries that may significantly increase the risk to the patient.

The objective for this work are listed as follows:

1. **Design a small expansion mechanism with the potential to expand at an anastomosis site.**
2. **Develop a suitable encapsulation technique for the device and its components to maintain biocompatibility when in vivo, to stop any cross contamination between the device and the surrounding tissues.**
3. **Determine a plausible, minimally invasive method for supplying power to the device when implanted.**
4. **Test the mechanism under laboratory conditions to ensure expansion potential.**
5. **Implant test the technology under clinically mimetic ex vivo conditions.**

14.1. Summary of Innovation

Designs for this device were based upon the idea of expanding a stainless steel strip in the form of a coiled structure that could be positioned in the anastomosis site. The most convenient drive mechanism for the expansion (uncoiling) of this apparatus was to utilise a single point expansion mechanism which comprised of a single micro motor. The design progressed through three iterative design stages based on this principal. Adapting both micro motor size and/or type at each stage to improve efficiency and placement potential.

These 3 iterations were as follows:

i. **1st Iteration – Worm Gear Concept (EC6)**

ii. **2nd Iteration – Worm Gear Concept (EC4)**

iii. **3rd Iteration - Ultrasonic Motor Concept**

Along-side the expansion mechanism design both power and control systems were created to perform an anastomotic expansion cycle from 12mm to 20mm in diameter over a number of years, from early childhood through to adolescence. This control system and power supply were altered in relation to changes in components and operating protocols that were present throughout the project.

A flow chart of how the project developed is shown in figure 135:

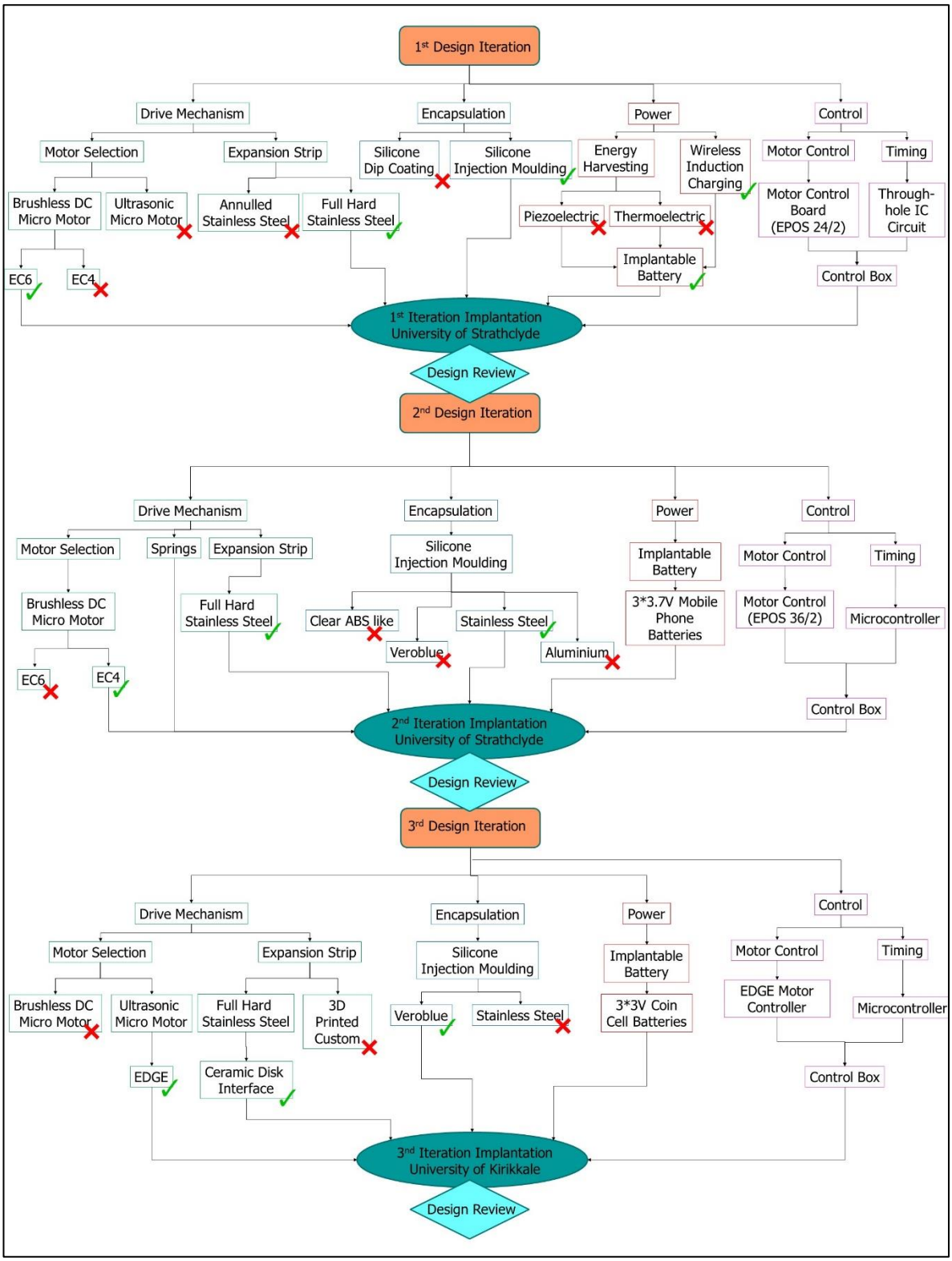

Figure 135 - R.E.A.D. Project Flow Chart

14.1.1. Concept Development - 1st Iteration Design (Worm Gear Concept)

During the development of the first iteration, a number of factors and components had to be determined such as expansion strip selection and motor orientation. To achieve, this early concept feasibility studies were carried out by designing a small expansion rig *(discussed in Chapter 7.1)* comprising of a micro motor with spur gear attachment, which successfully managed to expand an etched stainless steel strip with ease. However, on further examination it was clear that the perpendicular orientation of the motor to the strip would hinder the surrounding anatomy and would be much better suited if it was parallel. The decision to opt for a worm gear instead of the spur gear not only allowed this to be achieved but also reduced the force required and in turn the power needed for the motor to expand the strip. The motor selected for this iteration was the MAXON motor EC6, This was the largest of the 3 motors used throughout the iterative design process however its large torque was desirable to the functionality of the device. In addition to the worm gear an integrated gear head with the reduction ratio of 854:1 was used with the EC6 motor, this allowed the motor to continue to run at high speeds, reducing the risk of stalling and allow for the slow and controlled expansion needed for this application.

An aluminium housing support for the motor and strip were designed using a spring arm to allow movement of the strip in relation to the motor while maintaining contact at all times. A protective sheath was then designed using CREO 3.0 computer aided design software and 3D printed in an ABS like material. This provided a hard protective barrier for the drive mechanism.

The device was to be coated in a layer of silicone, this would act as a soft barrier between the device and the tissues so as not to cause harm or infection. This was achieved through use of an injection mould. The device was modelled in its entirety in CREO 3.0 and a negative cast created from it.

2 sewing rings were, modelled into this mould and reinforced with Dacron strips in order to sandwich the tissue in between and suturing through all 3 layers to ensure a secure hold onto the tissue.

For this first iteration of the device, due to the first implant study was carried out on a non-living animal, the control system was not tested in vivo, however an initial control system was created to run the device as if it were to be implanted in a live animal. It was designed on the basis of expanding the device from12mm to 20mm in diameter, 30 seconds a day over the course of 30 days. Using a combination of 2 timer IC's, one to count the on time (30 seconds) and one to count the off time (24 hours). The Motor and the control circuitry was powered externally using 10 x 1.2V rechargeable AAA batteries.

14.1.2. Outcomes

The purpose of the first implantation was to determine any potential impediments that would need to be addressed for implantation in live animal models. The exterior and internal wall sewing rings were removed to allow for easier implantation. The device itself was implanted successfully in the right ventricle using an interrupted suture to hold the device firmly in place. It was also seen that the device was too large in its current form. The control box was positioned in a backpack on the animals back, this was impractical for live animal models and they would be agitated by the cable and most likely interfere with the control mechanism during the recovery period.

14.2.1. Concept Development - 2nd Iteration Design (Worm Gear Concept continued)

Following from the previous iteration the main issue of the device size was the main concern. To address this, steps were taken to reduce the size of the expansion device considerably, this was achieved by using swapping the MAXON Motors (Berkshire, UK) EC6 with the smaller EC4 micro motor. The motor came was considerably smaller in size than its predecessor however it came with a smaller reduction gear box of 280:1. The aluminium housing and

springs were redesigned and optimised for the new motor size. A redesign of the sheath that protects the mechanics of the expansion mechanism was redesigned to stop any lateral travel of the worm gear and the expansion strip.

Further investigation was carried out on injection mould materials to determining that a mould made from 3D printed Stainless steel provided the best results, and the use of silicone grease was implemented to protect the devices moving parts during the encapsulation process.

The size of the power supply and control mechanisms were significantly reduced. The first iterations motor control board which was used to control the speed of the motor was replaced with a smaller version (approximately half of the original size.) Accompanying this, the two timer IC's in the timer control circuit were replaced by a single microcontroller, programmed with an updated duty cycle of 14.4 seconds a day for the 30 day implantation period. Over all this reduced the size of the timer and motor control system considerably, and were packaged together in a small control box designed in CREO 3.0 and 3D printed in ABS.

This iteration was powered by 3 x 3.7V mobile phone batteries, reducing the overall dimensions of the power supply. The two control components were deemed small enough to be implanted subcutaneously in the animal.

14.2.2. Outcomes

A total of 6 procedures were carried out. The experimental procedure for these is described in full in Chapter 11 where the animal was cooled and put on cardiopulmonary bypass before surgery took place. The device was implanted into each of the animals but the procedures were not successful as the long term objectives of the study were not be achieved.

14.3.1. Concept Development - 3rd Iteration Design (Piezoelectric Motor)

The option to reduce the size of the drive mechanism further was achieved by using the Nanomotion EDGE piezoelectric motor. This reduced the size and power consumption of the device, however the expansion method of the device had to be changed to accommodate this. Two different orientations were tried for this design settling on using the motor to turn a highly polished ceramic disk which, in turn, rotated a screw thread loosening off restraining wires to allow for slow expansion of the strip, this design is discussed in detail in Chapter 12. This was the most efficient way of utilising these small low powered ultrasonic motors to maximum effect, using the expansion force of the strip to be the primary method of expansion.

Accompanying the EDGE piezoelectric motor was its own control board which was again, significantly smaller than its predecessor in the second iteration. This control board was programmed to run the motor at a constant speed, and the 'on time' controlled by timer board designed for the second iteration. This programming however had to be altered slightly to accommodate for the functionality of the EDGE motor, as it was calculated that the on time for one week would need to be 4.5 seconds which was subdivided though the 7 day period leaving 638ms 'on time'. The total expansion time to 60 days rather than the original 30days. The cable that connected the motor to the control system was replaced by a 3.5mm stereo headphone jack and socket to allow for easy 'plug and play' of the device once implanted.

The size of the power supply was reduced further replacing the mobile phone batteries with 3 high capacity (1000mAh) 3V coin cell batteries.

14.3.2. Outcomes

3 procedures were carried out at the University of Kirikkale, in Ankara, Turkey. All animals survived the surgical procedure, one died on the 5th day of recovery with complications unrelated to the device itself. The remaining 2 survived the recovery and expansion period. Weight gain and social activity remained normal. Once the experimental period was over, the

animals were sacrificed and the implanted devices harvested. Unfortunately there was no sign of device expansion, and there were signs of breakdown in the connecting wires between the device itself to the power and control systems.

14.3. Objective Comparison

1. **Design a small expansion mechanism with the potential to expand at an anastomosis site.**

The design of the expansion mechanism had to take into account a number of factors, a) small in size as to not impede the surrounding tissues, b) Low power so that it can be powered either by energy harvesting or from minimally invasive charging sources, and c) have enough power to expand an expansion strip. Taking all of these attributes into account, the expansion mechanism for each iteration was designed around using a micro motor to expand a stainless steel strip. The first 2 design iterations used small profile motors from MAXON Motors (EC6 and EC4 respectively) and utilised a worm gear attached to the shaft to reposition the motor parallel to the strip expansion direction. This reduced the profile of the device and removed the possibility of the device partially obstructing a conduit when implanted. With each iteration the size of the expansion mechanism reduced significantly, and the power requirements followed suit. Resulting in a small low powered expansion mechanism which in which the expansion was tested before encapsulation of the device.

I feel that the limit of size and power has been achieved with this method of expansion, current technologies do not possess the power to size ratio that would be beneficial for this method of expansion.

The definitive solution to this problem may not involve any mechanical components at all, it could be entirely possible to use technologies such as 3D Bio printing discussed in Chapter 15.

2. **Develop a suitable encapsulation technique for the device and its components to maintain biocompatibility when in vivo, to stop any cross contamination between the device and the surrounding tissues.**

Cross contamination between the device mechanism and the tissues themselves is a major concern with a technology such as this. It was important to develop a way to protect both the electrical and mechanical components of the device from the surrounding tissues and for any debris that may be produced from the device leaking out into the body. This was successfully achieved using a 2 stage encapsulation process. A hard outer sheath was designed to provide a hard casing for the mechanical components and boxes were designed to house the electrical components such as the power supply and the control circuitry. Secondly a thin layer of silicone was applied through the use of injection moulding to completely encapsulate the device acting as a flexible barrier between the device and the tissues allowing maintaining functionality of the device. The sheath design and injection moulding was a method developed early on in the design process, and one that continued though the entire project.

This overall process **proved successful** due to the animals surviving the entire 3rd implantation study, proving the device did not cause any damage to the surrounding tissues when implanted resulting in a fully biocompatible device for this short 3 month implantation period.

A similar coating was applied to the connecting cables of the device. This proved problematic in the later implantation studies as it was seen that the coating was disrupted and pulled as the cables were threaded through the tissues. This could have potentially been the cause for device failure, causing a short in the power supply.

3. **Determine a plausible, minimally invasive method for supplying power to the device when implanted.**

Research was undertaken to determine the best method for powering the expansion mechanism. The ideal scenario being to harvest energy from the body itself to store energy to

power the device. Testing was carried out on commercially available piezoelectric material, which would convert the kinetic energy produced by the body, ideally the continuous movement of the diaphragm, to determine if this was in fact a viable solution for this device. The result of which was unfortunate as with current technologies available for piezoelectric materials, as the surface area needed and the amount it would need to deform would vastly more than would deem practical for this situation. The voltage and current produced by this material is minimal and more complex electronics would be needed to store and regulate power draw and storage. These materials are also quite ridged and brittle, so conforming to the bodily tissue without impeding function would be unlikely.

The next possible solution for this device is to use rechargeable batteries, which would be recharged transcutaniously through the skin using induction coils, this is currently used for such devices like pacemakers and cochlear implants, and would provide a viable solution to recharging the devices battery. A small experiment was carried out to see how simple it would be to create an effective induction coil power transfer system with success at transferring power to illuminate LED's, however these are fairly low powered devices (around $\leq$ 3V), therefore it is unclear what effects it would have trying to transmit the high voltage and current needed to recharge a battery power supply of around 9V (3 * 3V coin cell batteries used in the 3rd design iteration.) for example the burning of surrounding tissues. For short term testing and implantation purposes, Rechargeable battery packs were used consisting of a number of different rechargeable cells, each reducing in size with each iteration. It was concluded that for this technology, the viable long term method for powering the device as it stands would be to recharge an implantable battery periodically through its duty cycle through the use of induction coil which would transmit power wirelessly though the skin.

4. **Test the mechanism under laboratory conditions to ensure expansion potential.**

Bench testing of this device was successfully carried out on the device prior to encapsulation, It showed that for both expansion mechanisms (worm gear and ultrasonic) that it had the potential to increase the diameter of the expansion strip from 12mm to 20mm. Due to the time constraints of the project and strict deadlines for implantation of each of the iterations of the device, Bench testing was not carried out once the devices were encapsulated, this was because of the nature of the performing a 'one time only' operation it would have been unfeasible to remould the silicone around each device once it had been used and re-primed in the time frame implemented. It was thought that the thin silicone coating would have minimal effect on the expansion of the device itself.

5. **Implant test the technology under clinically mimetic ex vivo conditions.**

3 series of implantation studies were carried out over the duration of this project. The first set was implanted into a piglet cadaver to determine any potential impediments that would need to be addressed for implantation in the live animal models.

6 devices were built for the first set of live animal implantation surgeries. They were programmed to expand from 12mm to 20mm over a 4 week period. These implants were hindered however due to a number of technical difficulties involving: unusual anatomy, hypersensitivity and arrhythmia, ventilation and associated equipment, and tissue damage during surgery. These are outlines in Chapter 11. From these surgeries it was determined that it was possible to successfully establish CPB and the device can be deployed, however a new approach had to be determined with regards to RA cannulation. Further redesigns of the device in relation to size would be beneficial.

The second series of live animal implantation studies were carried out on three piglets at the University of Kirikkale in Ankera, Turkey. This time, the experiment duration was increased to 8 weeks accounting for the piezoelectric motor design. Discussed in Chapter 13. All three devices were implanted successfully, one of the piglets died on the 5th day of recovery with

complications unrelated to the device. The remaining two gained weight and made a full recovery. The animals were terminated and the implanted devices harvested. Unfortunately there was no sign of device expansion, and there were signs of breakdown in the connecting wires between the device itself to the power and control systems.

14.4. Other Potential Expansion Methods

The design for this device was based on using fundamental engineering principals to increase the diameter of the anastomosis site correlating with the growth of the surrounding anatomy. With this approach it was considered possible by applying a small constant force to the anastomosis tissues that they would be encouraged to adapt as the force increases leaving minimal scar tissue. However this may not be the ideal solution to this problem. An alternative solution which has come to light in recent years though the advancements in 3D printing technologies. Not only has it impacted the product and prototype manufacturing in industry, it has spilled over into the medical though the innovation of bioprinting. Bioprinting uses living cells and biocompatible support materials to produce functional living tissue structures. (Murphy et al. 2014). 3D printing of aortic valve conduits have already been achieved using hydrogel scaffolds with the incorporation of smooth muscle cells from the aortic root of a 12 year old girl. (Duan et al. 2013). These data prove that biocompatible implantable tissues can be 3D printed successfully however the nature of this problem is the growth of the conduit, specifically at the anastomosis site, it is yet to be determined if there are any complications regarding normal continued growth around these new tissue printed conduits such as scar tissue, and natural growth processes continue at the required rate. More importantly, this device focuses on the expansion of the anastomosis site and there is no confirmation that any other approaches to this have been successful. This issue would need to be investigated and monitored for to determine whether it is a viable solution.

14.5. Overall Achievements of Project Aims

The failure of the project to determine function implantation success may be regarded as an overall failure of the project. However, there are some clear successes. We were able to demonstrate after several iterations that it was possible to develop a functional expandable anastomosis mechanism using electromechanical means. The testing of functionality, was confirmed in vitro. The challenge of enhancing the biocompatibility of the device was met through silicone encapsulation of the device in such a way that functionality was not impaired. The power source was provided by rechargeable batteries that, although bulky, provided a more realistic solution than the initially proposed internal generation solution. Overall, technically the development was a success, producing an expandable, biocompatible and controllable solution to the continuous expansion of an anastomosis site. However, further work is required to prove functionality and efficacy of the technology under near-clinical conditions.

Chapter 15.

Future Work

This project is comprised of the very early stages in the iterative design process. Each component for this approach can still be improved and other methods for achieving the main aim are still to be investigated and developed further.

One large factor that is still missing from this device is a method of monitoring its progress. As it stands there is no way of knowing if the device is functioning properly, even though the device performed sufficiently on the bench, it was clear that further monitoring would have been beneficial throughout the implantation period. Information such as device expansion strip diameter, would allow for an early indication of device failure. Monitoring of device power consumption would allow for an estimate of how much power the motor is consuming which would be a representation of how much force is being applied to the surrounding tissues.

One idea that would coincide with this feedback system would be the ability to intervene with the mechanism during the experimental period, for example, if the motor stalls and requires more power to produce the torque needed to maintain functionality of the device, this could be achieved using wireless communication to the control system to adjust these parameters remotely.

Pressure sensors could aid in the visualisation of what is happening in relation to connecting tissues and if a conduit is applied, the flow rate of blood through the conduit. However issues surrounding the use of remote access software use in implantable technologies is security. Technologies such as those that transmit patient data or functional signals to and from implantable devices remotely can be susceptible to hacking attempts and interference. These attacks can cause a functional disruption in many implanted medical devices, with adverse events to the patient such as deafness and confusion to those with cochlear implants or in more serious cases or device failure and potential death, with devices aimed at cardiovascular and neurostimulation functions. (Camara et al. 2015)

Another task that will be carried out in the future development of this device is to make it conform to the European commission regulations to obtain its CE mark and be classified as a medical device The classification of medical devices is outlined in Annex IX of DIRECTIVE 93/42/EEC on medical devices. The level of classification corresponds to the level of potential hazards the device may hold. Due to the nature of this device, it would be labelled as a Class III medical device due to its surgical invasiveness during implantation, long term implantation and direct contact with the heart or cardiovascular tissues.

Chapter 16.

REFERENCES

REFERENCES

Advameg, I. (2016). "Artificial blood vessels." Medical Discoveries. from http://www.discoveriesinmedicine.com/Apg-Ban/Artificial-Blood-Vessels.html.

Al-Khalili, J. (2015). "The birth of the electric machines: a commentary on Faraday (1832) 'Experimental researches in electricity'." Philosophical Transactions of the Royal Society a-Mathematical Physical and Engineering Sciences **373**(2039).

ArcelorMittal (2010). "Stainless Steel and Corrosion." Stainless Europe. from http://www.aperam.com/uploads/stainlesseurope/Brochures/Leaflet%20corrosion_Eng_374Ko.pdf.

Ballermann, B. J. (1998). "Adding endothelium to artificial vascular grafts." Physiology **13**(3): 154-154.

Bar-Cohen, Y. (2004). EAP History, Current Status, and Influence. Electroactive Polymer (EAP) Actuators as Artificial Muscles, Reality, Potential and Challenges, Spie Press.

Bar-Cohen, Y., et al. (1998). Rotary ultrasonic motors actuated by traveling flexural waves. 5th Annual International Symposium on Smart Structures and Materials, International Society for Optics and Photonics.

Barbetseas, J., et al. (1998). "Differentiating thrombus from pannus formation in obstructed mechanical prosthetic valves: an evaluation of clinical, transthoracic and transesophageal echocardiographic parameters." Journal of the American college of cardiology **32**(5): 1410-1417.

Beardmore, R. (2013). "Worm Gears." from http://www.roymech.co.uk/Useful_Tables/Drive/Worm_Gears.html

Biglino, G., et al. (2013). "Modelling single ventricle physiology: Review of engineering tools to study first stage palliation of hypoplastic left heart syndrome." Frontiers in Pediatrics **1**(31).

Block, S. S. (2001). Disinfection, sterilization, and preservation, Lippincott Williams & Wilkins.

Bock, D. C., et al. (2012). "Batteries used to power implantable biomedical devices." Electrochimica acta **84**: 155-164.

Brawn, W. (2005). Atrioventricular septal defect. Key Topics in Cardiac Surgery. S. K. Ohri, A. Tang and L. W. Stephenson, Taylor & Francis Group**:** 258 - 261.

Bull, C. (1986). Atrial and ventricular dependent circulations. Congenital Heart Disease F. Macartney, UK and Europe: MTP Press Ltd**:** 35-54.

Camara, C., et al. (2015). "Security and privacy issues in implantable medical devices: A comprehensive survey." Journal of Biomedical Informatics **55**: 272-289.

Cameron, D. E. and L. A. Vricella (2004). Palliative Operations for Congenital Heart Disease. CURRENT THERAPY in Thoratic Cardiovascular Surgery. S. C. Yang and D. E. Cameron, Mosby**:** 722.

Carr, J. (2016). "Garth Pig Stockmanship Standards." from http://www.thepigsite.com/stockstds/17/growth-rate/.

Castro, C. F., et al. "ON THE MECHANICAL FAILURE OF ARTERIAL PROSTHESES."

Chapurina, Y., et al. (2015). "Synthesis of Thrombolytic Sol–Gel Coatings: Toward Drug-Entrapped Vascular Grafts." Journal of medicinal chemistry **58**(15): 6313-6317.

Chicago, U. o. (2014). "Hypoplastic Left Heart Syndrome." Pediatrics Clerkship. 2017, from https://pedclerk.bsd.uchicago.edu/page/hypoplastic-left-heart-syndrome.

Colas, A. and J. Curtis (2004). "Silicone biomaterials: history and chemistry." Biomaterials science: an introduction to materials in medicine **2**: 80-85.

Cole, J., et al. (2002). "Numerical investigation of the haemodynamics at a patched arterial bypass anastomosis." Medical engineering & physics **24**(6): 393-401.

Crow, S. (1993). "Sterilization processes. Meeting the demands of today's health care technology." The Nursing clinics of North America **28**(3): 687-695.

Culbertson, L. (2015). "Wireless Charging and Energy Harvesting to Revolutionize Medical Implants." from http://www.medicaldesignbriefs.com/component/content/article/mdb/features/22794.

Davis, F. and S. P. Higson (2007). "Biofuel cells—recent advances and applications." Biosensors and Bioelectronics **22**(7): 1224-1235.

de Leval, M. R. (2005). "The Fontan circulation: a challenge to William Harvey?" Nat Clin Pract Cardiovasc Med **2**(4): 202-208.

de Leval, M. R. (2005). "The Fontan circulation: a challenge to William Harvey?" Nature Clinical Practice Cardiovascular Medicine **2**(4): 202-208.

Delius, R. and J. Stark (1995). "Combined Rastelli and atrial switch procedure: anatomic and physiologic correction of discordant atrioventricular connection associated with ventricular septal defect and left ventricular outflow tract obstruction." European journal of cardio-thoracic surgery: official journal of the European Association for Cardio-thoracic Surgery **10**(7): 551-555.

Delius, R. E. and H. L. Walters III (2005). Truncus arteriosus. Key Topics in Cardiac Surgery. S. K. Ohri, A. Tang and L. W. Stephenson, Taylor &francis Group**:** 297 - 299.

Dennis, C. (1987). "Brief history of development of vascular grafts." P. Sawyer. New York: McGraw-Hill.

Desai, M., et al. (2011). "Role of prosthetic conduits in coronary artery bypass grafting." European journal of cardio-thoracic surgery **40**(2): 394-398.

Deyle, T. (2009). "Electroactive Polymers (EAP) as Artificial Muscles (EPAM) for Robot Applications." from http://www.hizook.com/blog/2009/12/28/electroactive-polymers-eap-artificial-muscles-epam-robot-applications.

Duan, B., et al. (2013). "3D Bioprinting of heterogeneous aortic valve conduits with alginate/gelatin hydrogels." Journal of Biomedical Materials Research Part A **101A**(5): 1255-1264.

Duncan, B. W. and R. B. B. Mee (2004). Transposition of the Great Arteries. CURRENT THERAPY in Thoratic and Cardiovascular Surgery. S. C. Yang and D. E. Cameron, Mosby**:** 755 - 758.

EACTS (2014). ECATS Congenital Database, Europein Association of Cardio-Thoratic Surgery.

Edelstahlwerke, D. (2007). "1.4104 - Chromium ferritic stainless steel with sulpher (Datasheet)." from http://www.dew-stahl.com/fileadmin/files/dew-stahl.com/documents/Publikationen/Werkstoffdatenblaetter/RSH/Datenblatt_4104_UK_.pdf.

Elkins, R. C., et al. (1994). "Pulmonary autograft in children: realized growth potential." The Annals of thoracic surgery **57**(6): 1387-1394.

Fontan, F., et al. (1971). "" Correction" of tricuspid atresia. 2 cases" corrected" using a new surgical technic." Annales de chirurgie thoracique et cardio-vasculaire **10**(1): 39.

Gallik, S. (2009). "Histology of the Heart Wall." from http://histologyolm.stevegallik.org/node/347.

Giboney, G. (1983). "Ventricular septal defect." Heart & lung: the journal of critical care **12**(3): 292-298.

GmbH, P. C. (2012). "Fundamentals of Piezo Technology." Technology. from http://www.piceramic.com/piezo-technology/fundamentals.html.

Gournay, V. (2011). "The ductus arteriosus: physiology, regulation, and functional and congenital anomalies." Archives of cardiovascular diseases **104**(11): 578-585.

Hardy, M. A. (1989). "The biology of scar formation." Physical therapy **69**(12): 1014-1024.

Haw, M. M. (2005). Hypoplastic left heart syndrome. Key topics in Cadiac Surgery. S. K. Ohri, A. Tang and L. W. Stephenson, Taylor & Francis Group**:** 282 - 286.

Higgins, R. A. (1968). Cold Working Process. Engineering Metallurgy, The English Universities Press LTD**:** 126.

Hoffman, J. I. and S. Kaplan (2002). "The incidence of congenital heart disease." Journal of the American college of cardiology **39**(12): 1890-1900.

Hopkins, R. A., et al. (1991). "Ross' first homograft replacement of the aortic valve." The Annals of thoracic surgery **52**(5): 1190-1193.

How, T. V. (1992). Mechanical Properties of Arteries and Arterial Grafts. Cardiovascular Biomaterials. G. W. Hastings. London, Springer London**:** 1-35.

Hunter, L. E. and J. M. Simpson (2014). "Prenatal screening for structural congenital heart disease." Nat Rev Cardiol **11**(6): 323-334.

Jahangiri, M., et al. (2000). "Repair of the truncal valve and associated interrupted arch in neonates with truncus arteriosus." The Journal of thoracic and cardiovascular surgery **119**(3): 508-514.

Jaques, L., et al. (1946). "Silicones and blood coagulation." Canadian Medical Association Journal **55**(1): 26.

Johnston, T. P., et al. (1990). "Controlled release of ethanehydroxy diphosphonate from polyurethane reservoirs to inhibit calcification of bovine pericardium used in bioprosthetic heart valves." International Journal of Pharmaceutics **59**(2): 95-104.

Jonas, R. A. (2009). Early primary repair of tetralogy of Fallot. Seminars in Thoracic and Cardiovascular Surgery: Pediatric Cardiac Surgery Annual, Elsevier.

Kapadia, M. R., et al. (2008). "A reproducible porcine ePTFE arterial bypass model for neointimal hyperplasia." Journal of Surgical Research **148**(2): 230-237.

Kapadia, M. R., et al. (2008). "Modified prosthetic vascular conduits." Circulation **117**(14): 1873-1882.

Keegan, G., et al. (2007). "Orthopaedic metals and their potential toxicity in the arthroplasty patient A REVIEW OF CURRENT KNOWLEDGE AND FUTURE STRATEGIES." Journal of Bone & Joint Surgery, British Volume **89**(5): 567-573.

Khan, A., et al. (2014). "Fabrication of zinc oxide nanoneedles on conductive textile for harvesting piezoelectric potential." Chemical Physics Letters **612**: 62-67.

Khlif, H., et al. (2011). "Contribution to the improvement of textile vascular prostheses crimping." Trends in Applied Sciences Research **6**(9): 1019.

King, A. (2009). "Surgery: Insights into patients' outcomes after the Ross procedure." Nat Rev Cardiol **6**(4): 263-263.

Lahey, F. (1946). "Comments made following the speech “Results from using Vitallium tubes in biliary surgery,” read by Pearse, HE before the American Surgical Association, Hot Springs, VA." Ann. Surg **124**: 1027.

Le Bas-Bernardet, S., et al. (2008). "Progress and prospects: genetic engineering in xenotransplantation." Gene therapy **15**(18): 1247-1256.

Lerouge, S. (2012). "Introduction to sterilization: definitions and challenges." Lerouge S, Simmons A, Sterilisation of Biomaterials and Medical Devices. Woodhead Publishing Series in Biomaterials: 1-19.

Martini, F. H. and J. L. Nath (2009). Blood Vessels and Circulation. Fundamentals of Anatomy and Physyology Pearson Benjamin Cummings**:** 719 - 774.

Martini, F. H. and J. L. Nath (2009). The Heart. Fundamentals of Anatomy and Physiology, Pearson Benjamin Cummings**:** 681 - 718.

Mavroudis, C. and C. L. Backer (2004). Coronary Artery Disease in Children. CURRENT THERAPY in Thoratic and Cardiovascular Surgery. S. C. Yang and D. E. Cameron, Mosby**:** 726 - 731.

Mavroudis, C. and C. L. Backer (2005). The Fontan circulation. Key Topics in Cardiac Surgery. S. K. Ohri, A. Tang and L. W. Stephenson, Taylor & Francis Group**:** 276 - 281.

Maxim Integrated, I. (2010). "Sterilisation Methods and Their Impact on Medical Devices Containing Electronics."

Mengeot, P., et al. (1985). "Effect of mechanical loading on displacements of chest wall during breathing in humans." Journal of Applied Physiology **58**(2): 477-484.

Migliavacca, F., et al. (2003). "Computational fluid dynamics simulations in realistic 3-D geometries of the total cavopulmonary anastomosis: the influence of the inferior caval anastomosis." Journal of biomechanical engineering **125**(6): 805-813.

Monahan, T. S. and F. W. LoGerfo (2007). "Endothelialization of Prosthetic Vascular Grafts." Cambridge University Press.

Monro, J. L. (2005). Vavular disease in children. Key Topics in Cardiac Surgery. S. K. Ohri, A. Tang and L. W. Stephenson, Taylor & Francis Group**:** 309 - 312.

Murphy, S. L., et al. (2013). "Deaths: final data for 2010." National vital statistics reports: from the Centers for Disease Control and Prevention, National Center for Health Statistics, National Vital Statistics System **61**(4): 1-117.

Murphy, S. V. and A. Atala (2014). "3D bioprinting of tissues and organs." Nat Biotech **32**(8): 773-785.

Nanomotion (2008). "The Piezoelectric Effect." from http://www.nanomotion.com/piezo-ceramic-motor-technology/piezoelectric-effect/.

Park, J. C., et al. (2001). "Calcification comparison of polymers for vascular graft." Yonsei medical journal **42**(3): 304-310.

Penny, D. J. and G. W. Vick (2011). "Ventricular septal defect." The Lancet **377**(9771): 1103-1112.

Podzolkov, V. P., et al. (1997). "Comparative assessment of Fontan operation in modifications of atriopulmonary and total cavopulmonary anastomoses." European journal of cardio-thoracic surgery **11**(3): 458-465.

Prevention, C. f. D. C. a. (2010). "Data Table for Boys Length-for-age and Weight-for-age Charts." National Center for Health Statistics. from http://www.cdc.gov/growthcharts/who/boys_length_weight.htm.

Prevention, C. f. D. C. a. (2010). "Data Table for Girls Length-for-age and Weight -for-age Charts." National Center for Health Statistics. from http://www.cdc.gov/growthcharts/who/girls_length_weight.htm.

Qin, Y., et al. (2008). "Microfibre–nanowire hybrid structure for energy scavenging." Nature **451**(7180): 809-813.

Quarteroni, A. (2010). "OPTIMAL CONTROL AND SHAPE OPTIMIZATION OF BYPASS." from http://cmcs.epfl.ch/applications/circulatorysystem.

Rastelli, G., et al. (1969). "Anatomic correction of transposition of the great arteries with ventricular septal defect and subpulmonary stenosis." The Journal of thoracic and cardiovascular surgery **58**(4): 545-552.

Repas, R. (2008). "Tiny Motors Make Big Moves." Machine Design. from http://machinedesign.com/archive/tiny-motors-make-big-moves.

Roche, J. (1987). "Explaining electromagnetic induction: a critical re-examination. The clinical value of history in physics." Physics Education **22**(2): 91.

Rodefeld, M. D., et al. (2005). Transposition of the great arteries. Key Topics in Cardiac Surgery. S. K. Ohri, A. Tang and L. W. Stephenson, Taylor & Francis Group**:** 287 - 292.

Roudaut, R., et al. (2007). "Thrombosis of prosthetic heart valves: diagnosis and therapeutic considerations." Heart **93**(1): 137-142.

Rutala, W. A., et al. (2008). Guidline for Disinfection and Sterilisation in Healthcare Facilities, 2008.

Salacinski, H. J., et al. (2001). "The mechanical behavior of vascular grafts: a review." Journal of biomaterials applications **15**(3): 241-278.

Sano, S., et al. (2003). "Right ventricle–pulmonary artery shunt in first-stage palliation of hypoplastic left heart syndrome." The Journal of thoracic and cardiovascular surgery **126**(2): 504-509.

Schniker, M. (1952). "Congenital anomalies of the heart and great vessels." Oxford University Press.

Sculpteo (2010). "Digital Light Processing (DLP) for Resin or Wax 3D Prints." Glossary. from http://www.sculpteo.com/en/glossary/dlp-definition/.

Sculpteo (2010). "Direct Metal Laser Sintering (DMLS) Fabrication Process for Metal 3D Prints." Glossary. from http://www.sculpteo.com/en/glossary/dmls-definition.

Sculpteo (2010). "Fused Deposition Modeling(FDM): 3D printing with filaments." Glossary. from http://www.sculpteo.com/en/glossary/fdm-fused-deposition-modeling-definition/.

Sculpteo (2010). "SLS (Selective Laser Sintering): 3D Printing Powder-based Process." Glossary. from http://www.sculpteo.com/en/glossary/selective-laser-sintering-sls-definition/.

Sculpteo (2010). "Stereolithography: 3D Printing by Laser solidifying Liquid-Resin." Glossary. from http://www.sculpteo.com/en/glossary/stereolithography-definition/.

Sircus, M. (2013). "Hyperthermia with Far-Infrared for Cancer and Pain." from http://drsircus.com/medicine/light-heat/hyperthermia-far-infrared-cancer-pain.

Snyder, G. J. (2008). "Small thermoelectric generators." The Electrochemical Society Interface **17**(3): 54.

Springett A and M. JK (2012). "Congenital Anomaly Statistics 2010: England and Wales." London: British Isles Network of Congenital Anomaly Registers.

Sterntech. "How Thermocouples Work." from http://www.sterntech.com/pdfs/thermocouples.pdf.

Stojanovic, I. (2013). "Mitral valve repair." from http://www.kardiohirurgija.rs/mitral-valve-repair.html.

Stratasys (2015). "How PolyJet 3D Printing Works." PolyJet Technology from http://www.stratasys.com/3d-printers/technologies/polyjet-technology.

Sue, C.-Y. and N.-C. Tsai (2012). "Human powered MEMS-based energy harvest devices." Applied Energy **93**: 390-403.

Sutton, M. S. J., et al. (1978). "Cardiac function in the normal newborn: additional information by computer analysis of the M-mode echocardiogram." Circulation **57**(6): 1198-1204.

Svensson, L. (2012). "Valve Sparing & Valve Preserving Surgery: Photos & Videos of Surgery." from https://my.clevelandclinic.org/health/articles/reimplantation-valve-sparing-surgery/photos-videos.

Teebken, O. E. and A. Haverich (2002). "Tissue engineering of small diameter vascular grafts." European Journal of Vascular and Endovascular Surgery **23**(6): 475-485.

Thomas, X. (2007). Silicones in Medical Applications. Inorganic Polymers R. De Jaege, Nova Science Publishers.

Thompson, J. E. (2001). History of Vascular Surgery. Surgery: Basic Science and Clinical Evidence. J. A. Norton, R. R. Bollinger, A. E. Chang et al. Berlin, Heidelberg, Springer Berlin Heidelberg**:** 969-985.

Tomaiuolo, M., et al. (2014). "A systems approach to hemostasis: 2. Computational analysis of molecular transport in the thrombus microenvironment." Blood **124**(11): 1816-1823.

Tomizawa, Y. (2003). "Vascular grafts: basic research and clinical applications." ADVANCES IN FLUID MECHANICS **34**: 1-40.

Townsend N, et al. (2013). "Children and young people statistics 2013." British Heart Foundation: London.

Ullom, R. L., et al. (1987). "The Blalock-Taussig shunt in infants: standard versus modified." The Annals of thoracic surgery **44**(5): 539-543.

Van Meurs-van Woezik, H., et al. (1987). "Growth of the internal diameters in the pulmonary arterial tree in infants and children." Journal of anatomy **151**: 107.

Vang, P. (2006). "Advantages and disadvantages between allograft versus autograft in anterior cruciate ligament replacement."

Wang, Z. L. and J. Song (2006). "Piezoelectric nanogenerators based on zinc oxide nanowire arrays." Science **312**(5771): 242-246.

Yasim, A., et al. (2006). "Gelatin-sealed Dacron graft is not more susceptible to MRSA infection than PTFE graft." European Journal of Vascular and Endovascular Surgery **32**(4): 425-430.

Yuan, S.-M. and H. Jing (2009). "Palliative procedures for congenital heart defects." Archives of cardiovascular diseases **102**(6): 549-557.

Zurbuchen, A., et al. (2013). "Energy harvesting from the beating heart by a mass imbalance oscillation generator." Annals of biomedical engineering **41**(1): 131-141.

APPENDIX

APPENDIX I – EC6 SPECIFICATION

maxon EC motor

EC 6 ∅6 mm, brushless, 1.2 Watt

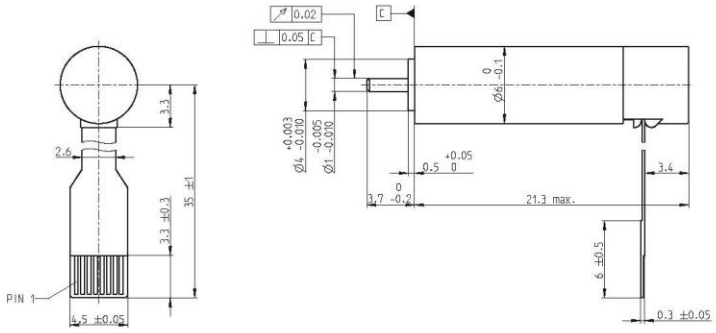

M 2.5:1

Stock program
Standard program
Special program (on request)

Article Numbers

		310599	250101
Motor Data (provisional)			
Values at nominal voltage			
1 Nominal voltage	V	6	12
2 No load speed	rpm	45100	34400
3 No load current	mA	53.1	19
4 Nominal speed	rpm	22400	11200
5 Nominal torque (max. continuous torque)	mNm	0.251	0.26
6 Nominal current (max. continuous current)	A	0.265	0.105
7 Stall torque	mNm	0.542	0.427
8 Starting current	A	0.48	0.147
9 Max. efficiency	%	45	41
Characteristics			
10 Terminal resistance phase to phase	Ω	12.5	81.5
11 Terminal inductance phase to phase	mH	0.0911	0.602
12 Torque constant	mNm/A	1.13	2.9
13 Speed constant	rpm/V	8470	3290
14 Speed/torque gradient	rpm/mNm	93800	92500
15 Mechanical time constant	ms	4.91	4.84
16 Rotor inertia	gcm²	0.005	0.005

Specifications

Thermal data

17	Thermal resistance housing-ambient	75 K/W
18	Thermal resistance winding-housing	5.0 K/W
19	Thermal time constant winding	0.467 s
20	Thermal time constant motor	80.2 s
21	Ambient temperature	-20...+100°C
22	Max. permissible winding temperature	+125°C

Mechanical data (preloaded ball bearings)

23	Max. permissible speed	100000 rpm
24	Axial play at axial load < 0.15 N	0 mm
	> 0.15 N	max. 0.06 mm
25	Radial play	preloaded
26	Max. axial load (dynamic)	0.1 N
27	Max. force for press fits (static)	10 N
28	Max. radial loading, 2 mm from flange	8 N

Other specifications

29	Number of pole pairs	1
30	Number of phases	3
31	Weight of motor	2.8 g

Values listed in the table are nominal.

Connection

Pin 1	Motor winding 3
Pin 2	Motor winding 2
Pin 3	Hall sensor 3
Pin 4	V_{Hall} 4.5...18 VDC
Pin 5	GND
Pin 6	Hall sensor 1
Pin 7	Hall sensor 2
Pin 8	Motor winding 1

Connector for Flexprint, Molex 52745-0897, FPC, 8 pole, pitch 0.5 mm, top contact style
Wiring diagram for Hall sensors see page 27

Operating Range

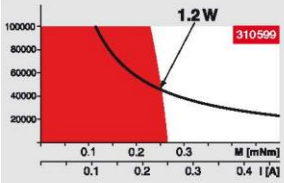

Comments

Continuous operation
In observation of above listed thermal resistance (lines 17 and 18) the maximum permissible winding temperature will be reached during continuous operation at 25°C ambient.
= Thermal limit.

Short term operation
The motor may be briefly overloaded (recurring).

Assigned power rating

maxon Modular System Overview on page 16 - 21

Planetary Gearhead
∅6 mm
0.002 - 0.03 Nm
Page 204

Encoder MILE
64 CPT,
3 channels
Page 262

Recommended Electronics:

DEC 24/1 **318305**	Page 297
DEC Module 24/2	298
EPOS2 24/2	312
EPOS2 Module 36/2	312
Notes	**20**

May 2012 edition / subject to change

Planetary Gearhead GP 6 A ∅6 mm, 0.002–0.03 Nm

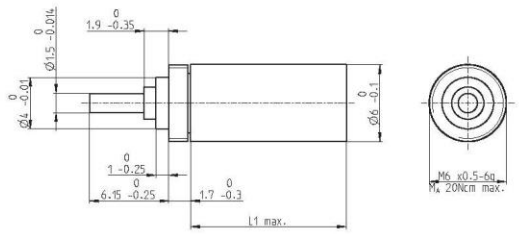

M 2.5:1

Technical Data					
Planetary Gearhead	straight teeth				
Output shaft	stainless steel				
Bearing at output	ball bearing				
Option	sleeve bearing				
Radial play, 5 mm from flange	max. 0.12 mm				
Axial play	0.02–0.10 mm				
Max. permissible axial load	5 N				
Max. permissible force for press fits	10 N				
Sense of rotation, drive to output	=				
Recommended input speed	< 40 000 rpm				
Recommended temperature range	-40...+100°C				
Number of stages	1	2	3	4	5
Max. radial load, 5 mm from flange	5 N	5 N	5 N	5 N	5 N

Stock program
Standard program
Special program (on request)

Article Numbers	304178	304179	304180	304181	304182
Gearhead Data					
1 Reduction	3.9 : 1	15 : 1	57 : 1	221 : 1	854 : 1
2 Reduction absolute	27/7	729/49	19683/343	531441/2401	14348907/16807
3 Max. motor shaft diameter mm	1	1	1	1	1
4 Number of stages	1	2	3	4	5
5 Max. continuous torque Nm	0.002	0.005	0.010	0.030	0.030
6 Intermittently permissible torque at gear output Nm	0.005	0.010	0.020	0.060	0.060
7 Max. efficiency %	88	77	68	60	52
8 Weight g	1.7	2.1	2.5	2.9	3.3
9 Average backlash no load °	1.8	2.0	2.2	2.5	2.8
10 Mass inertia gcm²	0.001	0.001	0.001	0.001	0.001
11 Gearhead length L1 mm	6.2	8.7	11.3	13.9	16.5

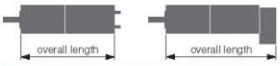

maxon Modular System

+ Motor	Page	+ Sensor/Brake	Page	Overall length [mm] = Motor length + gearhead length + (sensor/brake) + assembly parts				
RE 6, 0.3 W	50			21.9	24.4	27.0	29.6	32.2
RE 6, 0.3 W, Cap	50			25.9	28.4	31.0	33.6	36.2
EC 6, 1.2 W	138			28.4	30.9	33.5	36.1	38.7
EC 6, 1.2 W	138	MILE	262	28.8	31.3	33.9	36.5	39.1

Variant dimensions for the EC 6 combination (including assembly sleeve)

Combinations of EC 6 with GP 6

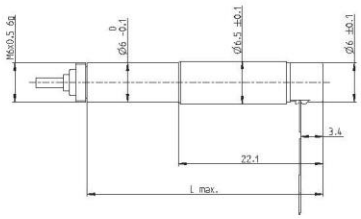

Combinations of EC 6 with MILE Encoder and GP 6

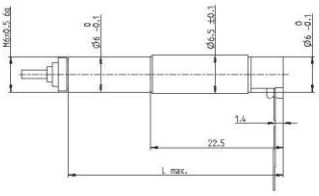

APPENDIX II – WORM GEAR SPECIFICATION

Schnecke / Worm		
no. of teeth z	Zähnezahl z	1
reference circle dm1	Mittenkreis dm1	2,4 mm
module m	Modul m	0,2 mm
flank direction	Flankenrichtung	rechtssteigend / clockwise
tooth width b1	Zahnbreite b1	7 mm
tip circle da1	Kopfkreis da1	2,8 mm
root circle df1	Fußkreis df1	1,9 mm
pitch angle γm	Mittensteigungswinkel γm	4,76°
diametral quotient q	Formzahl q	12
axial pitch px	Axialteilung px	0,628 mm
quality of thoothing	Verzahnungsqualität	7

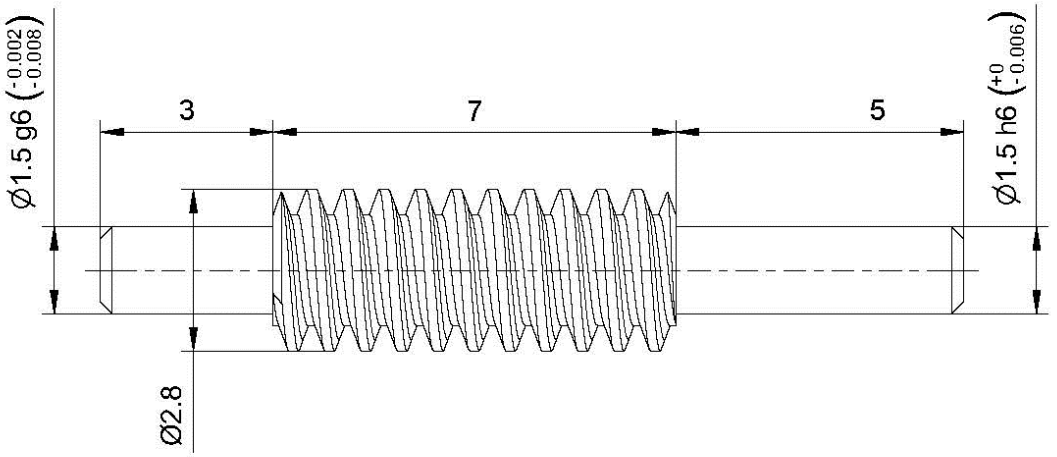

(2 : 1)

Rz 4

Werkstückkante /
work piece edges
DIN 6784

-0.1 +0.1

Micromotion PROPERTY

Diese Zeichnung ist unser geistiges Eigentum und darf ohne unsere Einwilligung weder kopiert, vervielfältigt noch an dritte weitergegeben werden.

This drawing and information herein is our property and is to be used in strict confidence. It shall not be copied or given to any third party without our written permission.

Allgemeintoleranzen / General Tolerances: ISO 2768-f

0,5	3	6	30	120	400	1000	2000
3	6	30	120	400	1000	2000	4000
± 0.05	± 0.05	± 0.1	± 0.15	± 0.2	± 0.3	± 0.5	/

micromotion®

Micromotion GmbH
An der Fahrt 13 Tel.: +49 (0)6131 66927-0
55124 Mainz Fax: +49 (0)6131 66927-20
Germany

Zus/Rev	Änderung / Modification	Datum/Date	Name

Ersatz für / Replacement for:

Ersetzt durch / Replaced by:

	Datum / Date	Name
Bear. Drawn	22.11.2012	SD
Gepr. Checked	22.11.2012	FK
Manufac. Checked		
Status		

Maßstab / Scale: 10 : 1

(Gewicht / Weight): 0,358 g

Material: 1.4104

(Benennung / Title): Worm-120604

(Zeichnungsnummer / drawing number): C-120604-100-001

(Version): C

Blatt/Sheet: 1 / 1

APPENDIX III –MFC SPECIFICATION

What is a Macro Fiber Composite (MFC)?

MFC benefits

- Flexible and durable
- Increased strain actuator efficiency
- Directional actuation / sensing
- Damage tolerant
- Available as elongator (d_{33} mode) and contractor (d_{31} mode)
- Conforms to surfaces
- Readily embeddable
- Environmentally sealed package
- Demonstrated performance
- Different piezo ceramic materials available

Schematic structure of the MFC

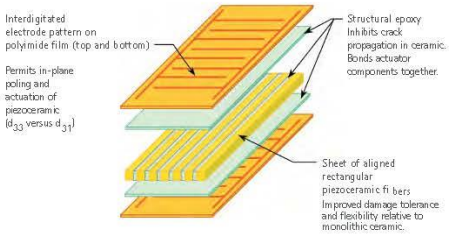

The Macro Fiber Composite (MFC) is the leading low-profile actuator and sensor offering high performance, durability and flexibility in a cost – competitive device.
The MFC was invented by NASA in 1996. Smart Material started commercializing the MFC as the licensed manufacturer and distributor of the patented invention* worldwide in 2002. Since then, the MFC has been continuously improved and customized to fit the customers' specific needs and to meet the requirements for new applications. Today more than 25 standard inventory sizes are available.
The MFC consists of rectangular piezo ceramic rods sandwiched between layers of adhesive, electrodes and polyimide film. The electrodes are attached to the film in an interdigitated pattern which tranfers the applied voltage directly to and from the ribbon shaped rods. This assembly enables in-plane poling, actuation and sensing in a sealed and durable, ready to use package. As a thin, surface conformable sheet it can be applied (normally bonded) to various types of structures or embedded in a composite structure. If voltage is applied it will bend or distort materials, counteract vibrations or generate vibrations. If no voltage is applied it can work as a very sensitive strain gauge, sensing deformations, noise and vibrations. The MFC is also an excellent device to harvest energy from vibrations.
The novel, pliable and conformable features of the MFC also allow for structural health monitoring applications, morphing and stiffening of structures, lambda wave generation and as a large area ultrasound 2–2 composite generator.
The MFC is available in d33 and d31 operational mode, a unique feature of the Macro Fiber Composite. The P1 type MFCs, including the F1 and S1 types are utilizing the d33 effect for actuation and will elongate up to 2000ppm if operated at the maximum voltage rate of -500V to +1500V. The P1 type MFCs are also very sensitive strain sensors. The P2, P3 type MFCs are utilizing the d31 effect for actuation and will contract up to 750ppm if operated at the maximum voltage rate of -60V to +360V. The P2 and P3 type MFCs are mostly used for energy harvesting and as strain sensors.

MFC P1 Type (d_{33} effect) Elongator
- powerful actuator
- sensitive sensor

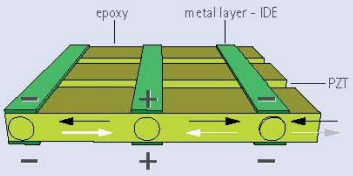

MFC P2 Type (d_{31} effect) Contractor
- Low Impedance sensor
- energy generator

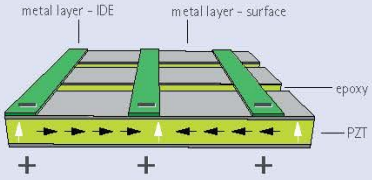

*protected under U.S. patent number 6,629,341, PCT/US00/18025; EP 1230689

APPENDIX IV – EC4 SPECIFICATION

maxon Flash No. 647
EC 4 / GP 4

February 8, 2013

From Michael Baumgartner
michael.baumgartner@maxonmotor.com
Tel. +41 (41) 662 42 84
Fax +41 (41) 666 16 50

To every e-mail address of mmb; mmi; mjc; mmcn; mmh; mmk; mmuk (only to William Mason, Patricia Wellman, Karen Whittaker); mpm; mmit (only to Luca Uberti, Alessia Moleri, Cinzia Bosani, Giovanni Stevenazzi); mmau; mmtw; Electrondart; mdp (only to Marc Rea, Florent Auternaud, Cédric Cadin, Anne Degrey); Electromate; Stork Drives; Aviton; Elsim; Servo Dynamics (Mr. Teo, Mr. Lau); Treffer; DNH Tradeserve, (only to info@dnhtrade.co.za), mpi, Kwapil

Copy Sales all, Marketing, Business Process Engineering

Ladies and Gentlemen,

you are looking at the best 4 mm micromotor in the world. An entire product program is already available: two motor sizes with two winding sizes each, with and without Hall sensors, as well as a matching planetary gearhead.

The evidence for the claim to being the best micromotor in the world can be found in the speed/torque gradient. With a value of 50,000 rpm mNm^{-1}, this motor-specific variable is alone at the top. With a continuous torque of 0.4 mNm, the EC 4 motor beats the performance of the competing products many times over.

The general problem encountered with micro drives is that the power output is too low for the customer's application, due to the physical dimensions. This stands in the way of many commercial applications.

Our challenge was to achieve maximum power in the smallest possible space. With the EC 4 platform, maxon explored the limits of the technical possibilities and is setting new benchmarks. With the innovative platform, we have created the prerequisites for opening up future-oriented fields of application.

The performance increase was achieved through no-compromise implementation of the latest winding technology, the most powerful magnets and optimum use of the air gap. Hall sensors make it possible to fully utilize the motor potential, right from standstill. The integration of Hall sensors is also unique for motors of this size.

To transfer the top performance characteristics of the motor in the application, a high-quality gearhead is necessary. The gearhead's ring gear and flange are a single part, the ring gear toothing is shaped; this provides optimum synchronous running. To make the products capable of withstanding the high input speeds and drive torques, high-performance ceramics are used for the planetary carrier. This makes a continuous torque of up to 15 mNm possible. The motor-gearhead interface is laser-welded and provides a constant diameter across the entire length of the combination.

This drive is a natural fit for applications in the fields of micropumps, analytic and diagnostic devices, ophthalmic surgical devices, laboratory robots, endoscopes and similar applications.

maxon gear GP 4
1 Output shaft
2 Flange
3 Ball bearings
4 Planetary wheels
5 Ceramic planetary carrier
6 Ring gear
7 Motor pinion (sun wheel)
maxon EC motor EC 4 (with Hall sensors)
8 Ball bearings
9 Permanent magnet
10 Winding
11 Stator stack
12 Housing
13 Ceramic bearing
14 Circuit board with Hall sensors
15 Shaft
16 Control magnet

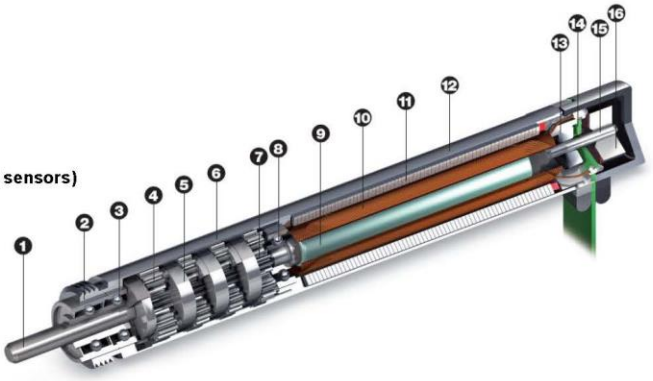

1/2

maxon motor
driven by precision

maxon modular system

The EC4 is available in two lengths:
- Short version with 0.5 W nominal power
- Long version with 1.0 W nominal power

For both versions, two windings each are available (3.0 V and 6.0 V nominal voltage). It is also possible to choose between versions with or without Hall sensors. The pin assignment and the layout of the flexprint are identical with the EC 8 motor. This means that existing adapter connectors can be used.

For the new GP 4 C planetary gearhead, three different reduction ratios are available. These correspond to a 2-stage, 3-stage and 4-stage version. In the 4-stage version, the max. continuous torque is approx. 15 mNm.

As control electronics for sample units, the DECS 50/5 (item S12044) for sensorless operation, as well as the new ESCON 36/3 EC (item 414533) can be provided.

Comparison with competitors

None of the competitors have remotely comparable powerful drives on offer.
A comparison of the characteristic speed/torque gradient:

Manufacturer	Motor type	Gradient rpm mNm^{-1}
maxon motor	EC4 long EC4 short	approx. **50,000** Approx. 93,000
Namiki	SBL 04-0829	Approx. 525,000
Faulhaber	Smoovie (Ø5mm) Smoovie (Ø3mm)	Approx. 300,000 Approx. 3,300,000

Prices
The prices for the motors are listed in the IFS price list, with the usual scaling according to the quantity (an extract is shown here).

EC 4 0.5 W with Hall sensors (short version)

Quantity	net CHF	gross CHF
1 – 4	99.40	187.40
50 – 149	88.80	121.10
500 – 749	81.50	95.30
1000 – 1999	78.60	87.30

EC 4 1.0 W with Hall sensors

Quantity	net CHF	gross CHF
1 – 4	105.70	199.40
50 – 149	94.50	128.80
500 – 749	86.80	101.40
1000 – 1999	83.60	92.90

GP 4 C, 2-stage (i=17:1)

Quantity	net CHF	gross CHF
1 – 4	63.70	120.00
50 – 149	56.90	77.60
500 – 749	52.20	61.10
1000 – 1999	50.30	55.90

GP 4 C, 3-stage (i=68:1)

Quantity	net CHF	gross CHF
1 – 4	74.00	139.50
50 – 149	66.10	90.10
500 – 749	60.70	71.00
1000 – 1999	58.50	65.00

GP 4 C, 4-stage (i=280:1)

Quantity	net CHF	gross CHF
1 – 4	84.80	159.90
50 – 149	75.80	103.30
500 – 749	69.60	81.30
1000 – 1999	67.00	74.50

Availability
Sample quantities of EC4 and GP4 units can currently be ordered via the sales check list.
Currently no modifications are possible.

Sales support

- The media release will be issued soon at www.maxonmotor.com .
- The "Mission to Minimize" product brochures are available in German and English (these can be ordered from Marketing Support).

We wish you every success.

Best regards,
maxon motor ag
Sales & Marketing
maxon medical
Steffen Zeller

Product Management
Michael Baumgartner

Attached: Data sheets

EC 4 ∅4 mm, brushless, 0.5 Watt

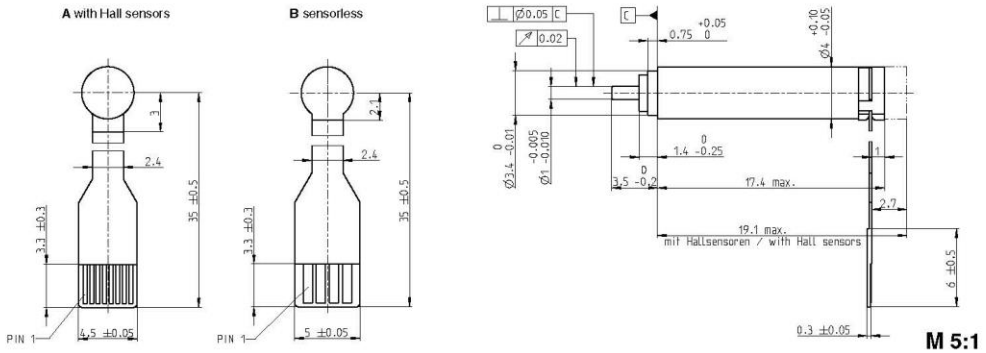

Stock program
Standard program
Special program (on request)

	Part Number	
A with Hall sensors	431555	431558
B sensorless	423518	423525

Motor Data (provisional)			
Values at nominal voltage			
1 Nominal voltage	V	3.0	6.0
2 No load speed	rpm	34700	35800
3 No load current	mA	23.4	12.1
4 Nominal speed	rpm	14000	15700
5 Nominal torque	mNm	0.219	0.226
6 Nominal current	A	0.297	0.157
7 Stall torque	mNm	0.397	0.415
8 Starting current	A	0.483	0.272
9 Max. efficiency	%	62	63
Characteristics			
10 Terminal resistance phase to phase	Ω	6.21	22.1
11 Terminal inductance phase to phase	mH	0.0231	0.0881
12 Torque constant	mNm/A	0.784	1.53
13 Speed constant	rpm/V	12200	6240
14 Speed/torque gradient	rpm/mNm	96400	90200
15 Mechanical time constant	ms	1.12	1.12
16 Rotor inertia	gcm²	0.00111	0.00111

Specifications

Thermal data

17	Thermal resistance housing-ambient	129 K/W
18	Thermal resistance winding-housing	2.39 K/W
19	Thermal time constant winding	0.113 s
20	Thermal time constant motor	78.0 s
21	Ambient temperature	-20 ... +80°C
22	Max. permissible winding temperature	+125°C

Mechanical data

23	Max. permissible speed	80000 rpm
24	Axial play	max. 0.06 mm
25	Radial play	preloaded
26	Max. axial load (dynamic)	0.1 N
27	Max. force for press fits (static)	3 N
28	Max. radial loading, 4 mm from flange	2 N

Other specifications

29	Number of pole pairs	1
30	Number of phases	3
31	Weight of motor	1.2 g

Values listed in the table are nominal.

Connection	with Hall sensors	sensorless
Pin 1	Motor winding 1	Motor winding 1
Pin 2	Motor winding 2	Motor winding 2
Pin 3	Motor winding 3	Motor winding 3
Pin 4	V_{Hall} 4.5...18 VDC	Y
Pin 5	GND	
Pin 6	Hall sensor 1	
Pin 7	Hall sensor 2	
Pin 8	Hall sensor 3	
Connector	**Part number**	**Part number**
MOLEX	52745-0896	52207-0485
MOLEX		52089-0419
TYCO		84953-4

Pin for design with Hall sensors:
FPC, 8-pol, Pitch 0.5 mm, top contact style
Wiring diagram for Hall sensors see catalogue p. 27

Operating Range

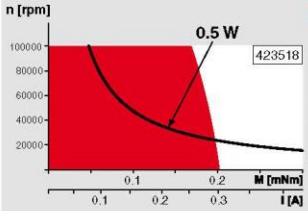

Comments

Continuous operation
In observation of above listed thermal resistance (lines 17 and 18) the maximum permissible winding temperature will be reached during continuous operation at 25°C ambient.
= Thermal limit.

Short term operation
The motor may be briefly overloaded (recurring).

Assigned power rating

maxon Modular System

Planetary Gearhead
∅4 mm
0.002–0.015 Nm
Page 6

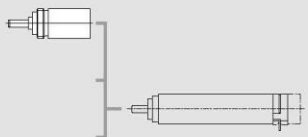

Recommended Electronics:

DECS 50/5	Page 6
ESCON 36/3	6

EC 4 ∅4 mm, brushless, 1.0 Watt

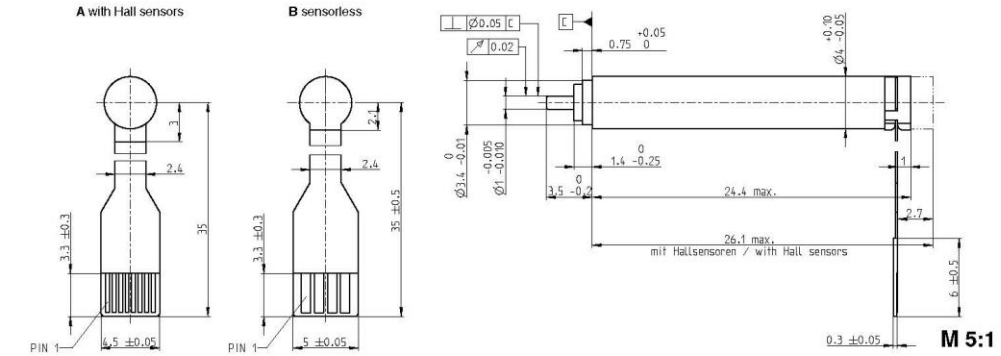

Stock program
Standard program
Special program (on request)

	Part Number	
A with Hall sensors	431182	431284
B sensorless	414402	423511

Motor Data (provisional)			
Values at nominal voltage			
1 Nominal voltage	V	3.0	6.0
2 No load speed	rpm	39900	29900
3 No load current	mA	40.6	14.1
4 Nominal speed	rpm	20200	11200
5 Nominal torque	mNm	0.383	0.400
6 Nominal current	A	0.587	0.229
7 Stall torque	mNm	0.799	0.660
8 Starting current	A	1.15	0.358
9 Max. efficiency	%	66	65
Characteristics			
10 Terminal resistance phase to phase	Ω	2.6	16.7
11 Terminal inductance phase to phase	mH	0.00946	0.0668
12 Torque constant	mNm/A	0.693	1.84
13 Speed constant	rpm/V	13800	5190
14 Speed/torque gradient	rpm/mNm	51800	47200
15 Mechanical time constant	ms	0.992	0.840
16 Rotor inertia	gcm²	0.00170	0.00170

Specifications

Thermal data	
17 Thermal resistance housing-ambient	97.4 K/W
18 Thermal resistance winding-housing	1.46 K/W
19 Thermal time constant winding	0.114 s
20 Thermal time constant motor	88.6 s
21 Ambient temperature	-20 ... +80°C
22 Max. permissible winding temperature	+125°C
Mechanical data	
23 Max. permissible speed	80000 rpm
24 Axial play	max. 0.06 mm
25 Radial play	preloaded
26 Max. axial load (dynamic)	0.1 N
27 Max. force for press fits (static)	3 N
28 Max. radial loading, 1 mm from flange	2 N
Other specifications	
29 Number of pole pairs	1
30 Number of phases	3
31 Weight of motor	2 g

Values listed in the table are nominal.

Connection	with Hall sensors	sensorless
Pin 1	Motor winding 1	Motor winding 1
Pin 2	Motor winding 2	Motor winding 2
Pin 3	Motor winding 3	Motor winding 3
Pin 4	V_{Hall} 4.5...18 VDC	Y
Pin 5	GND	
Pin 6	Hall sensor 1	
Pin 7	Hall sensor 2	
Pin 8	Hall sensor 3	
Connector	**Part number**	**Part number**
MOLEX	52745-0896	52207-0485
MOLEX		52089-0419
TYCO		84953-4

Pin for design with Hall sensors:
FPC, 8-pol, Pitch 0.5 mm, top contact style
Wiring diagram for Hall sensors see catalogue p. 27

Operating Range

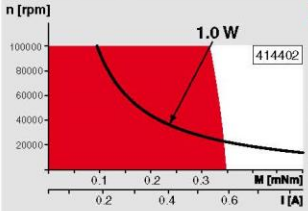

Comments

Continuous operation
In observation of above listed thermal resistance (lines 17 and 18) the maximum permissible winding temperature will be reached during continuous operation at 25°C ambient.
= Thermal limit.

Short term operation
The motor may be briefly overloaded (recurring).

Assigned power rating

maxon Modular System

Planetary Gearhead
∅4 mm
0.002–0.015 Nm
Page 6

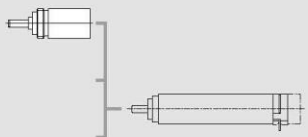

Recommended Electronics:

DECS 50/5	Page 6
ESCON 36/3	6

Planetary Gearhead GP 4 C Ø4 mm, 0.002 - 0.015 Nm

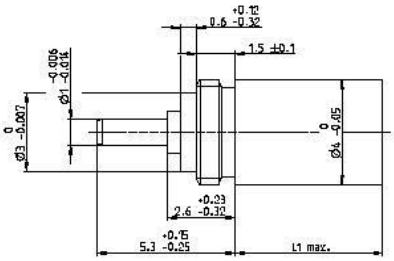

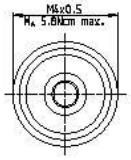

M 10:1

Technical Data			
Planetary Gearhead	special teeth		
Output shaft	stainless steel		
Bearing at output	ball bearings		
Radial play, 5 mm from flange	max. 0.14 mm		
Axial play at axial load	max. 0.2 mm		
Max. permissible axial load	5 N		
Max. permissible force for press fits	5 N		
Sense of rotation, drive to output	=		
Recommended input speed	< 40000 rpm		
Recommended temperature range	-15 ... +80°C		
Number of stages	2	3	4
Max. radial load, 5 mm from flange	1.5 N	3 N	5 N

Stock program
Standard program
Special program (on request)

Order Number			
	416148	417408	420531
Gearhead Data			
1 Reduction	17 : 1	68 : 1	280 : 1
2 Reduction absolute			
3 Max. motor shaft diameter mm	0.6	0.6	0.6
4 Number of stages	2	3	4
5 Max. continuous torque Nm	0.002	0.006	0.015
6 Intermittently permissible torque at gear output Nm	0.003	0.008	0.020
7 Max. efficiency %	76	70	65
8 Weight g	tb.d.	tb.d.	tb.d.
9 Average backlash no load °	3.9	4.2	4.5
10 Mass inertia gcm²	tb.d.	tb.d.	tb.d.
11 Gearhead length L1 mm	5.7	7.4	9.2

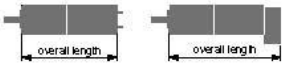

maxon Modular System						
+ Motor	Page	+ Sensor/Brake	Page	Overall length [mm] = Motor length + gearhead length + (sensor / brake) + assembly parts		
EC 4, 0.5 W, A	4			24.8	26.5	28.3
EC 4, 0.5 W, B	4			23.3	25.0	26.8
EC 4, 1 W, A	5			31.9	33.6	35.4
EC 4, 1 W, B	5			30.2	31.9	33.7

Control electronics for sample units.

For fast, easy and affordable commissioning of the EC 4 drive, we recommend the use of standard production electronic units. We offer two versions for motors with and without Hall sensors.

1-Q-EC sensorless amplifier DECS 50/5

- Digital speed control for sensorless EC motors
- Various start sequences can be selected
- Several options for specifying set values

Part no. DECS 50/5 S12044

4-Q EC amplifier ESCON 36/3 EC

- Digital speed control for EC motors with Hall sensors
- Several options for specifying set values
- 4-Q operation
- Easy commissioning

Part no. ESCON 36/3 EC 414533
Adapter 418723

APPENDIX V – EDGE MOTOR CONTROLLER SPECIFICATION

NANOMOTION
A Johnson Electric Company

XCD-EDGE-BD-01 Drive and Control

Application Recommendations

- Auto Focus/Zoom Modules
- Shutter & Aperture Control
- Filter Changers
- Pan and Tilt Modules

ORDERING INFORMATION

Part Number: XCD-EDGE-BD-01
Drive and Control

RELATED PRODUCTS/ ACCESSORIES

Part Number: EM1-S-0
EM1-V-0
EDGE motor

Part Number: XCDE150100-00
XCD EDGE Motherboard Assembly

Product Description

Nanomotion's XCD – Drive & Control redefines the art of miniaturized drive and control electronics with the smallest hardware for operating piezo ceramic servo motors. The XCD provides complete servo control for the OEM market, coupled with the power stage and drive electronics on one board. XCD will have an OEM specific, motherboard for connecting to the motor, position sensor, communication and power.

The XCD for the Edge motor is provided as a single axis board which can operate in the 'AB5' mode with brake on/off, or in the more traditional AB1A mode. The XCD for the Edge motors accepts a single ended encoder signal and is programmed via an IIC interface and the NanoCommander user software.

NANOMOTION
A Johnson Electric Company

www.nanomotion.com

XCD-1E-BD-00 Drive and Control

MECHANICAL DRAWINGS AND INTERFACE

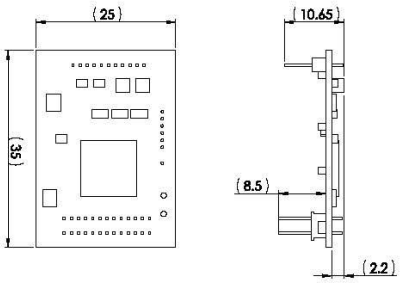

TECHNICAL SPECIFICATIONS

Dimensions:
35.0 x 25.0 x 10.65 mm
Motors supported : EDGE
Input Power: 5 V
Drive Mode AB5
(brake on/off) or AB1A mode
Communication IIC
Operating Temperature:
-40 to 85 °C

ELECTRICAL

Power Consumption:
500 mW (max)

ELECTRICAL INTERFACE

pin number	J2 Main Connector pin name	J2 Main Connector pin description	J1 Motor and Encoder Connector pin name	J1 Motor and Encoder Connector pin description
1	+5v	5vdc power input	+5v	5vdc power out
2	+5v	5vdc power input	a	encoder incremental signals
3	spi clk	spiclock	b	encoder incremental signals
4	spi en	spi enable	index	encoder reference mark
5	miso	master in slave out	gnd	system ground
6	mosi	master out slavein	limit sw right	limit switch right
7	n.c.	no connected	limit sw left	limit switch left
8	n.c.	not connected	gnd	system ground
9	rxd	rs232 receive	p1	motor phase 1
10	txd	rs232 transmit	com	motor common
11	sda	12c serial data	p2	motor phase 2
12	scl	12c serial clock		
13	gpi01	ppw		
14	gpi02	n/a		
15	gpi03	general purpose digital output 3		
16	gpi04	general purpose digital output 4		
17	an2	analog input 1		
18	an1	analog input 2		
19	emergency	emergency stop		
20	an3	analog input 3		
21	anlg_out2	analog output 2		
22	anlg_out1	analog output 1		
23	n.c.	n/a		
24	pwm_out	keep alive		
25	gnd	system ground		
26	gnd	system ground		

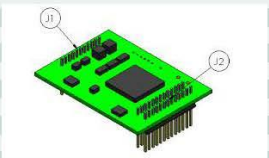

Nanomotion Ltd.
Worldwide Headquarters

Mordot HaCarmel Industrial Park
Yokneam 20692 Israel
t: +972 73 2498000
f: +972 73 2498099
e: nano@nanomotion.com

Nanomotion Inc.
U.S. Headquarters

1 Comac Loop, Suite 14B2
Ronkonkoma, New York 11779
t: (800) 821 6266
t: (631) 585 3000
f: (631) 585 1917
e: nanoUS@nanomotion.com

NANOMOTION
A Johnson Electric Company

www.nanomotion.com